Metabolic engineering of *Corynebacterium glutamicum* for production of L-lysine from mannitol and mannitol-rich seaweed extracts

Dissertation

zur Erlangung des Grades

des Doktors der Ingenieurwissenschaften

der Naturwissenschaftlich-Technischen Fakultät

der Universität des Saarlandes

von

Sarah Lisa Hoffmann

Saarbrücken

2020

Tag des Kolloquiums:	16.12.2020
Dekan:	Prof. Dr. Jörn Walter
Berichterstatter:	Prof. Dr. Christoph Wittmann
	Prof. Dr. Andriy Luzhetskyy
Vorsitz:	Prof. Dr. Uli Kazmaier
Akad. Mitarbeiter:	Dr. Frank Hannemann

Publications

Partial results of this work have been published in advance authorized by the Institute of Systems Biotechnology represented by Prof. Dr. Christoph Wittmann.

Peer-reviewed articles

Becker, J., Gießelmann, G., **Hoffmann, SL.**, Wittmann, C., 2016. *Corynebacterium glutamicum* for sustainable bioproduction: from metabolic physiology to systems metabolic engineering. In: Zhao, H., Zeng, A.P. (Eds.), Synthetic Biology - Metabolic Engineering. Advances in Biochemical Engineering/Biotechnology, vol. 162, Springer, Cham.

Hoffmann SL., Jungmann L., Schiefelbein S., Peyriga L., Cahoreau E., Portais JC., Becker J., Wittmann C., 2018. Lysine production from the sugar alcohol mannitol: Design of the cell factory *Corynebacterium glutamicum* SEA-3 through integrated analysis and engineering of metabolic pathway fluxes. Metabolic Engineering 47: 475-487.

Poblete-Castro, I., **Hoffmann, SL.**, Becker, J., Wittmann, C., 2020. Cascaded valorization of seaweed using microbial cell factories. Current Opinion in Biotechnology 65: 102-113.

Conference contributions

Hoffmann, SL., Jungmann, L., Schiefelbein, S., Becker, J., Wittmann, C., “Towards lysine production from seaweed: Design of a mannitol-using *Corynebacterium glutamicum* cell factory through integrated analysis and engineering of metabolic pathway fluxes.” 12th Metabolic Engineering Conference, June 24 - 28, 2018, Munich, Germany.

Hoffmann, SL., Jungmann, L., Schiefelbein, S., Becker, J., Wittmann, C., “Systems metabolic engineering of *Corynebacterium glutamicum* for the production of lysine from mannitol.” GASB II conference, September 27 - 28, 2018, Berlin, Germany.

Hoffmann, SL., Jungmann, L., Schiefelbein, S., Becker, J., Wittmann, C., “Towards 3G bio-production from ocean farms: Systems metabolic engineering of *Corynebacterium glutamicum* for the production of L-lysine from the major seaweed ingredient mannitol.” GIM conference, September 8 - 11, 2019, Pisa, Italy.

Hoffmann, SL., Jungmann, L., Schiefelbein, S., Becker, J., Wittmann, C., “Towards 3G bio-production from ocean farms: Systems metabolic engineering of *Corynebacterium glutamicum* for the production of L-Lysine from the major seaweed ingredient mannitol.” PhD day, November 6th, 2019, Saarland University, Saarbrücken, Germany.

Danksagung

Ganz herzlich bedanken möchte ich mich an erster Stelle bei Prof. Dr. Christoph Wittmann, der mir die Möglichkeit gegeben hat an diesem interessanten Thema zu arbeiten und mir stets bei allen möglichen Problemen zur Seite stand, immer einen guten Ratschlag parat hatte und vor allem mir den Glauben vermittelt hat, dass am Ende alles gut wird. Durch diese sehr tolle aber auch intensive Zeit konnte ich mich nicht nur wissenschaftlich sondern auch persönlich weiterentwickeln. Vielen lieben Dank!

Prof. Dr. Andriy Luzhetskyy danke ich für die Übernahme der Begutachtung meiner Arbeit. Auch bei Herrn Prof. Dr. Uli Kazmaier und bei Herrn Dr. Frank Hannemann möchte ich mich jeweils für die Übernahme der Leitung des Prüfungsverfahrens und den akademischen Prüfungsbeisitz bedanken.

Ganz herzlich möchte ich mich auch bei Dr. Judith Becker bedanken, die immer eine offene Tür hatte und mir immer mit guten Ratschlägen weiterhelfen konnte.

Ein besonderer Dank geht an Prof. Dr. Jean-Charles Portrais, Lindsay Peyriga und Edern Cahoreau für die Durchführung der NMR-Messungen und die tolle Zeit in Toulouse.

Ein weiterer Dank geht auch an Prof. Dr. Ignacio Poblete-Castro für die Bereitstellung der *D. antarcticta* Hydrolysate und die vielen tollen und interessanten Gespräche.

Bei Dr. Michael Hutter möchte ich mich für die tolle Zusammenarbeit und die enzymatischen Modellierungen bedanken.

Michel Fritz danke ich für seine Hilfsbereitschaft, seine Unterstützung während der Bearbeitung meines Projekts und vor allem für seine unendliche Geduld.

Bei den Mitarbeitern des Instituts für Systembiotechnologie möchte ich mich für die tolle Zeit, die tolle Unterstützung und vor allem die lustigen Momente bedanken. Christina, Gideon und Demian möchte ich ganz herzlich für die sehr tollen Gespräche und Ratschläge, sowohl beruflicher als auch privater Natur danken und dass ihr mich durch diese sehr schöne aber auch sehr extreme Zeit begleitet habt. Während der Zeit am Institut seid ihr für mich nicht nur zu sehr guten Arbeitskollegen geworden, auf die man immer zählen kann, sondern auch zu sehr guten Freunden. Ohne euch wäre die Zeit bestimmt nicht so schön und amüsant geworden. Auch bei Martin und Lars möchte ich mich für die fachlichen als auch privaten Konversationen aber auch für die tollen Erlebnisse rund ums Saarland oder in Italien bedanken. Nadja Barton danke ich für die Hilfe bei molekularbiologischen Arbeiten aber auch für die sehr tollen Momente die wir zusammen in China oder auch München verbringen durften. Weiterhin möchte ich mich

bei Susanne Haßdenteutel für die tollen Gespräche und ihre Hilfsbereitschaft bedanken und dass du egal zu welcher Situation immer einen passenden Spruch auf Lager hattest.

Ein besonderer Dank geht auch an Lukas, der mich seit dem Beginn meiner Arbeit sowohl als Bachelor- als auch als Masterstudent begleitet hat und trotz des anfänglich holprigen Startes mittlerweile nicht nur zu einem guten Arbeitskollegen sondern auch zu einem wichtigen Menschen geworden ist.

Bei meiner langjährigen besten Freundin Caro bedanke ich mich nicht nur für die tolle Unterstützung während dieser Zeit, sondern für die tolle Unterstützung seitdem wir uns kennen. Du hast mir immer mit Rat und Tat zur Seite gestanden und hattest immer die passenden Worte zur jeweiligen Situation parat. Auch für die schöne Zeit und die vielen lustige Momente bedanke ich mich rechtherzlich.

Philipp, danke für deine unendliche Geduld mit mir, deinen Glauben an mich, und dass du trotz schwieriger Momente immer hinter mir gestanden hast um mir den Rücken freizuhalten. Ich danke dir auch für die vielen tollen Momente die wir mit Diego oder wie du ihn auch liebevoll nennst, Diggi, Käpt’n Knoddel, Iggy Pop, hatten und dass du dich liebevoll um den Kleinen kümmerst.

Meiner Familie, danke für eure Unterstützung, für eure aufbauenden Worte, für eure Hilfsbereitschaft, für den Halt und für‘s da sein in schwierigen Zeiten.

Table of contents

Summary ..... **VIII**

Zusammenfassung ..... **IX**

1 Introduction **1**

2 Objectives **3**

3 Theoretical Background **4**

3.1 Alternative renewable feedstocks for bio-refinery applications 4

3.1.1 Seaweed - a third-generation renewable 5

3.2 *Corynebacterium glutamicum* as industrial workhorse 8

3.2.1 Discovery of *Corynebacterium glutamicum* - the L-glutamate story 8

3.2.2 Industrial application of *Corynebacterium glutamicum* 9

3.2.3 Industrial L-lysine production 10

3.2.4 Uptake and catabolism of industrially relevant sugars 14

3.2.5 Utilization of the sugar alcohol mannitol 15

3.2.6 L-Lysine biosynthesis 18

3.2.7 Central carbon metabolism 20

3.3 Metabolic engineering of L-lysine-producing *C. glutamicum* 21

3.3.1 Metabolic engineering of L-lysine biosynthesis and attenuation of competing pathways 22

3.3.2 Improvement of precursor supply and reducing power 23

3.3.3 Systems metabolic engineering 25

4 Material and Methods **30**

4.1 Bacterial strains 30

4.2 Primers and plasmids 31

4.3 Chemicals 33

4.4 Medium composition 33

4.4.1 Complex media 34

4.4.2 Mineral salt medium 35

4.4.3 Seaweed based medium 38

4.4.4 Industrial production media 39

4.5 Strain conservation 41

4.6 Strain construction 41

4.6.1 Isolation of plasmid DNA 41

4.6.2 Purification of DNA fragments 42

4.6.3 Construction of transformation vectors 42

4.6.4 Polymerase chain reaction 44

4.6.5 Site-directed mutagenesis 45

4.6.6 Gel electrophoresis 45

4.6.7 Preparation of heat shock competent *E. coli* cells ... 46
4.6.8 Transformation of *E. coli* cells by heat shock ... 47
4.6.9 Preparation of electro-competent *C. glutamicum* cells ... 47
4.6.10 Transformation of *C. glutamicum* ... 47
4.6.11 Second recombination ... 48
4.6.12 Computational modeling for protein engineering ... 48
4.6.13 Codon optimization ... 49
4.7 Cultivation ... 49
4.7.1 Batch cultivation in shake flasks ... 49
4.7.2 Fed-batch production of L-lysine from mannitol in a lab-scale bioreactor ... 49
4.8 Preparation of seaweed hydrolysates ... 50
4.8.1 Extraction of the brown seaweed *Durvillaea antarctica* ... 50
4.8.2 Extraction of the brown seaweed *Laminaria digitata* ... 51
4.8.3 Purification of alginate from seaweed extracts ... 51
4.8.4 Processing of seaweed hydrolysates for fermentative L-lysine production ... 51
4.9 Analytical methods ... 52
4.9.1 Quantification of cell concentration ... 52
4.9.2 Quantification of amino acids ... 53
4.9.3 Quantification of carbohydrates and organic acids ... 54
4.9.4 GC-MS analysis of ^{13}C labeling patterns ... 54
4.9.5 Qualitative quantification of seaweed hydrolysates ... 55
4.9.6 NMR analysis of ^{13}C labeling patterns ... 56
4.10 Biochemical methods ... 57
4.10.1 Preparation of crude cell extract ... 57
4.10.2 Quantification of protein concentration ... 57
4.10.3 Quantification of enzyme activity ... 57
4.11 Fluxomics ... 60
4.11.1 Metabolic modeling and flux estimation ... 60
4.11.2 Summed fractional labeling ... 66
4.11.3 *In silico* pathway modeling ... 66
4.12 Analysis of the cellular redox state ... 67
4.13 Statistical analysis ... 68
5 Results and Discussion ... 69
5.1 Activation of mannitol utilization in *C. glutamicum* ... 69
5.1.1 Deletion of the mannitol repressor protein MtlR ... 69
5.1.2 Metabolic fluxes of *C. glutamicum* SEA-1 ... 73
5.1.3 Protein engineering of mannitol 2-dehydrogenase in *C. glutamicum* ... 78
5.2 Elimination of fructose overflow ... 84
5.2.1 Connecting mannitol catabolism to the PP pathway ... 84
5.2.2 Metabolic fluxes of *C. glutamicum* SEA-2B ... 89
5.2.3 Extending the flux capacity of the EMP pathway ... 90

5.3 Systems wide engineering for maximized redox supply 97
5.3.1 Redox level in mannitol-grown L-lysine producing *C. glutamicum* 97
5.3.2 Co-factor balancing using transhydrogenase expression 99
5.4 Cascaded processing of seaweed into alginate and bioavailable monosaccharides 102
5.4.1 Hydrothermal extraction of *Laminaria digitata* 102
5.4.2 Enhanced process with combined enzymatic treatment 103
5.4.3 Extraction and purification of alginate as a high value side stream 105
5.5 Creation and benchmarking of a fully genome-based L-lysine-producing cell factory 106
5.5.1 Design, construction and evaluation of a fully genome-based producer 106
5.5.2 Redox status in *C. glutamicum* strains expressing the membrane-bound transhydrogenase PntAB 115
5.5.3 Metabolic pathway analysis 117
5.6 Establishment of a cascaded bioprocess for efficient L-lysine production using metabolically engineered *C. glutamicum* 120
5.6.1 Benchmarking of the final tailor-made L-lysine producer under industrial conditions 120
5.6.2 Production of L-lysine from pre-processed *Laminaria digitata* hydrolysates 123
5.6.3 Production of L-lysine from hydrolyzed *Durvillaea antarctica* waste 127
6 Conclusion and Outlook 129
7 Appendix 131
7.1 Primers 131
7.2 Codon optimization 132
7.3 ^{13}C Metabolic flux analysis 134
7.4 Elementary flux mode analysis 140
7.5 Data from ^{13}C metabolic flux analysis in *C. glutamicum* strains 143
8 Abbreviations and Symbols 147
9 References 152

Summary

Nowadays, *C. glutamicum* belongs to the most important industrial microbes, especially in the production of L-lysine, which is mainly applied as feed supplement in animal nutrition. L-Lysine is currently fermented from agricultural crops such as corn and sugar cane. Especially from a sustainability perspective, it is necessary to find non-food raw materials for production. In this regard, seaweed as 3rd generation renewable is highly promising. In a first round of metabolic engineering, the glucose-based L-lysine producing strain LYS-12 served as starting point to extend the substrate spectrum to mannitol, the most abundant seaweed carbohydrate, by deleting the constitutively expressed mannitol repressor MtlR/AtlR. However, only small amounts of L-lysine were produced by this mutant, designated SEA-1. To further upgrade this basic strain, several rounds of systems metabolic engineering were applied. These aimed at improving the NADPH supply and recycling excess NADH, originating from catabolic mannitol oxidation and posing inhibitory effects on the cell. The finally constructed L-lysine producer *C. glutamicum* SEA-7 revealed superior production performance and achieved a L-lysine titer of 76 g L^{-1} from mannitol in a fed-batch process. Finally, SEA-7 was implemented into a cascaded value chain towards maximal sustainability using seaweed extracts from *Laminaria digitata* and *Durvillaea antarctica*, yielding 0.29 mol mol^{-1} and 0.41 mol mol^{-1} of L-lysine, respectively.

Zusammenfassung

Heutzutage gehört das Bakterium *C. glutamicum* zu den wichtigsten industriellen Produzenten, insbesondere zur Herstellung von L-Lysin, welches vor allem Anwendung in der Futtermittelindustrie findet. L-Lysin wird derzeit hauptsächlich aus Nutzpflanzen wie Mais oder Zuckerrohr hergestellt. Insbesondere vor dem Hintergrund der Nachhaltigkeit ist die Erschließung alternativer Rohstoffe unumgänglich. Meeresalgen stellen diesbezüglich als 3. Generation nachwachsender Rohstoffe eine vielversprechende Ressource dar. Mittels *Metabolic Engineering* wurde das Substratspektrum des L-Lysin-Produzenten *C. glutamicum* LYS-12, der für die Produktion auf Glukose optimiert wurde, durch Deletion des Mannitolrepressors MtlR/AtlR um Mannitol, dem häufigsten Kohlenhydrat der Makroalgen, erweitert. Die so erzeugte SEA-1 Mutante bildete nur geringe Mengen L-Lysin. Um den Basisstamm zu verbessern, wurden weitere genetische Optimierungen vorgenommen. Diese zielten vor allem auf die Verbesserung der NADPH-Versorgung und das Recycling von überschüssigem NADH ab, das während der Mannitolverwertung akkumuliert und den Stoffwechsel hemmt. Der finale L-Lysin-Produzent *C. glutamicum* SEA-7 erzielte im Fed-Batch Prozess auf Mannitolbasis einen L-Lysin-Titer von 76 g L^{-1}. Letztendlich wurde SEA-7 in eine nachhaltige Wertschöpfungskette unter Verwendung von Algenextrakten aus *Laminaria digitata* und *Durvillaea antarctica* implementiert. Dabei wurden L-Lysin-Ausbeuten von 0,29 mol mol^{-1} und 0,41 mol mol^{-1} erzielt.

1 Introduction

With the Second World War and the advent of ready meals and spice mixtures about 80 years ago, the demand for L-glutamate as flavor enhancer increased, so that a large screening program was initiated to find natural L-glutamate-overproducing microbes (Kinoshita et al. 1957). This led to the discovery of the gram positive soil bacterium *Corynebacterium glutamicum*, initially named *Micrococcus glutamicus* (Abe et al. 1967; Kinoshita et al. 1957; Udaka 1960). It was found that not only L-glutamate can be produced by this organism, but also a variety of other amino acids such as L-alanine, L-aspartate, L-histidine, L-isoleucine, L-leucine, L-lysine, L-proline, L-tyrosine and L-valine (Kimura 1963). Over the past decades *C. glutamicum* was upgraded into a work horse, capable to produce a wide range of important products (Becker and Wittmann 2012a, 2012b). Today, *C. glutamicum* is one of the major cell factories for industrial production, including the amino acids L-glutamate and L-lysine (Becker and Wittmann 2012b; Eggeling and Bott 2015). Since L-lysine is one of the most limiting amino acid in animal nutrition, it is an important feed supplement (Wittmann and Becker 2007). In addition, it finds application in the polymer, the cosmetic and the pharmaceutical industry (Koffas and Stephanopoulos 2005). The L-lysine market grows by 6 - 7 % annually, and the production volume is expected to reach 4 million tons in 2023 (Cheng et al. 2018; Eggeling and Bott 2015). Currently, industrial L-lysine production is based on sugar-based feedstocks from cane and beet molasses and starch hydrolysates from corn, cassava and wheat (Ikeda 2003; Wittmann and Becker 2007). Unfavorably, these raw materials are derived from food crops and suffer from a continuous competition with human nutrition (Alaswad et al. 2015). The increasing need for a more sustainable production has turned the interest towards alternative resources, namely non-edible second-generation renewables such as straw, wood and grass, which are rich in lignocellulose (Balat 2011; Buschke et al. 2013a; Naik et al. 2010). Recently, superior *C. glutamicum* strains were created by systems wide metabolic engineering approaches, which produce large quantities of L-lysine (Anusree et al. 2016; Chen et al. 2019; Gopinath et al. 2011), plus other chemicals such as 1,5-diaminopentane (Buschke et al. 2013a; Buschke et al. 2011), 3-hydroxypropionic acid (Chen et al. 2017), xylonic acid (Yim et al. 2017) and xylitol (Dhar et al. 2016) from lignocellulosic sugars. However, the use of lignocellulosic biomass is challenged from an energy-costly processing of the lignocellulose into fermentable sugars and the formation of toxic compounds during the processing (Balat 2011; Buschke et al. 2013b). In addition, these raw materials consume valuable arable land, so that the use of third-generation renewables is increasingly becoming important, envisioning even more efficient and sustainable production. In this context, marine macroalgae (seaweed) show substantial potential as a most sustainable

feedstock because no fresh water, chemical fertilizer, arable land and extreme human intervention are needed for their cultivation (Goh and Lee 2010; Torres et al. 2019). Another major advantage of farming seaweed, apart from the simple extraction conditions for obtaining carbohydrates from milled algae (Poblete-Castro et al. 2020), and from the high photosynthetic activity and rapid growth (Alaswad et al. 2015; van Hal et al. 2014), is that it counteracts global warming by fixing CO_2 from the environment (Kraan 2013). Today, more than 30 million tons of seaweed are farmed in the oceans and the market volume is expected to increase to 500 million tons by 2050 (Poblete-Castro et al. 2020). The macroalgae, especially the brown species, are rich in carbohydrates such as the polysaccharides laminarin and alginate as well as the free sugar alcohol mannitol (Poblete-Castro et al. 2020; Torres et al. 2019; Wei et al. 2013). Depending on season and species, carbon levels of up to 55 % are observed (Kraan 2013; Wei et al. 2013). Mannitol thereby significantly contributes to the total carbohydrate content. It can form up to 30 % of the dry cell weight of seaweed (Iwamoto and Shiraiwa 2005). In this respect, the use of mannitol for the manufacture of industrial products such as L-lysine would make marine biomass accessible for sustainable production. Since L-lysine is one of the leading biotechnological products (Eggeling and Bott 2015), it appears promising to extend the substrate spectrum of *C. glutamicum* to mannitol. Naturally, the microbe cannot use the sugar alcohol. However, deletion of the MtlR/AtlR repressor enabled mannitol utilization in *C. glutamicum* (Laslo et al. 2012; Peng et al. 2011). Therefore, deletion of the repressor in *C. glutamicum* displayed a first promising target towards sustainable production of L-lysine from algal biomass, besides the conventional use of glucose-based raw materials.

2 Objectives

The overall aim of this work was to design and create strains of *C. glutamicum*, which produce the feed amino acid L-lysine from mannitol and from mannitol-rich extracts of seaweed. The L-lysine producing strain *C. glutamicum* LYS-12 should be taken as a starting point. In this regard, the first objective of this work was to extend the substrate spectrum of LYS-12 to mannitol, one of the main carbohydrates found in brown seaweed. Since mannitol-based L-lysine production was rather unexplored, the obtained strain should be analyzed at the level of metabolic fluxes, enzyme inventory and redox status to gain insights into its metabolism and identify targets to create a most efficient mannitol- to L-lysine cell factory. A further objective was to assess the production performance of the best producers in a fed-batch process under industrial conditions. Finally, this development should enable a value chain from aquatic biomass to L-lysine, including the use of seaweed and seaweed-derived extracts for production.

3 Theoretical Background

3.1 Alternative renewable feedstocks for bio-refinery applications

The world´s chemical market is mainly based on fossil coal, petroleum, and natural gas (Behera et al. 2015; Naik et al. 2010; Wyman et al. 2005). This extreme use leads to the depletion of fossil resources and hence to rising prices (Alaswad et al. 2015; Behera et al. 2015; Naik et al. 2010). Furthermore, it is ultimately unsustainable, as it increases the pollution of air and water and most critically drives climate change and global warming (Alaswad et al. 2015). Thus, the use of more sustainable and environmentally friendly resources appears inevitable to derive industrial products (Alaswad et al. 2015; Becker and Wittmann 2015). In recent years, several studies focused on the sustainable production of chemicals, materials and fuels by using highly engineered microbial cell factories such as *Escherichia coli* (Lee et al. 2009; Qian et al. 2011; Wang et al. 2011), *Saccharomyces cerevisiae* (Buijs et al. 2013; Nielsen et al. 2013; Zhang et al. 2006), and *Corynebacterium glutamicum* (Becker et al. 2011; Buschke et al. 2013a; Kind et al. 2014). So far, most of these production processes, particularly the production of fine and bulk chemicals, are based on food crops, i.e. cane and beet molasses, as well as starch hydrolysates from corn and cassava, containing glucose, fructose and sucrose as major carbon sources (Ikeda 2003; Ikeda 2017; Schneider et al. 2011). However, the first-generation renewables are only partly sustainable. They are derived from agricultural crops that require large areas of arable land for their plantation (Tan et al. 2008). In addition, the use of first-generation renewables for chemical production does unfavorably compete with human nutrition and leads to rising food prices (Naik et al. 2010; Schneider et al. 2011). Thus, promising attempts focused on the use of non-edible second-generation renewables such as wood, straw, and grass (Balat 2011; Naik et al. 2010). These materials are rich in lignocellulose, which is mainly consisting of cellulose (40 - 50 %), hemicellulose (20 - 30 %) and lignin (15 - 20 %) (Buschke et al. 2013b; Tan et al. 2008). Several studies demonstrated the utilization of second-generation sugars such as xylose (Buschke et al. 2013a; Kawaguchi et al. 2006; Sasaki et al. 2008; Shen et al. 2012), cellobiose (Kotrba et al. 2003; Ryu and Karim 2011; Soma et al. 2012), hemicellulose (Buschke et al. 2011; Ryu and Karim 2011), cellulose (Gaida et al. 2016; Ryu and Karim 2011), and lignin (Becker et al. 2018a; Kohlstedt et al. 2018; Sonoki et al. 2018; Vardon et al. 2015) to produce chemicals, materials and fuels. However, due to the complex composition and recalcitrance of lignocellulosic biomass, its difficult breakdown into fermentable monomers is usually accompanied with high pretreatment costs (Balat 2011; Becker and Wittmann 2019; Tan et al. 2008) as well as the accumulation of toxic ingredients (Buschke et al. 2013b). In addition, second-generation

renewables suffer from the extensive use of arable land and the associated food vs. fuel debate (Goh and Lee 2010; Naik et al. 2010). As a promising and even more sustainable resource, marine macroalgae (seaweed) are entering the stage at this point (Goh and Lee 2010).

3.1.1 Seaweed - a third-generation renewable

In order to achieve a sustainable production of industrially relevant products, a main challenge is to find a raw material which is sustainable and economically attractive. In this context, marine macroalgae are increasingly getting into the focus of research, since they are particularly rich in carbohydrates and widely abundant in nature (Kraan 2013). More than 10,000 different seaweed species are currently known, which can be divided into three groups based on their pigmentation, namely brown (Phaeophyceae), red (Rhodophyceae) and green (Chlorophyceae) seaweed (Alaswad et al. 2015; Torres et al. 2019). Traditionally, seaweed is used for food applications (Torres et al. 2019). In addition to its conventional application, seaweed is further used as feed additive, as fertilizer and in cosmetics (Poblete-Castro et al. 2020; Torres et al. 2019). Considering the historical background, the first industrial use of algae took place as early as 1914 during World War I, where the ash of seaweed was used for the production of black gunpowder (Neushul 1989). In recent years, the use of algae has become more and more important, particularly for the production of low-value biofuels like ethanol (Alfonsín et al. 2019; Hossain et al. 2008; Wargacki et al. 2012), diesel (Hossain et al. 2008) butanol (Hou et al. 2017; van der Wal et al. 2013) and biogas (Hughes et al. 2012; Vergara-Fernández et al. 2008). In addition, seaweed is now also used for the production of lactate (Mazumdar et al. 2014). The seaweed market has increased rapidly over the last years (Goh and Lee 2010). It is expected to grow from precisely 3 million tons of dry weight in 2012 to 500 million tons by 2050 (Bjerregaard et al. 2016; Poblete-Castro et al. 2020). Seaweed is mainly farmed in Asia, i.e. China, Indonesia, the Korean republic, the Philippines as well as Japan (FAO 2019). Thereby, the farming occurs especially in coastal areas and mainly includes the cultivation of *Saccharina*, *Euchema*, *Gracilara*, and *Porphyra* species (Kraan 2013; Poblete-Castro et al. 2020; Wei et al. 2013). Seaweed farming is of great advantage, because no arable land is needed for its cultivation (Kraan 2013; Torres et al. 2019). Beneficially, seaweeds are fast-growing compared to terrestrial plants and simultaneously highly-photosynthetically effective (Alaswad et al. 2015; van Hal et al. 2014). It has been reported that individual seaweed species are able to grow up to 60 m in length (McHugh 2003). As the cultivation of seaweed does not require fresh water, fertilizers, pesticides and herbicides, seaweed

seems almost an ideal sustainable feedstock (Behera et al. 2015; van Hal et al. 2014). In addition, its use has the positive side effect that greenhouse gases (GHG) are reduced due to the ability of seaweed to absorb CO_2 from the environment, hence reducing environmental impact (Kraan 2013). As another advantage, seaweed is rich in carbohydrates (Wei et al. 2013). Members of the group of brown macroalgae like *Laminaria japonica*, *Laminaria digitata* and *Sargassum fulvellum* contain up to 55 % of carbohydrates, including polymers such as laminarin and free mannitol (Jang et al. 2012; Kim et al. 2011; Manns et al. 2017). The latter can form up to 30 % of the dry weight (Iwamoto and Shiraiwa 2005; van Hal et al. 2014). Besides laminarin and mannitol, brown seaweed also contains the structural cell-wall polysaccharide alginate, which provides mechanical strength (Wei et al. 2013). As seaweed contains almost no lignin, mild extraction conditions are sufficient to break it down, a great benefit compared to lignocellulose (Behera et al. 2015; van Hal et al. 2014). Seaweed processing includes manual or mechanical harvesting and subsequent drying by sunlight, hot air and convection dryers (Torres et al. 2019). The recovery of carbohydrates from milled and dried seaweed can occur in different ways. In some approaches the use of H_2SO_4 or HCl (Chades et al. 2018; Kim et al. 2011) has been described for the recovery of carbohydrates, while other approaches use (hot) water (Chades et al. 2018; Horn et al. 2000a), and enzymatic hydrolysis (Hou et al. 2017; Kim et al. 2011). Since mannitol is present as a free sugar, i.e. not bound into polymers, its extraction can easily be done by using hot water (Poblete-Castro et al. 2020). The extraction of laminarin requires the use of enzymes such as ß-glucanase, laminarinase and cellulase to hydrolyze the polysaccharide into its glucose and mannitol monomers (Poblete-Castro et al. 2020; Wei et al. 2013). Seaweed is also a rich source of hydrocolloids (agars, carrageenan and alginates), vitamins (vitamin A, B, C and E), fatty acids (omega 3 and omega 6), proteins and amino acids (L-aspartate and L-glutamate), minerals (magnesium, potassium, iron and calcium), and pigments (fucoxanthin, ß-carotene, violaxanthin) (Torres et al. 2019).

In addition, the processing of algae often results in residues that are disposed of as waste (van Hal et al. 2014). In order to use the entire repertoire of algal compounds more efficiently, several studies suggested cascading biorefinery processes, i.e. the coupling of e.g. biofuel production to the simultaneous manufacturing of products with a high additive content (Figure 3-1) (Tedesco and Stokes 2017; Torres et al. 2019; van Hal et al. 2014). Such a cascading biorefinery approach would be of great advantage in using the entirety of algal compounds for the effective production of chemicals, materials and fuels while reducing or preventing the amount of waste produced (Torres et al. 2019). This concept thus promises sustainable and environmentally friendly production of value-added products and makes seaweed very attractive as a renewable resource.

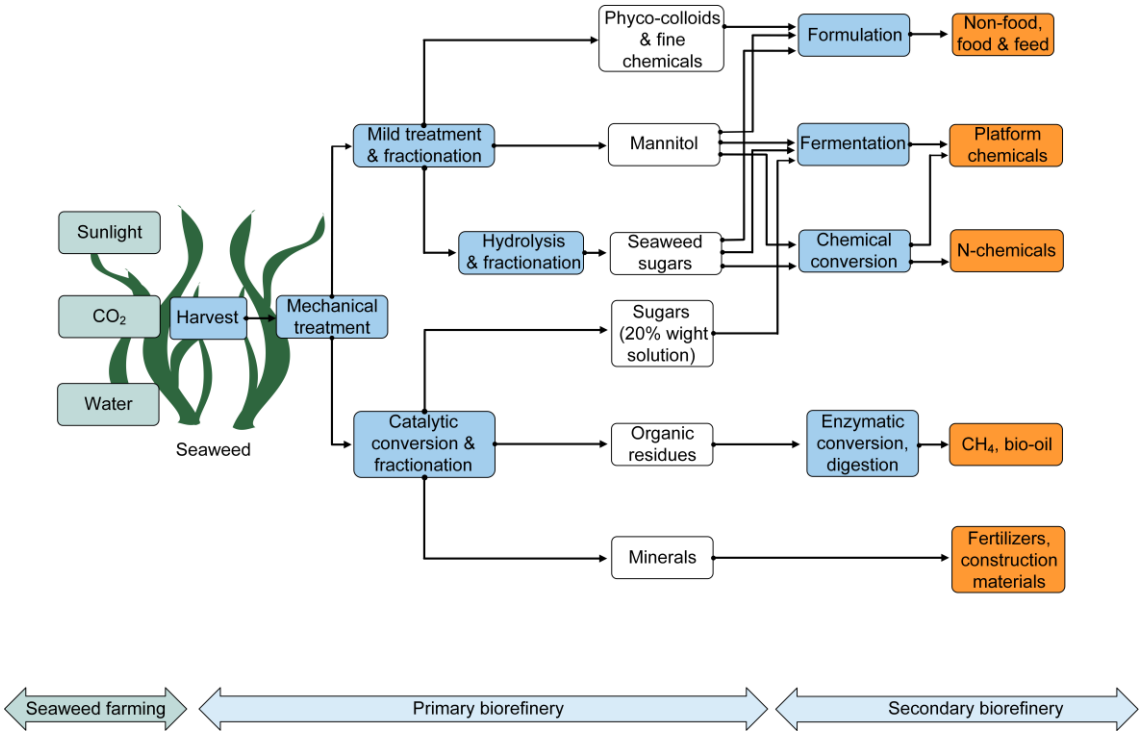

Figure 3-1: Schematic overview of a cascading seaweed biorefinery concept. The picture depicts starting materials (green boxes), conversion steps (blue boxes), intermediates (white boxes), and the final products (orange boxes) of a cascading biorefinery approach. The figure was adapted and modified from previous work (Kraan 2013; van Hal et al. 2014).

3.2 *Corynebacterium glutamicum* as industrial workhorse

3.2.1 Discovery of *Corynebacterium glutamicum* - the L-glutamate story

L-Glutamate, one of today's most important biotechnical products, was first isolated from legumes and chemically described in 1866 by Ritthausen (Ritthausen 1866; Vickery and Schmidt 1931). About 40 years later the Japanese researcher Prof. Kikunae Ikeda made a remarkable discovery during his work with seaweed. He identified the sodium salt L-glutamate as the component being responsible for the unique taste of kelp and defined the taste as umami, the fifth basic taste quality besides the four others, namely sweet, sour, salty and bitter (Ikeda 2002). His discovery led to the commercial production of monosodium L-glutamate, and within a short period of time L-glutamate was applied as an important food additive, particularly in Japan and China (Han 1929). Due to the food shortage after World War II, many Japanese were suffering from hunger. This starvation was the decisive factor to produce food protein commercially by fermentative approaches and led to the foundation of the first amino acid industry in Japan (Hirasawa and Shimizu 2017; Kinoshita 2005). The demand for L-glutamate continuously increased with the emergence of ready meals after World War II (Hirasawa and Shimizu 2017; Sand 2005). Therefore, it was important to find natural L-glutamate overproducing organisms. In a large screening program, a microorganism was isolated that secreted L-glutamate under biotin-limiting concentrations (Abe et al. 1967; Kinoshita et al. 1957; Shiio et al. 1962). The newly discovered L-glutamate secreting microorganism was initially named *Micrococcus glutamicus* (Udaka 1960). Further taxonomic studies revealed that this microorganism is a gram positive, non-sporulating, non-motile and rod-capable soil-bacterium which has a high GC-content of 53.8 % (Kalinowski et al. 2003; Liebl 2005).

Figure 3-2: Raster electron micrograph of glucose-grown *Corynebacterium glutamicum* ATCC 13032 (Bolten 2010).

However, the fact that the microbe has a unique cell wall composition with mycolic acid as lipophilic component, being typical for the envelopes of the genera of the suborder *Corynebacterineae*, led to a reclassification into *Corynebacterium glutamicum* (Goodfellow et al. 1976; Liebl 2005). In the present phylogenetic classification, *C. glutamicum* belongs to the class of *Actinobacteria*, the order *Actinomycetales*, the suborder *Corynebacterineae* and the family *Corynebacteriaceae* (Liebl 2005; Stackebrandt et al. 1997). The genome of *C. glutamicum* is fully sequenced (3,000 kb) (Ikeda and Nakagawa 2003; Kalinowski et al. 2003; Pompejus et al. 2004) and genetic engineering tools have been established (Kirchner and Tauch 2003; Sahm et al. 1995), which have led to the gradual transformation of *C. glutamicum* into an industrial workhorse with a broad product portfolio.

3.2.2 Industrial application of *Corynebacterium glutamicum*

As *C. glutamicum* is non-pathogenic (Liebl 2005), it was classified as a GRAS (generally recognized as safe) organism and suitable for the production of food and feed supplements, pharmaceuticals and medicine (Eggeling and Bott 2015; Wittmann and Becker 2007). The dominating chemicals produced with strains of *C. glutamicum* are the two amino acids L-glutamate and L-lysine, applied as flavor enhancer and food additive, respectively (Liebl 2005). In addition to these two amino acids, *C. glutamicum* efficiently produces other amino acids like L-methionine (Bolten 2010; Park et al. 2007), L-valine (Radmacher et al. 2002), L-arginine (Ikeda et al. 2009), L-tryptophan (Ikeda 2006), L-threonine (Eikmanns et al. 1991b), L-alanine (Jojima et al. 2010) L-serine (Peters-Wendisch et al. 2005), L-histidine (Mizukami et al. 1994), L-phenylalanine, L-tyrosine, and L-tryptophan (Ikeda and Katsumata 1992; Ikeda et al. 1994; Ikeda et al. 1993; Katsumata and Ikeda 1993). Furthermore, the bacterium is well-known for the efficient production of more than 70 other commercially attractive products (Becker et al. 2018b; Becker and Wittmann 2012a). Hereby, the combined application of fluxomics (Wittmann and Heinzle 2002; Wittmann et al. 2004a), metabolomics (Bolten et al. 2007; Wittmann et al. 2004c), transcriptomics (Sindelar and Wendisch 2007; Wendisch 2003) and proteomics (Schaffer et al. 2001; Silberbach et al. 2005), together with targeted genetic modification (Eikmanns et al. 1991a; Jäger et al. 1992; Ozaki et al. 1984) has provided *C. glutamicum* strains with world-leading production performance, regarding yield, titer and productivity (Becker et al. 2011; Gießelmann et al. 2019; Kind et al. 2010a). In the last decades, *C. glutamicum* has become an industrial workhorse for industrial biotechnology with a wide product portfolio (Baritugo et al. 2018; Becker et al. 2018b; Becker and Wittmann 2012a). Meanwhile, *C. glutamicum* cell factories provide

biofuels (e.g. ethanol, isobutanol) (Inui et al. 2004a; Smith et al. 2010; Yamamoto et al. 2013), bulk and fine chemicals (e.g., cadaverine, D-lactic acid, *cis, cis*-muconic acid) (Becker et al. 2018a; Kim et al. 2018; Kind et al. 2010b; Mimitsuka et al. 2007; Okino et al. 2008; Tsuge et al. 2019), extremolytes (e.g. ectoine, hydroxyectoine) (Becker et al. 2013; Gießelmann et al. 2019; Pérez-García et al. 2017b), polymers (e.g. poly-hydroxybutyrate, poly-lactate) (Liu et al. 2007b; Matsumoto et al. 2014) and feed additives (e.g. L-lysine, L-glutamate, L-threonine, pantothenate) (Becker et al. 2011; Hüser et al. 2005; Kase and Nakayama 1972; Sawada et al. 2010; Xu et al. 2018).

3.2.3 Industrial L-lysine production

With a production volume of 2.2 million tons per year, L-lysine belongs to the leading biotechnical products (Eggeling and Bott 2015). It is one of the eight essential amino acids (Eggeling 2013), which means that animals and humans are not able to produce it *de novo* and therefore must obtain it from food (Tonouchi and Ito 2017). Chemically, L-lysine consists of six carbon atoms, capped by two basic primary amino groups, which are positively charged under physiological conditions (Figure 3-3) (Berg et al. 2018).

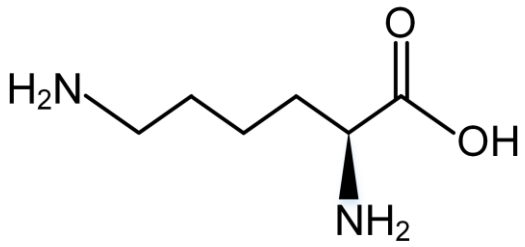

Figure 3-3: Chemical structure of L-lysine.

As animal feed is often based on wheat, barley and corn, all being naturally poor in L-lysine (Wittmann and Becker 2007), the amino acid is primarily used as feed additive in animal breeding (Eggeling and Sahm 1999; Wendisch 2017). Not only does L-lysine promote animal growth. It also prevents other amino acids from being taken up and metabolized in excess beyond their requirements. This lowers the excretion of nitrogen via manure into the environment, which otherwise negatively affects soil and water quality (Kircher and Pfefferle 2001; Wendisch 2017; Wittmann and Becker 2007). In addition, L-lysine is applied as a building block for polymers and as active ingredient in food, cosmetics, and pharmaceuticals (Ikeda 2003; Koffas and Stephanopoulos 2005).

The constantly growing world population and the increasing meat consumption lead to an increasing demand for L-lysine that has to be covered (Alexandratos and Bruinsma

2012; Wittmann and Becker 2007). The global meat consumption is projected to increase from recently 260 million tons to 370 million tons per year by 2030 and even to 455 million tons by 2050 (Alexandratos and Bruinsma 2012). As the L-lysine market currently grows by 6 - 7 % per year, global production is expected to increase from 2.2 million tons in 2015 to 4 million tons in 2023 (Cheng et al. 2018; Eggeling and Bott 2015; Insights 2016). In order to cover the enormous demand, the bacterial fermentation of sugars is getting more and more into the focus of research, since natural sources for L-lysine are limited (Eggeling and Sahm 1999). For large scale and commercial production of L-lysine, production sites are mainly located in the corn belts of China, North America, Brazil, Indonesia, and Russia. Major L-lysine producers currently include CJ Cehil-Jedang (South Korea), Global Bio-Chem Technology Group (China), Ajinomoto (Japan), Archer Daniels Midland (USA) and Evonik Industries (Germany) (Eggeling and Bott 2015; Ikeda 2017).

Today, most of L-amino acids inclusively L-lysine are produced by fed-batch, running fed-batch, repeated fed-batch and continuous fed-batch fermentation mode (Kelle et al. 2005). Thereby, the appropriate carbon source as well as nitrogen and other supplements are added to the process in a controlled way, in order to minimize the excessive formation of undesired products (Ikeda 2003; Kelle et al. 2005). A major advantage of a fed-batch process is the large concentration of product that can be achieved, which facilitates downstream processing. Regarding L-lysine, there is no technically relevant solubility limit in the fermentation broth. In commercial L-lysine production, large stirred tank reactors up to 750 m^3 are used (Kelle et al. 2005). The advantage of repeated fed-batch and continuous fed-batch processes are shorter downtimes, shorter lag-times of the bacteria, and higher volumetric productivity due to the shortened preparation time of reactor and inoculum (Hermann 2003). However, such procedures also entail an increased risk of contamination or strain instability (Hermann 2003; Ikeda 2003). Particularly, both the additional flows from and into the continuous-fermentation process go with an increased contamination risk (Hermann 2003). However, de Hollander et al. (1998) showed that even in a continuous process with coryneform bacteria the instability of strains can be reduced by a double limitation of carbon and phosphate (de Hollander et al. 1998). This also led to an increase in L-lysine productivity from 3.2 g L^{-1} h^{-1} to 3.8 g L^{-1} h^{-1} compared to a process with carbon limitation only (de Hollander et al. 1998).

Besides the operated fermentation mode also the choice of the carbon source plays an important role for process economics. Currently, the main carbon sources used to produce L-lysine are cane and beet molasses, sucrose, and starch hydrolysates (glucose

or dextrose) from corn, sugar cane, cassava and wheat (Ikeda 2003; Ikeda 2017). The choice of the carbon source highly depends on costs and availability in the respective region as it is the major cost factor for the production of bulk chemicals like L-lysine. While corn syrup and cassava, obtained from starch hydrolysates, are mainly used in North America, China, and South Asia, cane and beet molasses are the most popular carbon sources in Europe and South America (Ikeda 2003; Ikeda 2017). Sugar prices are often fluctuating and therefore have a major impact on the competitiveness of producers (Ikeda 2003) (Figure 3-4), which often brings sugar suppliers and L-lysine producers into alliances to produce L-lysine more economically (Wittmann and Becker 2007). Regarding the fermentation process, especially the conversion yield is of great importance to maximize financial gain (Wittmann and Becker 2007).

Figure 3-4: Historical price development of sugar from 2011 until 2020. The price is given in US dollar per pound (lb) (https://www.wallstreet-online.de/rohstoffe/zuckerpreis, March, 2020).

The crystalline form of L-lysine is preferred. L-lysine-HCl was the market-leading product for many years, because it is not as hygroscopic as $(L\text{-lysine})_2SO_4$ (Kelle et al. 2005). As shown in Figure 3-5, crystalline L-lysine-HCl is generally obtained over several steps of downstream processing, which includes cell separation and inactivation, the addition of sulfuric acid, followed by ion exchange chromatography and evaporation. Finally, L-lysine is neutralized with HCl, crystallized and dried for packaging (Ikeda 2003). While traditional downstream processes use sulfate or chloride as anions for crystalline L-lysine, more economical and environmentally friendly processes meanwhile use hydrogen carbonate and carbonate as counter ions (Kobayashi et al. 2011). Usually, CO_2 is released in high amounts during bacterial fermentation processes, mostly

produced during respiration. This CO_2 stemming from a second fermentation process, not related to L-lysine production, can be transferred to the broth of the L-lysine process. By actively shifting the pH to an alkaline level, elevated concentrations of both hydrogen carbonate and carbonate ions may be present, making them available as counter ions for L-lysine. In the end, hydrogen carbonate and carbonate ions can be discharged as CO_2 by heating the fermentation broth. This operation not only increases the content of the amino acid in the solid residue after downstream processing but also reduces the environmental loads as no extra counter ions have to be supplemented to the medium (Kobayashi et al. 2011).

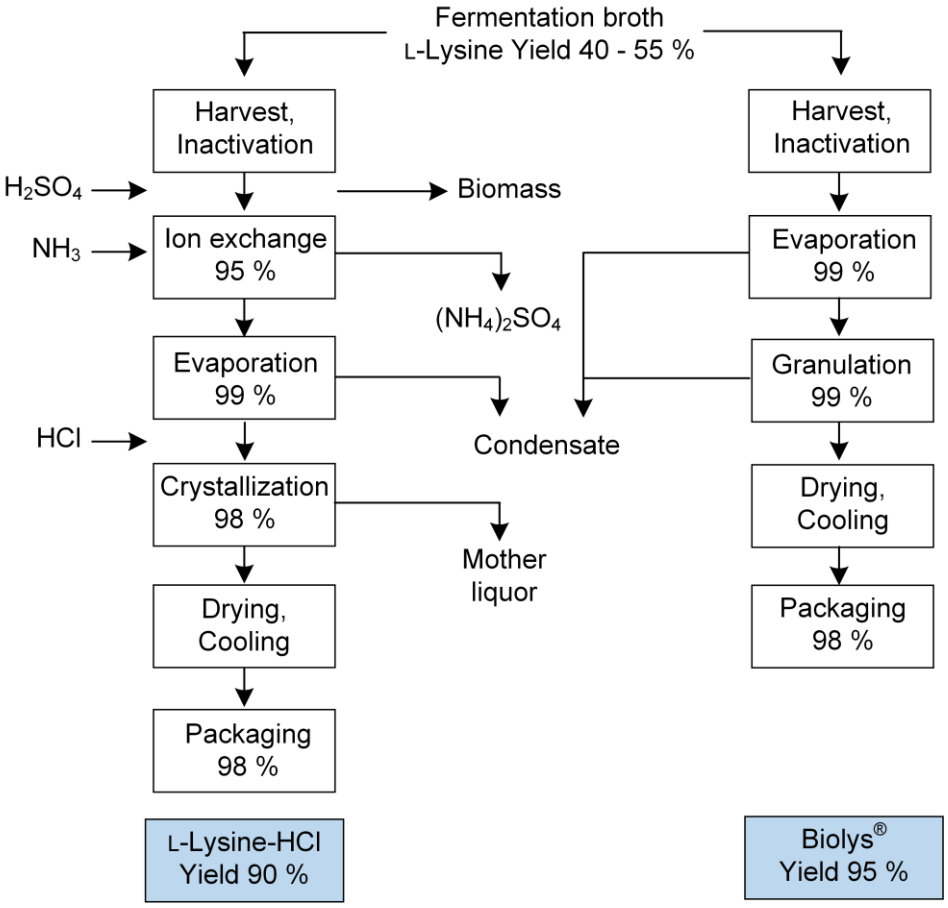

Figure 3-5: Flow diagram of two different downstream processes to produce feed-grade L-lysine from fermentation broth. The numbers in the brackets represent the yield (in %) for each processing step. The figure was adapted from previous work Kelle et al. (2005).

To minimize waste emissions, Evonik Degussa GmbH developed an alternative process by spray-drying the L-lysine culture broth (Figure 3-5). The product is sold as Biolys® (more than 54.6 % feed grade) (Evonik 2019), has a lower chloride content and additionally contains the entire culture broth, i.e. also nutritionally valuable by-products like additional amino acids along with granulated L-lysine sulfate (Evonik 2019; Kelle et al. 2005).

3.2.4 Uptake and catabolism of industrially relevant sugars

Today, most production processes are based on cane molasses, beet molasses and starch hydrolysates from corn and cassava, containing glucose, fructose and sucrose as major carbon sources (Ikeda 2003; Ikeda 2017). In *C. glutamicum*, the uptake of sugars occurs by the phosphotransferase systems (PTS) (Mori and Shiio 1987). Hereby, the sugar is transported across the membrane and simultaneously phosphorylated by transferring a phosphoryl group from phosphoenolpyruvate (PEP) to the sugar using several proteins (EI, HPr, EIIs) (Gorke and Stulke 2008) (Figure 3-6). Three sets of PTSs are present in *C. glutamicum*, specific for glucose/mannose, fructose and sucrose ($PTS_{Glc/Man}$, PTS_{Frc}, PTS_{Suc}), respectively. In addition, a fourth PTS with a yet unknown substrate specificity has been reported (Moon et al. 2007; Parche et al. 2001). Besides PTS associated sugar uptake, non PTS routes, including two *myo*-inositol transporters (*iolT1*, *iolT2*) are known (Ikeda et al. 2015; Lindner et al. 2011).

In contrast to other bacteria, the sugar uptake in *C. glutamicum* is not subjected to catabolite repression and thus constitutively expressed, which allows the parallel consumption of sugar mixtures in this bacterium (Yokota and Lindley 2005). This is of great advantage for industrial production processes with *C. glutamicum*, as many raw materials contain mixtures of sugars, i.e. molasses and starchy hydrolysates consisting of glucose, fructose, and sucrose (Ikeda 2003; Ikeda 2017). In this regard, *C. glutamicum* is able to use a broad range of hexose based sugars.

Unlike other bacteria, *C. glutamicum* utilizes only ribose as carbon five-sugar. Ribose uptake occurs by a specific ATP-binding cassette (ABC) transporter (Nentwich et al. 2009) (Figure 3-6). Screening studies revealed that most *C. glutamicum* strains are not able to use arabinose as pentose sugar (Kawaguchi et al. 2009). However, the *C. glutamicum* ATCC 31831 strain harbors a functional gene cluster for arabinose catabolism (Kawaguchi et al. 2009) (Figure 3-6). Natural utilization of xylose, as main sugar of hemicellulose, has not been reported so far for *C. glutamicum*. Although, the wild type strain ATCC 13032 is capable of taking up xylose into the cell and possesses a functional *xylB* gene, encoding xylulokinase activity, it lacks xylose isomerase activity, which is required to convert xylose to xylulose (Becker et al. 2016; Kawaguchi et al. 2006). The import of xylose occurs by a so far unidentified transporter (Sasaki et al. 2009). To broaden the substrate spectrum towards xylose as renewable feedstock, *C. glutamicum* has been metabolically engineered by the integration of the *xylAB* operon from *E. coli* (Buschke et al. 2013a; Buschke et al. 2011; Kawaguchi et al. 2006) (Figure 3-6). The utilization of the sugar alcohol mannitol by *C. glutamicum* is also of increasing interest due to its high content in macroalgae (Iwamoto and Shiraiwa 2005; Wei et al.

2013). However, the microbe is not able to utilize mannitol naturally due to a constitutively expressed transcriptional repressor MtlR (AtlR, SucR) (Laslo et al. 2012; Peng et al. 2011). Transcriptional analysis has shown that the deletion of this repressor protein enables mannitol utilization by *C. glutamicum* (Laslo et al. 2012) (Figure 3-6).

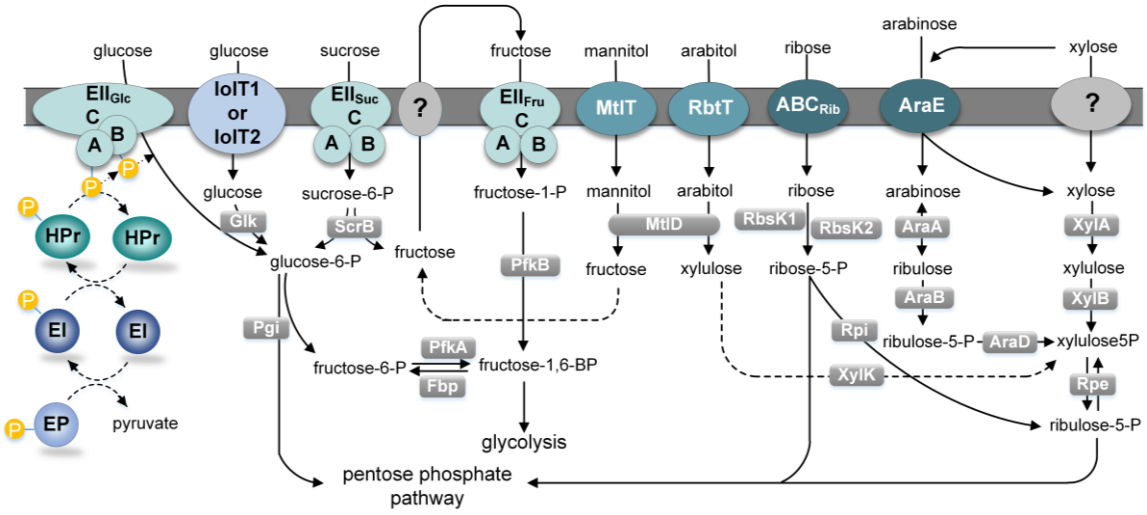

Figure 3-6: Schematic overview of pathways and uptake for different industrially relevant sugars and sugar alcohols. PTS, phosphotransferase system for uptake of glucose, fructose, sucrose; ABC_{Rib}, ATP-binding cassette transporter for ribose import; AraE, H^+-transporter for arabinose; MtlT/RbtT, MFS-type transporter for mannitol and arabitol import; IolT1/IolT2, *myo*-inositol transporter for non-PTS-mediated glucose uptake. Transporters for fructose export and xylose uptake are not known so far. An additional transporter for mannitol is probably present in *C. glutamicum*. Enzymes are represented in grey boxes. AraA, arabinose isomerase; AraB, ribulokinase; AraD, ribulose 5-phosphate 4-epimerase; EI, general PTS-component enzyme; EII_{Glc}, glucose-specific PTS component; EII_{Fru}, fructose-specific PTS component; EII_{Suc}, sucrose-specific PTS component; Fbp, fructose 1,6-bisphosphatase; Glk, glucokinase; HPr, histidine protein; MtlD, mannitol 2-dehydrogenase; MtlT/RbtT, mannitol/ribitol transporter; PEP, phosphoenolpyruvate; PfkA, 6-phosphofructokinase; PfkB, fructose 1-phosphate kinase; Pgi, phosphoglucoisomerase; RbsK, ribokinase 1 and 2; Rpe, ribulose 5-phosphate epimerase; Rpi, ribose 5-phosphate epimerase; ScrB, sucrose 6-phosphate hydrolase; XylA, xylose isomerase; XylB/XylK, xylulokinase. Figure adapted from Becker et al. (2016).

3.2.5 Utilization of the sugar alcohol mannitol

The utilization of sugar alcohols is promising, as it makes especially marine sources accessible for the production of bio-based chemicals. A major constituent of algal biomass is mannitol. This six carbon, non-cyclic sugar alcohol is one of the most abundant polyols occurring in nature (Iwamoto and Shiraiwa 2005; Wisselink et al. 2002). It acts as a storage compound, especially in brown algae, and makes up to 30 % of cell dry weight (Iwamoto and Shiraiwa 2005). Mannitol metabolism has been studied in several bacteria like *Escherichia coli* (Davis et al. 1988; Figge et al. 1994; Postma et al.

1993), *Bacillus* species (Akagawa et al. 1995; Henstra et al. 2000; Watanabe et al. 2003) or other bacteria such as *Clostridium actetobutylicum* (Behrens et al. 2001), *Vibrio cholera* (Kumar et al. 2011), and *Streptoccouss mutans* (Honeyman and Curtiss III 2000; Honeyman and Curtiss 1992). The mannitol uptake in these bacteria occurs via mannitol-specific PTS. Hereby, mannitol is transported across the membrane and simultaneously phosphorylated to mannitol 1-phosphate (Akagawa et al. 1995; Behrens et al. 2001; Davis et al. 1988; Henstra et al. 2000; Honeyman and Curtiss III 2000; Kumar et al. 2011; Watanabe et al. 2003). In bacteria such as *C. acetobutylicum* (Behrens et al. 2001) or *B. stearothermophilus* (Henstra et al. 2000; Henstra et al. 1999), mannitol utilization is regulated and controlled by mannitol-mediated catabolite repression, meaning that the absence of the inducer (mannitol) leads to phosphorylation of an activator (MtlR) which becomes inactive. In presence of the inducer, the former is imported and phosphorylated via PTS, leading to dephosphorylation and activation of MtlR (Behrens et al. 2001; Henstra et al. 2000). Unlike other bacteria, *C. glutamicum* naturally lacks the ability to utilize mannitol as sole substrate. Although the bacterium has a functional gene cluster, the bacterium is not able to utilize mannitol as sole carbon source because of the constitutively present repressor protein MtlR (AtlR, SucR), which prevents natural mannitol utilization (Peng et al. 2011). Hence, metabolic engineering strategies have been applied to make mannitol available for *C. glutamicum* (Laslo et al. 2012; Peng et al. 2011). The generation of *mtlR*-deficient mutants enabled the utilization of mannitol as sole carbon source, as the two structural genes *mtlT* and *mtlD* were released from repression and transcribed most likely as polycistronic mRNA (Peng et al. 2011) (Figure 3-7). The mannitol catabolic operon in *C. glutamicum* consists of the three genes in the order *mtlR*, *mtlT* and *mtlD*. (Peng et al. 2011). While the *mtlR* gene product encodes for an autoregulatory DeoR-type transcriptional repressor, the two genes *mtlT* and *mtlD* encode a MFS type transporter and a NAD-dependent mannitol 2-dehydrogenase, respectively (Peng et al. 2011). Recently, expression profiling and transcriptional analysis of different *C. glutamicum* mutants revealed, that the mannitol operon is rather an arabitol operon, consisting of the four genes *atlR* (*mtlR*), *xylB*, *rbtT* (*mtlT*) and *mtlD*, encoding the regulatory AtlR repressor, xylulokinase, ribitol (mannitol) transporter and mannitol 2-dehydrogenase, respectively. Thus, the gene products of XylB, RbtT, and MtlD are primarily necessary for the growth on arabitol, where the arabitol metabolism is further subjected to arabitol-dependent de-repression by AtlR (Laslo et al. 2012).

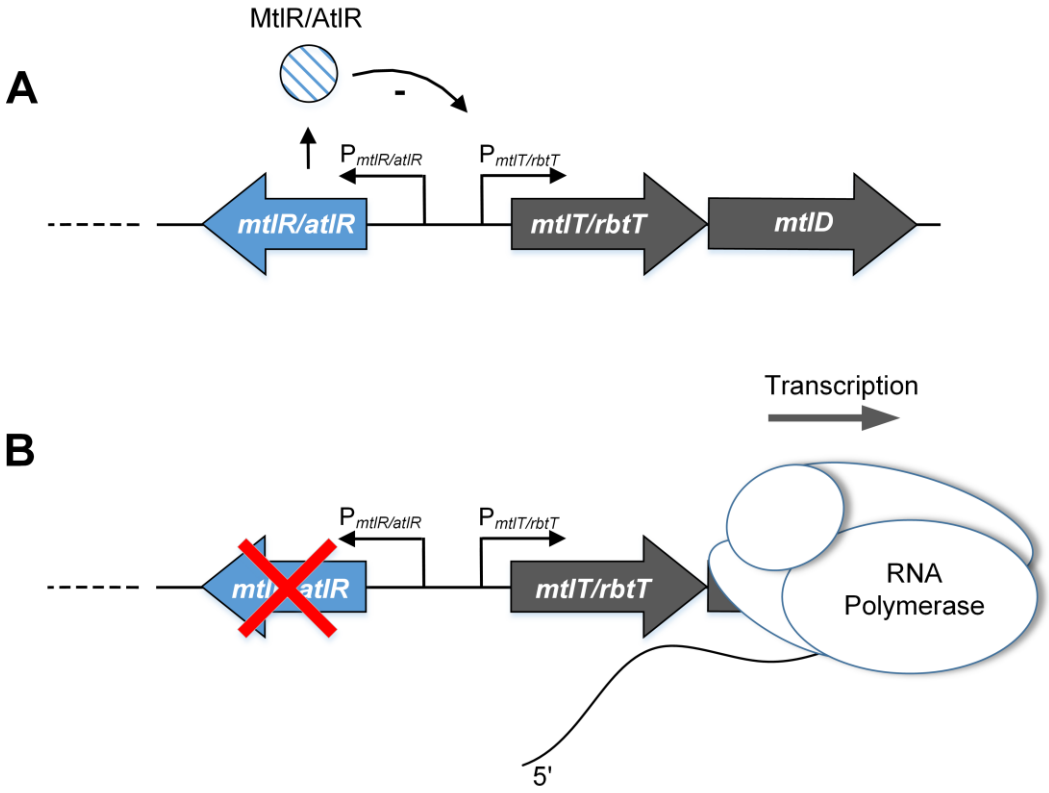

Figure 3-7: Catabolic operon for mannitol/arabitol utilization in *C. glutamicum* in the presence (A) and after deletion (B) of the transcriptional regulator MtlR/AtlR. The proteins are encoded by the corresponding genes: *mtlR*/*atlR*, transcriptional regulator; *mtlT*/*rbtT*, mannitol/ribitol transporter; *mtlD*, mannitol 2-dehydrogenase.

In addition, growth studies of a *ΔatlR ΔrbtT* double mutant revealed a growth behavior similar to that of the *ΔatlR* mutant. Therefore it was assumed that the RbtT transporter most probably represents an arabitol transporter and that there must exist a so far unknown transporter for additional mannitol uptake (Laslo et al. 2012). As depicted in Figure 3-6, in *C. glutamicum* the oxidation of arabitol into xylulose takes place via mannitol 2-dehydrogenase by using the co-substrate NAD^+. The formed xylulose is further phosphorylated to xylulose-5-phosphate by XylK before entering the central carbon metabolism (Laslo et al. 2012). The oxidation of mannitol into fructose is also mediated by mannitol 2-dehydrogenase (Peng et al. 2011). As *C. glutamicum* has no fructokinase, fructose metabolism involves the excretion of fructose by a hitherto unassigned transporter and re-uptake via the fructose-specific PTS. The carbon then reenters the lower glycolysis at the level of fructose 1,6-bisphospate (Moon et al. 2005; Moon et al. 2007; Wittmann et al. 2004a) (Figure 3-6 and Figure 3-8).

3.2.6 L-Lysine biosynthesis

In microbes, L-lysine formation can occur via two routes, the diaminopimelate route and the α-aminoadipate route. In the latter pathway, common particularly in higher fungi and some archaea such as *Thermoproteus neutrophilus*, oxoglutarate and acetyl-CoA serve as precursors for L-lysine biosynthesis (Velasco et al. 2002; Wittmann and Becker 2007). Especially in bacteria and plants, L-lysine synthesis occurs from the precursors pyruvate and L-aspartate via the diaminopimelate route (Wittmann and Becker 2007). There are four different types of the diaminopimelate route, the succinylase route, the acetylase route, the dehydrogenase route, and the aminotransferase route (Wittmann and Becker 2007). While the acetylase route, involving an acetyl residue as blocking group, is limited to some *Bacillus* species, the succinylase route with succinyl as residue occurs in gram negative as well as gram positive bacteria (Born and Blanchard 1999; Schrumpf et al. 1991; Weinberger and Gilvarg 1970; White 1983). Although most bacteria have only one of these pathways for L-lysine synthesis, some bacteria such as *C. glutamicum* possess two routes in parallel (Eikmanns et al. 1993). The coexisting pathways increase flexibility to react to changing environmental conditions (Sahm et al. 2000; Sonntag et al. 1993). The succinylase variant has a high affinity to ammonium and is energetically expensive (Becker et al. 2013; Sahm et al. 2000; Sonntag et al. 1993). The diaminopimelate variant is energetically less costly, but has a low ammonium affinity, thus this pathway is only active in the presence of high ammonium ion availability (Becker et al. 2013; Sahm et al. 2000; Sonntag et al. 1993). While *meso*-diaminopimelate, the precursor for L-lysine production, is formed in a single reaction by the enzyme diaminopimelate dehydrogenase (Ddh) in the dehydrogenase branch, the succinylase branch comprises four enzymes as shown in Figure 3-8 (Eikmanns et al. 1993). L-Lysine is formed from *meso*-diaminopimelate by decarboxylation reaction of diaminopimelate decarboxylase (LysA) (Ishino et al. 1988; Scapin et al. 1996; Yeh et al. 1988). The export of L-lysine is mediated by the L-lysine permease LysE (Bellmann et al. 2001; Vrljic et al. 1996). *Meso*-diaminopimelate not only serves as a precursor for L-lysine synthesis, it also serves as building block for peptidoglycan synthesis (Wehrmann et al. 1998; Yeh et al. 1988). In *C. glutamicum,* both L-lysine biosynthesis pathways require four mole NADPH to produce one mole L-lysine from oxaloacetate and pyruvate under the release of CO_2 (Marx et al. 1996). Therefore, the supply of NADPH and building blocks such as pyruvate and oxaloacetate is essential to drive L-lysine biosynthesis in *C. glutamicum* (Marx et al. 1996; Shiio et al. 1984; Wittmann and de Graaf 2005).

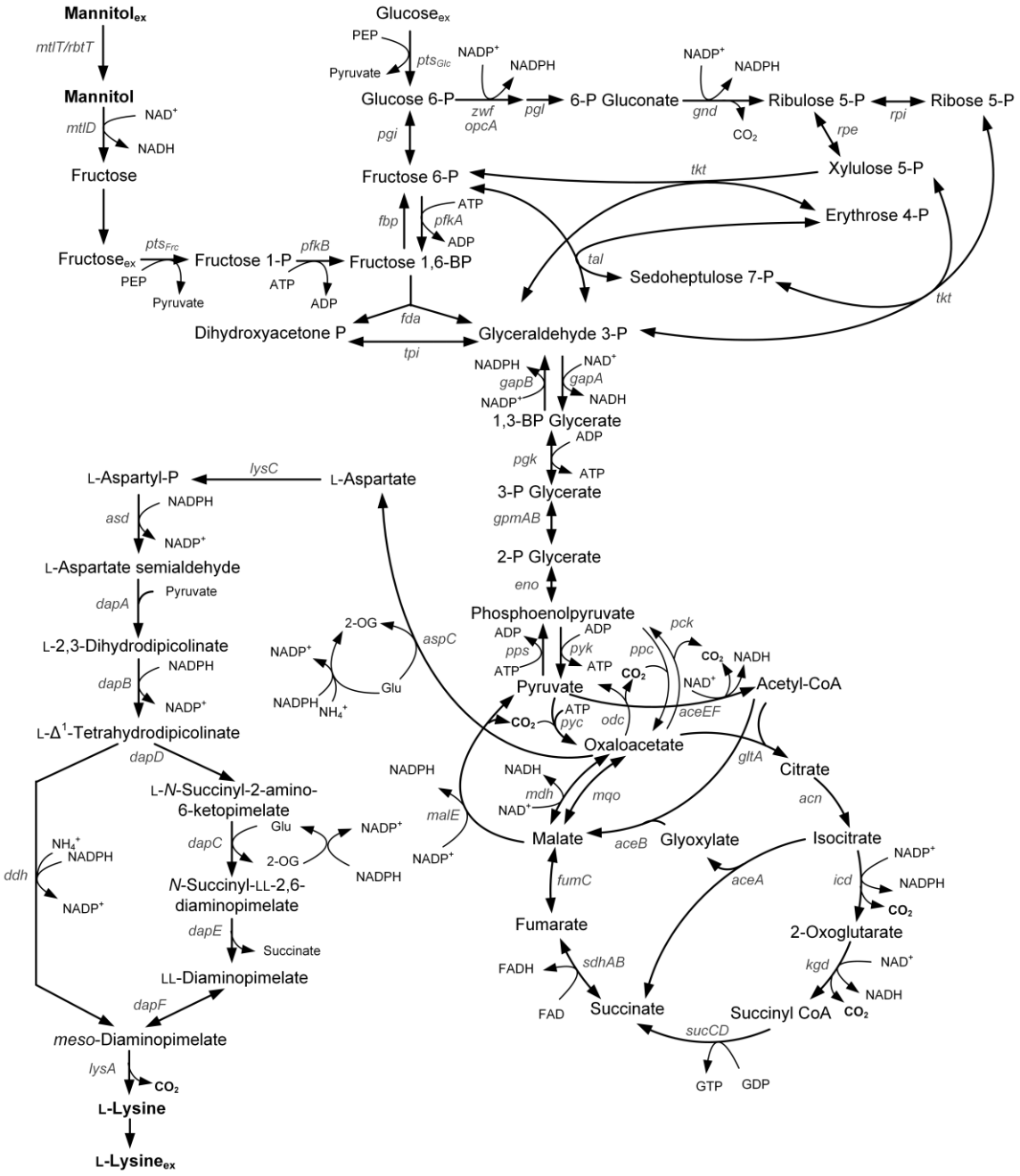

Figure 3-8: Central carbon metabolism and L-lysine biosynthesis (dehydrogenase and succinylase pathway) in *C. glutamicum*. The carbon core metabolism comprises the pathways for glucose and mannitol utilization, the Emden-Meyerhof-Parnas (EMP) pathway, the pentose phosphate (PP) pathway, the pyruvate node, and the tricarboxylic acid (TCA) cycle, the glyoxylate shunt and different anaplerotic reactions. The enzymes involved in mannitol metabolism are the mannitol/ribitol transporter (*mtlT/rbtT*) and mannitol 2-dehydrogenase (*mtlD*). The enzymes involved in L-lysine biosynthesis are aspartokinase (*lysC*), aspartate semialdehyde dehydrogenase (*asd*), dihydrodipicolinate synthase (*dapA*), dihydrodipicolinate reductase (*dapB*). At this branch point the metabolic pathway splits into (a) the succinylase pathway comprising tetrahydrodipicolinate succinylase (*dapD*), succinyl-aminoketopimelate transaminase (*dapC*), succinyl diaminopimelate desuccinylase (*dapE*), and diaminopimelate epimerase (*dapF*) and (b) the dehydrogenase pathway with diaminopimelate dehydrogenase (*ddh*). *Meso*-diaminopimelate, the product of the parallel pathways is then converted into L-lysine by diaminopimelate decarboxylase (*lysA*), and exported by a L-lysine permease (*lysE*).

3.2.7 Central carbon metabolism

After uptake into the cell, carbon is metabolized in the carbon core metabolism, which comprises the pathways of the Emden-Meyerhof-Parnas (EMP) pathway, the pentose phosphate (PP) pathway, the tricarboxylic acid (TCA) cycle, the glyoxylate shunt and anaplerotic reactions around the pyruvate node (Eikmanns 2005; Yokota and Lindley 2005). In contrast, the Entner-Doudoroff pathway does naturally not occur in *C. glutamicum* (von der Osten et al. 1989). The oxidative part of the PP pathway consists of glucose 6-phosphate dehydrogenase, 6-phoshogluconolactonase, and 6-phosphogluconate dehydrogenase and generates 2 NADPH (Moritz et al. 2000; Yokota and Lindley 2005) (Figure 3-8). As carbon dioxide is formed by the 6-phosphogluconate dehydrogenase reaction the oxidative route is irreversible (Yokota and Lindley 2005). Other enzymes involved in the PP pathway such as transketolase and transaldolase represent a reversible non-oxidative route. In general, the PP pathway is responsible for the supply of reducing power (NADPH) and precursors (ribose 5-phosphate, erythrose 4-phosphate), which are needed for biosynthesis of building blocks and furthermore for channeling excess carbon back into glycolysis (Yokota and Lindley 2005). As L-lysine biosynthesis is driven by NADPH supply, the entry point of the sugars into the carbon core metabolism has a strong influence on L-lysine formation (Kiefer et al. 2002; Sahm et al. 2000). Thus, tracer studies of L-lysine producing *C. glutamicum* showed that on the substrate fructose the PP pathway activity was significantly reduced (14 %) compared to that for glucose (62 %) (Kiefer et al. 2004).

Besides the oxidative PP pathway, NADPH is provided via isocitrate dehydrogenase in the TCA cycle (Eikmanns et al. 1995) and via malic enzyme (Gourdon et al. 2000) (Figure 3-8). The EMP pathway is the main route for breaking down sugars into PEP, pyruvate and acetyl-CoA with the simultaneous supply of energy and building blocks (Sauer and Eikmanns 2005). The regulation of the EMP pathway mainly occurs at the level of glyceraldehyde 3-phosphate dehydrogenase (GapDH) and pyruvate kinase, which are regulated by the NADH/NAD^+ ratio and the ATP/AMP ratio, respectively (Dominguez et al. 1998; Yokota and Lindley 2005). *C. glutamicum* naturally comprises two GapDH variants, namely GapA and GapB. While the NAD-dependent GapA enzyme is indispensable for growth on glucose and responsible for the utilization of glycolytic and gluconeogenic carbon sources, the GapB enzyme is only involved in gluconeogenesis and uses both NAD^+ and $NADP^+$ with a clear preference for $NADP^+$ (Ikeda and Nakagawa 2003; Omumasaba et al. 2004; Takeno et al. 2010). The opposite transcriptional regulation of the *gapA* and *gapB* genes reflects their different physiological function (Hayashi et al. 2002). Acetyl-CoA, which is derived from PEP and

pyruvate, represents the fueling substrate for the TCA cycle (Eikmanns 2005). The TCA cycle, also known as the citric acid cycle (Molenaar et al. 2000) or the Krebs cycle (Shiio et al. 1959) is a key metabolic pathway in *C. glutamicum* with important roles in anabolism and catabolism (Sauer and Eikmanns 2005). In particular, the cycle is responsible for the supply of energy (ATP, GTP) and reducing power (NADH, FADH, GTP) for biosynthetic purposes in *C. glutamicum* (Eikmanns 2005; Sauer and Eikmanns 2005) (Figure 3-8). As the TCA cycle intermediates are withdrawn for anabolism, the TCA cycle has to be replenished by anaplerotic reactions (Eikmanns 2005). The anaplerotic reactions are catalyzed by a number of enzymes, responsible for the interconversion of C_4 metabolites of the TCA cycle and C_3 metabolites of the glycolysis (Wittmann and Becker 2007; Wittmann and de Graaf 2005). The replenishment of the TCA cycle intermediate oxaloacetate is covered by two C_3 carboxylating enzymes, i.e. PEP carboxylase and pyruvate carboxylase. These reactions are of great importance, as they provide the precursor oxaloacetate, necessary for the production of amino acids belonging to the aspartate family such as L-lysine (Eikmanns 2005; Wittmann and de Graaf 2005). In addition, *C. glutamicum* also possesses three C_4-decarboxylating enzymes, i.e. PEP carboxykinase, malic enzyme, and oxaloacetate decarboxylase (Eikmanns 2005; Wittmann and de Graaf 2005).

3.3 Metabolic engineering of L-lysine-producing *C. glutamicum*

The main goal in developing amino acid producing strains is to channel as much carbon as possible from the carbon source towards the desired amino acid to increase product titer, yield and volumetric productivity (Ikeda 2003; Kelle et al. 2005; Wittmann and Becker 2007). First reports of improved production strains appeared only a short time after the discovery of *C. glutamicum* (Hagino and Nakayama 1974; Kase and Nakayama 1972; Nakayama et al. 1978). These were created by random mutagenesis using UV light irradiation and chemical agents followed by screening to select strains with the desired properties (Nakayama et al. 1978; Wittmann and Becker 2007). A milestone was the application of the L-lysine analogue S-(2-aminoethyl) cysteine (Nakayama and Araki 1973). This molecule cannot be metabolized by *C. glutamicum* and imitates L-lysine as feedback inhibitor of the aspartokinase. By randomly mutating the microbe and cultivating it on selection media, where L-lysine was substituted by its analogue, only clones with a mutated aspartokinase being released from L-lysine feedback inhibition were able to grow (Kalinowski et al. 1991; Nakayama and Araki 1973; Thierbach et al. 1990). Although these random mutagenesis approaches provided more efficient L-lysine producers, the uncontrolled introduction of detrimental mutations into the genome

appeared as a drawback (Ikeda et al. 2006). In further years, the decoding of the genome of *C. glutamicum* (Ikeda and Nakagawa 2003; Kalinowski et al. 2003; Yukawa et al. 2007) laid the foundation for the analysis of *C. glutamicum* using genomics (Brune et al. 2005; Mchardy et al. 2004), transcriptomics (Wendisch 2003), proteomics (Li et al. 2007; Schaffer et al. 2001), metabolomics (Bartek et al. 2008; Bolten et al. 2007; Woo et al. 2010), and fluxomics (Becker et al. 2007; Wittmann et al. 2004b). The genome-wide analysis of *C. glutamicum* enabled the targeted creation of new production strains through the use of genetic engineering approaches (Kirchner and Tauch 2003; Ohnishi et al. 2002). Metabolic engineering approaches allowed the targeted alteration of genomic DNA by integrating, deleting or interrupting the genes of interest (Ikeda et al. 2006; Jäger et al. 1992; Jetten and Sinskey 1995; Kirchner and Tauch 2003). To this end, metabolic engineering techniques such as the construction of cloning vectors or highly effective DNA transfer techniques have been developed in the last years (Cleto et al. 2016; Jäger et al. 1992; Kirchner and Tauch 2003; Tauch 2005). As the carbon core metabolism, particularly the PP pathway, the EMP pathway and the TCA cycle, provide precursors and energy for the biosynthesis of the amino acids of the aspartate family, metabolic engineering of these pathways was of great benefit for more effective production strains (Eikmanns 2005; Ikeda 2003).

3.3.1 Metabolic engineering of L-lysine biosynthesis and attenuation of competing pathways

Over the past, the L-lysine biosynthetic pathway in particular has received much attention to increase L-lysine production. The key enzyme studied was aspartokinase, encoded by *lysC* and catalyzing the conversion of aspartate to aspartyl phosphate (Cremer et al. 1991; Kalinowski et al. 1991; Kelle et al. 2005). Unlike *E. coli*, *C. glutamicum* does not possess different isozymes of the aspartokinase (Liu et al. 2007a; Mazat and Patte 1976; Sahm et al. 2000). The regulation of LysC and thereof the L-lysine biosynthetic pathway in *C. glutamicum* occurs via the allosteric feedback inhibition of aspartokinase by L-lysine and L-threonine via binding to the ß-subunit of the enzyme (Kalinowski et al. 1991). Different point mutations (e.g. T311I, T308I and S301Y in the ß-subunit of the aspartokinase) remove the feedback inhibition of LysC and result in increased L-lysine production (Cremer et al. 1991; Kalinowski et al. 1991; Kelle et al. 2005; Ohnishi et al. 2002). Furthermore, the overexpression of *lysC* further improved L-lysine production (Becker et al. 2011; Jetten et al. 1995). An important control of the L-lysine biosynthesis pathway also occurs at the level of aspartate semialdehyde, which is formed from aspartyl phosphate by aspartate semialdehyde dehydrogenase. As aspartate

semialdehyde represents a branching point, the carbon can be directed either to L-lysine biosynthesis or the competing L-threonine biosynthetic pathway (Eggeling and Bott 2015; Sahm et al. 2000). Homoserine dehydrogenase (*hom*) is the first enzyme in the L-threonine pathway and is regulated via feedback inhibition by L-threonine (Sahm et al. 2000; Shiio et al. 1973). To create L-lysine overproducing strains it was crucial to channel the carbon effectively towards L-lysine formation and downregulate L-threonine biosynthesis. The implementation of the Hom mutation V59A in combination with the LysC mutation T311I in the genome of *C. glutamicum* resulted in an improved L-lysine production strain (Ohnishi et al. 2002). Further improvement of L-lysine formation was achieved by overexpression of the genes *dapA* (Eggeling et al. 1998; Pisabarro et al. 1993), *dapF* and *dapC* (Hartmann et al. 2003), which encode for dihydrodipicolinate synthase, diaminopimelate epimerase and succinyl-amino-ketopimelate transaminase, respectively. While the introduction of a single mutation into the wild type strain often results in only slightly increased L-lysine production (Kim et al. 2006), the combination of different mutations is of great importance for efficient L-lysine production in *C. glutamicum* (Becker et al. 2011).

3.3.2 Improvement of precursor supply and reducing power

Reactions concerning the TCA cycle, particularly the pyruvate node, provide oxaloacetate as the precursor for amino acids of the aspartate family such as L-lysine (Eikmanns 2005; Gerstmeir et al. 2003). As mentioned before, the enzymes PEP carboxylase and pyruvate carboxylase are responsible to supply oxaloacetate and replenish the TCA cycle (Eikmanns 2005; Eikmanns et al. 1989; Wittmann and de Graaf 2005). Pyruvate carboxylase (Pyc) is the major enzyme for anaplerotic C_3 carboxylation in *C. glutamicum* (Petersen et al. 2000). The overexpression of *pyc* (Peters-Wendisch et al. 2001) and the amino acid exchange (P458S) (Ohnishi et al. 2002) led to increased L-lysine synthesis. In addition, the deletion of the gene *pck* encoding for PEP carboxykinase resulted in improved L-lysine production due to the increase in carbon net fluxes towards oxaloacetate (Riedel et al. 2001). Apart from PEP carboxykinase, also malic enzyme (MalE) is responsible for the conversion of C_4 metabolites derived from the TCA into C_3 metabolites with the simultaneous reduction of $NADP^+$ (Eikmanns 2005; Wittmann and de Graaf 2005). However, up to now the physiological function of malic enzyme is not totally clear, as neither the overexpression of *malE* nor the deletion leads to changes of the phenotype of *C. glutamicum* (Gourdon et al. 2000). However, it has been assumed that the enzyme might play an important role in NADPH generation on lactate or fructose (Dominguez et al. 1998; Eikmanns 2005; Gourdon et al. 2000). In

addition to the supply of precursors such as oxaloacetate and pyruvate, also the availability of NADPH is of great importance, since four moles of NADPH are required for the production of one mole L-lysine (Marx et al. 1996; Marx et al. 2003). Detailed findings concerning the NADPH metabolism of *C. glutamicum* were gained by ^{13}C metabolic flux analysis, and revealed that particularly the PP pathway is the major pathway for the generation of NADPH, when using glucose as substrate (Becker et al. 2005; Kiefer et al. 2002; Marx et al. 2003). However, it was noted that the PP pathway is significantly reduced in *C. glutamicum* strains growing on fructose (Kiefer et al. 2002). Various metabolic engineering approaches have, hence, been applied to optimize the PP pathway flux for increased NADPH availability and increased L-lysine synthesis. These approaches included, among others, the overexpression of the genes *fbp* (Becker et al. 2005; Georgi et al. 2005), *zwf* (Becker et al. 2007), and the entire *tkt*-operon (Becker et al. 2011). A further approach aimed at the amino acid substitution (S361F) in the 6-phosphogluconate dehydrogenase, encoded by *gnd*, in order to abolish the feedback repression by NADPH (Ohnishi et al. 2005). A further strategy to force more carbon through the PP pathway focused on the deletion of the *pgi* gene encoding for phosphoglucoisomerase (Marx et al. 2003). The deletion of *pgi* is only beneficial if sugars that enter the metabolism above fructose 6-phosphate are used as feed. However, sugars such as fructose, which have their entry point at the level of fructose 1,6-bisphosphate, need the *pgi* activity to pass the carbon through the PP pathway to provide NADPH (Kiefer et al. 2002; Wittmann et al. 2004a). Moreover, *pgi* deletion strains revealed several growth defects (Marx et al. 2003).

Recently, alternative routes for NADPH supply were implemented (Takeno et al. 2016; Takeno et al. 2010). As the native glyceraldehyde 3-phosphate dehydrogenase (GapA) of *C. glutamicum* has no $NADP^+$ activity, it was exchanged by the NADP-dependent glyceraldehyde 3-phosphate dehydrogenase (GapN) from *Streptococcus mutans* in order to couple the glycolytic flux to the formation of NADPH (Takeno et al. 2010). The expression of the GapN enzyme in a L-lysine producing strain improved L-lysine production (Takeno et al. 2010). Furthermore, the disruption of the PP pathway at the level of glucose 6-phosphate dehydrogenase had no significant effect on L-lysine production in *C. glutamicum* strains bearing the GapN enzyme, whereas a significant reduction in L-lysine production was observed in the parent strain bearing only the GapA enzyme (Takeno et al. 2016). A further study, aiming to couple the glycolytic flux to additional NADPH supply in *C. glutamicum* has shown that the use of an altered cofactor specificity of NAD^+ to $NADP^+$ in the native GapA enzyme increased L-lysine production (Bommareddy et al. 2014). In another approach, it was found that the use of the membrane-bound transhydrogenase PntAB from *E. coli* affects L-lysine production in a

beneficial way, as the enzyme provides additional NADPH by reducing $NADP^+$ via the oxidation of NADH (Kabus et al. 2007).

3.3.3 Systems metabolic engineering

The optimization of strains has been carried out traditionally by random mutagenesis, selection and genetic combination. The mutagenesis process of production strains mainly occurs by subjecting the organism and its genetic material to a variety of physical or chemical agents (Parekh et al. 2000). The drawback of random mutagenesis is the accumulation of detrimental mutations over the course of many mutagenesis cycles during strain development. Therefore, this approach often provides production strains with weak constitutions like growth deficiency or poor sugar consumption compared to corresponding wild type strains (Ikeda et al. 2006). These disadvantages led to the shift from conventional strain engineering strategies to metabolic engineering based on systems biology (Lee and Park 2010). Systems biology combines different omics technologies such as genomics, transcriptomics, proteomics, metabolomics and fluxomics, which are used to identify the best strategy for the genetic manipulation of organisms towards superior production performance (Becker and Wittmann 2015). An important milestone was thereby set by the availability of annotated genome sequences and thus the possibility to reconstruct genome-scale biochemical reactions for the prediction of possible targets for strain optimization (Kjeldsen and Nielsen 2009; Wittmann 2010). Genome-scale models have been constructed for several species such as *Saccharomyces cerevisiae* (Förster et al. 2003), *Escherichia coli* (Reed et al. 2003) and *C. glutamicum* (Kjeldsen and Nielsen 2009). The availability of genome sequences further led to a methodology called “genome breeding”. In this approach comparative analysis of different organisms allows the identification of beneficial mutations which are then reconstructed in a single wild type background (Ohnishi et al. 2002). Based on this approach a L-lysine-overproducing strain with improved L-lysine production was created, only due to the implementation of the modifications in the genes *hom*^{V59A}, *lysC*^{T311I}, and *pyc*^{P458S} in the *C. glutamicum* wild type strain ATCC 13032 (Ohnishi et al. 2002). Further studies have also shown the successful generation of overproducing strains containing a small number of key mutations required for the overproduction of L-lysine (Becker et al. 2011; Ikeda et al. 2006). In addition, it has been successfully demonstrated that *in silico* predictive analysis based on the genome sequence of *C. glutamicum* can help to identify specific genes that play an important role in the biosynthesis of amino acids. Thus, Mc Hardy et al. (2003) identified sixteen potential aminotransferase genes of which eleven were charactized in terms of their involvement in biosynthesis of branched-chain

amino acids (McHardy et al. 2003). Furthermore, also transcriptome analysis based on the common DNA microarray tool allowed to select a limited set from a variety of genes in different strains, which are highly relevant to get a deeper understanding of gene expression under different conditions such as the adaption and growth of *C. glutamicum* on various carbohydrates (Gerstmeir et al. 2004; Hayashi et al. 2002; Netzer et al. 2004), or to analyze the cell physiology and global regulation mechanisms due to the identification of regulons or stimulons (Lee and Park 2010; Wendisch 2003; Wendisch et al. 2006). Whole-genome DNA microarrays can also be applied to identify genes which are highly beneficial to improve product yields for recombinant proteins such as human insulin-like growth factor I fusion protein (IGF-If) in *E. coli* (Choi et al. 2003) or for amino acid production such as L-glutamate (Stansen et al. 2005) and L-lysine (Hayashi et al. 2006; Krömer et al. 2004). For example, the genes encoding for a methyltransferase and an ammonium uptake system have been successfully identified by comparative transcriptome analysis of the L-lysine producer MH20-22B and various other *C. glutamicum* strains. Subsequently the overexpression of these genes led to an increase in L-lysine production of about 40 % (Sindelar and Wendisch 2007). In addition, proteomics are useful to gain insights into biological systems and to investigate the impact of changing environmental conditions at the level of proteins (Lee and Park 2010; Schaffer and Burkovski 2005). For proteome analysis, 2-D gel electrophoresis, separating proteins to their isoelectric point, and subsequent identification of the proteins by mass spectrometry is a traditionally applied workflow (Bendt et al. 2003; Hermann et al. 2000; Hermann et al. 2001; Schaffer and Burkovski 2005; Schmid et al. 2000). First studies based on proteome analysis have been conducted to gain a better understanding of the response of *C. glutamicum* to nitrogen deficiency (Nolden et al. 2001; Schmid et al. 2000). Further on, the application of proteomics also provides the possibility to improve strain production. As an example, it was expected that overexpression of the *pspA* gene, encoding stress protein phage shock protein A, would be a useful engineering target to create a production strain with high production performance. In fact, it has been demonstrated that the overexpression of the *pspA* gene significantly increased the yield of soluble recombinant antibody fragment anti-CD18 $F(ab´)_2$ in *E. coli* (Aldor et al. 2005). Among the different omics technologies, also metabolomics represents a powerful tool to investigate cells and identify targets (Hasunuma et al. 2011). By this time, metabolome studies find application in various organisms such as *E. coli* (Chassagnole et al. 2002; Prasad Maharjan and Ferenci 2003; Tweeddale et al. 1998), *S. cerevisiae* (Raamsdonk et al. 2001; Theobald et al. 1997) and *C. glutamicum* (Krömer et al. 2004; Magnus et al. 2006; Moritz et al. 2000). The application of metabolome analysis has made an important contribution to obtain a better

understanding of various metabolic pathways for amino acids in *C. glutamicum*, including L-methionine (Krömer et al. 2005; Krömer et al. 2006a; Krömer et al. 2006b), L-valine and L-leucine (Magnus et al. 2006), and L-lysine (Krömer et al. 2004). While metabolomics consider the metabolite level of the cells, fluxomics are concerned with the metabolic fluxes between metabolite pools and are applied to gain a better understanding of metabolic processes and capabilities of the cell under various conditions (Kiefer et al. 2004; Wittmann and Heinzle 2001b, 2002; Wittmann et al. 2004a). The use of fluxome analysis further enables the investigation of the impact of genetic modifications and environmental conditions on the cell (Wittmann 2007; Wittmann and de Graaf 2005; Wittmann and Heinzle 2002). Metabolic flux studies involve the application of stable isotopes, mainly ^{13}C and ^{15}N, together with the application of GC-MS to measure metabolite labeling patterns being used to determine flux distributions in the cell. The metabolic flux analysis hereby includes two parts, i.e. an experimental part using single or multiple labelled tracer substrates for the cultivation of a desired organism and subsequent GC-MS measurement, as well as a computational part combining the labeling data with a global flux model to resolve unknown flux parameters (Wittmann 2002; Wittmann 2007). As example, when using [1-^{13}C] glucose or [1-^{13}C] fructose as the labeled substrate, the labeled carbon atom is split off and released as CO_2 when it is channeled through the PP pathway. The determination of the labeling pattern of proteinogenic L-alanine by GC-MS thus provides the flux partitioning between the PP pathway and glycolysis at the level of glucose 6-phosphate dehydrogenase (Wittmann 2007; Wittmann et al. 2004a). Metabolic flux studies have been extensively used to determine flux distributions in L-lysine-producing *C. glutamicum* cells by using glucose as carbon source (Becker et al. 2007; Becker et al. 2005; Becker et al. 2011; Marx et al. 1996; Marx et al. 1999; Marx et al. 2003) as well as other sugars such like sucrose (Wittmann et al. 2004a) and xylose (Buschke et al. 2013a). In order to generate production strains with superior production performance, the use of fluxomics in combination with other omics approaches has increased over the years. The combination of genome-scale models with omics technologies enabled an iterative approach, as shown in Figure 3-9, and led to tailor-made cell factories with precisely defined characteristics (Becker and Wittmann 2015; Kjeldsen and Nielsen 2009).

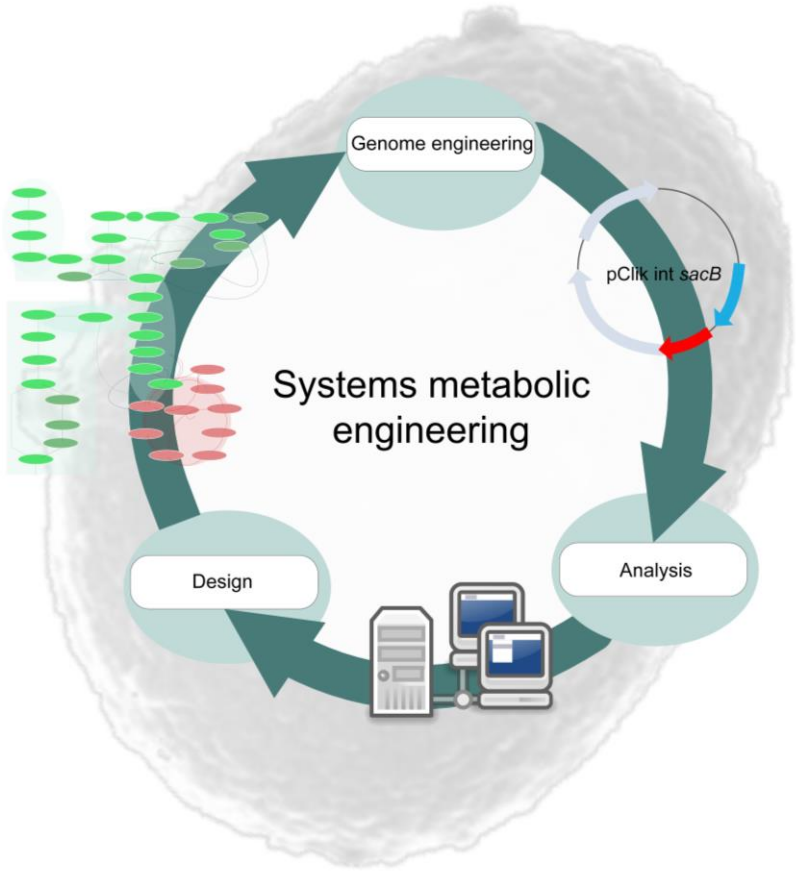

Figure 3-9: Systems metabolic engineering for the design and creation of a tailor-made cell factory. Figure adapted from Becker and Wittmann (2015).

In this regard, systems metabolic engineering has resulted in greatly improved amino acid producers over the years (Becker and Wittmann 2012b). The generation of the *C. glutamicum* L-lysine hyper-producing strain LYS-12 is an important example, where the combination of systems-level approaches has successfully led to a superior cell factory. The step-wise introduction of only 12 rational modifications into the wild type strain *C. glutamicum* ATCC 13032 turned this strain into a L-lysine hyper-producing strain, that exhibits superior production performance regarding yield, titer and productivity (Becker et al. 2011) (Figure 3-10). The first step to upgrade the wild type for L-lysine overproduction involved de-repression of the biosynthetic pathway. The feedback resistant aspartokinase variant, introduced for this purpose, exhibited the point mutation T311I, which led to the exchange of the amino acid L-threonine by L-isoleucine (Becker et al. 2005; Kim et al. 2006). Further improvement was achieved by upregulation of the carbon flux through L-lysine biosynthesis (overexpression of *lysC*, *dapB*, *ddh*, and *lysA*), attenuation of competing pathways (deletion of *pck* and downregulation of *icd* and *hom*), increased availability of the precursor oxaloacetate (overexpression and feedback decoupling of *pyc*), and increased supply of redox power (overexpression of *fbp* and the *tkt*-operon) (Becker et al. 2011).

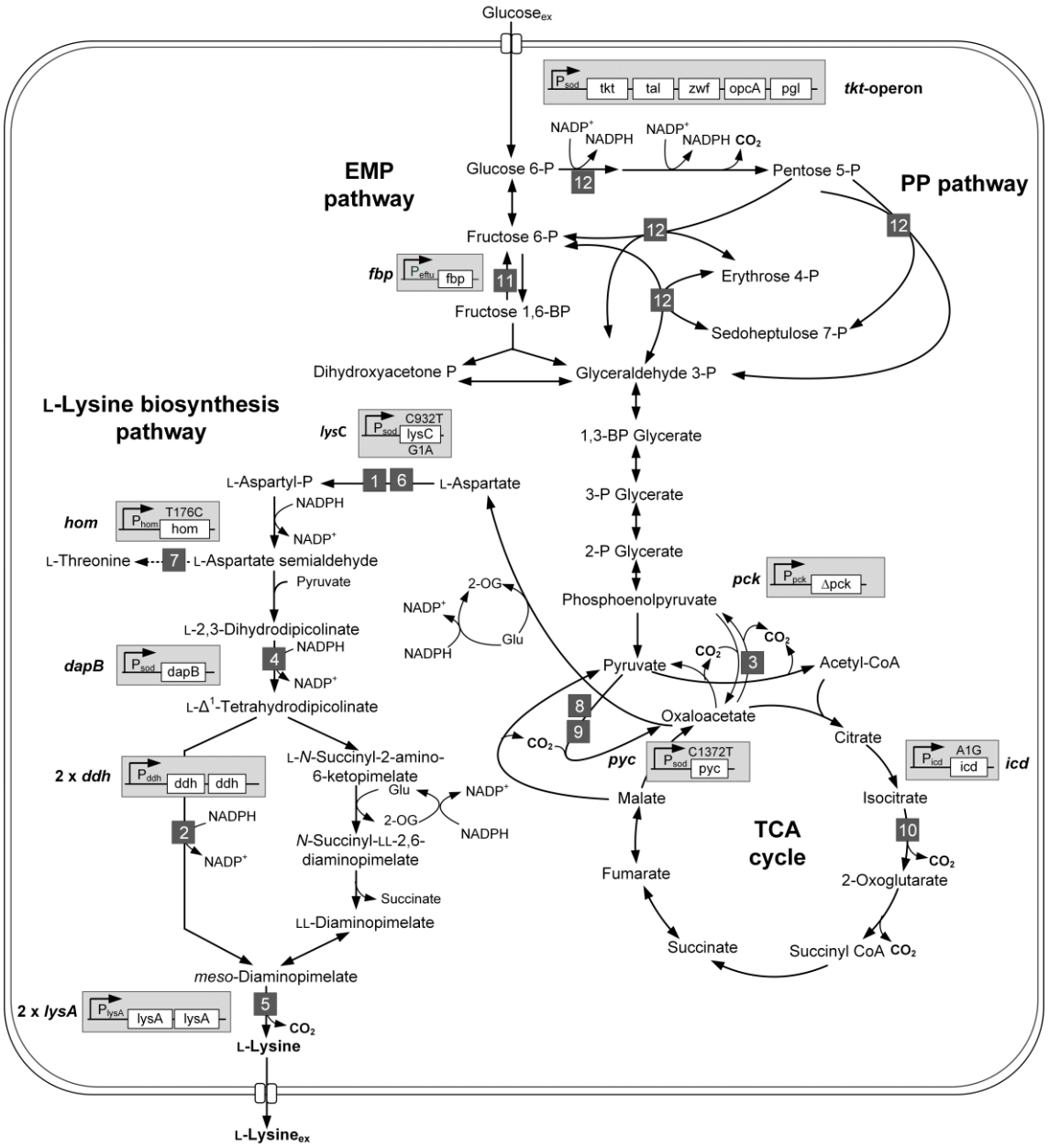

Figure 3-10: Central carbon metabolism and L-lysine biosynthesis in the L-lysine hyper-producing strain *C. glutamicum* LYS-12. The following traits were implemented in the genome of *C. glutamicum* wild type ATCC 13032 by Becker et al (2011) and depicted in gray boxes: 1, nucleotide exchange in *lysC* (*lysC*^{T311I}); 2, second copy of *ddh* (2x *ddh*); 3, deletion of *pck* (Δ*pck*); 4, overexpression of *dapB* (*P$_{sod}$ dapB*); 5, second copy of *lysA* (2x *lysA*); 6, overexpression of *lysC* (*P$_{sod}$ lysC*^{T311I}); 7, attenuation of *hom* (*hom*^{V59A}); 8, nucleotide exchange in *pyc* (*pyc*^{P458S}); 9, overexpression of *pyc* (*P$_{sod}$ pyc*^{P458S}); 10, attenuation of *icd* (*icd*^{GTG}); 11, overexpression of *fbp* (*P$_{eftu}$ fbp*); 12, overexpression of *tkt*-operon (*P$_{sod}$ tkt*). EMP pathway, Emden-Meyerhof-Parnas pathway; PP pathway, pentose phosphate pathway; TCA cycle, tricarboxylic acid cycle. Figure adapted from Becker et al. (2011).

4 Material and Methods

4.1 Bacterial strains

The previously developed L-lysine hyper-producing strain *C. glutamicum* LYS-12, containing 12 genome-based modifications to drive L-lysine biosynthesis from glucose (Becker et al. 2011), was used as starting point for strain engineering. The *E. coli* strains DH5α and NM522 were obtained from Invitrogen (Karlsruhe, Germany) and used as hosts for plasmid amplification and methylation, respectively. All strains used in this work are depicted in Table 4-1.

Table 4-1: Bacterial strains used in this work. Lukas Jungmann has contributed to the generation of the strain SEA-2B.

E. coli	**Description**	**Reference**
Strains		
E. coli DH5α	Heat shock competent cells for the amplification of the transformation vector	Invitrogen
E. coli NM522	Heat shock competent cells for the amplification and methylation of the transformation vector	Invitrogen
C. glutamicum	**Description**	**Reference**
Strains		
LYS-12	Wild type + P_{sod} *lysC*^{T311I}, overexpression of *lysC* (NCgl0247), encoding aspartokinase, by replacement of the native promoter by the *sod* promoter, and nucleotide exchange + 2x *ddh*, overexpression of *ddh* (NCgl2528), encoding diaminopimelate dehydrogenase, by implementation of an additional gene copy + Δpck, deletion of *pck* (NCgl2765), encoding PEP-carboxykinase + P_{sod} *dapB*, overexpression of *dapB* (NCgl1898), encoding dihydrodipicolinate reductase, by the *sod* promoter + 2x *lysA*, overexpression of *lysA* (NCgl1133), encoding diaminopimelate decarboxylase, by implementation of an additional gene copy + *hom*^{V59A}, nucleotide exchange in the *hom* (NCgl1136) gene, encoding homoserine dehydrogenase + P_{sod} *pyc*^{P485S}, overexpression of *pyc* (NCgl0659), encoding pyruvate carboxylase, by replacement of the native promoter by the *sod* promoter, and nucleotide exchange + *icd*$^{ATG \rightarrow GTG}$, attenuation of the *icd* (NCgl0634) gene, encoding isocitrate dehydrogenase, by replacement of the start codon + P_{eftu} *fbp*, overexpression of *fbp* (NCgl0976), encoding fructose 1,6 bisphosphatase, by replacement of the native promoter by the *eftu* promoter + P_{sod} *tkt*, overexpression of *tkt* operon containing the genes *tkt* (NCgl1512), encoding transketolase, *tal* (NCgl1513), encoding transaldolase, *zwf* (NCgl1514), encoding glucose 6-phosphate dehydrogenase, *opcA* (NCgl1515), encoding a putative subunit of glucose 6-phosphate dehydrogenase, and *pgl* (NCgl1516), encoding 6-phosphogluconolactonase	(Becker et al. 2011)

Table 4-1: *(Continued from previous page)* Bacterial strains used in this work.

C. glutamicum	**Description**	**Reference**
Strains		
SEA-1	LYS-12 + deletion of the *mtlR* gene (NCgl0110)	This work
SEA-2A	SEA-1 + genome-based integration of the *scrK* gene (ID1116607) from *Clostridium acetobutylicum* ATCC 824*,* encoding fructokinase, into the *crtEb* gene locus (NCgl0594)	This work
SEA-2B	SEA-1 + genome-based integration of the *mak* gene (EG11288) from *E. coli* K12-MG1655, encoding fructokinase, into the *crtEb* gene locus (NCgl0594) + replacement of the translational start codon GTG by ATG in the *mak* gene	This work
SEA-2C	SEA-1 + nucleotide exchange in the *mtlD* gene (NCgl0108) of *C. glutamicum*, encoding mannitol 2-dehydrogenase, resulting in the amino-acid exchange D75A	This work
SEA-2D	SEA-1 + genome-based integration of the *pntAB* gene (EG10744, EG10745) from *E. coli* K12-MG1655*,* encoding the membrane-bound nicotinamide nucleotide transhydrogenase PntAB, into the *crtB* gene locus (NCgl0598)	This work
SEA-2E	SEA-2B + empty plasmid pClik 5a MCS	This work
SEA-3	SEA-2B + plasmid-based expression of the *gapN* gene (SMU_676) from *Streptococcus mutans* UA159, encoding NADP-dependent glyceraldehyde 3-phosphate dehydrogenase	This work
SEA-4	SEA-2B + genome-based integration of the *pntAB* gene (EG10744, EG10745) from *E. coli* K12-MG1655*,* encoding the membrane-bound nicotinamide nucleotide transhydrogenase PntAB, into the *crtB* gene locus (NCgl0598)	This work
SEA-5	SEA-4 + empty plasmid pClik 5a MCS	This work
SEA-6	SEA-4 + plasmid-based expression of the *gapN* gene (SMU_676) from *S. mutans* UA159, encoding NADP-dependent glyceraldehyde 3-phosphate dehydrogenase	This work
SEA-7	SEA-4 + genome-based integration of the codon-optimized *gapN* gene (SMU_676) from *S. mutans* UA159, encoding NADP-dependent glyceraldehyde 3-phosphate dehydrogenase, into the *crtI*2 gene locus (NCgl0597)	This work

4.2 Primers and plasmids

For genomic modification (gene deletion, insertion, and mutation), the integrative plasmid pClik int *sacB* was applied (Becker et al. 2005). This vector has a size of 4.3 kb and contains a multiple cloning site, an origin of replication (ORI) for *E. coli*, a kanamycin resistance (kan^R) and the *sacB* gene from *Bacillus subtilis*, encoding levansucrase. The latter were used as selection markers for two subsequent genomic recombinations (Jäger et al. 1995; Jäger et al. 1992). As the plasmid does not have an ORI for

C. glutamicum, it forces genomic integration into the host. The plasmid pClik 5α MCS (5.1 kb) was used for plasmid-based overexpression in *C. glutamicum* (Buschke et al. 2011). It contained a multiple coning site, an ORI for *E. coli* and *C. glutamicum*, an open reading frame encoding the Rep-protein to initiate replication of the vector, and kan^R as selection marker. The plasmid pTC, which expresses the DNA methyltransferase for *C. glutamicum*, was used for DNA methylation (Kind et al. 2010a). This vector also contains an origin of replication for *E. coli* and tetracycline resistance (tet^R). To add the DNA methylation pattern of *C. glutamicum* to plasmid DNA, the pTC plasmid was co-expressed in *E. coli* NM522. For plasmid and primer construction the software Clone Manager Professional 9 (Sci-Ed Software, Denver, USA) was applied. To amplify the fructokinase genes *scrK* from *C. acetobutylicum* ATCC 824 (GeneBank Accession No. NC_003030) and *mak* from *E. coli* K12-MG1655 (GeneBank Accession No. NC_000913.3), genomic DNA of both organisms was obtained from the DSMZ (Braunschweig, Germany). All plasmids and primers created in this work are shown in Table 4-2 and in the appendix Table 7-1.

Table 4-2: Plasmids used in the present work for strain engineering of *C. glutamicum*. Lukas Jungmann has contributed to the construction of the following plasmids: pClik int *sacB* P_{sod} *mak,* pClik int *sacB* P_{tuf} *pntAB,* and pClik int *sacB* $mtlD^{GCA}$. The codon optimization of the *gapN* gene from *S. mutans* was performed by Eurofins (Eurofins, Ebersberg, Germany).

	Description	**Reference**
pTC	Expression vector for DNA-methyltransferase of *C. glutamicum*, containing an origin of replication (ORI) for *E. coli* and tet^R as selection marker	(Kind et al. 2010a)
pClik int *sacB*	Integrative transformation vector for genome-based modifications, comprising an MCS for *C. glutamicum*, an ORI for *E. coli*, and kan^R and *sacB* as selection markers	(Becker et al. 2005)
pClik int *sacB* Δ*mtlR*	Transformation vector for deletion of the *mtlR* gene from the genome of *C. glutamicum*	This work
pClik int *sacB* P_{sod} *scrK*	Transformation vector for integration of the *scrK* gene from *C. acetobutylicum* ATCC 824 into the *crtEb* gene locus under control of the *tuf* promotor	This work
pClik int *sacB* P_{sod} *mak*	Transformation vector for the integration of the *mak* gene from *E. coli* K12-MG1655 into the *crtEb* gene locus under control of the *tuf* promotor	This work

Table 4-2: *(Continued from previous page)* Plasmids used in the present work for strain engineering of *C. glutamicum*.

	Description	Reference
pClik int *sacB* P_{tuf} *pntAB*	Transformation vector for integration of the *pntAB* gene from *E. coli* K12-MG1655 into the *crtB* gene locus under control of the *tuf* promotor	This work
pClik int *sacB* P_{tuf} *gapN*	Transformation vector for integration of the codon-optimized *gapN* gene from *S. mutans* UA159 into the *crtI*2 gene locus under control of the *tuf* promotor	This work
pClik int *sacB* $mtlD^{GCA}$	Integrative transformation vector for exchanging the start codon of *mtlD* from GAT to GCA	This work
pClik 5a MCS	Episomal vector	(Buschke et al. 2011)
pClik 5a MCS *gapN*	Episomal vector with *gapN* from *S. mutans* UA159 (SMU_676) under control of its native promotor	(Schiefelbein 2014)

4.3 Chemicals

Peptone, beef extract, yeast extract, brain heart infusion (BHI) and agar were obtained from Difco Laboratories (Detroit, MI, USA). Tracer substrates i.e. 99 % [1-^{13}C] mannitol, 99 % [1-^{13}C] glucose and 99 % [1-^{13}C] fructose were purchased from Omicron Biochemicals Inc. (South Bend, IN, USA). All other chemicals were obtained from Sigma-Aldrich (Steinheim, Germany), Merck (Darmstadt, Germany), Fluka (Buchs, Switzerland) or Becton and Dickinson (Franklin Lakes, NJ, USA) and were of analytical or HPLC grade.

4.4 Medium composition

All media and solutions used in this work were prepared in ultrapure deionized water. Agar plates were prepared by addition of 20 g L^{-1} agar. Sterilization was carried out at 121 °C for 45 min or by filtration. If required, the antibiotics kanamycin (kan) and tetracycline (tet) were added to a final concentration of 50 µg ml^{-1} and 12.5 µg ml^{-1}, respectively.

4.4.1 Complex media

For agar plates and overnight cultures of *E. coli*, BHI medium was applied with either kanamycin or kanamycin and tetracycline, respectively. BHI medium was also used for agar plates and first pre-cultures of *C. glutamicum* (Table 4-3). For fed-batch fermentation, BHI medium with additional mannitol was applied. Mannitol was autoclaved separately and added to the medium to a final concentration of 15 g L^{-1}.

Table 4-3: Composition of BHI complex medium.

BHI	37 g
Add 1 L H_2O	
Autoclaved (121 °C, 45 min)	

After electroporation of *C. glutamicum* with plasmid DNA, BHI medium supplemented with 500 mM sorbitol (BHIS) was applied for regeneration of the cells. BHI solution and sorbitol solution were autoclaved separately and mixed together afterwards.

To initiate the first recombination event in *C. glutamicum*, cells were first cultivated in an overnight culture without selection pressure and subsequently plated on agar plates containing complex medium and sucrose (CM^{sac}). For strain selection of *C. glutamicum* during the second recombination event CM^{sac} plates and BHI plates additionally containing kanamycin (BHI^{kan}) were used. Thereby, *C. glutamicum* cells which had lost their plasmid were selected on CM^{sac} plates, while kanamycin deficient cells were selected on BHI^{kan} plates. Solutions of glucose, sucrose and urea, were autoclaved separately and supplemented to the medium after sterilization as shown in Table 4-4.

Table 4-4: Composition of CM complex medium.

CM medium	
Peptone	10 g
Beef extract	5 g
Yeast extract	5 g
NaCl	2.5 g
Add 725 mL H_2O	
Autoclaved (121°C, 45 min)	
Glucose (400 g L^{-1}), autoclaved (121 °C, 45 min)	25 mL
Urea (40 g L^{-1}), autoclaved (121 °C, 45 min)	50 mL
Sucrose (100 g L^{-1}), autoclaved (121 °C, 45 min)	200 mL

4.4.2 Mineral salt medium

To investigate *C. glutamicum* in shake flasks, chemically defined mineral salt medium (CDM) was used for the second pre-culture as well as for the main culture. For this purpose, stock solutions were prepared and sterilized separately (Table 4-5). The medium contained either glucose, fructose or mannitol as sole carbon source at a final concentration of 10 g L^{-1}.

Table 4-5: Composition of the stock solutions of the mineral salt medium used for cultivation studies of *C. glutamicum.*

Solution A	
NaCl	1 g
$CaCl_2$	55 mg
$MgSO_4 \cdot H_2O$	200 mg
Add 50 mL H_2O	
Autoclaved (121 °C, 45 min)	

Solution B	
$(NH_4)_2SO_4$	15 g
NaOH	pH 7.0
Add 100 mL H_2O	
Autoclaved (121 °C, 45 min)	

Buffer solution	
P1: K_2HPO_4	34.8 g
Add 1 L H_2O	
P2: KH_2PO_4	27.2 g
Add 1 L H_2O	
P1 and P2 were prepared separately	
Add P2 to P1 for pH 7.8	
Autoclaved (121 °C, 45 min)	

Substrate solution - Mannitol	
Mannitol	10 g
Add 100 mL H_2O	
Autoclaved (121 °C, 45 min)	

Substrate solution - Glucose	
Glucose	10 g
Add 100 mL H_2O	
Autoclaved (121 °C, 45 min)	

Substrate solution - Fructose	
Fructose	10 g
Add 100 mL H_2O	
Autoclaved (121 °C, 45 min)	

Vitamin solution	
Biotin	2.5 mg
Thiamin · HCl	5 mg
Pantothenic acid calcium salt	5 mg
Add 100 mL H_2O	
Filter sterilized	
Stored at 4 °C	

Fe solution	
$FeSO_4 \cdot 7H_2O$	20 mg
HCl	pH 1.0
Add 10 mL H_2O	
Filter sterilized	
Stored at 4 °C	

Trace element solution	
$FeCl_3 \cdot 6\ H_2O$	200 mg
$MnSO_4 \cdot H_2O$	200 mg
$ZnSO_4 \cdot H_2O$	50 mg
$CuCl_2 \cdot 2\ H_2O$	20 mg
$Na_2B_4O_7 \cdot 10\ H_2O$	20 mg
$(NH_4)_6Mo_7O_{24} \cdot 4\ H_2O$	10 mg
Add 1 L H_2O	
Filter sterilized	
Stored at 4 °C	

DHB solution	
3,4-Dihydroxybenzoic acid	300 mg
NaOH (6 M)	500 µL
Add 10 mL H_2O	
Filter sterilized	
Stored at 4 °C	

The different solutions were combined freshly before use according to the given composition as listed in Table 4-6.

Table 4-6: Final composition of the mineral salt medium used for cultivation of *C. glutamicum* strains

Mineral salt medium	
Solution A	50 mL
Solution B	100 mL
Buffer solution	100 mL
Substrate solution	100 mL
Vitamin solution	20 mL
Fe solution	10 mL
Trace element solution	10 mL
DHB solution	1 mL
Add 1 L H_2O	

In ^{13}C isotope studies for metabolic flux analysis, naturally labeled substrates were replaced by 99 % [1-^{13}C] mannitol, 99 % [1-^{13}C] glucose or 99 % [1-^{13}C] fructose (Omicron Biochemicals, South Bend, IN, USA).

4.4.3 Seaweed based medium

For cultivation of *C. glutamicum* on seaweed extracts from *Laminaria digitata* and *Durvillaea antarctica*, chemically defined mineral salt medium was prepared as described above. Instead of pure substrate, algal extract was supplemented to the main culture, equaling a final sugar concentration of 10 g L^{-1}.

4.4.4 Industrial production media

For fed-batch production of L-lysine in 1 L stirred tank bioreactors an industrially relevant mannitol-based medium (MDAP) was applied, which was supplemented with vitamins and trace elements as listed in Table 4-7.

Table 4-7: Composition of the stock solutions of the MDAP medium used for bioreactor fermentation of *C. glutamicum.*

Mannitol solution	
Mannitol	200 g
Add 1 L H_2O	
Autoclaved (121 °C, 45 min)	

Yeast extract solution	
Yeast extract	75 g
Add 1 L H_2O	
Autoclaved (121 °C, 45 min)	

Salt solution	
Citric acid	4 g
$(NH_4)_2SO_4$	50 g
KH_2PO_4	2.5 g
$Na_2HPO_4 \cdot 2\ H_2O$	3.1 g
$MgSO_4 \cdot 7\ H_2O$	2.5 g
$FeSO_4 \cdot 7\ H_2O$	140 mg
$ZnSO_4 \cdot 7\ H_2O$	60 mg
$MnSO_4 \cdot H_2O$	18 mg
$CaSO_4 \cdot H_2O$	266 mg
Add 1 L H_2O	
Autoclaved (121 °C, 45 min)	

MDAP trace element solution	
Citric acid	2.1 g
Boric acid	300 mg
$CoSO_4 \cdot 7\ H_2O$	428 mg
$CuSO_4 \cdot 5\ H_2O$	457 mg
$NiSO_4 \cdot 6\ H_2O$	338.0 mg
$(NH_4)_2MoO_4$	47.59 mg
Add 1 L H_2O	
Filter sterilized	

MDAP vitamin solution	
Biotin	300 mg
Thiamin · HCl	636 mg
Nicotinamide	600 mg
Pantothenic acid HCl	2.2 g
Add 1 L H_2O	
Filter sterilized	

The different solutions were freshly combined before use according to the given composition as shown in Table 4-8.

Table 4-8: Final composition of the MDAP medium used for bioreactor fermentation of *C. glutamicum.*

MDAP Medium	
Mannitol solution	200 mL
Yeast extract	89 mL
Salt solution	500 mL
MDAP trace element solution	1.4 mL
MDAP vitamin solution	15 mL
Antifoam 204	1 mL
Add 1 L H_2O	

Feeding was initiated, when the initial amount of the substrates (mannitol and fructose) was depleted. The components of the MDAP feed solution were sterilized by filtration, while mannitol was autoclaved and added to the medium after autoclaving and cooling down to 80 °C. The feeding solution was prepared according to the compositions listed in Table 4-9.

Table 4-9: Composition of the feeding solution used for fed-batch bioreactor fermentation of *C. glutamicum*.

MDAP feed solution	
Yeast extract	5 g
$(NH_4)_2SO_4$	13.3 g
Urea	14 g
MDAP vitamin solution	500 mL
Antifoam 204	1 mL
Add 620 mL H_2O	
Mannitol (500 g L^{-1}), autoclaved (121 °C, 45 min)	380 mL

4.5 Strain conservation

For strain conservation, cells of *E. coli* and *C. glutamicum* were cultivated in shake flasks (filled with 10 % BHI medium) at 30 °C and 230 rpm on an orbital shaker (Multitron, Infors AG, Bottmingen, Switzerland). If appropriate, kanamycin or tetracycline was added. During the exponential growth phase 800 µL of cell culture was mixed with 800 µL sterile, cooled glycerol (60 %, 4 °C) and the mixture was stored at -80 °C.

4.6 Strain construction

4.6.1 Isolation of plasmid DNA

For plasmid isolation from *E. coli* DH5α and *E. coli* NM522, the plasmid kit QIAprep Spin Miniprep Kit (Qiagen, Hilden, Germany) was used according to the manufacturer's instructions. All cultivations were conducted in baffled shake flasks (filled with 10 % BHI medium) incubated for 12 h at 37 °C and 230 rpm on an orbital shaker (Multitron, Infors AG, Bottmingen, Switzerland). Since plasmid isolation from *E. coli* DH5α was only used for plasmid assembly and amplification, individual isolations were performed using 2 mL of a BHI^{kan} culture. Plasmid DNA from *E. coli* NM522 was used for electroporation of *C. glutamicum*, where high DNA concentrations are required. For this purpose,

15 identical plasmid mini preparations were performed, using 2 ml of a BHI$^{kan+tet}$ culture, respectively. The DNA was pooled after the final elution step and concentrated by evaporation (SpeedVac Concentrator DNA 120, Thermo Fisher Scientific, Waltham, MA, USA). The elution of DNA from the QIAprep column was done in deionized water pre-warmed to 60 °C. Final DNA concentrations were determined by a spectrophotometer (NanoDrop1000, Thermo Fisher Scientific, Waltham, MA, USA).

4.6.2 Purification of DNA fragments

Amplified DNA from PCR reactions and digested DNA was purified by using a clean-up Kit (WIZARD SV Gel and PCR Clean-Up System, Promega Madison, WI, USA) according to the manufacturer's instructions. The final elution step was performed in deionized water pre-warmed to 60 °C. Final DNA concentrations were determined by a spectrophotometer (NanoDrop1000, Thermo Fisher Scientific, Waltham, MA, USA), and the correct DNA fragment sizes were verified by gel electrophoresis.

4.6.3 Construction of transformation vectors

For the construction of transformation vectors, isothermal assembly was used (Gibson et al. 2009). For this purpose, the DNA fragments for cloning were amplified by PCR using specific primers, containing 20 bp homologous overlap regions. The obtained DNA fragments were purified as described above and inserted into an empty vector (pClik int *sacB* or pClik 5αMCS), via the restriction sites. Therefore, the empty vector was isolated and digested with fast digest enzymes (Thermo Fisher Scientific, Rochester, NY, USA) as listed in Table 4-10.

Table 4-10: Reaction mixture used for enzymatic digestion.

Components	Volume [µL]	Final concentration
Template DNA	-	5 µg
FastDigest Buffer	5 µL	1x
Enzyme	5 µL	
Add 50 µL H_2O		

After enzymatic digestion, the transformation vector was purified as described above and checked for correctness by gel electrophoresis. For assembling the construction vector,

200 ng linearized transformation vector and an equimolar amount of PCR fragments were mixed with 15 µL of a Gibson master mix. Deionized water was added to a final volume of 20 µL and the mixture was incubated for 1 h at 50 °C (peQSTAR, Peqlab Biotechnolgy GmbH, Erlangen, Germany). The composition of the Gibson 5x assembly buffer and the Gibson master mix used in this work are listed in Table 4-11 and Table 4-12, respectively.

Table 4-11: Composition of Gibson 5x assembly buffer.

Gibson buffer	
Tris-HCl (1 M), pH 7.5	3 mL
$MgCl_2$ (100 mM)	300 µL
dGTP (100 mM)	60 µL
dATP (100 mM)	60 µL
dCTP (100 mM)	60 µL
dTTP (100 mM)	60 µL
DTT (1 M)	300 µL
PEG-800	1.5 g
NAD	20 mg
Add 6 mL H_2O	

Table 4-12: Composition of Gibson master mix.

Gibson buffer	
Gibson 5x assembly buffer	320 µL
T5 Exonuclease	0.64 µL
Phusion Polymerase	20 µL
Taq ligase	160 µL
Add 1200 µL H_2O	

For introduction of specific point mutations via PCR, primers containing the desired site-specific point mutation were used. Optionally, specifically modified primers and a kit for directed mutagenesis (QuikChance XL, Agilent, Waldbronn, Germany) were used according to the manufacturer's instructions to introduce an additional point mutation in the same gene.

4.6.4 Polymerase chain reaction

For DNA amplification and strain validation, polymerase chain reaction (PCR) was performed (peQSTAR, Peqlab Biotechnology GmbH, Erlangen, Germany). For verification of clones from transformation events, a Phire PCR master mix (Phire Green Hot Start II PCR Master Mix, Thermo Fisher Scientific, Rochester, NY, USA) was used. Cells from single colonies, transferred with a toothpick into a PCR reaction vessel, served as DNA template. For amplification of target fragments, the Phusion High-Fidelity PCR master mix (Thermo Fisher Scientific, Rochester, NY, USA) was used, containing Phusion polymerase with proof reading function. The PCR reaction was performed, using Phire PCR master mix or Phusion High-Fidelity PCR master mix, according to the composition listed in Table 4-13 and PCR was carried out corresponding to the program displayed in Table 4-14.

Table 4-13: Composition of the PCR reaction mixtures.

Components	Volume [µL]	Final concentration
2x PCR master mix (Phire or Phusion)	10	1x
Forward Primer (10 µM)	0.5	250 nM
Reverse Primer (10µM)	0.5	250 nM
Template DNA	1	5 - 500
DMSO	0.6	3 % (v/v)
Add 20 µL PCR grade H_2O		

Table 4-14: Temperature profile and time protocol used for PCR.

Step	Temperature [°C]	Time [min]	Number of cycles
Initial Denaturation	98	15	1
Denaturation	98	0.5	
Annealing	*	0.5	30
Elongation	72	**	
Final Elongation	72	5	1
Storage	8	∞	1

* depends on the G/C content of the primers

** depends on the length of the fragment to be amplified and the polymerase used

Phire polymerase: 15 sec kb^{-1}, Phusion polymerase: 30 sec kb^{-1}

The primer annealing temperature depended on the respective primers and was adjusted individually. The annealing temperature calculation was carried out with the software Clone Manager Professional 9 (Sci-Ed Software, Denver, USA). The obtained PCR products were purified and the concentration of DNA was determined spectrophotometrically as described above.

4.6.5 Site-directed mutagenesis

The introduction of specific point mutations in the genome of *C. glutamicum* was performed by PCR using transformation vectors, which were constructed as described above (see chapter 4.6.3) according to Gibson et al. (2009), and specific primers, containing the desired site-specific point mutation. To introduce additional point mutations in the same gene, specifically modified primers, and a directed mutagenesis kit (QuikChance XL, Agilent, Waldbronn, Germany) were used, according to the manufacturer's instructions.

4.6.6 Gel electrophoresis

To check PCR products, plasmids and plasmid digestions for correct size, samples were separated electrophoretically in a 1 % agarose gel (1 % (w/v) agarose in 1x TAE buffer). Separation was conducted in 1x TAE buffer prepared from a 50x concentrated stock solution (Table 4-15). If appropriate, samples were mixed with 1/5 volume loading dye (GelPilot Loading Dye 5x, Qiagen, Hilden, Germany) before loading the gel slots. To determine the band size of the samples, a 1 kb DNA ladder (1 kb/1000 bp BLUE DNA Ladder, GeneON, Ludwigshafen, Germany) was applied as standard.

Table 4-15: Composition of 50x TAE stock solution.

50x TAE stock solution	
Tris (2 M)	242.28 g
Acetic acid (100 %)	57 mL
EDTA (0.5 M), pH 8.0	100 mL
Add 1 L H_2O	

Electrophoresis was performed at 120 V for 40 - 60 min, depending on the size of the expected fragments (OWL EasyCast B1A, Thermo Fisher Scientific, Waltham, MA, USA, and MS300V, Major Science, Saratoga, CA, USA). For gel staining, the gel was incubated in a 2.5 mg L^{-1} ethidium bromide solution for about 20 min. Subsequently, the complexes of DNA molecules and ethidium bromide were visualized by UV-trans illumination in the ChemiDoc XRS+ System (Bio-Rad, Hercules, CA, USA).

4.6.7 Preparation of heat shock competent *E. coli* cells

The preparation of heat shock competent *E. coli* (*E. coli* DH5α and NM522) cells was performed by the inoculation of cells from a freshly streaked agar plate, incubated in 10 mL of BHI + 20 mM $MgSO_4$ for about 12 h at 37 °C and 230 rpm on an orbital shaker (Multitron, Infors AG, Bottmingen, Switzerland). Since *E. coli* NM522 contained the pTC plasmid, tetracycline was added to the culture medium to a final concentration of 12.5 µg mL^{-1}. After 12 h incubation time, the pre-culture was used to inoculate the main culture (250 mL BHI with 20 mM $MgSO_4$), which was incubated at 37 °C and 230 rpm on an orbital shaker (Multitron, Infors AG) until an OD_{600} of 0.4 - 0.6 was reached. Subsequently, the main culture was incubated for 10 min on ice and then harvested by centrifugation in pre-cooled 50 mL falcon tubes (10 min, 8800 x *g*, 4 °C). The obtained pellet was resuspended in 80 mL ice-cold TB buffer (Table 4-16) and incubated on ice for 10 min. After a second centrifugation step, cells were resuspended in 20 mL TB buffer containing 1.5 mL DMSO and incubated on ice again for 15 min. Subsequently, 220 µL aliquots of the cell suspension were dispensed in pre-cooled sterile 1.5 mL tubes and stored at -80 °C until use.

Table 4-16: Composition of TB-buffer.

TB-buffer	
Pipes-NaOH (0.5 M), pH 6.7	2 mL
$CaCl_2$ (0.5 M)	3 mL
KCl (2 M)	12.5 mL
$MnCl_2$ (1 M)	5.5 mL
Add 100 mL H_2O	

4.6.8 Transformation of *E. coli* cells by heat shock

For transformation of *E. coli* cells by heat shock, cells (prepared as described above) were thawed on ice and 100 - 500 ng plasmid DNA were added. After an incubation period of 30 min on ice, the heat shock was carried out in a water bath at 45 °C for 45 sec. Subsequently, cells were incubated on ice for 2 min followed by the addition of 900 µL BHI medium. The cell regeneration was performed for 1 h at 37 °C in a thermo block at 500 rpm (ThermoMixer, Eppendorf, Hamburg, Germany). After the regeneration, cells were harvested by centrifugation (3 min, 5700 x *g*). The supernatant was discarded and the obtained cell pellet was resuspended in about 100 µL of medium. For selection purposes, *E. coli* DH5α cells were then plated on BHI^{kan} agar and *E. coli* NM522 cells on a $BHI^{kan+tet}$ agar and incubated for 24 h at 37 °C. Verification of the obtained clones was performed by PCR as described above.

4.6.9 Preparation of electro-competent *C. glutamicum* cells

For preparation of electro-competent *C. glutamicum* cells, a freshly prepared agar plate was used as inoculum for the pre-culture, which was grown in 10 mL BHI for about 12 h at 30 °C on an orbital shaker (Multitron, Infors AG, Bottmingen, Switzerland). The pre-culture was then used as inoculum for the main culture, containing 50 mL BHI. After reaching an OD_{660} of 0.6 - 2, the main culture was harvested by centrifugation in pre-cooled 50 mL falcon tubes (5 min, 6500 x *g*, 4 °C) and washed twice with 5 mL ice cold 10 % (v/v) glycerol solution. Afterwards, cells were resuspended in 8 mL of 10 % (v/v) glycerol solution per gram cell wet weight and 200 µL aliquots of the cell suspension were transferred to 1.5 mL tubes and stored at -80 °C until use.

4.6.10 Transformation of *C. glutamicum*

Electroporation of *C. glutamicum* cells was conducted, using 200 µL cell suspension (prepared as described above), which was transferred to an electroporation cuvette (Gene Pulser cuvette with 0.2 cm gap, Bio-Rad, Hercules, CA, USA) and mixed with1 - 5 µg DNA. Subsequently, the suspension was coated with 800 µL 10 % (v/v) glycerol and incubated on ice for 2 min. Then, cells were transformed by electroporation using a Gene Pulser Xcell (3 kV, 25 µF and 200 Ω, Bio-Rad Laboratories Inc., Hercules, CA, USA). Cells were then directly transferred into 15 mL tubes containing 4 mL BHIS medium (pre-heated to 46 °C) and exposed to heat shock at 46 °C for 6 min in a water bath. For regeneration, cells were incubated at 30 °C for 2 h on an orbital shaker

(Multitron, Infors AG, Bottmingen, Switzerland). Finally, cells were harvested by centrifugation (5 min, 6500 x *g*). The obtained cell pellet was resuspended in 100 µL medium. For selection, the cell suspension was plated on $BHIS^{kan}$ agar and incubated at 30 °C for two days in order to obtain positive clones, which had completed the first recombination event. Since pClik int *sacB* has no ORI for *C. glutamicum*, it cannot replicate in this organism, only clones that had integrated the plasmid DNA into the genome via homologous recombination, were able to grow in the presence of kanamycin. Positive obtained clones were verified by PCR.

4.6.11 Second recombination

A single cell colony obtained from the first recombination event was transferred into 10 mL BHI medium and incubated at 30 °C for about 12 h on an orbital shaker (Multitron, Infors AG, Bottmingen, Switzerland) without kanamycin to stimulate the second recombination event. Subsequently, cells were plated on CM^{sac} agar plates and incubated for two days at 30 °C. Since the expression of *sacB*, encoding for levansucrase, is lethal for *C. glutamicum*, only cells without the plasmid backbone were able to grow in the presence of sucrose (Jäger et al. 1992). After incubation, sucrose-resistant single colonies were picked with a toothpick and patched on BHI^{kan} and CM^{sac} raster plates. The plates were then incubated at 30 °C for 24 h. For strain validation, colonies growing only on CM^{sac} agar were analyzed by PCR as described above and further validated by sequencing (LightRun, Eurofins GATC Biotech GmbH, Cologne, Germany).

4.6.12 Computational modeling for protein engineering

For altering the enzyme cofactor specificity, targeted protein modeling was conducted. For this purpose, available protein structures of the enzyme of interest were retrieved from the RCSB Protein Data Bank (PDB) and used to generate a homology model of the enzyme to be optimized in *C. glutamicum* by SWISS-MODEL (Benkert et al. 2011; Waterhouse et al. 2018). If necessary, missing atoms were manually added to the cofactor from the crystal structure and energetically optimized with the MM+ force field parameters implemented in HYPERCHEM (HYPERCHEM 1999) to obtain putative positions of the desired cofactor (e.g. P was added to NAD^+ to mimic $NADP^+$). The visualization of the native and modified enzyme structures was conducted using the Swiss-Pdb-Viewer (Guex 1999). Computational modeling for protein engineering was

performed by Dr. Michael Hutter (Computational Biology, Saarland University, Germany).

4.6.13 Codon optimization

To enhance the expression level of heterologous genes, the genes were adapted to the codon usage preferred by *C. glutamicum*. The codon-optimization was performed by Eurofins (Eurofins Genomics GmbH, Ebersberg, Germany), using the company's in-house bioinformatics algorithms.

4.7 Cultivation

4.7.1 Batch cultivation in shake flasks

Cultivation studies were conducted in baffled shake flasks (filled with 10 % medium) at 30 °C and 230 rpm on an orbital shaker (Multitron, Infors AG, Bottmingen, Switzerland). First, the pre-culture (10 mL BHI medium) was inoculated with a single colony from a BHI agar plate, which was incubated for two days at 30 °C. The cells were then incubated for 8 h (Multitron, Infors AG), collected by centrifugation (5 min, 8800 x *g*, room temperature), washed with chemically defined mineral salt medium (CDM) and used as inoculum for the second pre-culture (25 mL CDM medium). Cells were harvested during the exponential growth phase, washed twice as described above and used as the inoculum for the main culture (25 mL CDM medium). All shake flask studies were performed in triplicate. Where needed, dissolved oxygen was monitored using the PreSens shake-flask reader SFR (PreSens, Regensburg, Germany) based on fluorescence measurement. For measurement of dissolved oxygen the sensor device was fixed in the orbital shaker and shake flasks with immobilized optodes were used (Schneider et al. 2010). In isotope studies, the inoculum level was kept below 0.1 % of the later sampled cell concentration to exclude an interference of non-labeled biomass from the inoculum with later ^{13}C labeling analysis (Becker et al. 2011).

4.7.2 Fed-batch production of L-lysine from mannitol in a lab-scale bioreactor

The production performance of *C. glutamicum* from mannitol was assessed in a fed-batch process, using 1 L bioreactors (SR0700ODLS, DASGIP AG, Jülich, Germany). Cells (pre-grown for 12 h at 30 °C in 2 L baffled flasks with 200 mL BHI medium) were harvested (5 min, 8800 x *g*, room temperature), resuspended in 50 mL batch medium

and then used as inoculum. The initial batch process started with an initial volume of 300 mL. During the process, the temperature was kept at 30 °C ± 0.1 (CWD4 bioblock, DASGIP AG, Jülich, Germany). For pH online monitoring, a pH electrode was used (Mettler Toledo 405-DPAS-SC-K8S/225, Mettler Toledo, Giessen, Germany). A 25 % NH_4OH solution was added automatically (MP8 pump system, Eppendorf, Hamburg, Germany) to keep the pH stable at 7.0 ± 0.1. The dissolved oxygen level (pO_2) was monitored online by using a pO_2 electrode (VisiFerm DO 225; Hamilton, Höchst, Germany) and maintained above 30 % of saturation by adjusting the stirrer speed, the aeration rate and the oxygen fraction of the gas inflow. The composition of the exhaust gas (CO_2 and O_2) was measured online (GA4, DASGIP AG, Jülich, Germany). The initial stirrer speed was set to 600 rpm and the aeration rate to 18 sL h^{-1}. Feeding was initiated, when the initial amount of carbohydrates was exhausted. Feed pulses were manually added, when the pO_2 increased above 45 %. Data acquisition and process control were conducted by the DASGIP control software (DASGIP AG, Jülich, Germany).

4.8 Preparation of seaweed hydrolysates

4.8.1 Extraction of the brown seaweed *Durvillaea antarctica*

Durvillaea antarctica was collected in wintertime (August 2019) at Los Molles, Valparaiso, Chile (32º14'36''S, 71º31'00''W). Only the non-edible part, i.e. the mid stem of *D. antarctica* was used and washed with seawater to remove the sand and transported to the laboratory in plastic bags. The stem was cut into pieces (10 cm in length), dried at 60 ºC until constant weight and powdered with a blender for 15 min. For extraction, 10 g of the powder were mixed with 200 mL ethanol (80 % v/v) and stirred at 60 ºC for 2 h. Subsequently the ethanol was evaporated by heating to 80 ºC for 30 min. The resulting solution was resuspended in 250 mL sulfuric acid (4 % v/v), autoclaved (121 ºC, 40 min), cooled down to room temperature, stirred overnight, and then neutralized to pH 7.0 by adding KOH pellets (> 85 %). The supernatant was collected (10 min, 6000 x *g*, 20 ºC) and clarified by filtration (Whatman filter paper 6 µM, 55 mm, GE Health Care, Amersham, UK). The obtained hydrolysate was sterilized (121 °C, 15 min). Processing of the samples was done at the Biosystems Engineering laboratory (Center for Bioinformatics and Integrative Biology, Universidad Andrés Bello, Santiago, Chile).

4.8.2 Extraction of the brown seaweed *Laminaria digitata*

Dried leaves (50 g) of *Laminaria digitata* (Makrobiotik, Hohrenk, Germany) were powdered with a blender. The powder was resuspended in 500 mL deionized water and autoclaved (121 °C, 18 min), which yielded a mannitol-rich hydrolysate. Optionally, enzymatic hydrolysis was conducted after the heating step, in order to increase the sugar level. For this purpose, the extract was additionally amended with a cocktail of enzymes, i.e. Celluclast 1.5 L (10 mg g^{-1}) and Viscozyme L (10 mg g^{-1}) (Sigma-Aldrich, Steinheim, Germany) and incubated at 50 °C and pH 5.5 for 48 h. Subsequently, the hydrolysate was clarified from debris and collected (15 min, 5000 x *g*, 4 °C) and alginate was precipitated as described below.

4.8.3 Purification of alginate from seaweed extracts

The extraction of sodium alginate from hydrolysate of *L. digitata* was adapted from previous work (Haug et al. 1974; Latifi et al. 2015). Therefore, $CaCl_2 \cdot 2H_2O$ (0.1 g g^{-1}) was added. The mixture was stirred (15 min, 200 rpm). The precipitated raw alginate was separated from the supernatant by filtration, resuspended in 2 % (w/v) $CaCl_2$ for 2 h and then washed with deionized water. Subsequently the polymer was treated with 40 % formaldehyde for 2 h and then extracted twice with 50 mL 0.2 M HCl. Afterwards it was washed three times with deionized water. Finally, the alginate was dissolved in 400 mL 3 % (w/v) Na_2CO_3 and incubated for two days. Then, the solution was centrifuged (30 min, 10000 x *g*) to remove solids and the obtained supernatant was mixed with an equal volume of ethanol to precipitate alginate as sodium salt. Finally, the obtained sodium alginate was washed twice with acetone and dried for 24 h at room temperature and then for 24 h at 80 °C.

4.8.4 Processing of seaweed hydrolysates for fermentative L-lysine production

The extract, obtained from *D. antarctica* (see chapter 4.8.1), was directly used for cultivation experiments, while the extract from *L. digitata* was further processed after the separation of alginate to achieve a higher carbohydrate content. For this purpose, the alginate-free extract (215 - 230 mL) was filtered by Whatman filter paper (6 µM, 55 mm, GE Health Care, Amersham, UK) and concentrated (3 h, Vacuum Concentrator RVC 2-33 IR, Christ, Osterode, Germany) to a volume of 30 mL. In all cases, the pH of the algal extract was neutralized to pH 7.4 with 6 M NaOH and the final solution was sterilized by autoclaving (121 °C, 20 min), prior to cultivation.

4.9 Analytical methods

4.9.1 Quantification of cell concentration

Optical density. For determination of the optical density, 0.5 mL to 1 mL sample was collected and transferred into a 1.5 mL reaction vessel. The exact sample amount was monitored on an analytical balance (Quintix 224-1S, Sartorius, Göttingen, Germany). The cell concentration was determined spectrophotometrically (UV-1600PC spectrophotometer, Radnor, PA, USA) by measuring the optical density (OD) at 660 nm against water as reference.

Cell dry weight. The cell dry weight (CDW) was determined gravimetrically. Therefore, 15 mL plastic tubes were dried at 80 °C to constant weight (72 h). Afterwards, the dried tubes were cooled down in a desiccator (1 h) and then their weight was determined on a balance (Quintix 224-1S, Sartorius, Göttingen, Germany). For determination of the CDW, 10 mL culture broth was sampled into the pre-dried tubes. Again, the exact sample amount of the remaining sample was determined on an analytical balance (Quintix 224-1S, Sartorius, Göttingen, Germany). Cells were harvested by centrifugation (10 min, 9800 x *g*, 4 °C) and washed three times with deionized water. Finally, the samples were dried at 80 °C to a constant weight and weighed again. Parallel analysis of CDW and OD_{660} yielded a linear correlation (Figure 4-1).The resulting correlation factor was CDW [g L^{-1}] = 0.352 x OD_{660}. All measurements were conducted in three biological replicates.

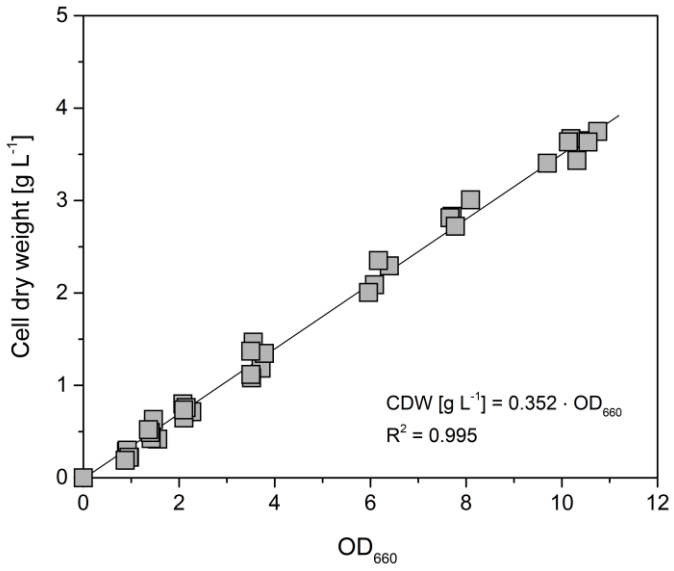

Figure 4-1: Correlation between optical density (OD_{660}) and cell dry weight for *C. glutamicum* SEA-1 grown on mannitol as carbon source.

4.9.2 Quantification of amino acids

Culture supernatant (5 min, 8800 x *g,* 4 °C) was diluted 1:10 with internal standard solution (α-amino butyric acid, 222.22 µM) on an analytical balance (Quintix 224-1S, Sartorius, Göttingen, Germany). The amino acids were separated using HPLC (Agilent 1200 Series, Agilent Technology, Waldbronn, Germany) on a reversed phase column (Gemini, 5 µm, C18, 110 A, 150 x 4.6 mm, Phenomenex, Aschaffenburg, Germany) and a guard pre-column (SecurityGuard Cartriges, Gemini C18, 4 x 3 mm; Phenomenex). After automatic pre-column derivatization with *o*-phthalaldehyde (OPA), samples were injected into the system and separated with a gradient of eluent A (40 mM NaH_2PO_4, pH 7.8) and eluent B (45 % (v/v) methanol, 45 % (v/v) acetonitrile and 10 % (v/v) water) with a flow rate of 1 mL min^{-1} at 40 °C (Krömer et al. 2005). Separation of proteinogenic amino acids was performed according to the standard protocol in Table 4-17. A shorter protocol was applied for the quantification of only L-lysine, L-glutamate, L-glycine, and L-alanine. Here, the separation was carried out on a reversed phase column (Gemini, 3 µm, C18, 110 A, 100 x 4.6 mm, Phenomenex) equipped with a pre-column as described above. Detection was performed by fluorescence measurement (340 nm excitation, 540 nm emission; fluorescence detector G1321A, Agilent Technologies, Waldbronn, Germany) and quantification was based on α-amino butyric acid (222.22 µM) as internal standard (Krömer et al. 2005).

Table 4-17: Gradient of eluent A (40 mM NaH_2PO_4, pH 7.8) and B (45 % (v/v) methanol, 45 % (v/v) acetonitrile and 10 % (v/v) water) for separation and quantification of amino acids.

Standard protocol			**Short protocol**		
Time [min]	Eluent A [%]	Eluent B [%]	Time [min]	Eluent A [%]	Eluent B [%]
0.00	100.0	0.0	0.00	100.0	0.0
44.50	55.5	44.5	12.50	37.5	62.5
45.00	39.0	61.0	13.00	0.0	100.0
47.00	39.0	51.0	15.00	0.0	100.0
48.00	18.0	82.0	15.50	100.0	0.0
48.50	0.0	100.0	17.50	100.0	0.0
50.50	0.0	100.0			
51.00	100.0	0.0			
53.00	100.0	0.0			

4.9.3 Quantification of carbohydrates and organic acids

Quantification of trehalose and organic acids (lactate, acetate) was conducted by isocratic HPLC (1260 Infinity Series, Agilent Technology), using an Aminex HPX-87H column (300 x 7.8 mm, Bio-Rad, Hercules, CA, USA) at 55 °C with 50 mM H_2SO_4 as mobile phase and a flow rate of 0.5 ml min^{-1} (Barton et al. 2018). Detection and quantification of the analytes was performed via refraction index measurement and external standards.

Mannitol, glucose and fructose were quantified using HPLC (1260 Infinity Series, Agilent Technology) with a Metacarb 87C column (300 x 7.8 mm, Agilent Technology), preceded by a Metacarb 87C guard column (50 x 7.8 mm, Agilent Technology) and a desalting column (Micro-Guard Deashing Cartridge, Bio-Rad). Separation was carried out at 85 °C using demineralized water as mobile phase at a flow rate of 0.5 mL min^{-1}. Refraction index measurement was used for detection and external standards were used for quantification.

4.9.4 GC-MS analysis of ^{13}C labeling patterns

For ^{13}C labeling analysis, mass isotopomer distributions (MIDs) of amino acids from the cell protein of *C. glutamicum* were quantified by gas chromatography-mass spectrometry (GC-MS) (GC 7890A, 5975C quadrupole detector, Agilent Technologies) (Kiefer et al. 2004; Wittmann et al. 2002). For this purpose, cells (approximately 1 mg CDW) were harvested during the exponential growth phase (5 min, 8800 x *g*, 4 °C), washed two times with deionized water, and hydrolyzed in 6 M HCl for about 24 h (Wittmann 2007). Afterwards, the supernatant was clarified by filtration (0.2 µm, Merck, Millipore, Darmstadt, Germany) and then dried under nitrogen for about 20 min. The derivatization of proteinogenic amino acids was performed by adding 50 µL dimethylformamide (0.1 % pyridine) and 50 µL *N*-methyl-*N*-tert-butyldimethylsilyl-trifluoroacetamide (MBDSTFA; Macherey-Nagel, Düren, Germany) and incubating the mixture for 35 min at 80 °C (Krömer et al. 2004; Wittmann et al. 2002). GC-MS based analysis of the derivatized amino acids was carried out as described previously (Kiefer et al. 2004) using a temperature profile (Table 4-18) and an amino acid standard as reference. In order to exclude isobaric interference between the analytes of interest and the samples, samples were first measured in scan mode. Derivatization of amino acids with the reagent MBDSTFA resulted in a typical fragmentation pattern that comprised the following mass fragments: [M-57], [M-85], and [M-159]. For flux determination, only the [M-57] fragment,

containing the complete carbon backbone of the appropriate amino acid, was determined via selective ion monitoring (Wittmann 2007).

Table 4-18: Temperature profile of the GC oven used for the analysis of labeled amino acids.

Time [min]	Temperature [°C]
0.0	120
2.0	120
12.0	200
24.0	325
27.0	325

The obtained mass isotopomer distributions (MIDs) were corrected for natural isotope abundance (MID_{corr}) (van Winden et al. 2002) (see appendix Table 7-3) and used together with stoichiometric data on substrate uptake, product formation, growth and biomass composition for the calculation of metabolic fluxes in mannitol-grown *C. glutamicum* cells.

4.9.5 Qualitative quantification of seaweed hydrolysates

In order to determine carbohydrates from seaweed hydrolysates of *Laminaria digitata*, 1 mL extract was incubated at 80 °C for about 20 h. Subsequently 400 µL HCl (2 M) was added to the dried sample. Afterwards, the supernatant was clarified by filtration (0.2 µm, Merck, Millipore, Darmstadt, Germany) and then dried under nitrogen for about 20 min. Sample preparation included a two-step derivatization as previously described (Kiefer et al. 2004; Schwechheimer et al. 2018), however, only using another silylation reagent. In short, the dried supernatant was first resuspended in 50 µL pyridine (2 % methoxylamine) for 25 min at 80 °C and then derivatized with 50 µL *N*-methyl-*N*-trimethylsilyl-trifluoroacetamide (MSTFA; Macherey-Nagel, Düren, Germany) for 30 min at 80 °C. Determination of carbohydrates was carried out by GC-MS (GC 7890A, 5975C quadrupole detector, Agilent Technologies) using pure standards as reference (Kiefer et al. 2004; Krömer et al. 2008; Wittmann et al. 2002). The obtained derivates of carbohydrates were measured in scan mode. Table 4-19 represents the temperature profile used for analysis of carbohydrates present in *L. digitata* hydrolysates (glucose, fructose, mannitol).

Table 4-19: Temperature gradient used for GC-MS analysis of sugars.

Time [min]	Temperature [°C]
0.0	120
3.0	150
13.0	300
16.0	300
17.0	325

4.9.6 NMR analysis of ^{13}C labeling patterns

For ^{13}C NMR analysis, cells (approximately 50 mg CDW) were hydrolyzed for 12 h in 2 mL HCl (6 M) at 110 °C. The obtained hydrolysate was dried, washed twice in D_2O, and resuspended in 200 µL D_2O (0.1 % DCl, 1 mM 3-(trimethylsilyl)propionic-2,2,3,3-d_4 acid (TSPd_4)). NMR measurements were then performed on a Bruker Avance III spectrometer operating at 800 MHz proton frequency equipped with a QPCI cryogenic probe head at 280.0 K. The isotopic enrichment of the L-alanine carbons was obtained using a combination of 2D-zeroquantum filtered-TOCSY (ZQF-TOCSY) and 1D (^1H) ^{13}C with long d1 delay of 30 s to allow full relaxation of ^{13}C magnetization between scans. Briefly, the proton decoupled ^{13}C NMR provided the relative intensities of ^{13}C carbons only (^{12}C carbons were not detectable in a direct ^{13}C-NMR carbon experiment). The ZQF-TOCSY then gave access to the partition between ^{12}C- and ^{13}C-linked ^1H and furthermore to the ^{13}C specific enrichment of protonated carbons C_3 and C_2 of L-alanine. The ^{13}C enrichment of the L-alanine carbons C_1 and C_2 was then recalculated from the ^{13}C relative intensities between C_1, C_2 and C_3 from 1D ^{13}C, calibrated from the C_3 enrichment, measured with ZQF-TOCSY. For each sample, the signal to noise ratio (SNR) was measured either with ^{13}C 1D or 2D TOCSY acquisitions. The standard errors of the presented measurements were calculated from the respective SNR. NMR measurements were performed by Lindsay Peyriga and Edern Cahoreau (Institute Ingénierie des Systèmes Biologiques et des Procédés (INSA), Toulouse University, France)

4.10 Biochemical methods

4.10.1 Preparation of crude cell extract

Exponentially growing cells were harvested by centrifugation (5 min, 8800 x *g*, 4 °C), washed once with an enzyme specific disruption buffer (see below) and then resuspended to a final concentration of 1 g (cell wet mass) mL^{-1}. Cell disruption was then performed by mechanical treatment. Therefore, the extract was transferred to FastPrep-24 vials containing silica beads (0.1 mm diameter; MP Biomedicals, Illkirch-Graffenstaden, France) and then disrupted in a ribolyzer (5500 rpm, 2 x 30 s with 2 min break on ice, Precellys-24, Bertin Technologies, Montignyle-Bretonneux, France). Finally, cell debris was removed by centrifugation (5 min, 13000 x *g*, 4 °C).

4.10.2 Quantification of protein concentration

To quantify the protein content in cell extracts, the BCA protein assay kit (Pierce BCA Protein Assay Kit, Thermo Fisher Scientific, Rockford, IL, USA) was used according to the manufacturer's instructions, using bovine serum albumin (BSA) as calibration standard. In short, standard and sample dilution series were prepared on an analytical balance (Quintix 224-1S, Sartorius, Göttingen, Germany). After the samples were transferred to a 96-well microplate (Microtest Plate 96 Well.F, Sarstedt, Nümbrecht, Germany), the reaction was initiated by adding 200 µL of the BCA reagent mix, followed by incubation for 30 min at 37 °C. Afterwards, the measurement of absorption at 540 nm was conducted in a microplate reader (iEMS Reader MF, Labsystems, Thermo Electron Corporation LED GmbH, Langenselbold, Germany). All measurements were carried out in triplicate.

4.10.3 Quantification of enzyme activity

Determination of enzyme activity in crude cell extracts was conducted in a total volume of 1 mL in triplicate. The reactions were monitored by the change in absorbance at 340 nm, referring to the change of redox equivalents, in a spectrophotometer (SPECORD 50 Plus, Analytik Jena, Jena, Germany). Negative controls were carried out without substrate or crude cell extract, respectively. All measurements were conducted in the same way. For this purpose, a pre-warmed master mix without substrate and cell extract was prepared from stock solutions and used to initiate the reaction. All measurements were carried out in 1.5 mL cuvettes (Sarstedt, Nümbrecht, Germany) for 10 min at 30 °C. An extinction coefficient of ε_{340} = 6.22 L $mmol^{-1}$ cm^{-1} for NAD(P)H was

used to determine the enzyme activity based on the change in absorbance [A min^{-1}] at 340 nm. As an exception, the membrane-bound transhydrogenase was assayed at 375 nm. Enzyme activities are given as specific activity [U mg^{-1}] correlated to the protein concentration in the extract. One unit [U] was defined as 1 µmol per minute.

Fructokinase

For determination of fructokinase activity, cell disruption buffer containing 100 mM Tris-HCl (pH 7.8), 10 mM $MgCl_2$, and 0.75 mM dithiothreitol (DTT) was used. Activity measurement of fructokinase was adapted from previous work (Helanto et al. 2006) using phosphoglucose isomerase (PGI) and NADP-dependent glucose 6-phosphate dehydrogenase (G6PDH) as coupling enzyme, which allowed online monitoring via the change in absorbance at 340 nm. The assay was performed at 30 °C in a total volume of 1 mL, containing 100 mM Tris-HCl (pH 7.8), 10 mM $MgCl_2$, 1 mM NADP, 1 U glucose 6-phosphate dehydrogenase, 2 U phosphoglucose isomerase, 2 mM ATP, 2 mM fructose, and 25 µL crude cell extract.

Mannitol 2-dehydrogenase

Preparation of crude cell extract was performed using 100 mM Tris-HCl (pH 7.8), 10 mM $MgCl_2$, and 0.75 mM DTT as disruption buffer. The activity measurement of mannitol 2-dehydrogenase, adapted from previous work (Peng et al. 2011), was performed in 1 mL disruption buffer, additionally containing 25 µL crude cell extract, 80 mM mannitol, and 1 mM NAD and NADP, respectively, at 30 °C.

Glyceraldehyde 3-phosphate dehydrogenase

Prior to determination of glyceraldehyde 3-phosphate dehydrogenase (GapDH) activity, cells were disrupted in 100 mM Tris-HCl (pH 8.3), 10 mM $MgCl_2$, and 0.75 mM DTT. The activity of GapDH was measured at 30 °C as previously described (Crow and Wittenberger 1979). The activity of GapDH was analyzed at 30 °C in 1 mL 100 mM Tris-HCl buffer, containing 25 µl crude cell extract, 2 mM glyceraldehyde 3-phosphate, and either 1 mM NAD^+ or $NADP^+$, respectively, to assay both variants, i.e. the native NAD-dependent glyceraldehyde 3-phosphate dehydrogenase (GapA) and the NADP-dependent glyceraldehyde 3-phosphate dehydrogenase (GapN).

Malic enzyme

Cells were disrupted in a buffer containing 100 mM Tris-HCl (pH 7.8), 200 mM KCl, and 0.75 mM DTT. Malic enzyme activity was then analyzed at 30 °C as described previously (Gourdon et al. 2000) using a total volume of 1 mL, containing 100 mM Tris-HCl (pH 7.8), 200 mM KCl, 2 mM $MgCl_2$, 1 mM NADP, 40 mM malate, and 50 µL crude cell extract. Malate was added from a stock solution (1 M Tris-HCl, pH 7.8).

Membrane-bound transhydrogenase

The protocol for analysis of membrane-bound transhydrogenase (PntAB) was adapted from previous work (Kabus et al. 2007). In short, a membrane fraction was prepared from cells, harvested by centrifugation (10 min, 4500 x *g*, 4 °C), and washed with one culture volume of TE buffer (10 mM Tris-HCl, 1 mM EDTA, pH 8.0). The cell pellet was resuspended in 1 mL TE buffer, containing 40 µL complete protease inhibitor (Roche Diagnostics, Penzberg, Germany). Cells were then transferred into FastPrep-24 vials and disrupted as described above (see chapter 4.10.1). Cell debris was removed by centrifugation (20 min, 5000 x *g*, 4 °C). The obtained crude extract was subjected to ultracentrifugation (90 min, 150,000 x *g*, 4 °C). The sedimented membrane fraction was washed in 1 mL Tris-HCl buffer (10 mM, pH 8.0) and subsequently resuspended in 0.5 mL of the same buffer. Transhydrogenase activity was then analyzed in a 1 mL mixture containing 50 mM potassium phosphate (pH 7.0), 100 mM NaCl, 10 mM ß-mercaptoethanol, 0.1 mM NADPH, 0.1 mM 3-acetylpyridine-NAD^+, and 25 µL of resuspended membrane protein solution, monitoring the increase in absorbance at 375 nm. The assay was performed with a spectrophotometer (SPECORD® 50 Plus, Analytik Jena, Jena, Germany) at 30 °C. One unit of activity was defined as 1 µmol 3-acetylpyridine-NADH produced per minute.

4.11 Fluxomics

4.11.1 Metabolic modeling and flux estimation

The metabolic network of ^{13}C flux analysis of mannitol-grown *C. glutamicum* cells considered all relevant carbon core pathways, i.e. the EMP pathway, the PP pathway, the TCA cycle, and anaplerotic carboxylation and decarboxylation reactions. In addition, the biosynthetic routes of L-lysine as well as relevant by-products and precursors of anabolic pathways into biomass (Becker et al. 2011) were implemented. For the analysis of mutant strains, the network considered the genetic modifications introduced case wise, i.e. (i) mannitol uptake by the native mannitol/ribitol transporter (MtlT/RbtT), (ii) mannitol oxidation into fructose by the native mannitol 2-dehydrogenase (MtlD), (iii) phosphorylation of fructose into fructose 1-phosphate by the native fructose-specific phosphotransferase system (PTS_{Frc}), (iv) phosphorylation of fructose into fructose 6-phosphate by heterologous fructokinase (Mak), (v) NADP-dependent conversion of glyceraldehyde 3-phosphate into 3-phosphoglycerate by heterologous glyceraldehyde 3-phosphate dehydrogenase (GapN), and (vi) interconversion of oxidized/reduced NADP(H) by heterologous membrane-bound transhydrogenase (PntAB), respectively. The flux approach assumed steady-state of the investigated cells, which was verified for the conducted experiments from metabolic and isotopic analysis (Figure 5-4, Figure 7-2 - 7-5, Table 5-9, Table 5-11).

Since mannitol is a symmetric molecule, labeling studies using mannitol tracers, i.e. parallel studies with [1-^{13}C] mannitol and an equimolar mixture of naturally labeled plus [$^{13}C_6$] mannitol, respectively, did not provide an unique flux optimum with fine structures such as bidirectional and reversible reactions, of a fully resolved network by using global parameter estimation. Therefore, the major net fluxes through central carbon core metabolism were determined using a simplified approach, which was based on metabolite balancing and selected labeling information (Hoffmann et al. 2018).

Relative oxidative PP pathway flux on glucose and fructose, respectively. First, the relative flux into the oxidative PP pathway, i.e. the flux via glucose 6-phosphate dehydrogenase (v_{Zwf}), was determined by an isotope experiment with 99 % [1-^{13}C] glucose and [1-^{13}C] fructose, respectively. Cells, grown on the tracer were analyzed for the ^{13}C labelling pattern of proteinogenic L-alanine (see appendix Table 7-3). The lower boundary (Ib) for the entry flux into the PP pathway at the level of glucose 6-phosphate dehydrogenase ($v_{Zwf,lb}$) was determined from the ratio between the fraction of the single labeled (M+1) and the non-labeled mass isotopomer (M) of L-alanine ($I_{M+1/M}$), corrected

for natural isotope abundance (van Winden et al. 2002), using the followed equation (Eq. 1).

$$v_{Zwf,lb} = \frac{1 - I_{M+1/M}}{1 + {}^{2}/_{3} \cdot I_{M+1/M}} \cdot 100 \qquad \text{(Eq. 1)}$$

The obtained result for $v_{Zwf,lb}$ was used to derive the relative flux into the oxidative PP pathway (v_{Zwf}), using a correlation factor ($f = 1.49$) according to Eq. 2

$$v_{Zwf} = f \cdot v_{Zwf,lb} \qquad \text{(Eq. 2)}$$

The obtained value also represented the flux through 6-phosphogluconate dehydrogenase (v_{Gnd}), downstream of glucose 6-phosphate dehydrogenase. The correlation factor f was derived from previous flux studies of *C. glutamicum*, which revealed a constant ratio between ($v_{Zwf,lb}$) and (v_{Zwf}) (see appendix Table 7-2). The ^{13}C flux data of wild type and twelve L-lysine-producing strains, demonstrating this, were taken from previous work (Becker et al. 2011).

Relative oxidative PP pathway flux on mannitol. For mannitol, the lower boundary of the oxidative PP pathway flux was derived using Eq. 3. Cells, grown on the tracer were again analyzed for the ^{13}C labeling pattern of proteinogenic L-alanine (see appendix Table 7-3). Different to glucose and fructose, the calculation now considered the fact that the used tracer [1-^{13}C] mannitol was a symmetric molecule (Cherniak et al. 1998), which provided only 50 % [1-^{13}C] glucose 6-phosphate at the entry point into the oxidative PP pathway, so that the labeling release in the PP pathway was roughly halved.

$$v_{Zwf,lb} = 2 \cdot \frac{1 - I_{M+1/M}}{1 + {}^{2}/_{3} \cdot I_{M+1/M}} \cdot 100 \qquad \text{(Eq. 3)}$$

Subsequently, the relative flux through glucose 6-phosphate dehydrogenase (v_{Zwf}) and 6-phosphogluconate dehydrogenase (v_{Gnd}) was again calculated using Eq. 2 (see appendix Table 7-4).

Fluxes at the fructose node in the SEA-1 strain (see appendix Table 7-5). The flux of fructose phosphorylation ($v_{Frc,in}$), i.e. the carbon flux entering central metabolism, directly resulted from the measured flux of mannitol uptake ($v_{Mtl,in}$) and fructose accumulation ($v_{Frc,out}$) (Eq. 4). It matched the flux of the fructose specific phosphotransferase system PTS_{Frc} (Eq. 5).

$$v_{Frc,in} = v_{Mtl,in} - v_{Frc,out} \quad \text{(Eq. 4)}$$

$$v_{PTS,Frc} = v_{Frc,in} \quad \text{(Eq. 5)}$$

Fluxes at the fructose node in the strains harboring fructokinase activity (see appendix Table 7-5). In strains SEA-2B, SEA-3, and SEA-7, the total flux of fructose phosphorylation was split between the PTS_{Frc} and the additionally expressed fructokinase (Mak). Here, it was assumed that the observed flux increase into the oxidative PP pathway, as compared to the parent strain SEA-1 without fructokinase activity, was exclusively due to the novel enzyme (Eqs. 6 A-C). This appeared justified, because the massive amplification of fructose 1,6-bisphosphate and the entire *tkt*-operon, already in place in the parent strain (Becker et al. 2011), obviously failed to push carbon into the PP pathway. The PTS_{Frc} flux was then derived by balancing (Eq. 7).

$$v_{Mak,SEA-2B} = v_{Zwf,SEA-2B} - v_{Zwf,SEA-1} \quad \text{(Eq. 6 A)}$$

$$v_{Mak,SEA-3} = v_{Zwf,SEA-3} - v_{Zwf,SEA-1} \quad \text{(Eq. 6 B)}$$

$$v_{Mak,SEA-7} = v_{Zwf,SEA-7} - v_{Zwf,SEA-1} \quad \text{(Eq. 6 C)}$$

$$v_{PTS,Frc} = v_{Frc,in} - v_{Mak} \quad \text{(Eq. 7)}$$

Flux through the lower glycolysis at the level of glyceraldehyde 3-phosphate dehydrogenase in strains SEA-1, SEA-2B, and SEA-2-D (see appendix Table 7-6). The flux through the native glyceraldehyde 3-phosphate dehydrogenase GapA (v_{GapA}) was obtained by balancing. The calculation considered the influx from fructose ($v_{Frc,in}$), the lumped flux withdrawing carbon above the glyceraldehyde 3-phosphate node, i.e. the formation of trehalose ($v_{G6P,Tre}$) (Table 5-8 and Table 5-10), the demand for anabolism, and the carbon dioxide release in the PP pathway (Eq. 8). The demand for

anabolism was taken from the biomass yield (Table 5-8 and Table 5-10), and the cellular composition of *C. glutamicum* (Wittmann and de Graaf 2005).

$$v_{GapA} = (v_{Frc,in} - v_{G6P,Tre} - v_{G6P,Ana} - v_{F6P,Ana} - v_{R5P,Ana} - v_{E4P,Ana} - v_{Gap,Ana} - {}^{v_{Zwf}}/_{6}) \cdot 2 \quad \text{(Eq. 8)}$$

Flux through the lower glycolysis at the level of glyceraldehyde 3-phosphate dehydrogenase in strains SEA-3 and SEA-7 (see appendix Table 7-6). SEA-3 and SEA-7 exhibited two enzymes, catalyzing the conversion of glyceraldehyde 3-phosphate into 1,3-bisphosphoglycerate and 3-phosphoglycerate, respectively: the native NAD-dependent (GapA) and the heterologous NADP-dependent glyceraldehyde 3-phosphate dehydrogenase (GapN). The relative contribution of both enzymes was derived by assuming that the contribution of GapA was the same as in the previous SEA-2B strain (Eqs. 9 A and B), and that GapN matched the glycolytic flux increase resulting from its heterologous expression (Eq. 10 A and B).

$$v_{GapA,SEA-3} = v_{GapA,SEA-2B} \quad \text{(Eq. 9 A)}$$

$$v_{GapA,SEA-7} = v_{GapA,SEA-2B} \quad \text{(Eq. 9 B)}$$

$$v_{GapN,SEA-3} = \left(\left(v_{Frc,in} - v_{G6P,Tre} - v_{G6P,Ana} - v_{F6P,Ana} - v_{R5P,Ana} - v_{E4P,Ana} - v_{Gap,Ana} - {}^{v_{Zwf}}/_{6}\right) \cdot 2\right) - v_{GapA,SEA-2B}$$

(Eq. 10 A)

$$v_{GapN,SEA-7} = \left(\left(v_{Frc,in} - v_{G6P,Tre} - v_{G6P,Ana} - v_{F6P,Ana} - v_{R5P,Ana} - v_{E4P,Ana} - v_{Gap,Ana} - {}^{v_{Zwf}}/_{6}\right) \cdot 2\right) - v_{GapA,SEA-2B}$$

(Eq. 10 B)

Flux through the lower glycolysis at the level of enolase in the SEA-1, SEA-2B, and the SEA-2D strain (see appendix 7-7). The flux through enolase (v_{Eno}) was derived by stoichiometric balancing according to Eq. 11, considering the withdrawal of 3-phosphoglycerate for L-glycine formation (Table 5-8 and Table 5-10) and anabolism. The latter was taken from the biomass yield (Table 5-8 and Table 5-10), determined for each strain, and the cellular composition of *C. glutamicum* (Wittmann and de Graaf 2005).

$$v_{Eno} = v_{GapA} - v_{3P,Ana} - v_{3P,Gly} \quad \text{(Eq. 11)}$$

Flux through the lower glycolysis at the level of enolase in the SEA-3 and SEA-7 strain (see appendix Table 7-7). The flux through enolase (v_{Eno}) was derived by stoichiometric balancing according to Eq. 12, considering the withdrawal of 3-phosphoglycerate for L-glycine formation (Table 5-9 and Table 5-11) and anabolism. The latter was taken from the biomass yield (Table 5-9 and Table 5-11), determined for each strain, and the cellular composition of *C. glutamicum* (Wittmann and de Graaf 2005).

$$v_{Eno} = v_{GapA} + v_{GapN} - v_{3P,Ana} - v_{3P,Gly} \quad \text{(Eq. 12)}$$

Flux through anaplerotic carboxylation (see appendix Table 7-8). The lumped net flux through anaplerosis ($v_{Pyc,net}$), fueling the TCA cycle via carboxylation of glycolytic carbon three intermediates, was calculated via stoichiometric balancing as described previously (Wittmann and Heinzle 2002). The calculation (Eq. 13) considered the withdrawal of oxaloacetate and α-ketoglutarate for L-lysine formation and L-glutamate formation, respectively (Table 5-8, Table 5-9 and Table 5-11). In addition, the anabolic demand of the two precursors was determined from the biomass yield (Table 5-8, Table 5-9 and Table 5-11) and the cellular composition of *C. glutamicum* (Wittmann and de Graaf 2005).

$$v_{Pyc,net} = v_{OAA,Ana} + v_{Akg,Ana} + v_{Akg,Glu} + v_{OAA,Lys} \quad \text{(Eq. 13)}$$

Flux through pyruvate dehydrogenase (see appendix Table 7-9). The flux through pyruvate dehydrogenase at the entry into the TCA cycle (v_{Pdh}) was calculated via stoichiometric balancing. The calculation (Eq. 14) considered the withdrawal of pyruvate for L-lysine and by-product formation (Table 5-8, Table 5-9 and Table 5-11). In addition, the anabolic demand of phosphoenolpyruvate and pyruvate was inferred from the biomass yield (Table 5-8, Table 5-9, and Table 5-11) and the cellular composition of *C. glutamicum* (Wittmann and de Graaf 2005).

$$v_{Pdh} = v_{Eno} - v_{PEP,Ana} - v_{Pyr,Ana} - v_{Pyc,net} - v_{Pyc,Lac} - v_{Pyr,Ala} - v_{Pyr,Lys} \quad \text{(Eq. 14)}$$

Fluxes through the TCA cycle (see appendix Table 7-10). The relative TCA cycle flux at the level of citrate synthase (v_{Cis}), isocitrate dehydrogenase (v_{Icd}), and α-ketoglutarate dehydrogenase (v_{Akd}) was calculated via stoichiometric balancing (Eq. 15 and 16), assuming an inactive glyoxylate shunt (Wittmann and Heinzle 2002). The anabolic demand for acetyl-CoA and α-ketoglutarate was taken from the biomass yield (Table 5-8, Table 5-9, and Table 5-11) and the cellular composition of *C. glutamicum* (Wittmann

and de Graaf 2005). In addition, the withdrawal of α-ketoglutarate for L-glutamate formation was considered.

$$v_{Cis} = v_{Icd} = v_{Pdh} - v_{AcCoA,Ana} \quad \text{(Eq. 15)}$$

$$v_{Akd} = v_{Cis} - v_{Akg,Ana} - v_{Akg,Glu} \quad \text{(Eq. 16)}$$

Flux through malic enzyme (see appendix Table 7-12). The relative flux through malic enzyme (v_{Mae}) was inferred using a combined approach of *in vitro* activity analysis and NADPH balancing. Hereby, the enzyme assay revealed the presence or absence of the enzyme (via the measured *in vitro* activity) and the upper boundary of the malic enzyme flux (Lange et al. 2017). Malic enzyme was found active in all cases (see appendix Table 7-11). *C. glutamicum* naturally generated NADPH by the following reactions: glucose 6-phosphate dehydrogenase (v_{Zwf}), 6-phosphogluconate dehydrogenase, (v_{Gnd}), isocitrate dehydrogenase (v_{Icd}), and malic enzyme (v_{Mae}). The mutant SEA-7 potentially supplied additional NADPH using heterologous NADP-specific glyceraldehyde 3-phosphate dehydrogenase (v_{GapN}). On the other hand, NADPH was required for anabolism ($v_{NADPH,Anabolism}$) and L-lysine-formation, i.e. 4 NADPH per L-lysine (Kiefer et al. 2004; Wittmann and de Graaf 2005; Wittmann and Heinzle 2001a). While glucose-grown *C. glutamicum* might exhibit an apparent excess of supplied NADPH under certain situations, an apparent shortage has not been described, when using ^{13}C metabolic flux analysis (Wittmann and de Graaf 2005; Wittmann and Heinzle 2002). In addition, the extremely low PP pathway flux of mannitol-grown cells did not make an apparent NADPH excess likely (Figure 5-5, Figure 5-18, and Figure 5-23). It therefore appeared justified to infer the flux of malic enzyme in strains SEA-1, SEA-2D, and SEA-7 from an inspection of the redox balance (Eq. 17) and use the enzymatic constraint as an additional validation. The relative contribution of malic enzyme in strains SEA-2D and SEA-7 (both additionally expressing the membrane-bound transhydrogenase PntAB) was assumed to be equal to that of SEA-1, based on the malic enzyme activity (see appendix Table 7-11).

$$v_{Mae} = v_{NADPH,Anabolism} + 4v_{Lys} - v_{Zwf} - v_{Gnd} - v_{GapN} - v_{Icd} \quad \text{(Eq. 17)}$$

Flux through membrane bound transhydrogenase (see appendix Table 7-14). The relative flux through the membrane-bound transhydrogenase (v_{PntAB}) in strain SEA-2D and SEA-7 was inferred again using redox balancing. As for malic enzyme, enzymatic analysis of the transhydrogenase was used as a validation constraint (see appendix Table 7-13).

$$v_{PntAB} = v_{NADPH,Anabolism} + 4v_{Lys} - v_{zwf} - v_{Gnd} - v_{GapN} - v_{Icd} - v_{Mae} \quad \text{(Eq. 18)}$$

4.11.2 Summed fractional labeling

In order to calculate the summed fractional labeling (SFL), i.e. the total ^{13}C enrichment of the carbon backbone of a compound with n atoms (Christensen et al. 2000), the obtained MIDs were corrected for natural isotopes (MID_{corr}) according to Eq. 19. The obtained SFL data were expressed as percentage. While 100 % means that no carbon is split off from the carbon skeleton of the compound and a fully labeled ^{13}C carbon backbone is obtained, i represents the number of ^{13}C atoms of the underlying isotopomer

$$SFL = \sum_{i=1}^{n+1} \frac{i \cdot MID_{i,corr}}{n} \cdot 100 \quad \text{(Eq. 19)}$$

4.11.3 *In silico* pathway modeling

To predict theoretical (maximum) yields, optimal pathway usage and identify promising genetic targets for strain engineering, elementary flux mode analysis was applied (Melzer et al. 2009). The genome scale model of *C. glutamicum* was used as a template to derive a large-scale model with all pathways relevant for this work (Kjeldsen and Nielsen 2009). The large-scale metabolic network comprised all central metabolic pathways including the PP pathway, the EMP pathway, the TCA cycle and reactions for the interconversion of C_4 metabolites of the TCA cycle and C_3 metabolites of glycolysis. For the modeling of mutants, the network was extended by the mannitol utilization pathway, by heterologous fructokinase (Mak), the transhydrogenase (PntAB), and NADP-dependent glyceraldehyde 3-phosphate dehydrogenase (GapN) reactions (see appendix Table 7-15). The cellular composition of *C. glutamicum* cells was inferred from previous work (Wittmann and de Graaf 2005).

4.12 Analysis of the cellular redox state

The protocol used for quenching the intracellular metabolism during sampling was adapted from previous work (Moritz et al. 2000; Wittmann et al. 2004c). Therefore, 5 mL culture broth was mixed with 10 mL pre-cooled methanol (-58 °C, 60 % (v/v)) and centrifuged (5 min, 9400 x *g*, -10 °C). The temperature of quenched samples was always kept below -20 °C. The obtained cell pellet was directly used for extraction.

For extraction of nicotinamide adenine dinucleotides the protocol according to the manufacturer's instructions was applied (EnzyChrom™ $NAD(P)^+$/NAD(P)H Assay Kit; BioAssay System, Hayward, CA, USA). Cells were washed in ice-cold PBS buffer (Table 4-20) and harvested (5 min, 9400 x *g*, 4 °C). Since the applied assay could not distinguish between oxidized and reduced nicotinamide adenine dinucleotides, extraction of NAD^+/$NADP^+$ and NADH/NADPH was performed separately. For later determination of $NAD(P)^+$ the cell pellet was resuspended in $NAD(P)^+$ extraction buffer, while for determination of NAD(P)H the cell pellet was resuspended in NAD(P)H extraction buffer. Afterwards, the extracts were kept for 5 min at 60 °C. Subsequently, 20 µL assay buffer was added. In addition, 100 µL of the opposite extraction buffer was added to neutralize the extracts. After mixing, debris was separated by centrifugation (5 min, 9400 x *g*, 4 °C), and the supernatant was used for quantification of the NAD^+/NADH and the $NADP^+$/NADPH ratio using the EnzyChrom™ NAD^+/NADH Assay Kit (E2ND-100; BioAssay System, Hayward, CA, USA) and EnzyChrom™ $NADP^+$/NADPH Assay Kit (ECNP-100; BioAssay System, Hayward, CA, USA), respectively.

Table 4-20: Composition of PBS-buffer

PBS-buffer	
NaCl (137 mM)	8 g
Na_2HPO_4 (10 mM)	1.42 g
KH_2PO_4 (1.98 mM)	0.27 g
KCl (2.7 mM)	0.2 g
HCl	pH 7.4
Add 1 L H_2O	

Nicotinamide adenine dinucleotides were quantified using enzymatic cycling as described previously (Bernofsky and Swan 1973; Matsumura and Miyachi 1980). For

quantification of NAD^+/NADH, lactate dehydrogenase based cycling was applied. In the initial reaction, lactate was oxidized into pyruvate via LDH. The formed NADH reduced a formazan reagent (MTT), which was detected at 565 nm. The quantification of $NADP^+$/NADPH was based on glucose dehydrogenase cycling. Glucose 6-phosphate (G6P) was converted into 6-phosphogluconate (6PG) and the formed NADPH reduced a formazan reagent, which was detectable at 565 nm. The measured change in absorbance was proportional to the concentration of NAD^+/NADH and $NADP^+$/NADPH, respectively. The quantification of nicotinamide adenine dinucleotides was carried out in a 96-well plate (Microtest Plate 96 Well.F, Sarstedt, Nümbrecht, Germany). For this purpose, 40 µL of a sample or standard was added per well. As standard, a NAD^+ and $NADP^+$ dilution series (0 to 10 µM) was prepared on an analytical balance (Quintix 224-1S, Sartorius, Göttingen, Germany). The measurement was then conducted in a microplate reader (iEMS Reader MF, Labsystems, Thermo Electron Corporation LED GmbH, Langenselbold, Germany) for 15 min (NAD^+/NADH) and 30 min ($NADP^+$/NADPH). All measurements were carried out in triplicate.

4.13 Statistical analysis

All data shown are expressed as mean value ± standard deviation. For significance analysis, the data were subjected to one-way analysis of variance (ANOVA), followed by the Fisher's Least Significant Difference (LSD) test and Duncan’s multiple range test. Values were considered statistically significant, when the P value was less than 0.05 ($P < 0.05$, *). The software SPSS 24.0 (SPSS Inc, Chigaco, IL, USA) was used for statistical analysis.

5 Results and Discussion

5.1 Activation of mannitol utilization in *C. glutamicum*

5.1.1 Deletion of the mannitol repressor protein MtlR

The use of seaweed as a third-generation renewable is of great advantage for the sustainable production of industrially relevant products (Goh and Lee 2010), because it requires no arable land, but only water, sunlight and CO_2. Seaweed is abundant in nature and contains up to 55 % of dry weight of carbohydrates (Wei et al. 2013). Especially members of the group of brown macroalgae, including *Laminaria digitata* and *Laminaria japonica* are rich in mannitol, a six carbon polyol, which constitutes up to 30 % of their dry weight (Iwamoto and Shiraiwa 2005; van Hal et al. 2014). Due to this, the utilization of mannitol by *C. glutamicum* is of great interest. Initial studies investigated whether *C. glutamicum* was able to naturally utilize mannitol. The recently created L-lysine hyperproducing strain *C. glutamicum* LYS-12 was grown on minimal medium with mannitol as the sole carbon source (Figure 5-1).

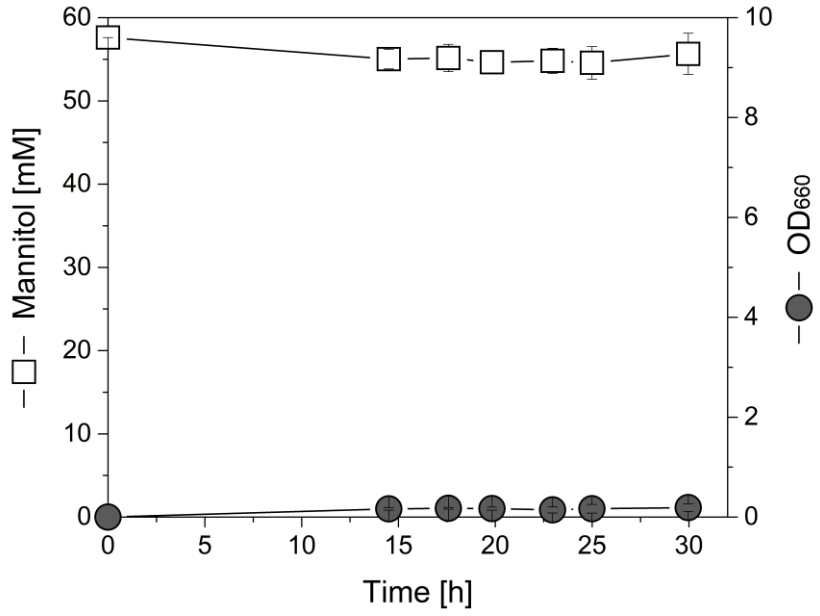

Figure 5-1: Growth experiment of L-lysine producing *C. glutamicum* LYS-12 (Becker et al. 2011) on mineral salt medium containing mannitol as sole carbon source. The data represent mean values and corresponding standard deviations from three biological replicates. When cultivated for an extended time (100 h), a spontaneous mutant arose, which was capable to utilize mannitol. Sequencing of this mutant revealed a point mutation in the *mtlR* gene, replacing L-alanine by L-valine at position 152 (A152V).

As shown, *C. glutamicum* LYS-12 was not able to utilize mannitol as the sole carbon source, unlike other bacteria such as *Escherichia coli* (Postma et al. 1993),

Clostridium acetobutylicum (Behrens et al. 2001), *Vibrio cholera* (Kumar et al. 2011) and *Streptococcus mutans* (Honeyman and Curtiss III 2000; Honeyman and Curtiss 1992). This seemed due to its constitutively expressed mannitol/arabitol dependent transcriptional repressor MtlR/AtlR (Laslo et al. 2012; Peng et al. 2011). For this reason, the initial strategy to extend the substrate spectrum of *C. glutamicum* LYS-12 to mannitol aimed at complete deletion of the *mtlR* gene from the genome. The introduction of the amino acid exchange A152V in the *mtlR* gene, suggested as alternative from sequencing of a spontaneously observed mannitol-using wild type mutant (Figure 5-1), was not considered because it appeared more sensitive to a potential reversal. Deletion of the *mtlR* gene from the genome of *C. glutamicum* LYS-12 was achieved by using the integrative pClik int *sacB* plasmid, harboring a 705 bp construct being composed of two homologous recombination sequences of 405 bp (upstream of the *mtlR* gene) and 300 bp (downstream of the *mtlR* gene), respectively (Table 4-1, appendix Table 7-1). The downstream construct contained 100 bp of the terminal end of the coding *mtlR* gene sequence. After confirmation of a positive clone after the second recombination using PCR and sequencing, the obtained strain was designated *C. glutamicum* SEA-1. It was tested for growth and production performance (Figure 5-2).

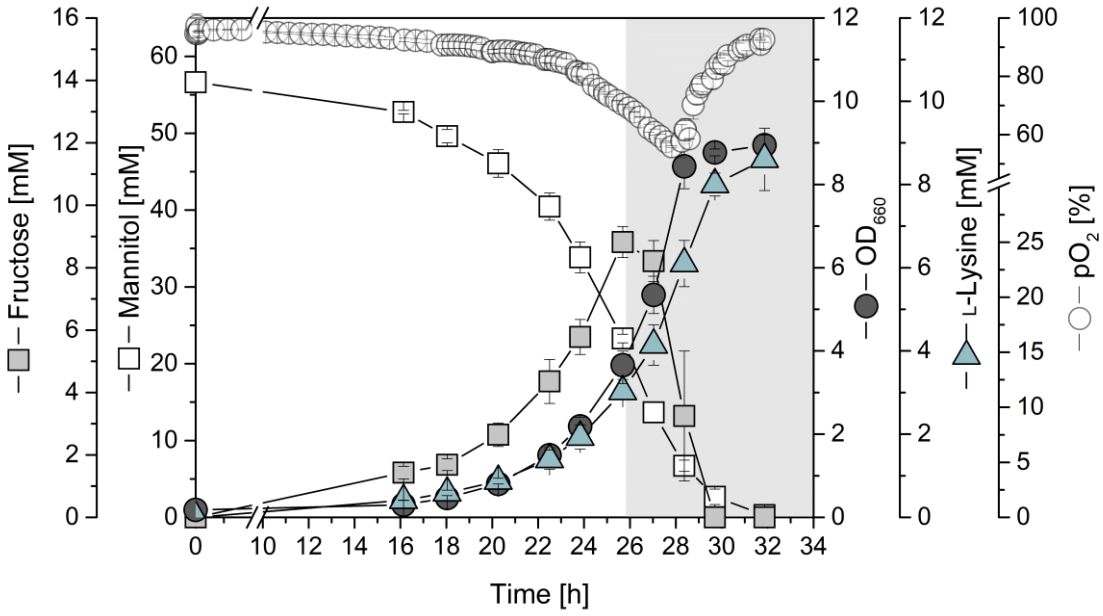

Figure 5-2: Growth and production characteristics of L-lysine producing *C. glutamicum* SEA-1 on mineral salt medium containing mannitol as the sole carbon source. The two phases of fructose accumulation (phase I) and fructose and mannitol consumption (phase II) are displayed in white and grey, respectively. The data represent mean values and corresponding standard deviations from three biological replicates.

When considering the cultivation profile of SEA-1, the deletion of the *mtlR* gene enabled utilization of mannitol. The mutant exhibited a specific growth rate and a biomass yield of $0.26 \pm 0.00\ h^{-1}$ and $54.3 \pm 2.2\ g\ mol^{-1}$, respectively (Table 5-1, and Table 5-2). L-Lysine was produced and excreted throughout the entire cultivation period, reaching a final titer of 8.7 mM L-lysine. Notably, SEA-1 revealed two phases: a main growth phase (phase I), in which mannitol was consumed and fructose, the intermediate product of mannitol oxidation, temporarily accumulated up to 8.8 mM, and a subsequent second phase (phase II), in which the accumulated fructose was again depleted and co-consumed together with the remaining mannitol (Figure 5-2 and 5-3). L-Lysine production differed between the two phases. While during the first phase L-lysine was formed at a yield of 90 mmol mol^{-1}, the yield was more than doubled (196 mmol mol^{-1}) during the second phase (Figure 5-3 and Table 5-1). The successful conversion of mannitol into L-lysine was an important proof of concept towards using *C. glutamicum* on the seaweed sugar.

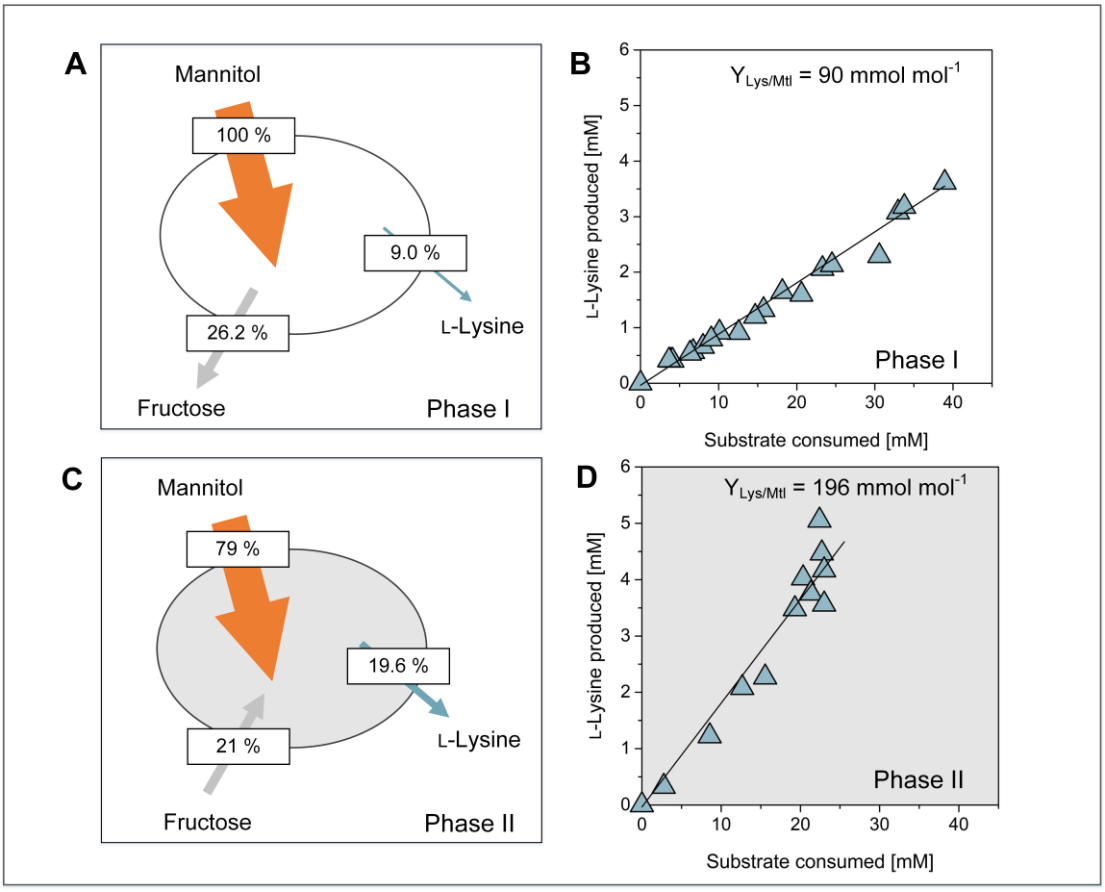

Figure 5-3: L-Lysine production of *C. glutamicum* SEA-1, related to the two cultivation phases (phase I and phase II) (Figure 5-2). The L-lysine yield in phase I referred to the consumption of mannitol (A, B), while the L-lysine yield in phase II referred to the joint consumption of mannitol and fructose (C, D). The two phases of fructose accumulation (phase I) (A, B) and re-consumption (phase II) (C, D) are displayed in white and grey, respectively. The data represent mean values and corresponding standard deviations from three biological replicates.

To check if SEA-1 was sufficiently aerated, the dissolved oxygen (pO_2) was monitored online. As shown in Figure 5-2, the pO_2 level did not drop below 50 %, confirming that the strain grew aerobically throughout the entire cultivation. Besides L-lysine, small levels of by-products (trehalose, L-glutamate, L-glycine, L-alanine, acetate, and lactate) were observed (Table 5-1).

Table 5-1: Growth and production characteristics of L-lysine producing *C. glutamicum* SEA-1 during the first phase (phase I, Figure 5-2) of batch cultivation on defined mineral salt medium with mannitol. The given data comprise the specific rates for growth (μ), mannitol uptake (q_{Mtl}), and L-lysine production (q_{Lys}) and the yields for L-lysine ($Y_{Lys/Mtl}$), biomass ($Y_{X/Mtl}$) and secreted by-products (fructose (Frc), trehalose (Tre), L-glycine (Gly), L-glutamate (Glu), lactate (Lac), acetate (Ace), and L-alanine (Ala)). The data represent mean values and deviations from three biological replicates.

Strain	SEA-1
Phase I	
μ [h^{-1}]	0.26 ± 0.00
q_{Lys} [mmol g^{-1} h^{-1}]	0.55 ± 0.10
q_{Mtl} [mmol g^{-1} h^{-1}]	6.1 ± 1.1
$Y_{Lys/Mtl}$ [mmol mol^{-1}]	90.1 ± 1.1
$Y_{X/Mtl}$ [g mol^{-1}]	40.2 ± 2.0
$Y_{Frc/Mtl}$ [mmol mol^{-1}]	262.1 ± 14.2
$Y_{Lac/Mtl}$ [mmol mol^{-1}]	9.9 ± 1.0
$Y_{Glu/Mtl}$ [mmol mol^{-1}]	6.3 ± 0.3
$Y_{Gly/Mtl}$ [mmol mol^{-1}]	2.3 ± 0.1
$Y_{Tre/Mtl}$ [mmol mol^{-1}]	2.6 ± 0.2
$Y_{Ace/Mtl}$ [mmol mol^{-1}]	1.8 ± 0.9
$Y_{Ala/Mtl}$ [mmol mol^{-1}]	0.7 ± 0.2

Table 5-2: Production performance of metabolically engineered *C. glutamicum* SEA-1 during growth on mannitol. The data comprise the mean specific rate for L-lysine production (q_{Lys}), and the yields for L-lysine ($Y_{Lys/Mtl}$) and biomass ($Y_{X/Mtl}$), calculated over the entire cultivation period. The kinetic and stoichiometric data represent mean values and deviations from three biological replicates.

Strain	SEA-1
q_{Lys} [mmol g^{-1} h^{-1}]	0.73 ± 0.02
$Y_{Lys/Mtl}$ [mmol mol^{-1}]	153.16 ± 11.5
$Y_{X/Mtl}$ [g mol^{-1}]	54.3 ± 2.2

However, in contrast to the higher L-lysine yield of the parent strain LYS-12 grown on glucose (Becker et al. 2011), *C. glutamicum* SEA-1 showed only weak performance on

mannitol. L-Lysine yield (153.16 mmol mol^{-1}) and specific L-lysine production rate (0.73 mmol g^{-1} h^{-1}) (Table 5-2) were far below the values of *C. glutamicum* LYS-12 grown on glucose (258.4 mol mol^{-1}, 1.2 mmol g^{-1} h^{-1}).

This posed the question, why the two substrates caused such a huge difference. Based on previous findings, the redox metabolism was inspected in more detail. Since four mole NADPH are required for the formation of one mole L-lysine, the supply of NADPH is crucial for L-lysine production (Wittmann and Heinzle 2001a). In live, ^{13}C tracer studies with *C. glutamicum* cells grown on glucose showed high PP pathway activity and consequently efficient L-lysine production (Becker et al. 2007; Becker et al. 2005; Becker et al. 2011). Due to the fact that NADPH in *C. glutamicum* is mainly generated through the PP pathway (Takeno et al. 2016; Wittmann and Heinzle 2002), the entry point of the applied carbon source into the carbon core metabolism has a strong influence on L-lysine production (Kiefer et al. 2002; Kiefer et al. 2004). Tracer studies with *C. glutamicum* revealed that fructose as a carbon source led to a significantly reduced PP pathway activity (14 %), because the carbon enters the lower glycolysis via fructose 1,6-bisphoshate, generating significantly less NADPH. As a consequence, L-lysine formation by fructose-grown *C. glutamicum* strains was reduced compared to glucose grown strains (Kiefer et al. 2004). *C. glutamicum* LYS-12, grown on glucose, confirmed the impact of the PP pathway flux. This strain showed a PP pathway activity of almost 84 %, obviously promoting superior L-lysine production (Becker et al. 2011). Since mannitol entered the lower glycolysis via fructose, it seemed that most substrate bypassed the PP pathway. It appeared important to study the mannitol-grown strain SEA-1 on the level of metabolic fluxes and get a direct insight into the use of the PP pathway on this substrate.

5.1.2 Metabolic fluxes of *C. glutamicum* SEA-1

Common methods to resolve metabolic fluxes in *C. glutamicum*, including studies on different sugars such as glucose (Kiefer et al. 2004; Wittmann and Heinzle 2002), fructose (Kiefer et al. 2004), sucrose (Wittmann et al. 2004a) and xylose (Buschke et al. 2013a) used parallel tracer studies and parameter estimations via computerized flux models. Hereby, position specific enrichment of ^{13}C in selected carbon atoms of the tracer substrate provided highly informative ^{13}C labeling patterns within the cell that could be used to deduce the flux information. However, mannitol is a symmetric molecule (Cherniak et al. 1998). As a result, parallel mannitol tracer studies (on 1-^{13}C and 50 % U-^{13}C) did not elucidate the intracellular metabolic fluxes to the same extent (data not shown). Accordingly, a simplified flux approach was established, which enabled to

infer the net fluxes through the core pathway without resulting exchange fluxes and flux reversibility. This approach used the ^{13}C labeling pattern of L-alanine to derive the lower boundary of the PP pathway flux in mannitol-grown cells (see Eq. 3, chapter 4.11.1). A correlation factor between this lower boundary and the real PP pathway flux was then obtained from glucose-grown cells and used to derive the true PP pathway flux on mannitol. Using metabolite balancing, the other net fluxes in the network could then be calculated. As described above, the flux via malic enzyme was estimated by redox balancing, additionally considering the measured activity of malic enzyme as a constraint and consistency check (see appendix Table 7-11). As depicted in Figure 5-4, SEA-1 exhibited metabolic steady state (indicated by the constant production performance). Isotopic steady-state was indicated by the constant ^{13}C labeling pattern of proteinogenic amino acids for growth on [1-^{13}C] mannitol. These findings demonstrated that the alternatively chosen flux approach was practicable.

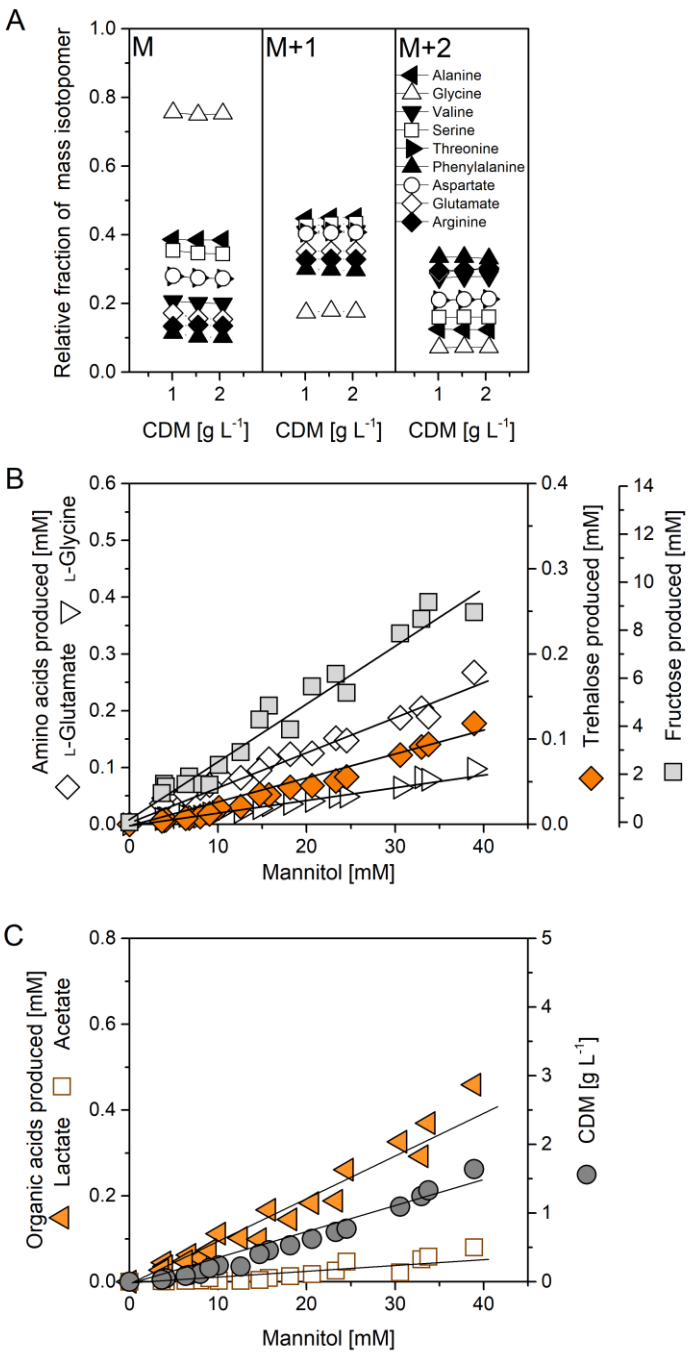

Figure 5-4: Verification of isotopic (A) and metabolic (B, C) steady-state of L-lysine-producing *C. glutamicum* SEA-1 on mineral salt medium containing mannitol as the sole carbon source. The data derived from three biological replicates and represent the initial growth phase of the cultivated *C. glutamicum* SEA-1 mutant, which was determined by fructose accumulation and is displayed in white in the cultivation profile (Fig. 5-2).

Figure 5-5 represents the metabolic flux distribution of *C. glutamicum* SEA-1 on mannitol.

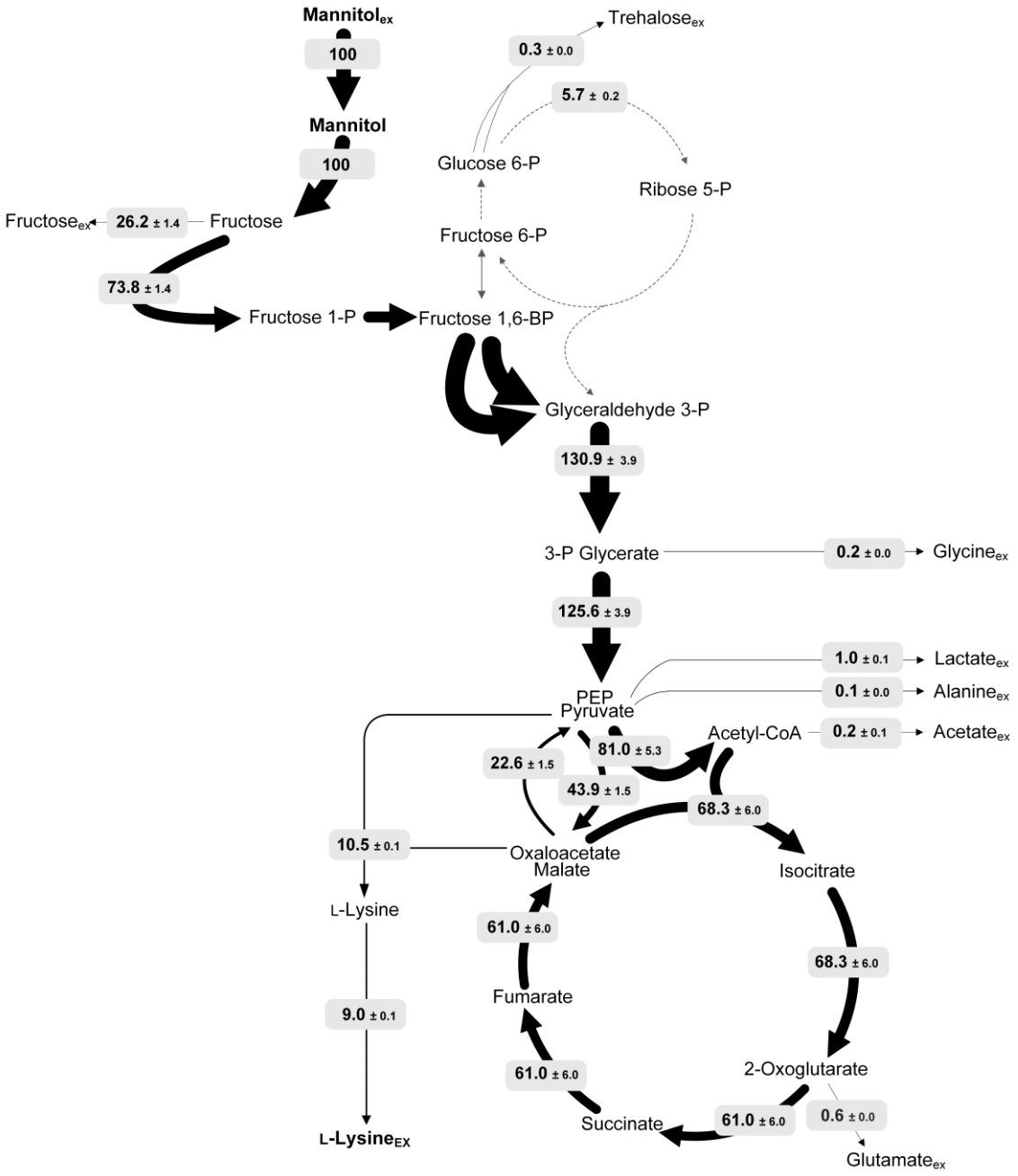

Figure 5-5: *In vivo* carbon flux distribution of L-lysine-producing *C. glutamicum* SEA-1 during growth on mineral salt medium containing mannitol as the sole carbon source. All fluxes are given as a molar percentage of the corresponding mean specific mannitol uptake rate (q_{Mtl} = 6.1 mmol g^{-1} h^{-1}), which was set to 100 %. The thickness of the reaction arrows represents the flux amount. The anabolic fluxes into biomass are not displayed.

It became obvious that only a minor part of carbon (6 %) was channeled through the PP pathway to generate NADPH. In contrast, a PP pathway flux of 84 % was observed for the parent strain *C. glutamicum* LYS-12 on glucose (Becker et al. 2011). Additional

insights into the PP pathway were gained from a quantitative inspection of the amounts of ^{13}C remaining in L-alanine on different [1-^{13}C] labeled substrates (Table 5-3).

Table 5-3: Isotopic labeling pattern of L-alanine obtained from *C. glutamicum* SEA-1 cells grown on 99 % [1-^{13}C] mannitol, 99 % [1-^{13}C] glucose, and 99 % [1-^{13}C] fructose, respectively. The table shows the summed fractional labeling (SFL) obtained via GC-MS (SFL_{MS}) and NMR (SFL_{NMR}), respectively. The data represent mean values and deviations from three biological replicates. For comparison the SFL of the substrates was 16.7 %.

Substrate	SFL_{MS} [%]	SFL_{NMR} [%]
[1-^{13}C] mannitol	16.6 ± 0.01	17.1 ± 0.4
[1-^{13}C] glucose	7.4 ± 0.00	n.d.*
[1-^{13}C] fructose	16.0 ± 0.01	n.d.*

*n.d. = not determined

Almost no ^{13}C label was cleaved off in [1-^{13}C] mannitol-grown SEA-1. The analysis by GC-MS (SFL_{MS}) and NMR (SFL_{NMR}) revealed values of 16.6 % and 17.1 %, practically identical to the ^{13}C enrichment of the substrate (Table 5-3). Comparative studies on [1-^{13}C] glucose indicated a much stronger use of the PP pathway (Table 5-3). The SFL_{MS} of L-alanine on [1-^{13}C] fructose was similar to that for mannitol and identified a similar weak use of the PP pathway (Table 5-3). Despite its genetically enhanced PP pathway (Becker et al. 2005; Becker et al. 2011), mannitol-grown SEA-1 revealed one of the lowest PP pathway fluxes ever observed in *C. glutamicum* (Becker et al. 2007; Becker et al. 2005; Becker et al. 2011; Buschke et al. 2013a; Kiefer et al. 2004; Kind et al. 2013; Wittmann and Heinzle 2002; Wittmann et al. 2004a).

The metabolic flux distribution for mannitol-grown *C. glutamicum* SEA-1 further revealed that mannitol was completely oxidized intracellularly into fructose (Figure 5-5). From there, the carbon was efficiently channeled via the fructose-specific phosphotransferase system (PTS_{Frc}) to the lower glycolysis (74 %), whereas the rest was excreted. It seemed that the NADH formed during mannitol oxidation was involved in fructose accumulation, since excess NADH has an impairing effect on glyceraldehyde 3-phosphate dehydrogenase in *C. glutamicum* (Kiefer et al. 2004; Yokota and Lindley 2005). *C. glutamicum* SEA-1 was not able to phosphorylate fructose inside the cell due to missing fructokinase activity (Moon et al. 2005; Moon et al. 2007). Regarding the large extent of fructose lost into the medium, the underlying export mechanism is not known (Moon et al. 2005; Moon et al. 2007). However, the observed overflow of fructose indicated a bottleneck in mannitol-grown SEA-1. Previous studies reported fructose excretion in *C. glutamicum* strains during growth on sucrose, which was assigned to

missing fructokinase activity in *C. glutamicum* (Dominguez and Lindley 1996; Moon et al. 2005; Moon et al. 2007). As a consequence of this pathway architecture, the carbon exclusively entered the lower glycolysis at the level of fructose 1,6-bisphosphate and was then directed to the lower glycolysis. Thus, *C. glutamicum* SEA-1 exhibited a high glycolytic flux at the level of glyceraldehyde 3-phosphate dehydrogenase (131 %). This high flux was to a large extent directed into the TCA cycle. The cycle carried much higher flux (68 % at the level of isocitrate dehydrogenase), as compared to glucose-grown *C. glutamicum* LYS-12 (31 %) (Becker et al. 2011).

A relatively low flux from the pyruvate node was channeled into the TCA cycle to oxaloacetate (44 %) and further towards L-lysine (11 %), as compared to glucose-grown LYS-12 (Becker et al. 2011). At the pyruvate node, a high cyclic flux (23 %) was observed between the oxaloacetate/malate pool and the PEP/pyruvate pool, much higher than the flux for glucose-grown LYS-12 (6 %) (Becker et al. 2011). Due to the deletion of the *pck* gene in SEA1, encoding for phosphoenolpyruvate carboxykinase (Becker et al. 2011), the back flux from the TCA cycle to the glycolysis was likely catalyzed by malic enzyme, eventually to generate additional NADPH (Eikmanns 2005; Wittmann and de Graaf 2005). Previous reports suggested that malic enzyme might serve as NADPH source during growth on lactate and fructose (Dominguez et al. 1998; Eikmanns 2005; Gourdon et al. 2000), which both are linked to a low PP pathway flux. Based on this work, the same seemed to be the case for mannitol. Taken together, the flux analysis provided the first insight into mannitol-grown *C. glutamicum* on the flux level and appeared valuable to guide further strain engineering.

5.1.3 Protein engineering of mannitol 2-dehydrogenase in *C. glutamicum*

In *C. glutamicum* mannitol is oxidized by mannitol 2-dehydrogenase into fructose, which is coupled to the reduction of NAD^+ into NADH. Hence, catabolism of mannitol delivers substantial amounts of NADH. Inherently, NADH has an inhibitory effect on glyceraldehyde 3-phosphate dehydrogenase, an important enzyme in the EMP pathway (Kiefer et al. 2004; Yokota and Lindley 2005). On top of the apparent excess for NADH, NADPH was obviously limiting (Figure 5-5). This imbalance suggested the engineering of redox metabolism as promising strategy (Chemler et al. 2010). First, we decided to improve the production performance of SEA-1 by engineering enzymatic cofactor specificity (Bommareddy et al. 2014; Cahn et al. 2017; Ma et al. 2010). Mannitol 2-dehydrogenase appeared as an excellent target, because a shift of its cofactor preference promised to kill two birds with one stone: eliminate the undesired NADH excess and NADPH limitation.

In this regard, a next round of metabolic engineering aimed to change the cofactor specificity of mannitol 2-dehydrogenase (MtlD), from NAD^+ to $NADP^+$. Based on computational modeling, a homology model of *C. glutamicum* MtlD was constructed, using the crystallographic protein structure of *Pseudomonas fluorescens* MtlD (pdb entry 1M2W.pdb) as template, since no crystallographic protein structure of *C. glutamicum* MtlD was available. The template structure revealed 44 % sequence identity and therefore suggested satisfying predictive power. To predict the putative position of the phosphate substituent in the $NADP^+$ molecule, the phosphate group was manually added to the crystal structure of *P. fluorescens* and energetically optimized.

The structure of the cofactor binding pocket of the obtained NADP-dependent mannitol 2-dehydrogenase is depicted in Figure 5-6.

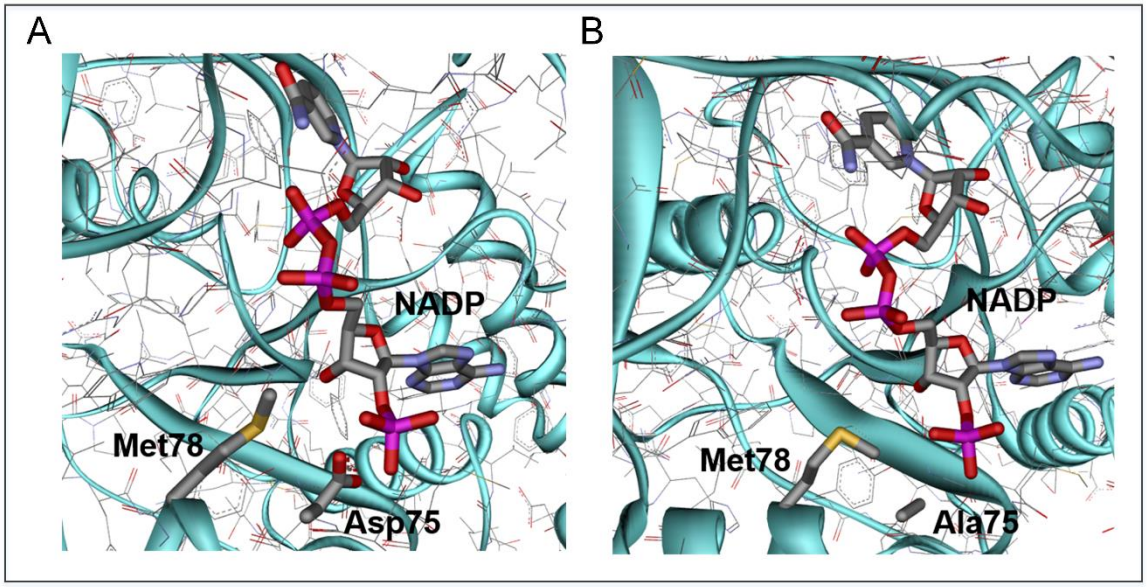

Figure 5-6: Homology model of the wild type mannitol 2-dehydrogenase of *C. glutamicum* (A) and the predicted mutant (B), both complexed with $NADP^+$. The different atoms are visualized by the following colors: yellow, sulphur; blue, nitrogen; red, oxygen; pink, phosphate. For computation modeling, the crystallographic protein structure of *P. fluorescens* MtlD (pdb entry 1M2W.pdb) was used, as no crystallographic protein structure of *C. glutamicum* MtlD was available.

From a chemical point of view, $NADP^+$ distinguishes structurally from NAD^+ by an additional attached phosphate group at the 2'-position of the adenine ribose (Voet et al. 1999). Due to this difference, the position of amino acids in the cofactor binding pocket differs between the two co-substrates (Bottoms et al. 2002; Cahn et al. 2017; Cirilli et al. 2003; Scrutton et al. 1990). The negatively charged carboxyl group of amino acid residues such as L-aspartate typically present in NAD-specific enzymes can form a hydrogen bond with the 2'- and 3'-hydroxyl groups of the adenosyl-ribose ring, the

binding of NAD^+ is therefore favored over that of $NADP^+$ (Bommareddy et al. 2014; Cirilli et al. 2003; Reddy et al. 1996). Such a residue was also present in the mannitol 2-dehydrogenase of *C. glutamicum*. As depicted in Figure 5-6 A the negatively charged carboxylate group of Asp75 unfavorably repelled the negatively charged phosphate group of $NADP^+$, explaining the preference of the enzyme for NAD^+. To enable the binding of $NADP^+$ without steric and electrostatic collision the negative charge obviously had to be removed. In line, an exchange of L-aspartate 75 by L-alanine 75 (D75A) implemented an amino acid with only a small and neutral charged side chain (Figure 5-6 B). Based on computational modeling, amino acid exchange of L-methionine by L-lysine at position 78 (M78K) was also considered beneficial, because L-lysine had a positively charged side chain that allowed a better interaction with the negatively charged phosphate group of the $NADP^+$ molecule. Both enzyme variants were constructed. In order to introduce the site-specific D75A point mutation into the *mtlD* gene, specific primers were used to construct the transformation vector (see chapter 4.6.3 and 4.6.5). After confirmation of a positive clone after the second recombination event by sequencing, the obtained strain was designated *C. glutamicum* SEA-2C. For the additional amino acid exchange M78K in SEA-2C, modified primers and a directed mutagenesis kit were applied (see chapter 4.6.5). However, this second exchange was detrimental, because the two point *mtlD* mutant was no longer able to grow on mannitol (data not shown), which was probably due to the fact that the enzyme was no more functional.

Subsequently, the native MtlD enzyme and the novel D75A MtlD variant, were characterized. To this end, their cofactor specificity was studied, i.e. the NAD^+ and $NADP^+$ activity was measured in the novel SEA-2C and the parent strain (Table 5-4). The parent strain *C. glutamicum* SEA-1, harboring the native MtlD enzyme, exhibited activity only with NAD^+ ($V_{max,NAD}$: 379.9 ± 14.5 mU mg^{-1}), but not with $NADP^+$ ($V_{max,NADP}$: 0.9 ± 0.2 mU mg^{-1}). Beneficially, nucleotide exchange D75A in *mtlD* created the desired NADP-specific activity ($V_{max,NADP}$: 12.9 ± 0.7 mU mg^{-1}) in addition to NAD-specific activity ($V_{max,NAD}$: 148.9 ± 4.3 mU mg^{-1}) (Table 5-4). The mutant even revealed a higher affinity for $NADP^+$ ($K_{M,NADP}$: 0.7 ± 0.1 mM) than for NAD^+ ($K_{M,NAD}$: 1.1 ± 0.1 mM) (Table 5-4). Admittedly, the mutation resulted in an almost two fold decreased NAD^+ activity.

Table 5-4: Enzyme kinetics of mannitol 2-dehydrogenase in *C. glutamicum* SEA-1 and *C. glutamicum* SEA-2C, respectively. The basic strain *C. glutamicum* SEA-1 served as reference. The cultivation was conducted in mannitol mineral salt medium at 30 °C. The data represent mean values and deviations from three biological replicates.

Strain	$K_{M,NAD}$ (mM)	$V_{max,NAD}$ (mU mg^{-1})	$K_{M,NADP}$ (mM)	$V_{max,NADP}$ (mU mg^{-1})
SEA-1	0.8 ± 0.1	379.9 ± 14.5	n.d.*	< 0.9
SEA-2C	1.1 ± 0.1	148.9 ± 4.3	0.7 ± 0.1	12.9 ± 0.7

*n.d. = not determined

To investigate how the modified enzyme affected the performance of *C. glutamicum* SEA-1, shake flask studies with mannitol were conducted (Table 5-5, Table 5-6, Figure 5-7). Strikingly, the novel mutant accumulated 18.8 mM L-lysine, corresponding to an almost twofold higher L-lysine yield (280 mmol mol^{-1}) compared to the parent strain (Figure 5-7, Table 5-6). The substantially improved yield indicated that carbon was more efficiently channelled towards L-lysine biosynthesis by the modified enzyme. Furthermore, the novel mutant revealed a 40 % increased specific L-lysine production rate (Table 5-6). As shown, it did not excrete fructose, as observed for the parent strain SEA-1. However, the modified MtlD caused an impaired growth and reduced cellular fitness. The new strain required almost 40 h, 7 h more than the parent strain, for complete utilization of mannitol (Figure 5-7). The reduced growth behaviour was probably related to reduced mannitol conversion. Considering the total activity of the mutated enzyme (Table 5-4), which was reduced almost twofold (162 mU mg^{-1}), it seemed that the mutated mannitol 2-dehydrogenase was limiting mannitol catabolism. The by-product spectrum revealed slightly increased levels of trehalose and L-glutamate, while no levels of acetate and lactate were detected compared to those in the parent strain. Levels of other by-products remained unaffected (Table 5-5). Taken together, the amino-acid exchange in MtlD appeared to be highly efficient with respect to NADPH formation and L-lysine biosynthesis in *C. glutamicum*. However, the amino acid exchange partly impaired the growth of the *C. glutamicum* SEA-2C mutant.

Table 5-5: Kinetics and stoichiometry of L-lysine-producing *C. glutamicum* SEA-1 and SEA-2C during growth on mineral salt medium containing mannitol as the sole carbon source. The data represent the initial growth phase of the SEA-1 strain, which was determined by fructose accumulation and is highlighted in white in the cultivation profile (Figure 5-7), and the entire cultivation period of the SEA-2C strain. The given data comprise the specific rates for growth (μ), mannitol uptake (q_{Mtl}), and L-lysine production (q_{Lys}) and the yields for L-lysine ($Y_{Lys/Mtl}$), biomass ($Y_{X/Mtl}$) and by-products (fructose (Frc), trehalose (Tre), L-glycine (Gly), L-glutamate (Glu), lactate (Lac), acetate (Ace), and L-alanine (Ala)). The data represent mean values and deviations from three biological replicates

Strain	SEA-1	SEA-2C
μ [h^{-1}]	0.26 ± 0.00	0.16 ± 0.02
q_{Lys} [mmol g^{-1} h^{-1}]	0.55 ± 0.10	1.02 ± 0.03
q_{Mtl} [mmol g^{-1} h^{-1}]	6.1 ± 1.1	3.7 ± 0.1
$Y_{Lys/Mtl}$ [mmol mol^{-1}]	90.1 ± 1.1	279.8 ± 18.1
$Y_{X/Mtl}$ [g mol^{-1}]	40.2 ± 2.0	43.1 ± 4.0
$Y_{Frc/Mtl}$ [mmol mol^{-1}]	262.1 ± 14.2	< 0.01
$Y_{Lac/Mtl}$ [mmol mol^{-1}]	9.9 ± 1.0	< 0.01
$Y_{Glu/Mtl}$ [mmol mol^{-1}]	6.3 ± 0.3	22.3 ± 2.9
$Y_{Gly/Mtl}$ [mmol mol^{-1}]	2.3 ± 0.1	2.0 ± 0.4
$Y_{Tre/Mtl}$ [mmol mol^{-1}]	2.6 ± 0.2	3.1 ± 0.5
$Y_{Ace/Mtl}$ [mmol mol^{-1}]	1.8 ± 0.9	<0.01
$Y_{Ala/Mtl}$ [mmol mol^{-1}]	0.7 ± 0.2	<0.01

Table 5-6: Production characteristics of *C. glutamicum* strains SEA-1 and SEA-2C, engineered for L-lysine production from mannitol. The data comprise the mean specific rate for L-lysine production (q_{Lys}), and the yields for L-lysine ($Y_{Lys/Mtl}$) and biomass ($Y_{X/Mtl}$), calculated over the entire cultivation period. The data represent mean values and deviations from three biological replicates.

Strain	SEA-1	SEA-2C
q_{Lys} [mmol g^{-1} h^{-1}]	0.73 ± 0.02	1.02± 0.03
$Y_{Lys/Mtl}$ [mmol mol^{-1}]	153.16 ± 11.5	279.8 ± 18.1
$Y_{X/Mtl}$ [g mol^{-1}]	54.3 ± 2.2	43.1 ± 4.0

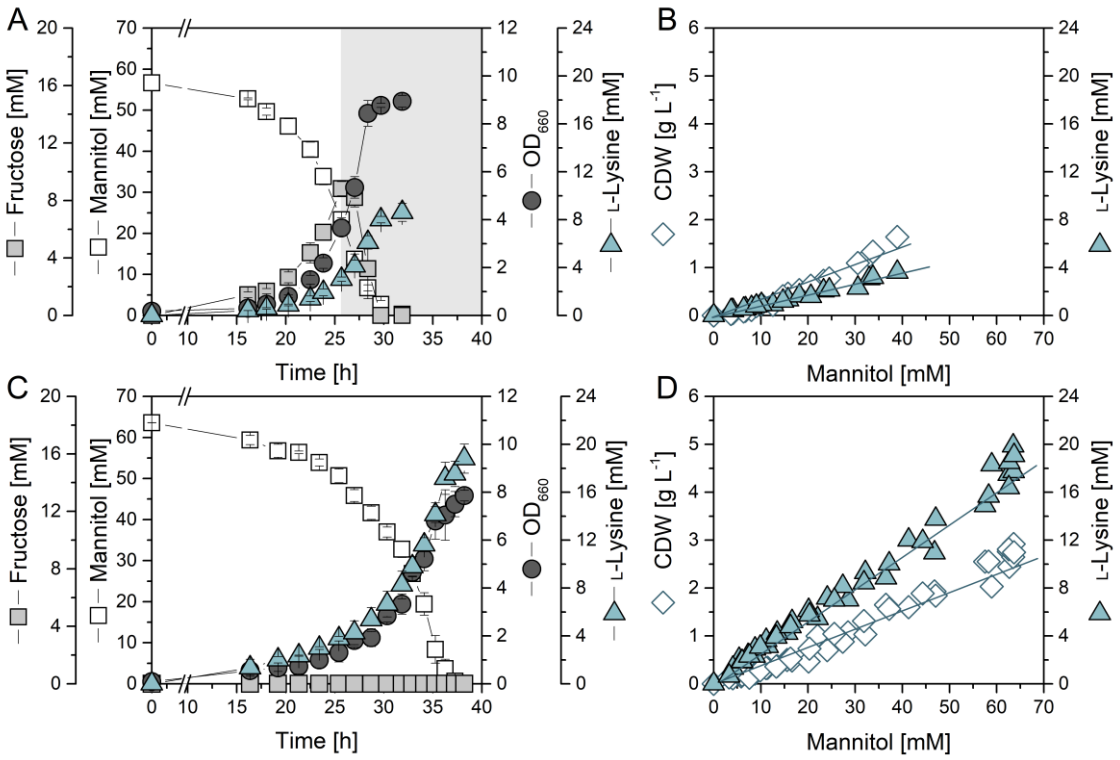

Figure 5-7: Growth and production characteristics of L-lysine-producing *C. glutamicum* SEA-1 (A-B) and *C. glutamicum* SEA-2C (C-D) on mineral salt medium containing mannitol as the sole carbon source. The cultivation profiles represent growth, product formation, fructose accumulation, and mannitol as well as fructose consumption over the entire cultivation period and represent mean values and corresponding standard deviations from three biological replicates (A, C). The two phases of fructose accumulation (phase I) and re-consumption (phase II) are displayed in the cultivation profile in white and grey, respectively. Yields for L-lysine and biomass were determined by linear regression of L-lysine and biomass formation, respectively, plotted against mannitol consumption (B, D). These data reflect the initial growth phase, linked to fructose accumulation (shown in white) for strain SEA-1 and the entire cultivation period of the non-fructose accumulating strain SEA-2C.

5.2 Elimination of fructose overflow

5.2.1 Connecting mannitol catabolism to the PP pathway

As discussed, the entry point of mannitol into metabolism had a strong impact on the strain performance. As mannitol-grown *C. glutamicum* SEA-1 revealed excessive fructose accumulation, a redirection of intracellular fructose was necessary. The intracellular phosphorylation of fructose into fructose 6-phosphate appeared promising, because it opened the possibility to reduce fructose overflow and (at the same time) enhance the PP pathway flux (Becker et al. 2005). Since *C. glutamicum* lacks fructokinase activity (Moon et al. 2005; Moon et al. 2007), two different heterologous fructokinases, i.e. ScrK from *Clostridium acetobutylicum* and Mak from *Escherichia coli* were tested.

Expression of ScrK fructokinase from *C. acetobutylicum*. To phosphorylate the formed fructose intracellularly into fructose 6-phosphate, the *scrK* gene encoding fructokinase (EC 2.7.1.4) from *C. acetobutylicum* ATCC 824 was genomically expressed in the basic producer SEA-1. For expression, the gene was implemented into the *crtEb* gene locus (NCgl0594), encoding for a lycopene elongase (Heider et al. 2012). The designed gene construct comprised two homologous flanking regions, located upstream (500 bp) and downstream (520 bp) of the *crtEb* gene locus, the *scrK* gene itself (951 bp) and a 192 bp-sized DNA fragment, harboring the superoxide dismutase (*sod*) promoter of *C. glutamicum* for constitutive overexpression (Becker et al. 2007). As depicted in Figure 5-8, disruption of the *crtEb* gene and introduction of *scrK* was visualized by the change of the cell color from yellow to pale pink. The pale pink cell color was caused by the accumulation of lycopene (Heider et al. 2012).

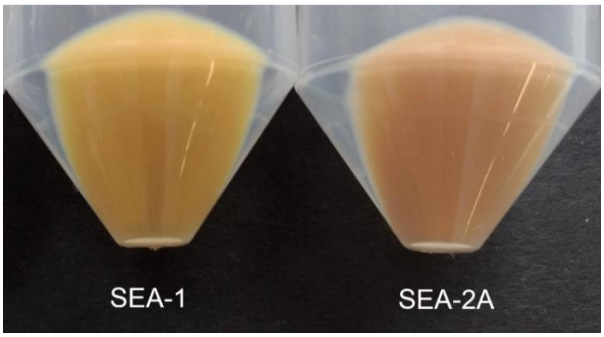

Figure 5-8: Visualization of the correct insertion of the *scrK* gene from *C. acetobutylicum* ATCC 824 into the *crtEb* gene locus of *C. glutamicum* SEA-1, encoding for lycopene elongase. Disruption of the *crtEb* gene and thus correct insertion of the *scrK* gene turned the normally yellowish color for wild type cells into a pale pink color in mutant cells.

The newly created SEA-2A strain was further investigated. In order to confirm functionality of the fructokinase in *C. glutamicum*, its activity in crude cell extract was determined. *C. glutamicum* SEA-2A revealed the desired fructokinase activity (108 ± 1 mU mg^{-1}), while no activity was measurable in the parent strain *C. glutamicum* SEA-1 (< 0.1 mU mg^{-1}) (Table 5-7). The ScrK enzyme showed high affinity for ATP and fructose of $K_{M,ATP}$ = 470 ± 3 µM and $K_{M,Frc}$ = 330 ± 1 µM, respectively. To evaluate the production performance of the mutant, cultivation studies on mineral salt medium containing mannitol as the sole carbon source were performed (Figure 5-9).

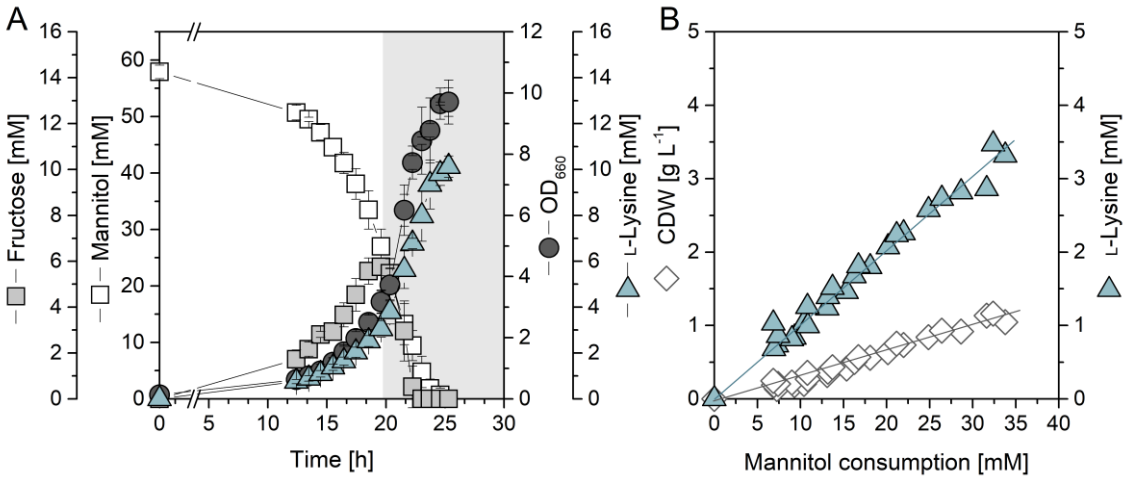

Figure 5-9: Growth and production characteristics of L-lysine-producing *C. glutamicum* SEA-2A on mineral salt medium containing mannitol as the sole carbon source. The cultivation profile represents growth, product formation, fructose accumulation, and mannitol as well as fructose consumption over the entire cultivation period and represents mean values and corresponding standard deviations from three biological replicates (A). Yields for L-lysine and biomass were determined by linear regression of L-lysine and biomass formation, respectively, plotted against mannitol consumption (B) from three biological replicates.

The novel mutant exhibited a slightly improved production performance. It accumulated L-lysine to a titer of 10.1 mM (Figure 5-9 A), slightly more than observed for the ancestor SEA-1 (Figure 5-2). Hereby, fructokinase expression increased the L-lysine yield by 14 % to 102 mmol mol^{-1} (Figure 5-9, Table 5-8). SEA-2A grew well on mannitol and completely consumed the substrate within 25 h, much faster than the parent strain, which required 32 h (Figure 5-2). Beneficially, fructose accumulation was reduced by 29 %. Admittedly, it could not be completely eliminated as initially desired. This was different to previous findings in sucrose-grown *C. glutamicum*, when the heterologous expression of *scrK* from *C. acetobutylicum* abolished fructose-overflow metabolism (Moon et al. 2005). This might relate to the fact that sucrose catabolism forms fructose only by a relative flux of 50 %, whereby mannitol-derived fructose accumulates at a relative flux of 100 %, in

combination with a higher specific uptake rate of mannitol (Wittmann et al. 2004a). The by-product spectrum revealed slightly increased levels of L-glutamate, L-glycine and trehalose, while acetate, L-alanine and lactate were not detected (Table 5-8).

Expression of Mak fructokinase from *E. coli*. Next, the Mak fructokinase from *E. coli* was tested as an alternative. For genome-based expression of the *mak* gene, it was also introduced into the *crtEb* gene locus of *C. glutamicum* SEA-1 under control of the constitutive *sod* promoter using a gene construct with the *mak* gene (909 bp) and the same homologous flanking regions located upstream (500 bp) and downstream (520 bp) of the *crtEb* gene locus, as described for *scrK*. As the start codon of a gene influences the translational efficiency of the encoded enzyme (Becker et al. 2010), the rare naturally present variant GTG was replaced by the stronger triplet ATG. The correct insertion was again visualized by the cell color, and it was further confirmed by PCR (fragment size 2121 bp) and by sequencing. The obtained strain was designated *C. glutamicum* SEA-2B and further investigated. Expression of *mak* yielded a specific fructokinase activity of 161 ± 1 mU mg^{-1} in the crude cell extract. Compared to SEA-2A, fructokinase activity was 49 % higher. It also revealed better affinity for ATP ($K_{M,ATP}$ = 410 ± 7 mM). In contrast, the K_M for fructose was notably higher for Mak, as compared to ScrK (Table 5-7).

Table 5-7: Enzyme kinetics of the fructokinase ScrK from *C. acetobutylicum* and Mak from *E. coli*, expressed in *C. glutamicum* SEA-2A and *C. glutamicum* SEA-2B, respectively. The L-lysine basic producer *C. glutamicum* SEA-1 served as reference. The cultivation of the different strains was conducted in mannitol mineral salt medium at 30 °C. The data represent mean values and deviations from three biological replicates.

Strain	$K_{M,ATP}$ (µM)	$K_{M,Frc}$ (µM)	V_{max} (mU mg^{-1})
SEA-1	n.d.*	n.d.*	< 0.01
SEA-2A	470 ± 3	330 ± 1	108 ± 1
SEA-2B	410 ± 7	540 ± 2	161 ± 1

*n.d. = not determined

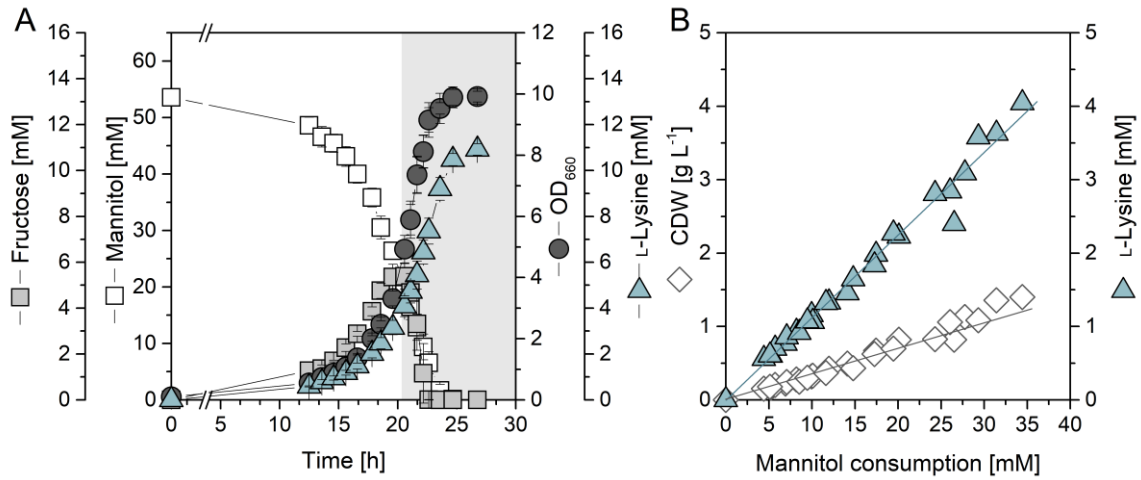

Figure 5-10: Growth and production characteristics of L-lysine-producing *C. glutamicum* SEA-2B on mineral salt medium containing mannitol as the sole carbon source. The cultivation profile represents growth, product formation, fructose accumulation, and mannitol as well as fructose consumption over the entire cultivation period and represents mean values and corresponding standard deviations from three biological replicates (A). Yields for L-lysine and biomass were determined by linear regression of L-lysine and biomass formation, respectively, plotted against mannitol consumption (B). The data represent the initial growth phase, which was determined by fructose accumulation (shown in white).

Cultured on mannitol, SEA-2B exhibited faster mannitol consumption, resulting in substrate depletion after 27 hours (Figure 5-2 and 5-10). The expressed fructokinase enabled a substantial improvement in L-lysine formation (Figure 5-10). The novel mutant accumulated 10.9 mM L-lysine, more than 25 % more than the *C. glutamicum* SEA-1 strain (Figure 5-2). SEA-2B also showed a higher L-lysine yield and a higher specific L-lysine production rate, increased by 31 % and 25 %, respectively (Figure 5-11). Notably, expression of the Mak fructokinase reduced fructose accumulation by 30 % (Table 5-8). SEA-2B was further analyzed at the metabolic flux level to clarify the effects of fructokinase expression in more detail.

Table 5-8: Kinetics and stoichiometry of L-lysine-producing *C. glutamicum* SEA-1, SEA-2A and SEA-2B during growth on mineral salt medium containing mannitol as the sole carbon source. The data represent the initial growth phase of the cultivated mutants, which was determined by fructose accumulation and is highlighted in white in the cultivation profiles (Figure 5-2, Figure 5-9 and Figure 5-10). The given data comprise the specific rates for growth (μ), mannitol uptake (q_{Mtl}), and L-lysine production (q_{Lys}) and the yields for L-lysine ($Y_{Lys/Mtl}$), biomass ($Y_{X/Mtl}$) and by-products such as fructose (Frc), trehalose (Tre), L-glycine (Gly), L-glutamate (Glu), lactate (Lac), acetate (Ace), and L-alanine (Ala). The data represent mean values and deviations from three biological replicates.

Strain	SEA-1	SEA-2A	SEA-2B
μ [h^{-1}]	0.26 ± 0.00	0.23 ± 0.00	0.25 ± 0.02
q_{Lys} [mmol g^{-1} h^{-1}]	0.55 ± 0.10	0.67 ± 0.08	0.72 ± 0.05
q_{Mtl} [mmol g^{-1} h^{-1}]	6.1 ± 1.1	6.5 ± 0.4	6.3 ± 0.4
$Y_{Lys/Mtl}$ [mmol mol^{-1}]	90.1 ± 1.1	102.4 ± 6.9	113.6 ± 6.1
$Y_{X/Mtl}$ [g mol^{-1}]	40.2 ± 2.0	35.7 ± 1.3	39.8 ± 3.3
$Y_{Frc/Mtl}$ [mmol mol^{-1}]	262.1 ± 14.2	186.4 ± 12.7	183.9 ± 13.3
$Y_{Lac/Mtl}$ [mmol mol^{-1}]	9.9 ± 1.0	< 0.01	< 0.01
$Y_{Glu/Mtl}$ [mmol mol^{-1}]	6.3 ± 0.3	10.5 ± 1.6	9.0 ± 1.0
$Y_{Gly/Mtl}$ [mmol mol^{-1}]	2.3 ± 0.1	4.1 ± 0.2	4.5 ± 0.4
$Y_{Tre/Mtl}$ [mmol mol^{-1}]	2.6 ± 0.2	3.5 ± 0.1	3.2 ± 0.3
$Y_{Ace/Mtl}$ [mmol mol^{-1}]	1.8 ± 0.9	< 0.01	< 0.01
$Y_{Ala/Mtl}$ [mmol mol^{-1}]	0.7 ± 0.2	< 0.01	< 0.01

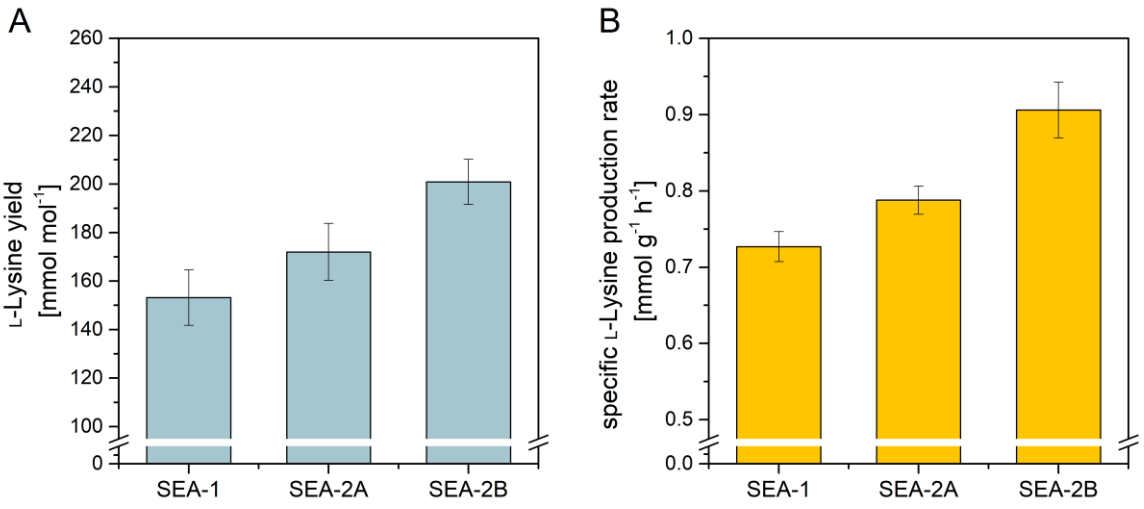

Figure 5-11: Production characteristics of *C. glutamicum*, engineered for L-lysine production from mannitol. The figure shows the mean specific L-lysine yield (A) and the specific L-lysine production rate (B) for the strains SEA-1, SEA-2A and SEA-2B over the entire cultivation period. The data represent mean values and deviations from three biological replicates.

5.2.2 Metabolic fluxes of *C. glutamicum* SEA-2B

In order to gain a better understanding how fructokinase expression influenced the metabolism of *C. glutamicum* SEA-2B, it was analyzed for its intracellular flux distribution (Figure 5-12). During cultivation on [1-^{13}C] labeled mannitol, cells exhibited isotopic and metabolic steady state, indicated by constant growth and production performance as well as constant ^{13}C labeling of the measured amino acids (see appendix Figure 7-2, Table 5-8). The determined distribution of intracellular fluxes of the *C. glutamicum* SEA-2B strain is given in Figure 5-12.

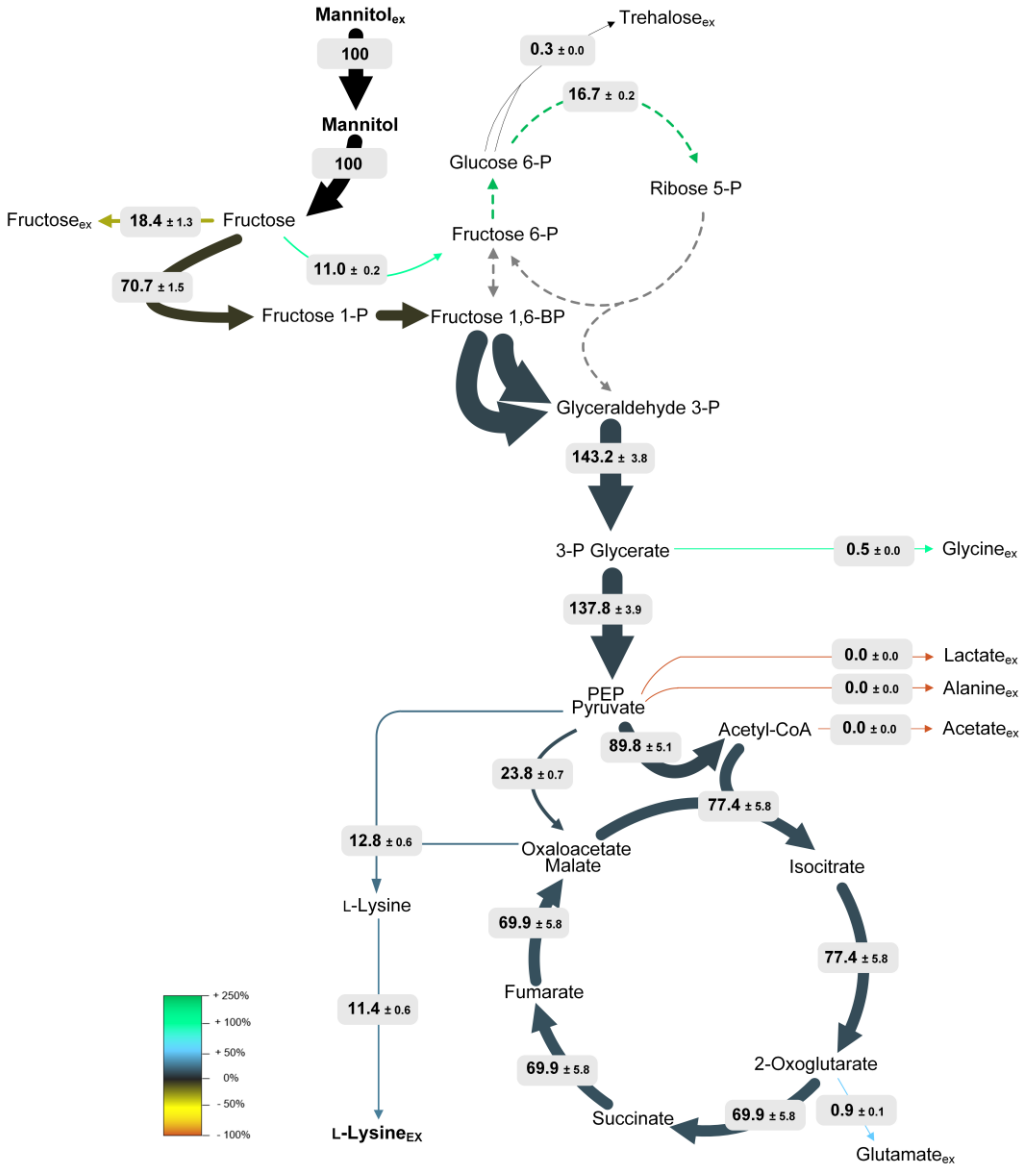

Figure 5-12: *In vivo* carbon flux distribution of L-lysine-producing *C. glutamicum* SEA-2B during growth on mineral salt medium containing mannitol as the sole carbon source. All fluxes are expressed as the molar percentage of the corresponding mean specific mannitol uptake rate (q_{Mtl} = 6.3 mmol g^{-1} h^{-1}), which was set to 100 %. The thickness of the reaction arrows represents the flux amount, while the color code reflects the flux differences compared to the L-lysine basic producer *C. glutamicum* SEA-1. The anabolic fluxes into biomass are not displayed.

When regarding the metabolic fluxes at the fructose node, a generally higher flux into the carbon metabolism was observed in SEA-2B, as compared to the basic producer SEA-1 (Figure 5-12). As direct response to fructokinase expression, fructose secretion into the medium was reduced to 18 %. Thus a higher flux (82 %) entered the core metabolism and was available for growth and L-lysine production. Hereby, the carbon was mostly channeled via fructose 1-phosphate to the lower glycolytic chain (71 %), whereas a weak but significant flux (11 %) was channeled via fructokinase towards the PP pathway. As a consequence, the PP pathway was activated in SEA-2B compared to SEA-1 (Figure 5-5 and Figure 5-12). Nonetheless, the mannitol-grown SEA-2B strain still supplied much less NADPH via the PP pathway as compared to glucose-grown *C. glutamicum* strains, which revealed relative PP pathway fluxes between 47 % and 84 % (Becker et al. 2005; Becker et al. 2011; Bommareddy et al. 2014; Kind et al. 2013; Wittmann and Heinzle 2002). *C. glutamicum* SEA-2B carried a high flux of carbon towards the pyruvate node. When considering the pyruvate node, an enhanced flux towards L-lysine biosynthesis was observed (Figure 5-12). A substantial carbon fraction entered the TCA cycle via pyruvate dehydrogenase (90 %), and resulted in a high TCA cycle flux (77 %) at the level of isocitrate dehydrogenase, much higher than that of engineered L-lysine producing *C. glutamicum*, growing on glucose (Becker et al. 2005; Becker et al. 2011; Bommareddy et al. 2014; Kiefer et al. 2004; Kind et al. 2013). Since NADPH is formed by isocitrate dehydrogenase in *C. glutamicum*, *C. glutamicum* SEA-2B obviously used this enzyme to compensate for the rather low NADPH supply via the PP pathway. Admittedly, the high TCA cycle activity led to an undesired loss of carbon as CO_2 (via isocitrate dehydrogenase as well as via α-ketoglutarate dehydrogenase) which became unavailable for L-lysine production. Taken together, the heterologous fructokinase reduced fructose accumulation substantially, but not completely. In addition, it did not promote the PP pathway to the high extent necessary to provide sufficient NADPH for higher L-lysine yield. As a consequence, most of the carbon bypassed the PP pathway and was channeled through the lower EMP pathway.

5.2.3 Extending the flux capacity of the EMP pathway

Considering the PP pathway flux in both strains, *C. glutamicum* SEA-1 and SEA-2B, it became obvious that the expressed fructokinase redirected carbon flux partially, but not to the extent, known from glucose-grown *C. glutamicum* (Bae et al. 2016; Moon et al. 2005). Obviously, the remaining major entry of mannitol via fructose 1-phosphate and fructose 1,6-bisphosphate in mannitol-grown cells still revealed a high influx into the EMP pathway. In addition, the (at least partially) remaining fructose overflow indicated that the

capacity of the EMP pathway was likely not sufficient. In this regard, it appeared promising to further enhance glycolytic flux capacity (Figure 5-12). The chosen strategy involved heterologous expression of NADP-dependent glyceraldehyde 3-phosphate dehydrogenase (Figure 5-13). *C. glutamicum* naturally comprises two glyceraldehyde 3-phosphate dehydrogenases (GapDHs), GapA and GapB, which differ in respect to cofactor specificity and physiological function (Hayashi et al. 2002; Takeno et al. 2016; Takeno et al. 2010). While the GapA enzyme prefers NAD^+ as cofactor and is involved in the utilization of both glycolytic as well as gluconeogenic carbon sources, the GapB enzyme harbors a dual cofactor signature but clearly prefers $NADP^+$ and is only active in the gluconeogenic direction (Ikeda and Nakagawa 2003; Omumasaba et al. 2004; Takeno et al. 2010). However, unlike other organisms, such as *C. acetobutylicum* (Iddar et al. 2002) and *Streptococcus mutans* (Crow and Wittenberger 1979), *C. glutamicum* does not possess a GapDH enzyme to catalyze the irreversible and NADP-dependent conversion of glyceraldehyde 3-phosphate to 3-phosphoglycerate in the glycolytic direction (Crow and Wittenberger 1979; Takeno et al. 2016). In this regard, the introduction of an additional NADPH-generating glyceraldehyde 3-phosphate dehydrogenase promised two beneficial effects at the same time: (i) a further reduction of fructose accumulation by the increased glycolytic capacity and (ii) extra NADPH formation. The *gapN* gene, encoding the non-phosphorylating NADP-dependent glyceraldehyde 3-phosphate dehydrogenase from *S. mutans* UA159 was selected, as the candidate. It was expressed using an episomal replicating vector. Consequently, the resulting mutant contained GapN together with the native NAD-dependent GapA enzyme (Figure 5-13).

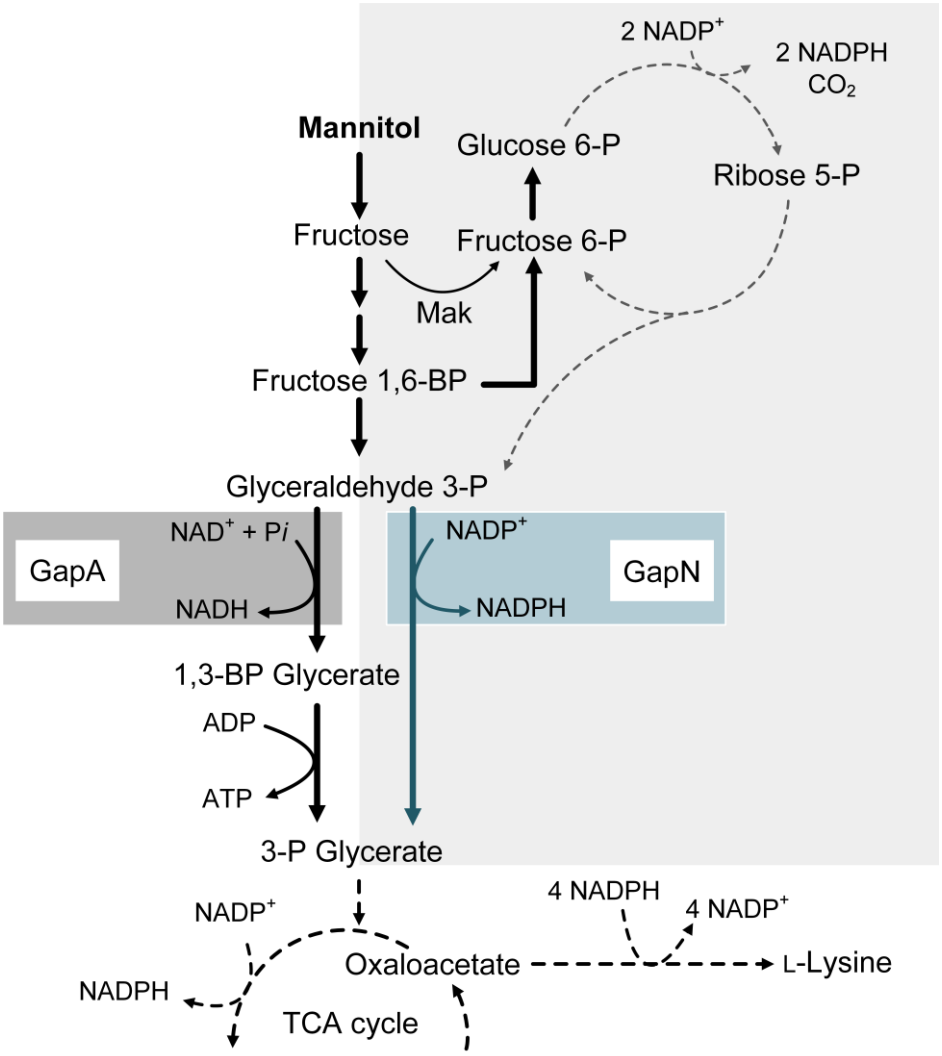

Figure 5-13: Blueprint of the designed carbon core metabolism in the L-lysine producing strain SEA-3, visualizing the metabolic engineering strategy, to enhance the glycolytic flux capacity and couple the EMP pathway to the generation of NADPH.

For expression of *gapN*, the gene was inserted into the episomally replicating vector pClik 5α MCS under the control of its native promotor. After transformation and subsequent verification of positive clones by PCR and sequencing, one of the clones was designated SEA-3. The strain SEA-2E, expressing the empty plasmid served as reference strain.

To confirm the functionality of GapN in SEA-3, its activity was measured in crude cell extract. The SEA-3 mutant revealed the desired NADP-dependent GapN activity (250 ± 11 mU mg^{-1}) in addition to its NAD-specific GapA activity (420 ± 25 mU mg^{-1}), whereas the control strain SEA-2E (bearing the empty plasmid) only revealed activity for NAD^+ (397 ± 34 mU mg^{-1}), but not for $NADP^+$ (< 0.1 mU mg^{-1}). The novel NADP-dependent activity was therefore completely attributed to GapN. These findings are in

agreement with previous results (Takeno et al. 2010), which revealed only NAD-dependent GapDH activity (440 ± 19 mU mg^{-1}) in *C. glutamicum* wild type ATCC 13032. In order to investigate how GapN affected the production performance of *C. glutamicum* SEA-3, the strain was further investigated (Figure 5-14).

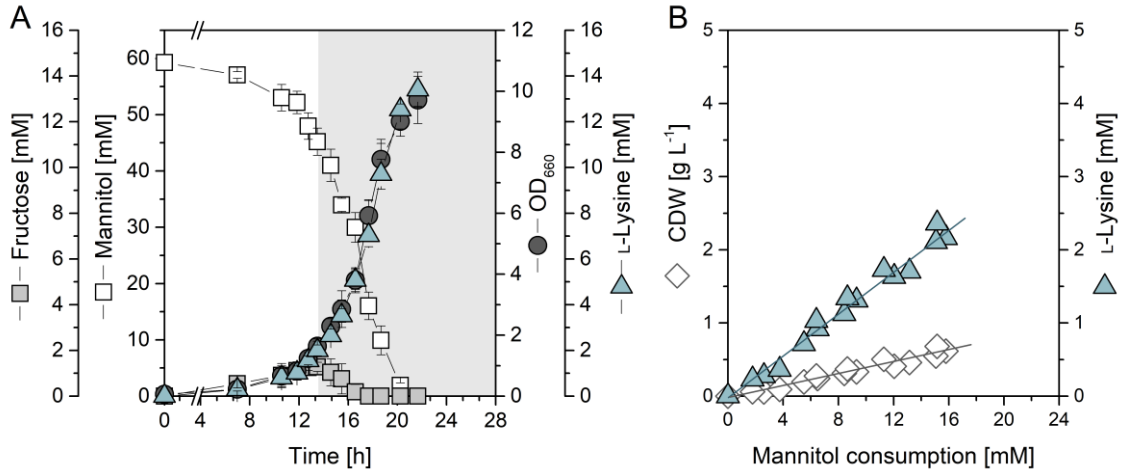

Figure 5-14: Growth and production characteristics of *C. glutamicum* SEA-3 on mannitol mineral salt medium. The cultivation profile shows growth, substrate consumption and product formation and represents mean values and corresponding standard deviations from three biological replicates (A). Yields for L-lysine and biomass were determined by linear regression of L-lysine and biomass formation, respectively, plotted against mannitol consumption (B). The data represent the initial main growth phase, which was linked to fructose accumulation (shown in white).

Cultured on mannitol, the novel mutant showed a substantial increase in L-lysine production (Figure 5-14). Furthermore, NADP-dependent GapN expression positively affected growth, as mannitol was consumed in only 22 h. SEA-3 accumulated 13.4 mM L-lysine, more than 54 % more than SEA-1 and almost 23 % more than SEA-2B (Figure 5-15). In line, the overall L-lysine yield (226 mmol per mol^{-1}) was almost 48 % and 13 % higher (Figure 5-15). Moreover, the specific L-lysine production rate as well as the mannitol uptake rate were increased markedly (Figure 5-15, Table 5-9). Interestingly, mannitol-grown *C. glutamicum* SEA-3 reached the excellent production performance of the L-lysine hyperproducer *C. glutamicum* LYS-12, which showed a specific L-lysine production rate of 1.27 mmol g^{-1} h^{-1} and a L-lysine yield of 258 mmol mol^{-1}, respectively, when cultivated on glucose (Becker et al. 2011). Recent studies also have demonstrated a positive influence of GapN expression on L-lysine production from glucose (Takeno et al. 2010). On glucose, GapN can even compensate for an artificially removed PP pathway in terms of NADPH supply (Takeno et al. 2016). Beneficially, fructose accumulation was almost completely abolished (Figure 5-14, Figure 5-16 and Table 5-9).

Table 5-9: Kinetics and stoichiometry of L-lysine-producing *C. glutamicum* SEA-1, SEA-2B, SEA-3 and SEA-2E during growth on mannitol. The data represent the initial growth phase of the cultivated strains, which was characterized by fructose accumulation (Figure 5-2, Figure 5-10 and Figure 5-14). The data comprise the specific rates for growth (μ), mannitol uptake (q_{Mtl}), and L-lysine production (q_{Lys}) and the yields for L-lysine ($Y_{Lys/Mtl}$), biomass ($Y_{X/Mtl}$) and by-products (fructose (Frc), trehalose (Tre), L-glycine (Gly), L-glutamate (Glu), lactate (Lac), acetate (Ace), and L-alanine (Ala)). The data represent mean values and deviations from three biological replicates.

Strain	SEA-1	SEA-2B	SEA-2E	SEA-3
μ [h^{-1}]	0.26 ± 0.00	0.25 ± 0.02	0.24 ± 0.02	0.30 ± 0.02
q_{Lys} [mmol g^{-1} h^{-1}]	0.55 ± 0.10	0.72 ± 0.05	0.69 ± 0.03	1.08 ± 0.02
q_{Mtl} [mmol g^{-1} h^{-1}]	6.1 ± 1.1	6.3 ± 0.4	6.0 ± 0.03	7.5 ± 0.6
$Y_{Lys/Mtl}$ [mmol mol^{-1}]	90.1 ± 1.1	113.6 ± 6.1	113.1 ± 1.5	144.8 ± 9.5
$Y_{X/Mtl}$ [g mol^{-1}]	40.2 ± 2.0	39.8 ± 3.3	39.5 ± 2.0	40.0 ± 4.3
$Y_{Frc/Mtl}$ [mmol mol^{-1}]	262.1 ± 14.2	183.9 ± 13.3	208.3 ± 18.4	82.2 ± 18.0
$Y_{Lac/Mtl}$ [mmol mol^{-1}]	9.9 ± 1.0	< 0.01	< 0.01	< 0.01
$Y_{Glu/Mtl}$ [mmol mol^{-1}]	6.3 ± 0.3	9.0 ± 1.0	3.0 ± 0.1	10.3 ± 1.2
$Y_{Gly/Mtl}$ [mmol mol^{-1}]	2.3 ± 0.1	4.5 ± 0.4	3.0 ± 0.3	6.6 ± 1.2
$Y_{Tre/Mtl}$ [mmol mol^{-1}]	2.6 ± 0.2	3.2 ± 0.3	3.4 ± 0.3	3.0 ± 0.4
$Y_{Ace/Mtl}$ [mmol mol^{-1}]	1.8 ± 0.9	< 0.01	< 0.01	< 0.01
$Y_{Ala/Mtl}$ [mmol mol^{-1}]	0.7 ± 0.2	< 0.01	< 0.01	< 0.01

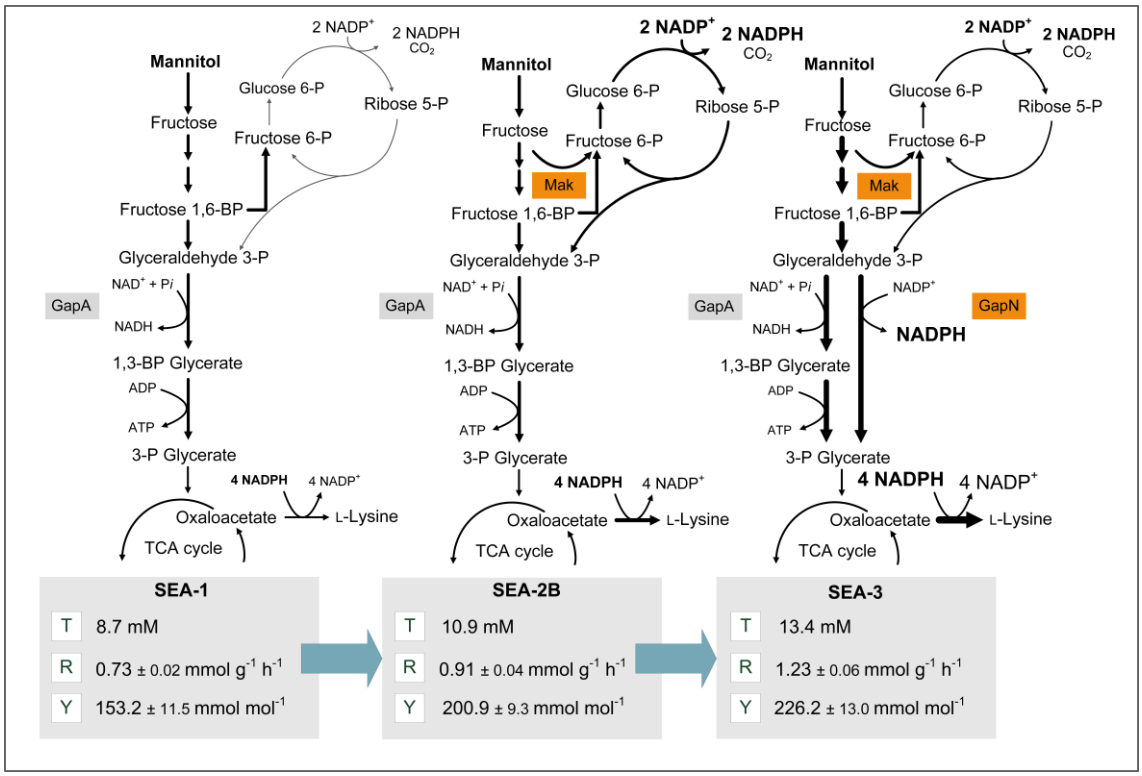

Figure 5-15: Production characteristics of tailor-made L-lysine producing *C. glutamicum* strains SEA-1, SEA-2B and SEA-3, cultivated on mannitol. The figure shows the L-lysine yield ($Y_{Lys/Mtl}$), the specific L-lysine production rate (q_{Lys}) and the L-lysine titer over the entire cultivation period. The data represent mean values and deviations from three biological replicates. The thickness of the arrows schematically highlights the influence of the implemented modifications on the metabolism in the different strains. Orange boxes represent the implemented modified genetic targets in the respective strain. T, L-lysine titer; R, specific L-lysine production rate; Y, L-lysine yield.

The effect of heterologous GapN expression could also be observed at the level of the metabolic fluxes (Figure 5-16). Again, the used flux approach relied on isotopic and metabolic steady state, which was inferred from constant growth and production performance as well as constant ^{13}C labeling pattern of amino acids over time (Table 5-9, appendix Figure 7-3). As a result of GapN expression, the EMP pathway was strongly upregulated to 166 %, with GapN catalyzing 23 % of the flux. The PP pathway was found less active than in the parent strain. The demand for NADPH was now mainly covered by GapN (Figure 5-16). As direct response to the elevated EMP pathway flux, a high flux entered the pyruvate node and substantially triggered L-lysine formation (Figure 5-16). Moreover, the pathways fueling the TCA cycle were found more active. The TCA cycle was strongly upregulated by additional GapN expression. Interestingly and different to the findings here, the TCA cycle activity decreased in glucose-grown L-lysine producing *C. glutamicum* strains bearing the additional NADP-dependent GapN enzyme (Takeno et al. 2016). The exact reason remains unclear, but the strong different behavior of the

GapN mutants on the different substrates underlines the high impact of the raw material for strain behavior and also strain design. Eventually, the significant GapN activity and thus the reduced ATP formation by phosphoglycerate kinase, triggered the TCA cycle and ATP formation via the respiratory chain.

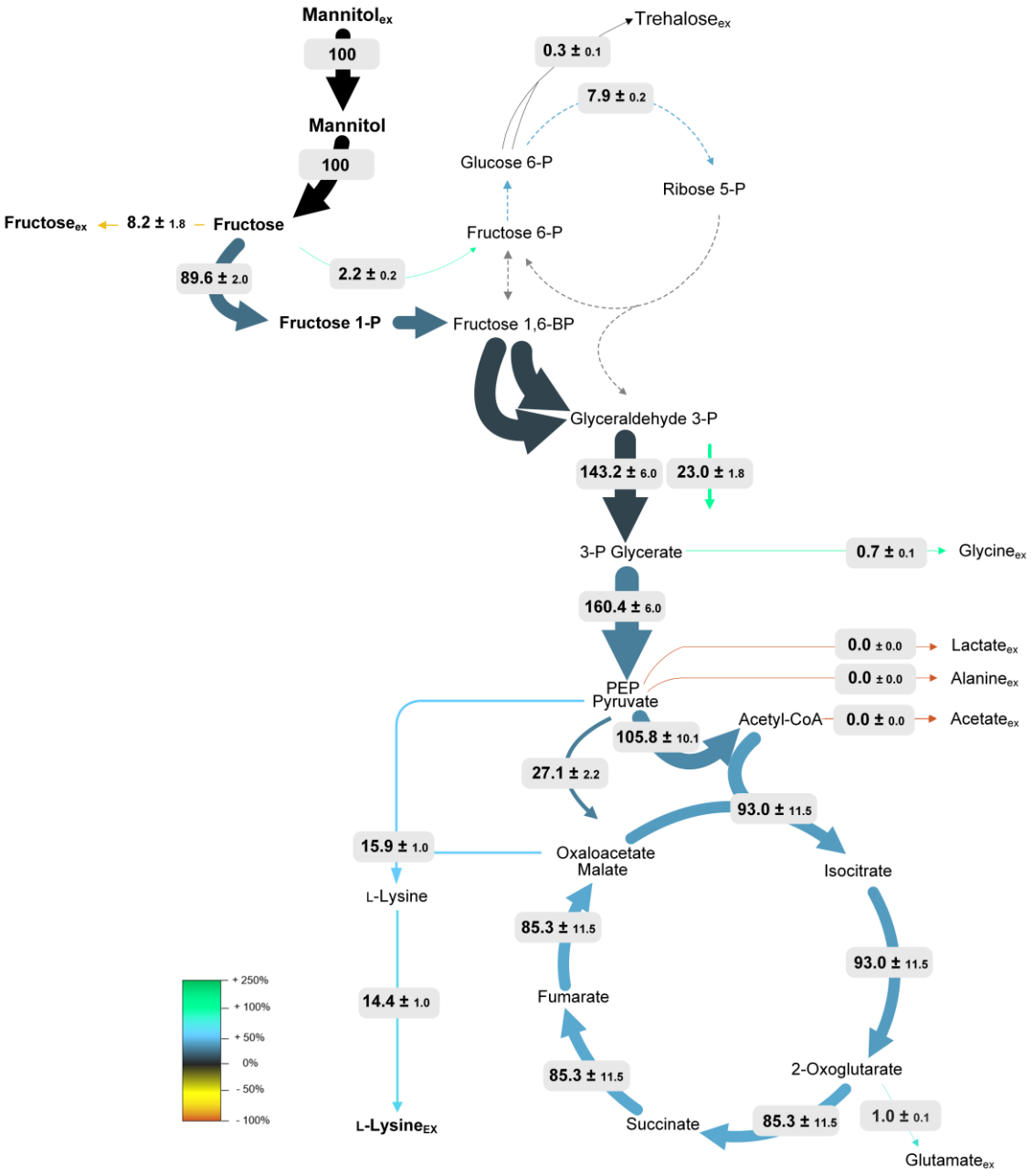

Figure 5-16: *In vivo* carbon flux distribution of L-lysine-producing *C. glutamicum* SEA-3 during growth on mannitol. All fluxes are given as a molar percentage of the corresponding mean specific mannitol uptake rate (q_{Mtl} = 7.5 mmol g^{-1} h^{-1}), which was set to 100 %. The thickness of the reaction arrows represents the flux amount, while the color code reflects the flux difference compared to the basic L-lysine producer *C. glutamicum* SEA-1. The anabolic fluxes into biomass are not displayed.

5.3 Systems wide engineering for maximized redox supply

5.3.1 Redox level in mannitol-grown L-lysine producing *C. glutamicum*

The redox status, i.e. the ratio of NADPH/$NADP^+$ and NADH/NAD^+, has a strong influence on the metabolism (Spaans et al. 2015; Xu et al. 2019). Chemically, NAD^+/NADH and $NADP^+$/NADPH appear similar, as they only differ in one phosphate group. From a biochemical point of view, however, they fulfill very different functions. While NADH primarily transfers electrons to the respiratory chain to yield ATP, NADPH is involved in various anabolic reduction reactions (Sauer et al. 2004). As an example, the biosynthesis of L-lysine is strongly dependent on the availability of reducing power (Wittmann and Heinzle 2001a). Four moles of NADPH were needed to produce one mole of L-lysine (Wittmann and Heinzle 2001a). Generally, NADPH has to be in excess (NADPH >> $NADP^+$) (Sauer et al. 2004; Spaans et al. 2015) to drive L-lysine biosynthesis and other anabolic routes (Becker et al. 2005; Jiang et al. 2013; Wittmann and de Graaf 2005; Zhan et al. 2019). Hence, a sufficient supply of NADPH is crucial for efficient L-lysine formation. Regarding the NADH/NAD^+ ratio, growth on glycolytic substrates requires a surplus of NAD^+ over NADH (NAD^+ >> NADH) to provide sufficient thermodynamic driving force, and the efficient regeneration of NADH is one of the key tasks to keep glycolysis in efficient operation (Berg et al. 2018; Inui et al. 2004b; Spaans et al. 2015). Otherwise, excess NADH might impair the activity of glycolytic enzymes such as glyceraldehyde-3-phosphate dehydrogenase (Kiefer et al. 2004; Yokota and Lindley 2005). When growing *C. glutamicum* on mannitol, huge amounts of NADH were generated during oxidation of the carbon source into fructose.

In order to gain a better understanding of the different *C. glutamicum* strains and understand how the redox metabolism was altered by the imposed genetic manipulations, it appeared straightforward to determine the intracellular redox level, i.e. the ratio of the intracellular NADH/NAD^+ and NADPH/$NADP^+$, respectively. For this purpose, strains of interest were grown on mannitol and glucose and harvested in the early-exponential phase (Figure 5-17).

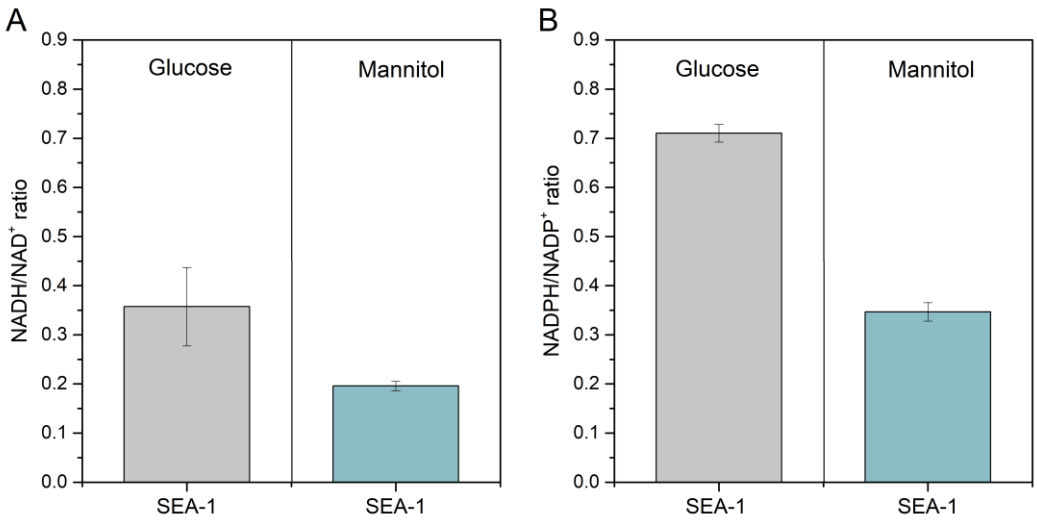

Figure 5-17: Redox metabolism in L-lysine producing *C. glutamicum* on glucose and mannitol. The figure shows the NADH/NAD$^+$ ratio (A) and the NADPH/NADP$^+$ ratio (B). The data represent mean values and deviations from three biological replicates.

The NADPH/NADP$^+$ ratio of glucose-grown SEA-1 (0.71 ± 0.02) was approximately twice as high as the value observed for growth on mannitol (Figure 5-17 B). First, the significant difference for the two substrates nicely matched with production performance. The yield for L-lysine in the genetically almost identical producer LYS-12 on glucose (Becker et al. 2011) was much higher than that of SEA-1 on mannitol (Figure 5-3, Table 5-1, Table 5-2). Apparently, the extent of NADPH excess acted as a driving force to form the amino acid. Second, it seemed that the differences in redox level directly emerged from differences in flux distribution. While glucose-grown LYS-12 (Becker et al. 2011) exhibited a high PP pathway flux (84 %) to form NADPH, mannitol-grown SEA-1 channeled only 6 % of the flux through this pathway, resulting in a more than 93 % reduced supply of the cofactor via this route, known to be the main one to generate NADPH in *C. glutamicum* (Becker et al. 2005; Kiefer et al. 2002; Marx et al. 1996; Wittmann and Heinzle 2001a).

A surprise was the outcome of the analyses of the NADH/NAD$^+$ ratio on both substrates. Intuitively, one would have expected an increased ratio on mannitol due to the inherently linked high formation of NADH during mannitol oxidation. However, the opposite was the case. On mannitol, SEA-1 strain revealed a 44 % decreased value (0.20 ± 0.01), as compared to that of glucose-grown SEA-1 cells (0.36 ± 0.08) (Figure 5-17 A). As high amounts of NADH are generated during the oxidation of mannitol to fructose. It is likely that the reduced NADH/NAD$^+$ ratio in the mannitol-grown SEA-1 strain is due to the cells attempting to get rid of excess NADH via the respiratory chain.

5.3.2 Co-factor balancing using transhydrogenase expression

Based on findings up to this point, indicating a low efficiency of mannitol-grown cells to use the PP pathway for redox supply (even after several genetic changes aiming at increased flux), further improvement of L-lysine production aimed at activating alternative routes to generate NADPH. The membrane-bound transhydrogenase PntAB from *E. coli*, able to provide NADPH from NADH appeared most promising. Driven by the proton motive force, the enzyme oxidizes NADH to NAD^+ while simultaneously reducing $NADP^+$ to NADPH (Jackson 2003; Kabus et al. 2007). For expression of PntAB, the genes *pntAB* (EG10744, EG10745) from the genome of *E. coli* K12-MG1655 (GenBank Accession No. NC_000913.3), were introduced into the *crtB* (NCgl0598) gene locus of SEA-1. The designed gene construct comprised two 600 bp homologous flanking regions, the *pntAB* gene itself (2932 bp) and a 200 bp-sized DNA fragment, harboring the *tuf* promoter (NCgl0480) for constitutive overexpression (Becker et al. 2005). A positive clone, obtained from the second recombination event, exhibited the correct PCR fragment of 4.3 kb and the correct sequence and was designated SEA-2D. In order to confirm transhydrogenase activity, the enzyme was assayed via monitoring the reduction of 3-acetylpyridine-NAD^+ by NADPH in the membrane fraction of *C. glutamicum* cells. The novel SEA-2D strain revealed the desired transhydrogenase activity (497.9 ± 30.8 mU mg^{-1}), whereas the parent strain *C. glutamicum* SEA-1 did not (< 0.1 mU mg^{-1}) (see appendix Table 7-13). Subsequently, the performance of SEA-2D was evaluated (Table 5-10). Supported by the PntAB expression, L-lysine production of SEA-2D was strongly enhanced. The strain produced L-lysine almost exclusively with a final titer of 12.8 mM. The L-lysine yield and specific production rate were increased by 47 % (to 225 mmol per mol mannitol) and by 25 % (to 0.91 mmol g^{-1} h^{-1}), respectively, compared to the parent strain (Table 5-2, Table 5-10). Moreover, the newly constructed mutant SEA-2D revealed improved fitness. It consumed mannitol completely within 26 h. Most strikingly, PntAB expression abolished fructose overflow (Table 5-10). It can therefore be assumed that fructose accumulation in the parent strain SEA-1 indicated a persistent bottleneck in the carbon core metabolism, stemming from the NADH generated during mannitol oxidation. This excess reducing power most presumably had an impairing effect on the glycolytic chain, particularly on glyceraldehyde 3-phosphate dehydrogenase (Kiefer et al. 2004; Toyoda and Inui 2016; Yokota and Lindley 2005). In this context, it is likely that the additional expression of PntAB not only boosted the NADPH supply, but also released the strain from redox stress by converting NADH to NAD^+. Ultimately, PntAB expression solved two problems at once, the NADPH shortage limiting L-lysine production as well as the high NADH/NAD^+ ratio impairing cell fitness and substrate catabolism.

Table 5-10: Growth and production characteristics of L-lysine producing *C. glutamicum* SEA-2D during batch cultivation using defined mineral salt medium with mannitol. The data comprise the specific rates for growth (μ), mannitol uptake (q_{Mtl}), and L-lysine production (q_{Lys}) and the yields for L-lysine ($Y_{Lys/Mtl}$), biomass ($Y_{X/Mtl}$) and by-products (fructose (Frc), trehalose (Tre), L-glycine (Gly), L-glutamate (Glu), lactate (Lac), acetate (Ace), and L-alanine (Ala)). The data represent mean values and deviations from three biological replicates.

Strain	SEA-2D
μ [h^{-1}]	0.21 ± 0.01
q_{Lys} [mmol g^{-1} h^{-1}]	0.91 ± 0.04
q_{Mtl} [mmol g^{-1} h^{-1}]	4.0 ± 0.1
$Y_{Lys/Mtl}$ [mmol mol^{-1}]	224.9 ± 5.0
$Y_{X/Mtl}$ [g mol^{-1}]	52.0 ± 3.9
$Y_{Frc/Mtl}$ [mmol mol^{-1}]	< 0.01
$Y_{Lac/Mtl}$ [mmol mol^{-1}]	< 0.01
$Y_{Glu/Mtl}$ [mmol mol^{-1}]	3.8 ± 0.1
$Y_{Gly/Mtl}$ [mmol mol^{-1}]	1.5 ± 0.1
$Y_{Tre/Mtl}$ [mmol mol^{-1}]	3.4 ± 0.2
$Y_{Ace/Mtl}$ [mmol mol^{-1}]	< 0.01
$Y_{Ala/Mtl}$ [mmol mol^{-1}]	< 0.01

To gain a better understanding how the expression of PntAB affected the intracellular flux distributions, the strain *C. glutamicum* SEA-2D was further analyzed at the metabolic flux level (Figure 5-18) using the approach as described above (see chapter 4.11.1). The fluxes via malic enzyme and PntAB were estimated by redox balancing, additionally considering the measured activity of malic enzyme and PntAB as a constraint and consistency check (see appendix Table 7-11, Table 7-13). Using this approach, the metabolic pathway activities of SEA-2D were determined (Figure 5-18). During the cultivation on [1-^{13}C] mannitol, cells exhibited isotopic and metabolic steady state (appendix Figure 7-4, Table 5-10). As direct response to the PntAB expression, no fructose accumulation could be observed compared to the parent strain SEA-1 (Figure 5-18). Consequently, a high carbon flux was channeled via fructose 1-phosphate to the lower EMP pathway. The PP pathway was found to be even less active than in the parent strain. Even though a very low PP pathway activity was observed in the SEA-2D mutant, the mutant showed a high carbon flux (24 %) towards the L-lysine biosynthetic pathway, while the fluxes fueling the TCA cycle remained unaffected. This finding suggests that the high demand for NADPH to drive L-lysine biosynthesis is covered by the interconversion reaction of NADH and $NADP^+$ into NADPH and NAD^+ by the transhydrogenase reaction (Kabus et al. 2007). Accordingly, a transhydrogenase activity of 66 % was observed. This finding impressively demonstrates that solely the expression

of PntAB in mannitol-grown cells is sufficient to increase L-lysine production to a high extent and furthermore confirms the success of the applied strategy.

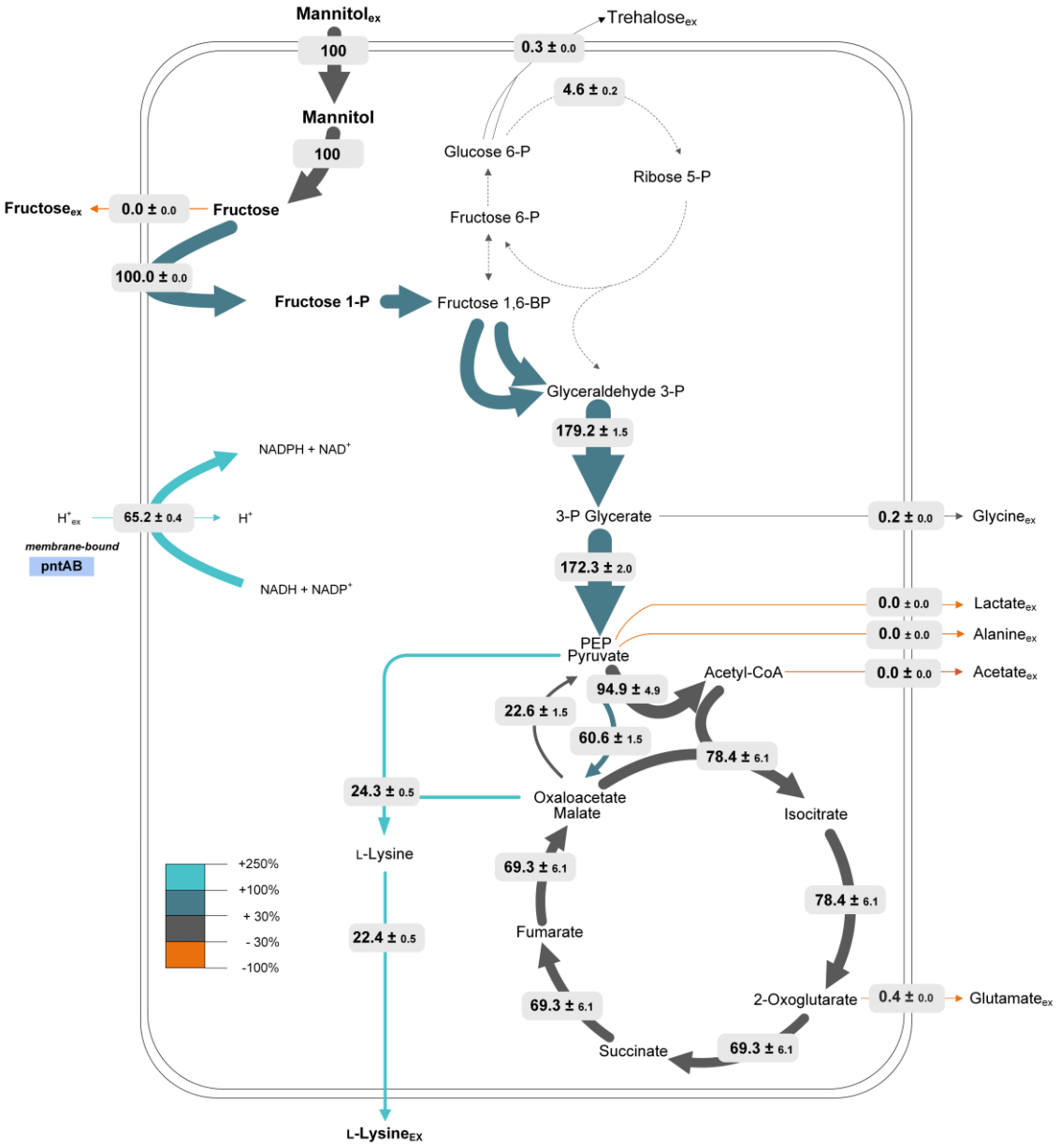

Figure 5-18: *In vivo* carbon flux distribution of L-lysine-producing *C. glutamicum* SEA-2D during growth on mineral salt medium containing mannitol as the sole carbon source. All fluxes are expressed as the molar percentage of the corresponding mean specific mannitol uptake rate (q_{Mtl} = 4.0 mmol g^{-1} h^{-1}), which was set to 100 %. The thickness of the reaction arrows represents the flux amount, while the color code reflects the flux differences compared to the L-lysine basic producer *C. glutamicum* SEA-1. The anabolic fluxes into biomass are not displayed.

5.4 Cascaded processing of seaweed into alginate and bioavailable monosaccharides

5.4.1 Hydrothermal extraction of *Laminaria digitata*

As discussed above, aquatic biomass is getting more and more into the focus of research, as it is more sustainable than terrestrial feedstocks (Kraan 2013). Members of the group of brown macroalgae, including *Laminaria digitata*, are rich in polysaccharides (laminarin, alginate) and in particular, free mannitol. The sugar alcohol forms up to 30 % of the dry weight, depending on the seasonal harvest of the algae (Iwamoto and Shiraiwa 2005; Poblete-Castro et al. 2020; Wei et al. 2013). In this regard, the mannitol-based L-lysine process developed in this work should now be tested on real seaweed streams. For this purpose, *L. digitata* was processed in order to get mannitol-rich extracts. The developed cascaded work flow for crushing, extraction and depolymerization of the algal biomass is shown in Figure 5-19.

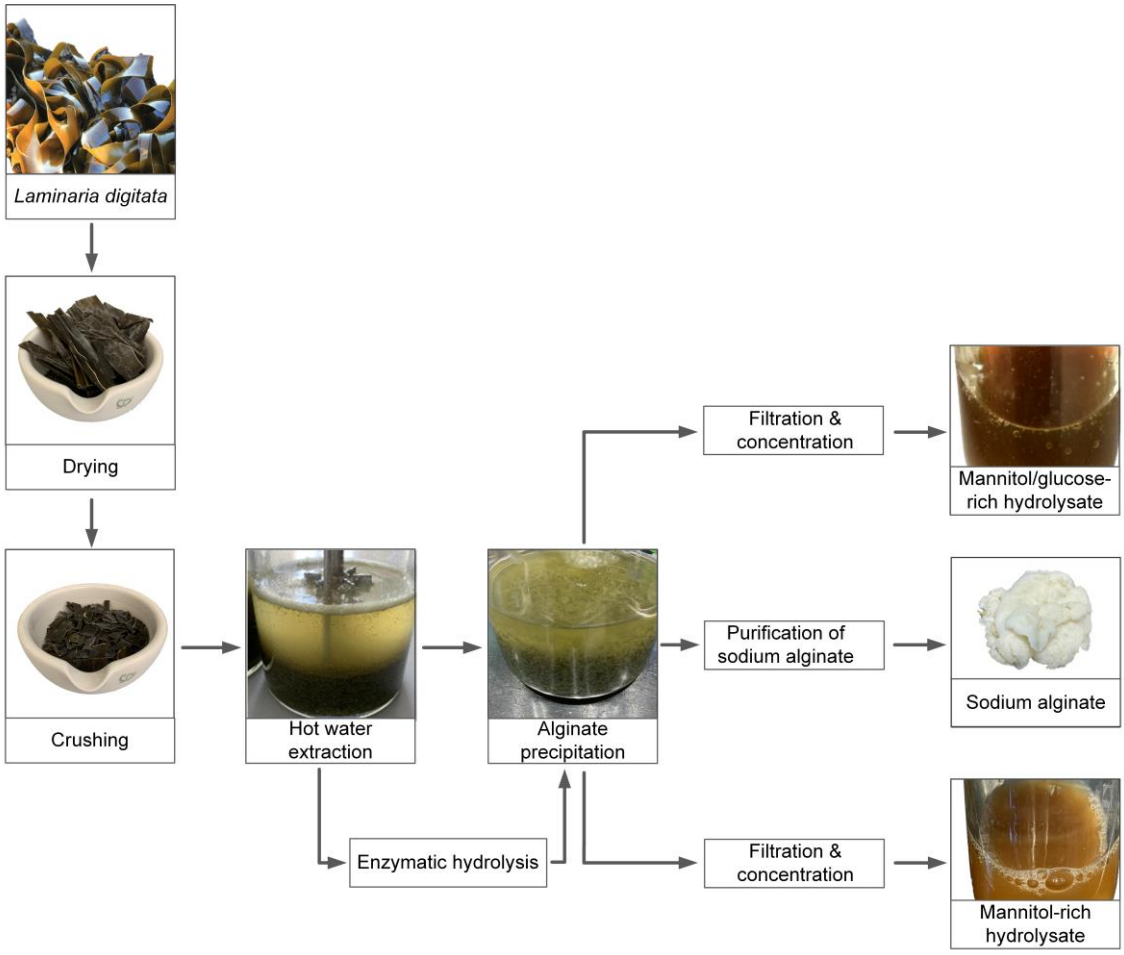

Figure 5-19: Cascaded processing of the brown algae *L. digitata* into alginate and sugar-rich hydrolysates. The conversion steps are described in the boxes.

After several rounds of optimization, sugar-rich hydrolysates could be obtained via a cascade of process steps, which included crushing of the algae, hydrothermal extraction optionally combined with enzymatic hydrolysis, alginate precipitation and purification, as well as filtration and concentration of the extract into a fermentable hydrolysate. The protocol was developed out of previous workflows, using extraction in hot water (Horn et al. 2000b), acid hydrolysis (Chades et al. 2018; Kim et al. 2011), and enzymatic hydrolysis (Kim et al. 2011) for seaweed extracts. In order to minimize the use of reagents and avoid an increased salt content, hot water (121 °C) was chosen first to extract mannitol. After the treatment, the solely detectable carbohydrate was mannitol (Figure 5-20). In addition to mannitol, the hot water extract contained traces of L-alanine, L-glutamate and L-aspartate. These are the most abundant amino acids in algal biomass (Hou et al. 2015; Manns et al. 2017). The mannitol concentration in the extract ranged between 6 g L^{-1} and 12 g L^{-1} for different *L. digitata* batches. The fluctuation appeared due to seasonal variation of the mannitol content in seaweed. Mannitol accumulates during summer and autumn as a storage compound, and is re-utilized during winter (Schiener et al. 2015). Next, we tested acid hydrolysis, shown to increase the mannitol yield during extraction (Chades et al. 2018). However, extraction at 50 °C using 0.1 M HCl resulted in a mannitol concentration, similar to that observed for hot water extraction. Even though the pH was adjusted after the extraction using NaOH, *C. glutamicum* did not grow on acid-derived hydrolysates. Probably, the high concentration of chloride ions and/or sodium ions were inhibiting cell growth. Consequently, the acid-based treatment for sugar extraction was not further pursued. Towards higher substrate levels for the subsequent fermentation experiment, the extracts were concentrated 7-fold. Thus, extracts containing up to 50 g L^{-1} of mannitol were obtained. The high level of mannitol appeared advantageous as cultivation studies could be performed at higher substrate levels. It had, however, to be tested, whether the concentration steps did not increase the abundance of other ingredients to inhibitory levels.

5.4.2 Enhanced process with combined enzymatic treatment

Laminarin, a glucose-containing polymer capped by mannitol at its reducing end, can form up to 40-50 % of the dry weight of certain seaweed species (Torres et al. 2019; Wang et al. 2016a; Wei et al. 2013). It also occurs in *L. digitata*, although to a lower extent (Kadam et al. 2015; MacArtain et al. 2007). It appeared beneficial to make it available for L-lysine production towards increased efficiency. Previous studies have approached the degradation of Laminarin by enzymatic hydrolysis (Hou et al. 2017; Kim

et al. 2011). In line, an enzymatic step was added after the extraction, using an commercial enzyme cocktail, composed of cellulosic enzymes complexed with a broad range of carbohydrate depolymerizing activities (Celluclast 1,5 L, Viscozyme L). As depicted in Figure 5-20, the enzymatic treatment formed glucose and fructose in addition to mannitol.

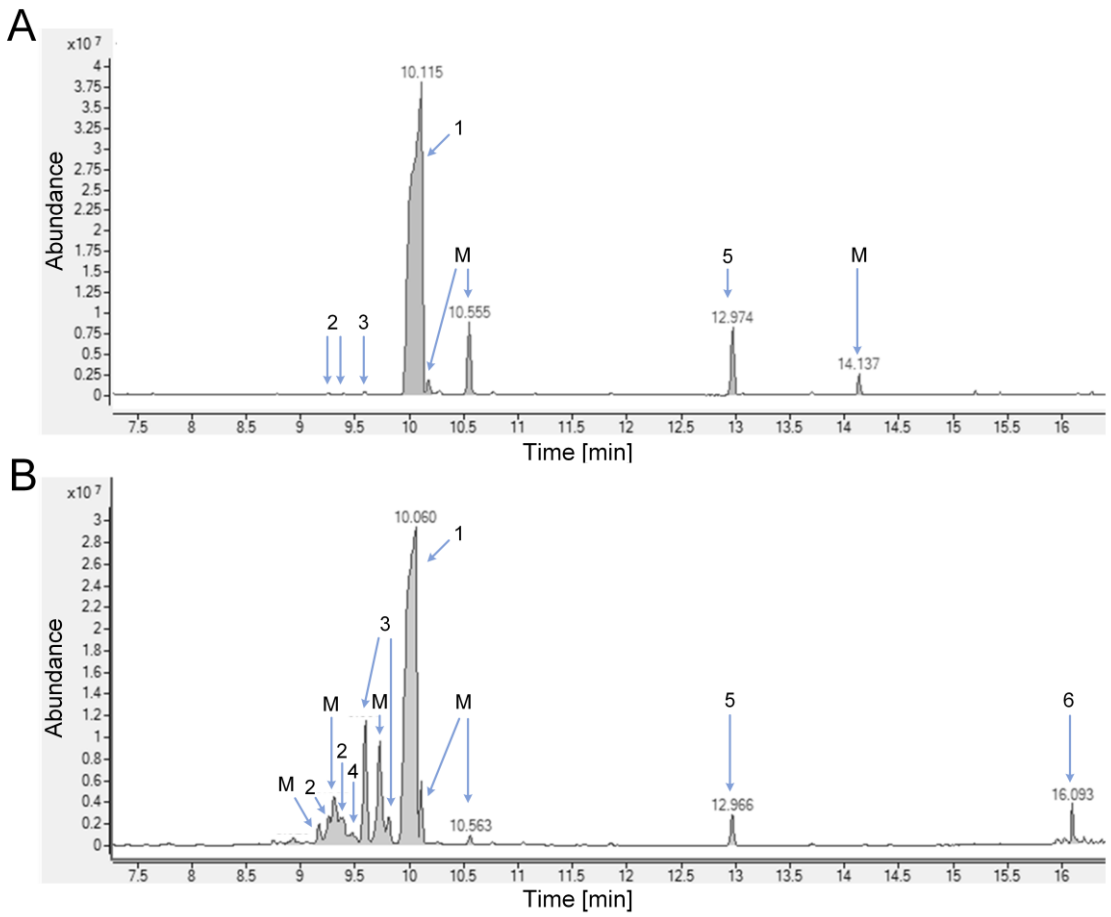

Figure 5-20: GC-MS analysis of processed *L. digitata* hydrolysates after thermal extraction (A) and after thermal extraction with subsequent enzymatic hydrolysis using Celluclast 1,5 L and Viscozyme L (B). The samples were derivatized with MSTFA for GC-MS measurement. The carbohydrates were identified based on retention time and mass spectrum as compared to pure standards. The following TMS-derivatives were detected: 1, mannitol (91 % identity); 2, fructose (91 %); 3, glucose (93 %); 4, galactose (83 %)/mannose (72 %). The presence of other sugars was suggested, although at rather low spectrum identity: 5, sedoheptulose (45 %)/mannonic acid (45 %); 6, maltose (58 %). Other signals (M) either belonged to the sample matrix or background noise.

In addition to the sugars, small amounts of L-glutamate, L-aspartate and L-alanine were found.

The obtained extracts were generally quite viscous after combined thermal and enzymatic treatment, likely linked to the presence of alginate (Figure 5-19) (Chades et al. 2018; Hou et al. 2015).

5.4.3 Extraction and purification of alginate as a high value side stream

Alginate was extracted and purified into sodium alginate (Figure 5-19). Through several steps of separation, decolorization and purification, sodium alginate was finally recovered as a clean, white gum (Figure 5-19). In total, the alginate yield was 7.4 % after subsequently drying for 24 h at 80 °C. The structural polysaccharide is an industrially relevant product. It is widely used in the food, cosmetic, pharmaceutical, and paper industry, mainly due to its superior gelling, thickening and stabilization properties (Fertah et al. 2017; Torres et al. 2019). In this regard, the purification of alginate as a side stream maximized the valorization degree of seaweed as raw material. *C. glutamicum* is naturally unable to use alginate as a carbon source. One could imagine to breakdown alginate during the hydrolysis (would, however, require more harsh conditions and energy) and the implementation of catabolic pathways for breakdown of the alginate monomers guluronic acid and mannuronic acid (Hou et al. 2015; Wang et al. 2016a) in *C. glutamicum* in the future, as an alternative. This would require substantial engineering efforts. However, the combined use of alginate plus mannitol could create interesting synergies. As an example, engineered *E. coli* can metabolize alginate and mannitol simultaneously for the production of ethanol. This approach is promising, as the fermentation of alginate to ethanol requires NADH, which on the other hand is provided by the mannitol catabolism (Wargacki et al. 2012). After precipitation of alginate, the remaining extracts were concentrated 7-fold using vacuum concentration. The major carbohydrate observed in the concentrated hydrolysate was mannitol (Figure 5-20). It varied between 53 g L^{-1} and 74 g L^{-1} for different *L. digitata* batches. The enzyme treated alginate-depleted hydrolysates revealed substantial levels of glucose (16 g L^{-1} to 22 g L^{-1}) and fructose (0.5 g L^{-1} to 3.5 g L^{-1}). Taken together, the combination of hydrothermal and enzymatic treatment followed by vacuum concentration provided rich hydrolysates. The recovery of pure alginate as a side stream integrates well into emerging cascaded biorefinery processes envisioning to use the entire seaweed biomass more efficiently (van Hal et al. 2014).

5.5 Creation and benchmarking of a fully genome-based L-lysine-producing cell factory

5.5.1 Design, construction and evaluation of a fully genome-based producer

Based on all the insights gained from metabolic engineering, the most beneficial traits should now be combined towards maximum efficiency. The cell factory to be created should only display genomic modifications, implemented into the genome for the sake of strain stability and strain safety and a production process without selection markers. The basic L-lysine producer SEA-1 was taken as a starting point. It was based on the L-lysine hyperproducer LYS-12 and coined twelve modifications to enhance L-lysine formation on glucose (Becker et al. 2011) and additionally lacked the mannitol repressor (MtlR) to enable mannitol utilization (Laslo et al. 2012; Peng et al. 2011). As a second-generation strain, SEA-2D, expressing the membrane-bound transhydrogenase PntAB was selected, due to its excellent production capacity (Table 5-10, Figure 5-18). Since *C. glutamicum* SEA-2D supplied NADPH almost exclusively via isocitrate dehydrogenase in the TCA cycle and the novel transhydrogenase reaction (Figure 5-18), the next round of metabolic engineering aimed to activate the PP pathway as additional route for NADPH supply. This strategy promised to reduce carbon loss in the TCA cycle via CO_2 formation (Kiefer et al. 2004). Based on the findings in this work, the fructokinase Mak from *E. coli* was co-expressed. The genomic implementation was performed in the same way as described above. The obtained mutant was designated *C. glutamicum* SEA-4.

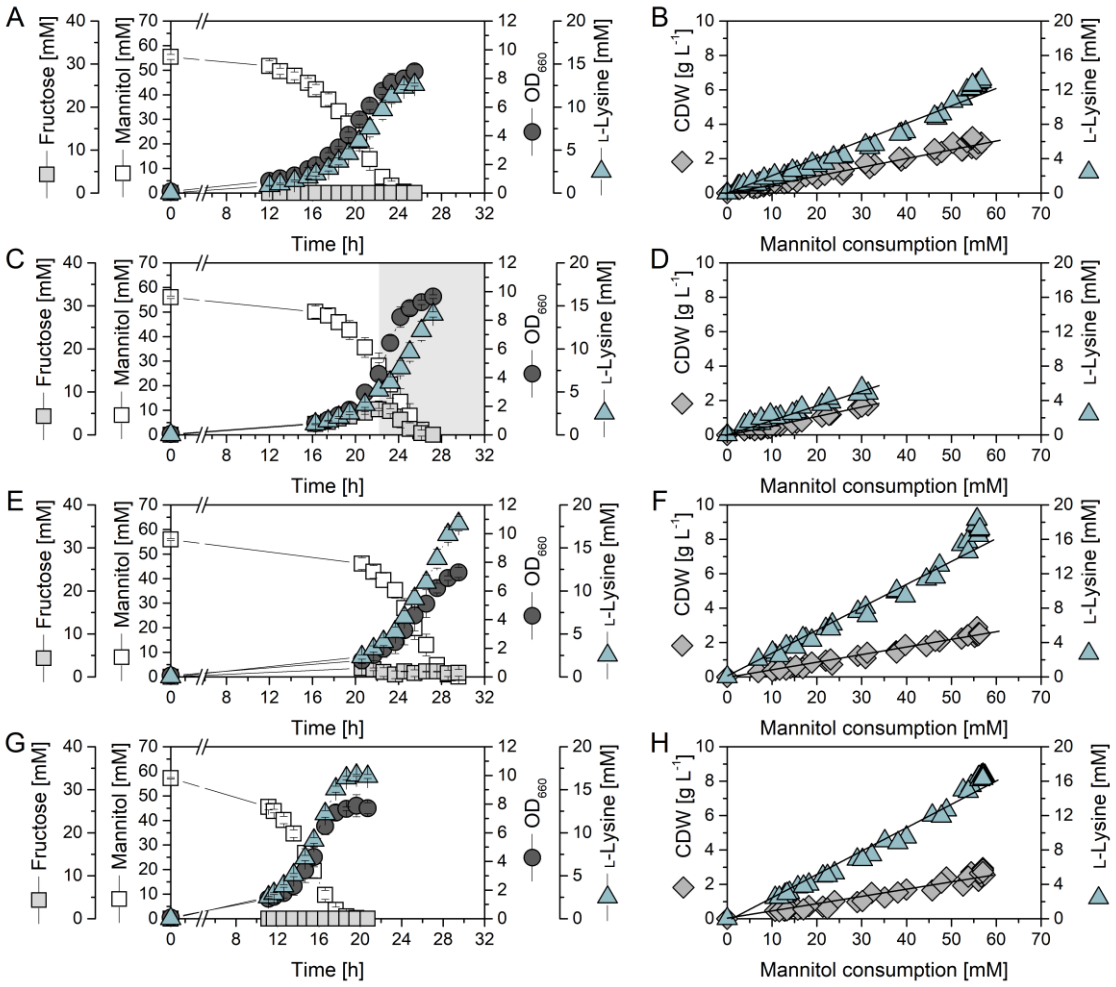

Figure 5-21: Genealogy of L-lysine producing *C. glutamicum* strains SEA-2D (A-B), SEA-4 (C-D), SEA-6 (E-F), and SEA-7 (G-H) on mineral salt medium containing mannitol as the sole carbon source. The cultivation profiles represent mean values and corresponding standard deviations from three biological replicates (A, C, E, G). Yields for L-lysine and biomass were determined by linear regression of L-lysine and biomass formation, respectively, plotted against mannitol consumption (B, D, F, H). These data reflect the initial growth phase, linked to fructose accumulation (shown in white) for strain SEA-4 and the entire cultivation period for the other non-fructose accumulating strains.

Table 5-11: Kinetics and stoichiometry of L-lysine-producing *C. glutamicum* strains on mannitol. The data represent the initial growth phase, linked to fructose accumulation (shown in white, Figure 5-21) for strain SEA-4 and the entire cultivation period for the other non-fructose accumulating strains SEA-2D, SEA-6 and SEA-7. In addition, the control strain SEA-5 is shown, harboring the empty pClik 5α MCS plasmid. The data comprise the specific rates for growth (μ), mannitol uptake (q_{Mtl}), and L- lysine production (q_{Lys}) and the yields for L-lysine ($Y_{Lys/Mtl}$), biomass ($Y_{X/Mtl}$) and by-products (fructose (Frc), trehalose (Tre), L-glycine (Gly), L-glutamate (Glu), lactate (Lac), acetate (Ace), and L-alanine (Ala)). The data represent mean values and deviations from three biological replicates.

Strain	SEA-2D	SEA-4	SEA-5	SEA-6	SEA-7
μ [h^{-1}]	0.21 ± 0.01	0.29 ± 0.03	0.24 ± 0.06	0.24 ± 0.02	0.25 ± 0.02
q_{Lys} [mmol g^{-1} h^{-1}]	0.91 ± 0.04	0.85 ± 0.01	0.84 ± 0.02	1.59 ± 0.03	1.58 ± 0.05
q_{Mtl} [mmol g^{-1} h^{-1}]	4.0 ± 0.1	5.4 ± 0.3	5.2 ± 0.2	5.1 ± 0.1	5.3 ± 0.1
$Y_{Lys/Mtl}$ [mmol mol^{-1}]	224.9 ± 5.0	159.3 ± 8.1	163.3 ± 9.1	311.9 ± 7.6	299.5 ± 4.8
$Y_{X/Mtl}$ [g mol^{-1}]	52.0 ± 3.9	53.5 ± 1.8	45.9 ± 9.3	47.2 ± 3.0	47.8 ± 5.4
$Y_{Frc/Mtl}$ [mmol mol^{-1}]	< 0.01	179.3 ± 8.7	239.9 ± 13.4	< 0.01	< 0.01
$Y_{Lac/Mtl}$ [mmol mol^{-1}]	< 0.01	< 0.01	< 0.01	< 0.01	< 0.01
$Y_{Glu/Mtl}$ [mmol mol^{-1}]	3.8 ± 0.1	8.5 ± 1.5	6.6 ± 1.6	4.6 ± 1.3	9.5 ± 0.2
$Y_{Gly/Mtl}$ [mmol mol^{-1}]	1.5 ± 0.1	3.4 ± 0.2	4.5 ± 0.4	4.7 ± 0.2	5.2 ± 0.4
$Y_{Tre/Mtl}$ [mmol mol^{-1}]	3.4 ± 0.2	4.2 ± 0.1	3.5 ± 0.3	2.7 ± 0.2	1.8 ± 0.2
$Y_{Ace/Mtl}$ [mmol mol^{-1}]	< 0.01	< 0.01	< 0.01	< 0.01	< 0.01
$Y_{Ala/Mtl}$ [mmol mol^{-1}]	< 0.01	< 0.01	< 0.01	< 0.01	< 0.01

When considering the entire cultivation of strain SEA-4, the expression of the Mak enzyme resulted in a substantial increase in the overall L-lysine yield 273 mmol mol^{-1} (Figure 5-22 A). When considering the initial cultivation phase, however, the additional expression of the Mak enzyme appeared detrimental on a first glance (Figure 5-21 C). The mutant secreted fructose, which was quite surprising, because the implemented enzyme should have rather enhanced the intracellular consumption of fructose. The exact reason remained unclear. One explanation could be the subsequently enhanced mannitol influx in the novel strain, resulting from the combined expression of PntAB and Mak. Apparently, the two enzymes synergistically worked together towards faster growth and substrate uptake. This triggered an extra influx of mannitol, which could not be handled. Indeed the excreted fructose flux almost exactly matched this extra uptake of mannitol. In addition, *C. glutamicum* SEA-4 showed an elevated L-lysine production rate (1.4 mmol g^{-1} h^{-1}), which represented an increase of 54 %, as compared to the SEA-2D strain (Figure 5-22 B).

In order to eliminate fructose accumulation, a next round of metabolic engineering aimed to abolish this overflow. As shown, the expression of GapN beneficially reduced fructose excretion (Figure 5-14, Figure 5-16). Therefore, native *gapN*, coding for non-phosphorylating NADP-dependent glyceraldehyde 3-phosphate dehydrogenase from *S. mutans* (Crow and Wittenberger 1979; Takeno et al. 2010) was episomally expressed in *C. glutamicum* SEA-4 (see chapter 5.2.3). The newly created strain, designated SEA-6, expressed *gapN* under control of its native promotor. The correctness of the mutant was verified by PCR and sequencing. When tested in shaking flasks, it showed an even better production performance. SEA-6 accumulated L-lysine to a titer of 17.8 mM, corresponding to a L-lysine yield of 312 mmol mol^{-1} (Figure 5-21 E, F, Figure 5-22 A). Furthermore, the strain exhibited an increased specific L-lysine production rate compared to the parent strain (Figure 5-22 B). Since a control strain (SEA-5), which harbored the empty plasmid did not reveal this improvement, but rather matched the characteristics of the ancestor strain, the enhanced performance could be directly attributed to the GapN enzyme. Notably, fructose accumulation was completely abolished by the GapN expression, confirming the success of the applied strategy.

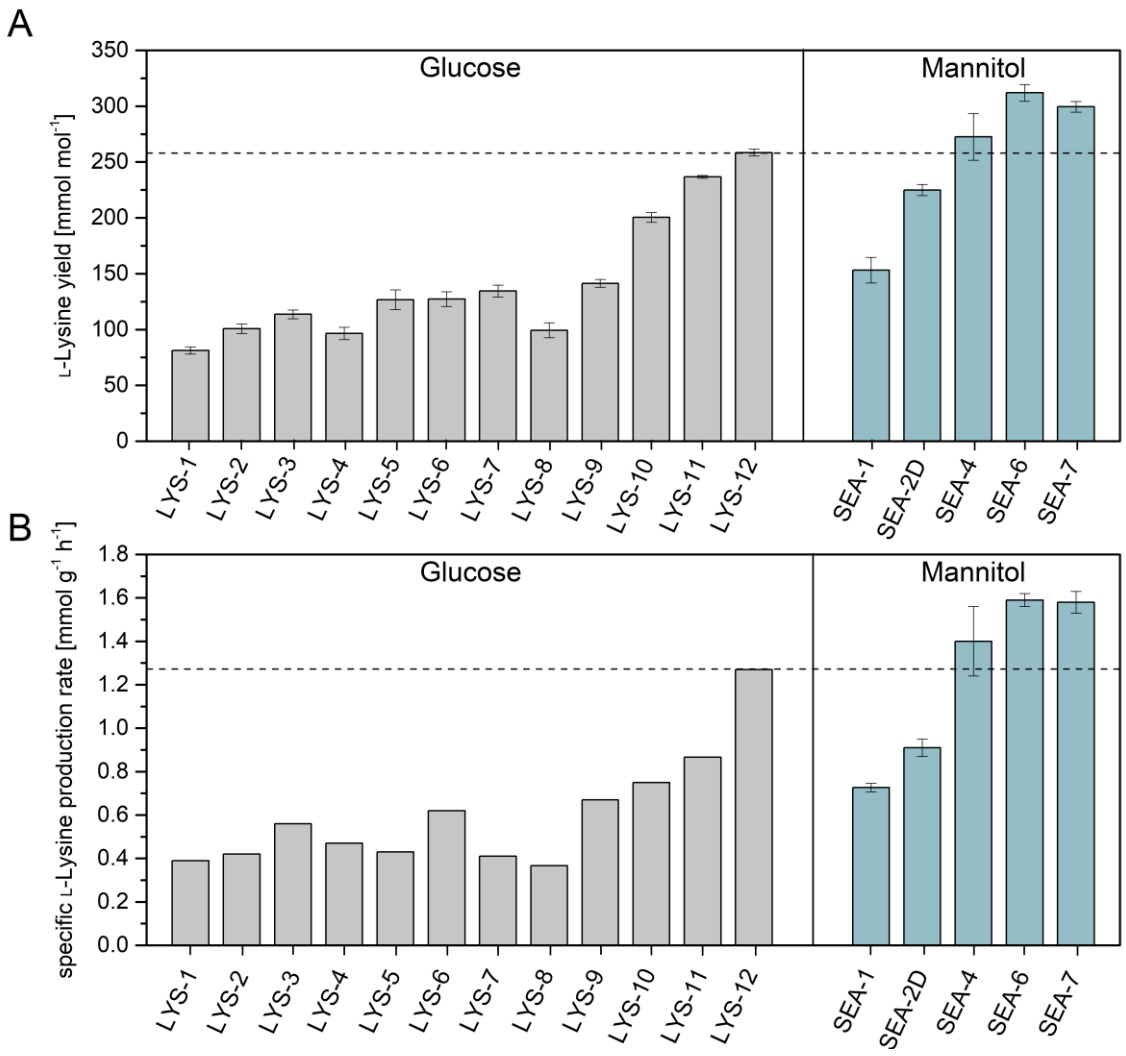

Figure 5-22: Production characteristics of *C. glutamicum* strains, engineered for L-lysine production from mannitol. The figure shows the mean specific L-lysine yield (A) and the specific L-lysine production rate (B) calculated for the constructed strains SEA-1, SEA-2D, SEA-4, SEA-6 and SEA-7 over the entire cultivation period (turquoise bars). The data represent mean values and deviations from three biological replicates. For comparison the L-lysine yield (A) and the specific L-lysine production rate (B) of previous metabolic engineered glucose-optimized *C. glutamicum strains*, i.e. L-lysine producers LYS-1 to LYS-12, are shown (grey bars) (Becker et al. 2011).

An important final round of engineering replaced the plasmid-based *gapN* gene by a genome-based copy to obtain a fully genome-engineered strain. To compensate for the fact that a genomic *gapN* gene would occur only as a single copy, as compared to likely several or even multiple copies of a plasmid-based *gapN* gene, the expression efficiency was tuned. First, the *gapN* gene from *S. mutans* was adapted to the preferred codon usage of *C. glutamicum* (see appendix Figure 7-1). Second, the translational start codon of *gapN* (GTG) was changed by the more common and stronger variant ATG in order to promote translational efficiency (Becker et al. 2010). Third, the native promoter was

replaced by the *tuf* promoter, proven to mediate high expression efficiency in *C. glutamicum* (Becker et al. 2005). The designed construct for implementation of *gapN* into the *crtI*2 gene locus (NCgl0597) of *C. glutamicum* SEA-4 comprised the *gapN* gene itself (1428 bp) under control of the constitutive *tuf* promoter as well as two homologous flanking regions (483 bp and 447 bp) of the 5' and 3' regions of the *crtI*2 locus. The strain *C. glutamicum* SEA-7, obtained after the second recombination event, was verified by PCR and sequencing. In order to confirm the functionality of the codon-optimized GapN, enzymatic measurement was conducted as described above. The novel mutant revealed the desired NADP-dependent activity (462.6 ± 2.4 mU mg^{-1}), whereas no $NADP^+$ activity was detectable in its ancestor strain. Compared to the native plasmid-based GapN (250 ± 11 mU mg^{-1}), an almost doubled activity was found for the codon-optimized version, which was an excellent measure of success of the implemented genetic optimization at the level of codon usage, promoter strength and translational efficiency. Moreover, it indicated a substantial extension of the glycolytic flux capacity in the SEA-7 strain. Supported by codon-optimized GapN expression, SEA-7 consumed mannitol within only 20 h (Figure 5-21 G), much faster than all parent strains. The engineering of the glycolytic flux capacity also completely eliminated fructose overflow (Figure 5-21 G). Metabolic flux analysis of SEA-7 revealed a high carbon flux towards lower glycolysis (Figure 5-23), while the carbon flux through the PP pathway was rather low (6 %). The lower glycolysis was strongly activated by the additional GapN, which contributed 36 % to the total EMP pathway flux. In this regard, the genome-based optimized GapN was much more efficient as the plasmid-based native copy, which increased the flux by only 23 %. Thus, a substantial flux (32 %) was directed to the L-lysine pathway, while the TCA cycle flux was mainly unaffected (Figure 5-23).

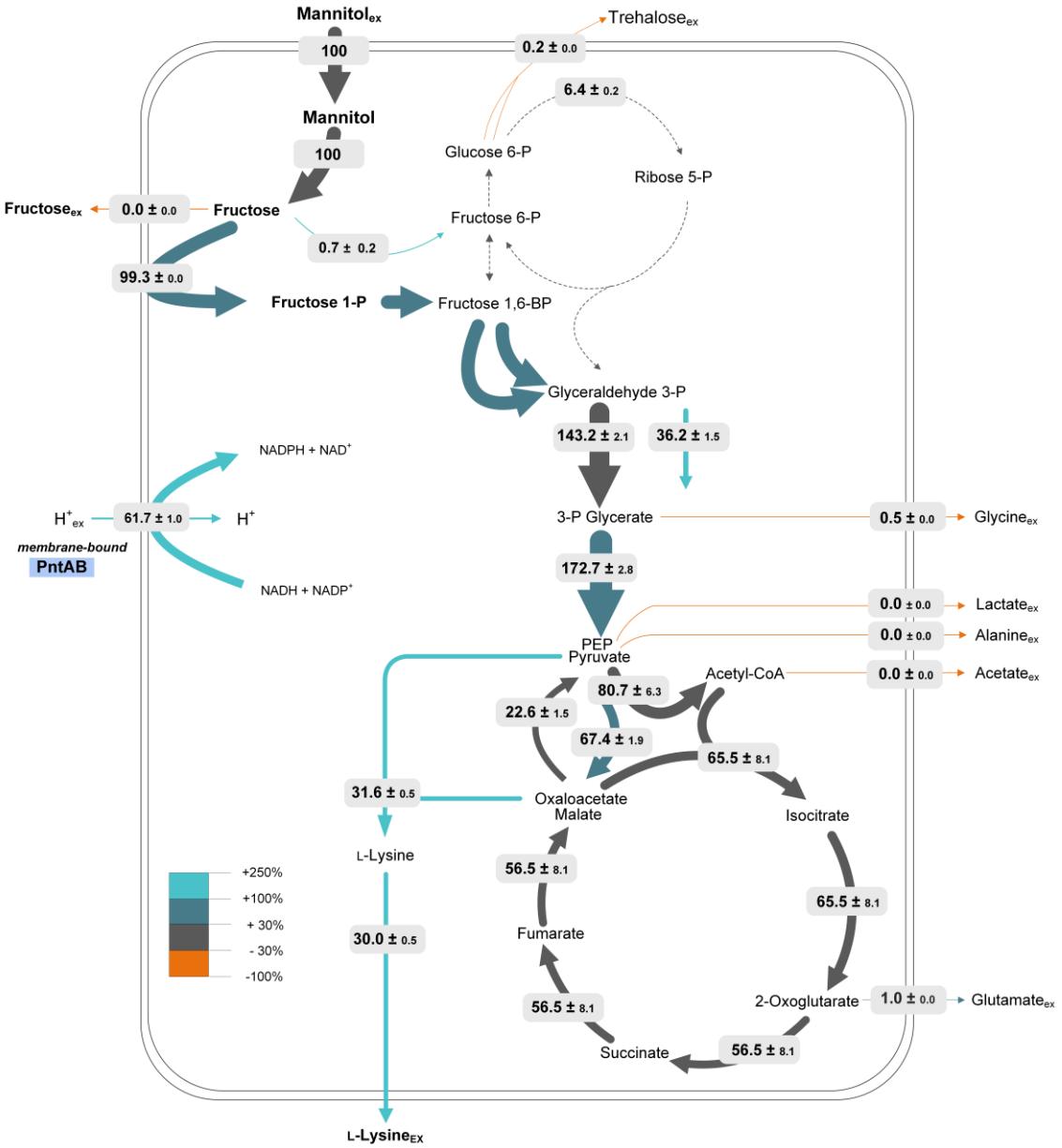

Figure 5-23: *In vivo* carbon flux distribution of the tailor-made L-lysine-producing strain *C. glutamicum* SEA-7 during growth on mannitol. All fluxes are given as a molar percentage of the corresponding mean specific mannitol uptake rate (q_{Mtl} = 5.3 mmol g^{-1} h^{-1}), which was set to 100 %. The thickness of the reaction arrows represents the flux amount, while the color code reflects the flux difference compared to the basic L-lysine producer *C. glutamicum* SEA-1. The anabolic fluxes into biomass are not displayed.

Regarding L-lysine yield (300 mmol mol^{-1}) and specific L-lysine production rate (1.6 mmol g^{-1} h^{-1}), the novel SEA-7 strain was as good as the plasmid-based variant (Figure 5-22, Table 5-11). The finally designed, L-lysine-producing *C. glutamicum* SEA-7 comprised sixteen genomic modifications in total, which enabled efficient L-lysine production from mannitol. The genomic traits included i) the activation of mannitol utilization by deletion of the MtlR repressor, ii) the improvement of precursor supply,

iii) the attenuation of undesired by-products, iv) the upregulation of the L-lysine biosynthetic pathway, v) the enhancement of NADPH supply, and vi) the recycling of excess NADH (Figure 5-24). When comparing the L-lysine yield and the specific L-lysine production rate of the recently created L-lysine hyperproducing strain *C. glutamicum* LYS-12 (Becker et al. 2011) with those of the SEA-7 strain (Figure 5-22), it becomes obvious that the constructed mutant surpassed the L-lysine yield and the specific L-lysine production rate by nearly 16 % and 24 %, respectively.

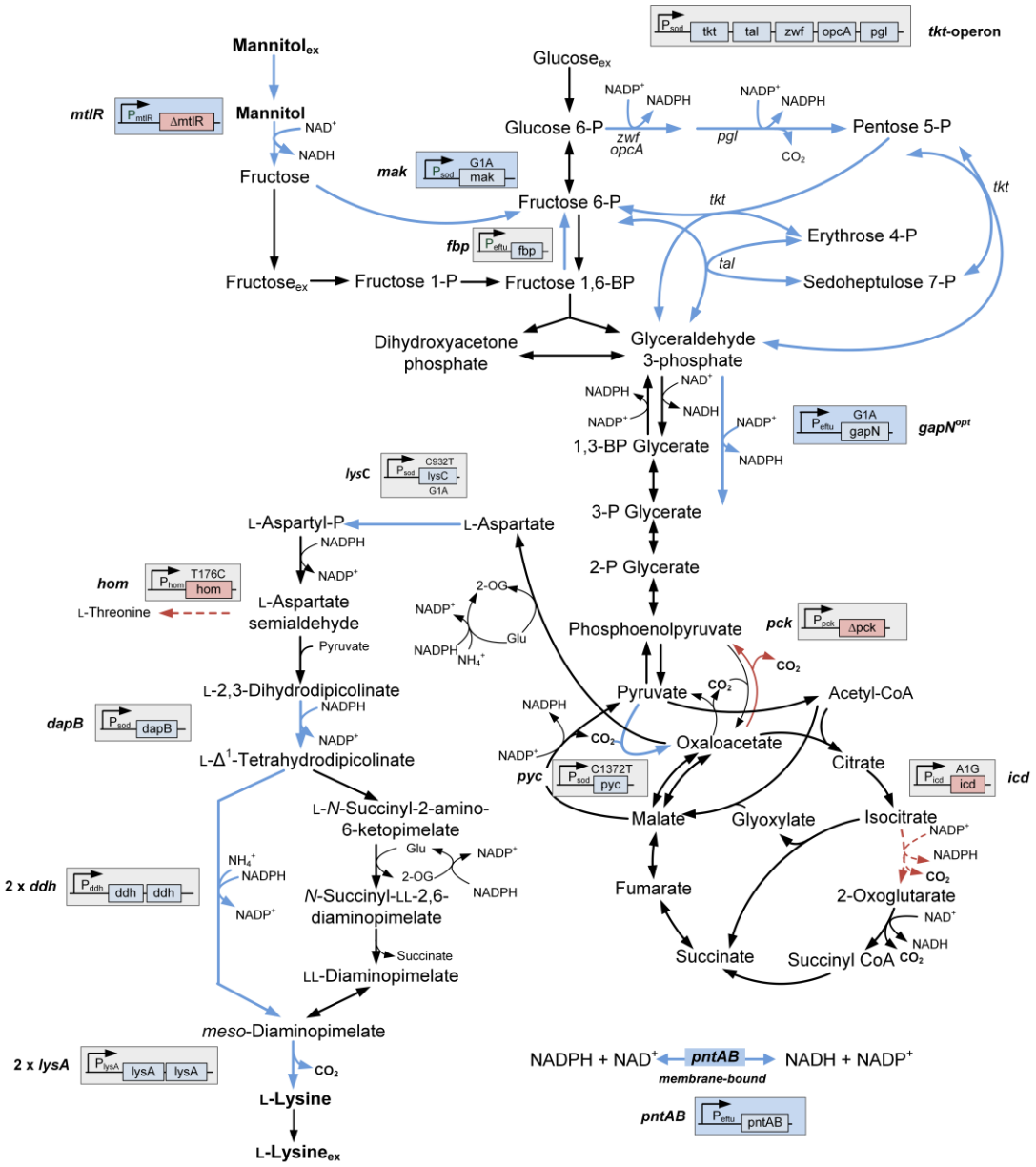

Figure 5-24: Design of tailor-made L-lysine producing *C. glutamicum* SEA-7 by systems wide metabolic engineering. The cell factory comprised the following genetic traits: deletion of the mannitol repressor (Δ*mtlR*), overexpression of fructokinase from *E. coli* (P_{sod} *mak*), overexpression of codon-optimized NADP-dependent glyceraldehyde 3-phosphate dehydrogenase (*gapN*) from *S. mutans* (P_{eftu} *gapN*^{opt}), overexpression of membrane-bound transhydrogenase (*pntAB*) from *E. coli* (P_{eftu} *pntAB*), overexpression of the transketolase operon (P_{sod} *tkt*), overexpression of fructose 1,6-bisphosphatase (P_{eftu} *fbp*), overexpression and feedback decoupling of pyruvate carboxylase (P_{sod} *pyc*^{P458S}), overexpression and feedback decoupling of aspartokinase (P_{sod} *lysC*^{T311I}), deletion of phosphoenolpyruvate carboxykinase (Δ*pck*), attenuation of isocitrate (*icd*^{GTG}) dehydrogenase and homoserine dehydrogenase (*hom*^{V59A}), overexpression of 4-hydroxy-tetrahydrodipicolinate reductase (P_{sod} *dapB*), overexpression of diaminopimelate dehydrogenase (2x *ddh*), and overexpression of L-lysine decarboxylase (2x *lysA*). Blue arrows indicate gene amplification, while red arrows indicate gene deletion and red dashed arrows gene attenuation. The depicted gray boxes represent modified genetic traits, which were implemented in the genome of *C. glutamicum* by. Becker et al. (2011), while the blue boxes show the genetic traits of this work. All genetic modifications were stably implemented into the genome of *C. glutamicum*.

5.5.2 Redox status in *C. glutamicum* strains expressing the membrane-bound transhydrogenase PntAB

When considering all experiments, particularly the redox measurements in the selected *C. glutamicum* strains (Figure 5-25, Figure 5-26), it becomes clear that a balanced NADH/NAD^+ ratio as well as the sufficient supply of NADPH is crucial for an improved L-lysine production from the sugar alcohol mannitol. It was shown, that the PP pathway is the common route in L-lysine producing *C. glutamicum* strains to provide NADPH for the formation of L-lysine (Becker et al. 2007; Becker et al. 2005; Becker et al. 2011; Kiefer et al. 2004). However, this is not the case for *C. glutamicum* strains grown on mannitol, as they show a significantly low PP pathway activity. (Figure 5-5, Figure 5-12, Figure 5-16, Figure 5-18, Figure 5-23). Although the PP pathway provides large amounts of reduction power, the production of NADPH is inevitably concomitant with the loss of carbon in form of CO_2 that is no longer available for L-lysine formation (Marx et al. 1996; Takeno et al. 2016). For this reason, a different strategy was pursued, which aimed to supply the cell with sufficient NADPH while reducing the high NADH/NAD^+ ratio. Thus, by combining the expression of GapN and PntAB in mannitol-grown cells, the highest L-lysine yield ever observed in mannitol-grown *C. glutamicum* cells was achieved (Figure 5-22, Figure 5-26). Also the redox state of the cell was shown to be enhanced markedly after the expression of either PntAB or PntAB and GapN (Figure 5-25 B, Figure 5-26), confirming that the increased NADPH/$NADP^+$ ratio improves L-lysine production in a substantial manner. These findings confirm, that besides the PP pathway the NADPH supply via the glycolytic chain is also highly promising for the overproduction of L-lysine in mannitol-grown *C. glutamicum* cells. Takeno et al. (2016) for instance, demonstrated that an efficient L-lysine synthesis is possible solely via a NADPH coupled glycolysis. Thereby, they disrupted the PP pathway at the level of glucose 6-phosphate and showed that the PP pathway activity is not essential for efficient L-lysine biosynthesis when instead GapN is expressed (Takeno et al. 2016).

When it comes to redox power, not only the delivery of NADPH is crucial, but also the NADH/NAD^+ ratio in the cell. Considering the NADH/NAD^+ ratio in the selected strains, it becomes obvious that a nearly constant NADH/NAD^+ ratio was obtained when the strains SEA-1 (0.196 ± 0.009), SEA-2D (0.215 ± 0.019), and SEA-4 (0.265 ± 0.07) were cultivated on mannitol (Figure 5-25 A). However, it could be shown that the additional GapN expression in SEA-7 led to a reduced NADH/NAD^+ ratio in the cell. Metabolic flux analysis of strain SEA-7 revealed that GapN contributed 36 % to the total flux of the EMP pathway (Figure 5-23), hence the reduced NADH/NAD^+ ratio is likely due to the lower contribution of the native NAD-dependent GapA enzyme.

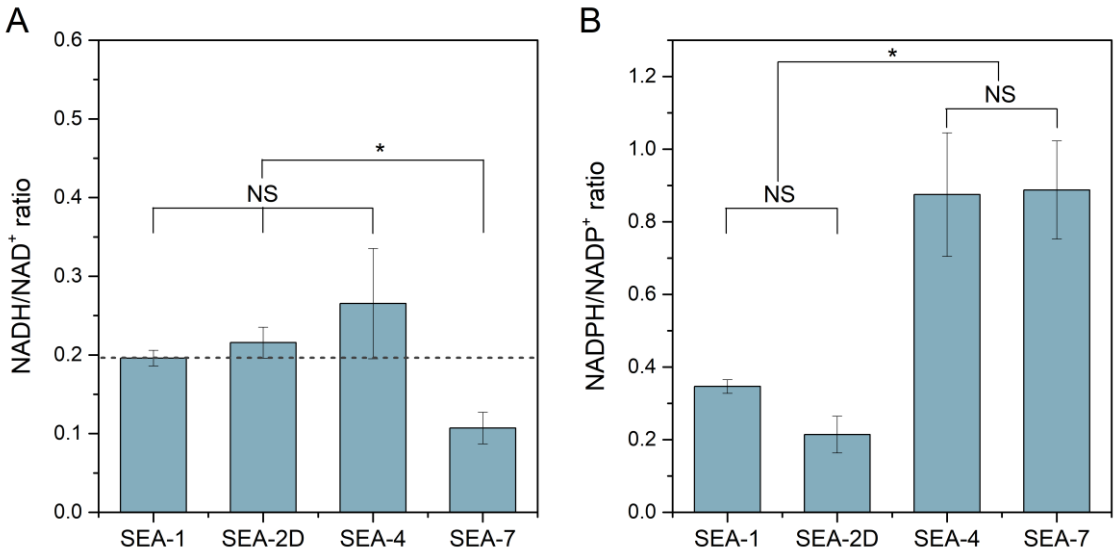

Figure 5-25: Redox metabolism in selected *C. glutamicum* strains grown on mannitol. The figure shows the NADH/NAD$^+$ ratio (A) and the NADPH/NADP$^+$ ratio (B). The data represent mean values and deviations from three biological replicates. For statistical significance analysis, the data were subjected to one-way analysis of variance (ANOVA), followed by Fisher's Least Significant (LSD) test. NS, not significant; *, significant ($P < 0.05$).

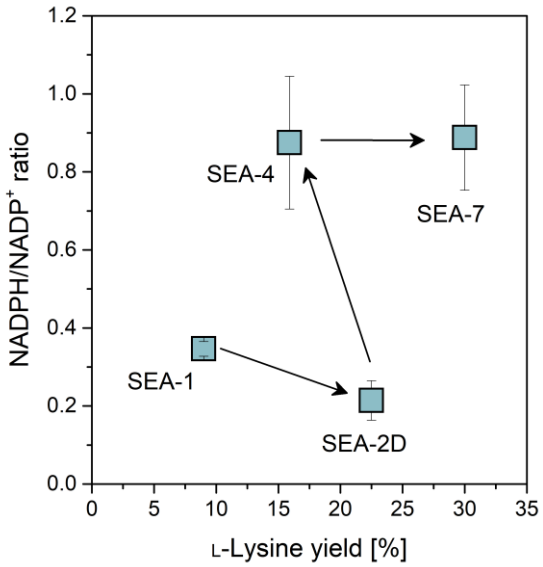

Figure 5-26: Correlation between the NADPH/NADP$^+$ ratio and the reached L-lysine yield during the initial growth phase in selected *C. glutamicum* strains. The data represent mean values and deviations from three biological replicates.

5.5.3 Metabolic pathway analysis

To evaluate the constructed production strains with regard to their theoretical production potential, *in silico* elementary flux mode analysis was conducted (Buschke et al. 2013a; Chen et al. 2009; Kind et al. 2014). In order to predict the theoretical maximum yield as well as the optimal pathway use from mannitol, the elementary fluxes for the different metabolic networks of the created *C. glutamicum* strains were computed (Melzer et al. 2009). For strain evaluation, the experimentally observed production performance was implemented into the calculated flux space (Figure 5-27).

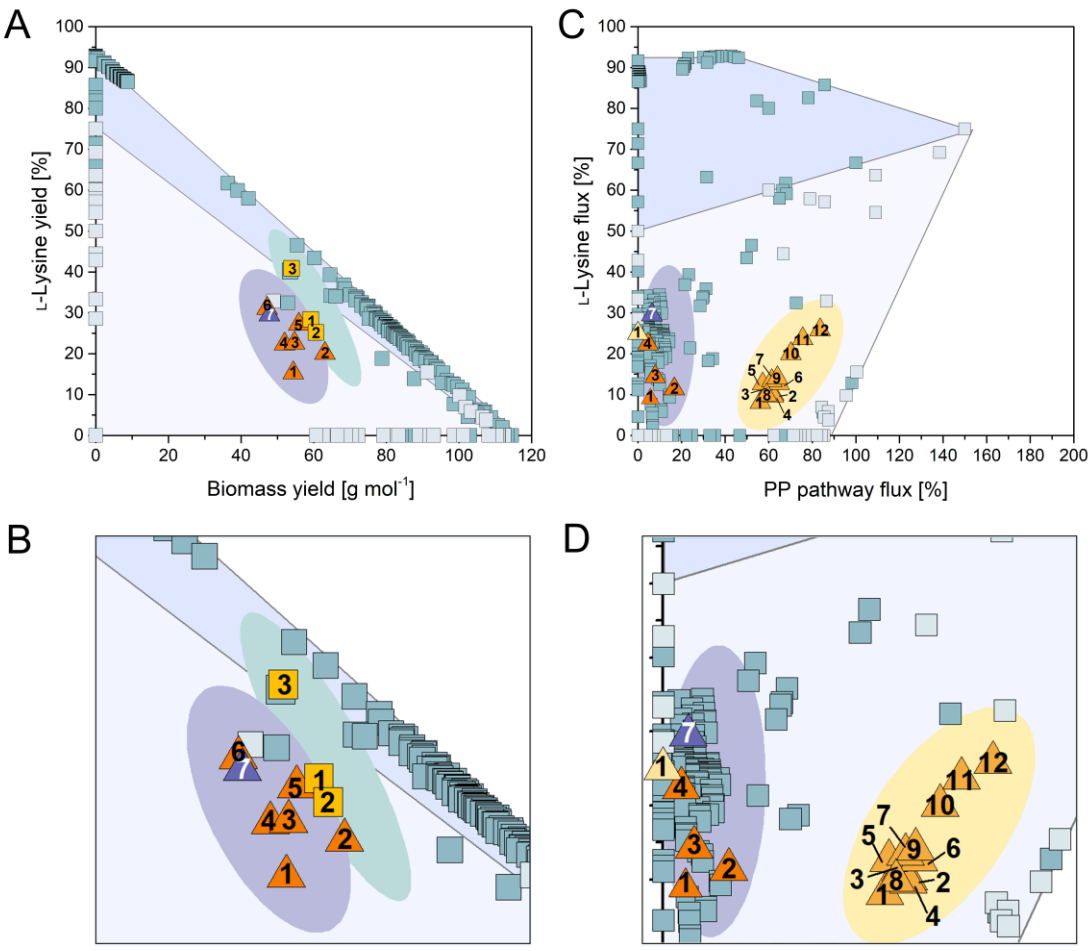

Figure 5-27: Evaluation of tailor-made L-lysine-producing *C. glutamicum* strains by elementary flux mode analysis. The *in silico* flux space for L-lysine production from mannitol was calculated by using the basic L-lysine producer strain SEA-1 (network see appendix Table 7-15) and the superior L-lysine producer strain SEA-7 (network see appendix Table 7-15). The yields for L-lysine and biomass, corresponding to individual elementary modes of SEA-1 (light grey squares) and SEA-7 (light grey squares plus green squares) are shown in A and B. The integrated experimental data reflect the engineered strains cultivated on mannitol, displayed as orange triangles: SEA-1 (1), SEA-2B (2), SEA-3 (3) SEA-2D (4), SEA-4 (5), SEA-6 (6). The best strain SEA-7 is highlighted as purple triangle (7). In addition, the experimental data of *C. glutamicum* strain SEA-7 on algal extract are displayed as light orange squares: cultivation on mannitol-rich extract from *L. digitata* (1), cultivation on mannitol- and glucose-rich extract from *L. digitata* (2), and cultivation on extract from *D. antarctica* (3). The underlying genetic changes for each strain are summarized in Table 4-1.

Table 5-27: *(Continued from previous page)* The correlation between L-lysine flux and the flux through the PP pathway was calculated by elementary flux mode analysis for the basic strain SEA-1 (light grey squares) and SEA-7 (light grey squares plus green squares) (C, D). Additionally, experimental data from the previously engineered GapN-expressing mutant *C. glutamicum* RE2/pCAK311, producing L-lysine from glucose (yellow triangle) (Takeno et al. 2016), and the *C. glutamicum* strain genealogy LYS-1 to LYS-12 (dark yellow triangles) (Becker et al. 2011), producing L-lysine from glucose, are displayed.

As depicted in Figure 5-27 A-B, the maximum predicted L-lysine yield for the basic producer *C. glutamicum* SEA-1 from mannitol was 750 mmol mol^{-1}, achieved for zero growth. Considering the obtained production performance of SEA-1, the L-lysine yield (153 mmol mol^{-1}) was still far from this optimum. This mutant exhibited only a low PP pathway flux, so that only little quantities of NADPH were provided via this route, which is required for an efficient L-lysine production in *C. glutamicum* (Becker et al. 2007; Becker et al. 2005; Becker et al. 2011; Wittmann and de Graaf 2005; Wittmann and Heinzle 2001a). In contrast to mannitol-grown *C. glutamicum* strains, a generally high carbon flux through the PP pathway was observed for L-lysine-producing *C. glutamicum* strains grown on sugars (Becker et al. 2007; Becker et al. 2005; Buschke et al. 2013a; Kiefer et al. 2004; Wittmann et al. 2004a). As illustrated by the elementary flux mode analysis, a maximum L-lysine flux of 75 % in the mannitol-grown SEA-1 strain would require a high PP pathway flux of 150 % (Figure 5-27 C, D). Despite the fact, that strain SEA-1 was derived from the L-lysine hyperproducer *C. glutamicum* LYS-12, which had a massively engineered PP pathway (Becker et al. 2011), its PP pathway flux was very low, explaining the weak performance as compared to glucose. In this respect, an additional NADPH supplying route appeared to be essential for efficient L-lysine production. For example, it has recently been shown that the heterologous expression of GapN in glucose-grown *C. glutamicum* strains can compensate the NADPH supply in the cell when the NADPH supply via the PP pathway, which is the most commonly used way for NADPH generation in *C. glutamicum*, is not present (Takeno et al. 2016) (Figure 5-27 C, D). In fact, another round of metabolic engineering aimed at the heterologous expression of glyceraldehyde 3-phosphate dehydrogenase in mannitol-grown strains. It was shown that analogously to strains grown on glucose, GapN has a beneficial effect on L-lysine production on mannitol. By coupling the NADPH production to glycolysis, L-lysine production in strain SEA-3 was significantly increased to a final L-lysine yield of 226 mmol per mol mannitol (Figure 5-15, Figure 5-27 A, B). The strain even showed a good L-lysine production performance comparable to that of the L-lysine hyperproducing strain LYS-12 on glucose (Becker et al. 2011). In addition, the SEA-3 mutant showed an increase in L-lysine flux, while the PP pathway flux decreased by 53 % compared to the

parent strain *C. glutamicm* SEA-2B (Figure 5-27 C, D). These results confirmed, that efficient L-lysine production does not necessarily depend on NADPH supply via the PP pathway, as shown before (Takeno et al. 2016). Since the additional plasmid-based expression of the NADH-insensitive GapN enzyme in the mannitol-grown SEA-6 mutant led to the abolishment of the fructose secretion, it can be assumed that particularly high NADH levels strongly impair the metabolism. Thus, previous studies reported that glyceraldehyde 3-phosphate dehydrogenase, a central enzyme of glycolysis, was strongly inhibited by too high NADH/NAD^+ ratios in the cell (Kiefer et al. 2004; Yokota and Lindley 2005). As shown in Figure 5-26, the contribution of the membrane-bound PntAB transhydrogenase in combination with GapN positively influences L-lysine production in mannitol-grown *C. glutamicum*. Thus, the final production strain *C. glutamicum* SEA-7 revealed superior production performance and exhibited a high L-lysine yield of 300 mmol mol^{-1}, while a marginally low PP pathway activity was observable (Figure 5-27). The additional expression of PntAB in *C. glutamicum* led to an enormous enlargement of the realizable flux space. As a result, the maximum predicted L-lysine yield increased by 20 % compared to the SEA-1 strain to a value of 900 mmol mol^{-1}. Most crucially, however, the expression of transhydrogenase allowed the theoretically predicted maximum L-lysine yield to be achieved with a low contribution of the PP pathway (Figure 5-27 C, D). In sum, these results clearly demonstrate that for a high-grade L-lysine production with mannitol-grown *C. glutamicum*, the organism needs to be optimized with respect to both NADPH provision and NADH/NAD^+ redox state, and that the PP pathway activity is not strictly necessary, if PntAB and GapN are expressed. With the superior L-lysine producing SEA-7 strain in hands, it was now interesting to assess the production performance of the tailor-made cell factory in a fed-batch fermentation under industrial conditions.

5.6 Establishment of a cascaded bioprocess for efficient L-lysine production using metabolically engineered *C. glutamicum*

5.6.1 Benchmarking of the final tailor-made L-lysine producer under industrial conditions

In order to evaluate the performance of the created producer *C. glutamicum* SEA-7 under industrial conditions, a fed-batch process with mannitol-based medium was performed for L-lysine production (Figure 5-28). In short, the process was started as a batch with initially 41 g L^{-1} mannitol, followed by extended feeding in which further amounts of mannitol were added. Mannitol was added to the culture first from a concentrated feed. Due to the fact that SEA-7 was still performing well, when larger amounts of the feed had been added and the reactors approached their maximum filling capacity, the feed was switched to mannitol as a solid through the end of the culture. Different to sugars such as glucose and sucrose, which exhibited excellent solubility, mannitol is significantly less soluble (216 g L^{-1}), so that the liquid feed applied was rather diluted and more quickly filled up the reactor. Considering the initial batch phase, the cells started exponential growth without a lag-phase and accumulated L-lysine from early on (Figure 5-28 A). The strain completely used the batched mannitol and formed 5 g L^{-1} of L-lysine until the end of the batch phase (6 h) (Figure 5-28 A), whereby a L-lysine yield of 0.21 mol mol^{-1} was observed (Figure 5-28 B). In addition, fructose accumulation was observed, which peaked to approximately 14 g L^{-1}, indicating a remaining bottleneck in metabolism when high levels of mannitol are provided. Then, the first feeding phase was started (Figure 5-28 A). The concentrated mannitol feed was added pulse-wise. The mannitol level in the process was continuously monitored, which allowed to maintain it in the range of 5 - 10 g L^{-1}. The L-lysine concentration continually increased from 5 g L^{-1} at the end of the batch phase to 32 g L^{-1} after 17 h. Fructose, which accumulated during the initial batch phase, was immediately re-consumed during the feeding phase, thus the fructose level was 1 g L^{-1}. The cells produced L-lysine almost exclusively. Lactate (5 g L^{-1}) accumulated as the only by-product. The formation of lactate as a fermentation product usually occurs, when the oxidation of NADH via the respiratory chain is limited (Bott and Niebisch 2003). Since in *C. glutamicum* lactate is formed from pyruvate by NADH-dependent lactate dehydrogenase (Blombach et al. 2011), it seemed the cells formed lactate to at least partly regenerate excess NADH that was produced during the oxidation of mannitol to fructose. Such a phenomenon, however, was not observed during the previous shake flasks cultivation of the strain. In addition, the level of dissolved oxygen was sufficiently high (> 40 % of saturation) during the entire process. As another

explanation, lactate was formed as a by-product because the cell growth had stopped at this time point.

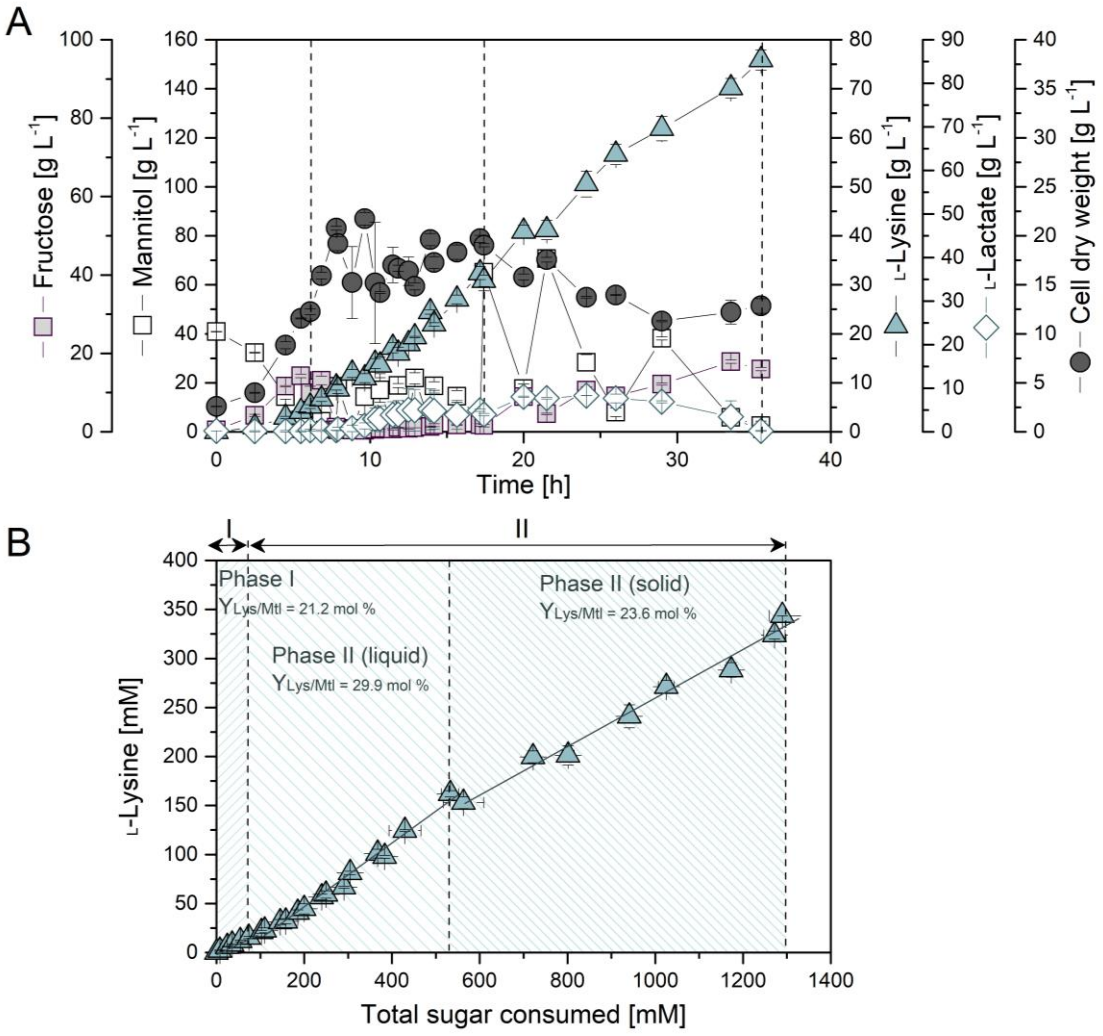

Figure 5-28: Growth and production performance of L-lysine producing *C. glutamicum* SEA-7 in a fed-batch process on mannitol. The figure represent the cultivation profile of the producing strain (A), and the achieved L-lysine yields in the different cultivation phases (B). The data represent mean values and deviations from two independent fermentation experiments.

After 17 h, the liquid feeding had to be stopped due to the fact that the reactors had been filled up rather completely. Then, the final feeding phase with solid mannitol was initiated. Technically, mannitol doses were added every few hours through one of the tree reactor ports. Each dose increased the mannitol level up to 50 g L^{-1}. The L-lysine level further increased to a final titer of 76 g L^{-1} after 35 h (Figure 5-28A). Thereby, the feeding was stopped after 29 h to ensure the depletion of remaining carbon. The short cultivation time is comparable to that of the molasses-based fed-batch process of *C. glutamicum* LYS-12 (Becker et al. 2011) and indicated a high efficiency of SEA-7. Lactate was

completely taken up towards the end of the process. With the start of the second feeding phase slight accumulation of fructose was again observed. It seemed, that the strain could handle the replenishment of high mannitol concentrations and the eventually high concentrations of NADH formed during mannitol oxidation. This assumption is supported by the observation that fructose accumulation was almost completely eliminated during the first feeding phase, when only small amounts of mannitol were added, while fructose accumulation was again observed in the second and final feeding phase due to the high added mannitol concentrations of 50 g L^{-1} similar to the batch phase. Admittedly, the addition of solid mannitol in big pulses was a rather artificial way of feeding, realized because of limited reactor capacity. The consideration of sufficient reactor volume for continuous liquid feeding would allow to avoid such a phenomenon. Notably, the obtained seaweed extracts contained mannitol to a lower extent so that a strategy for efficiently fermenting this more diluted raw material has to be worked out. Different L-lysine yields were obtained for the batch (0.21 mol mol^{-1}), the first feed phase (0.30 mol mol^{-1}) and the second feed phase (0.24 mol mol^{-1}) (Figure 5-28 B). The main space time yield for L-lysine was 2.1 ± 0.1 g L^{-1} h^{-1}. Over the entire process, production took place at more than half of the maximum rate (1.5 g L^{-1} h^{-1}) touching the performance of glucose-based processing (Becker et al. 2018b; Becker and Wittmann 2012a; Becker et al. 2011).

The high industrial relevance of L-lysine results in constant efforts to improve overproducing strains towards maximal L-lysine titer, productivity and yield (Becker and Wittmann 2012b). Beyond classical breeding, systems metabolic engineering had meanwhile created and designed L-lysine producers with superior production performance, typically using glucose, fructose and sucrose based raw materials (Becker et al. 2011; Ikeda et al. 2006; Ohnishi et al. 2002; Shiratsuchi et al. 1995; Xu et al. 2018). For the first time, this work demonstrated L-lysine production from the sugar alcohol mannitol. The performance of the created strain SEA-7 touched that of glucose-based L-lysine production. The development of this strain is therefore of great interest, as mannitol is a major constituent of algal biomass, especially of brown macroalgae (Iwamoto and Shiraiwa 2005; Wei et al. 2013). In the following, L-lysine production should be further demonstrated using real seaweed raw material.

5.6.2 Production of L-lysine from pre-processed *Laminaria digitata* hydrolysates

One of the main objectives of this work was to establish the production of L-lysine from algal hydrolysates. Since *L. digitata* was known to be rich in mannitol (Adams et al. 2011), this species was used to demonstrate the value chain. After processing *L. digitata* (Figure 5-19) into a mannitol and/or a mannitol/glucose-rich hydrolysate as described above (see chapter 4.8.2), it was now used as a raw material. For conversion of the carbohydrates into L-lysine, the best producing strain *C. glutamicum* SEA-7 was used as cell factory (Figure 5-29).

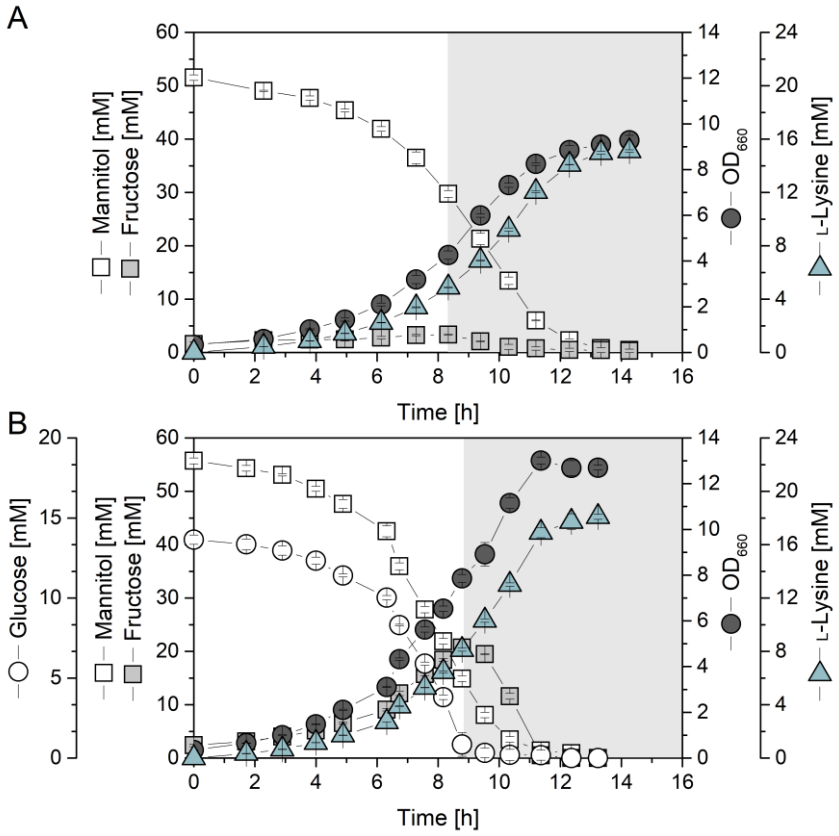

Figure 5-29: Growth and production performance of the tailor-made L-lysine producer *C. glutamicum* SEA-7 on mannitol-rich (A), and mannitol/glucose-rich hydrolysate of *L. digitata* (B). Cultivation was performed on mineral salt medium, supplemented with algal extract to a final mannitol concentration of 10 g L^{-1}. The two phases of fructose accumulation (phase I) and fructose re-consumption (phase II) are shown in white and grey, respectively. The data represent mean values and corresponding standard deviations from three biological replicates.

First tested on mannitol-rich extract, which additionally contained small traces of fructose, SEA-7 completely consumed the sugar alcohol within 14 h (Figure 5-29 A). SEA-7 grew even faster on the hydrolysate than on pure mannitol as substrate (Figure 5-21 G, Figure 5-29 A). The strain grew exponentially with growth-coupled

L-lysine secretion. The final L-lysine titer of 15.1 mM, and the L-lysine yield of 284 mmol per mol mannitol plus fructose (Figure 5-30), indicated that high levels of carbon were channeled into L-lysine formation. On the hydrolysate it reached a maximum specific growth rate of 0.33 h^{-1}, which was almost 32 % higher (Table 5-12). This could been due to growth promoting ingredients in the extract, such as vitamins (vitamins A, B, C and E), fatty acids (omega 3 and omega 6), proteins and amino acids (L-aspartate and L-glutamate), minerals (magnesium, potassium, iron and calcium) and pigments (fucoxanthin, ß-carotene, violaxanthin) (Torres et al. 2019). Considering the biomass formation, the mutant also revealed a slightly increased biomass yield when using the hydrolysate as carbon source (Table 5-12). A slight and transient fructose accumulation was observed during the first 8 h of cultivation (Figure 5-29 A), different to the use of pure mannitol (Table 5-12).

Since *C. glutamicum* is also able to metabolize glucose, it was now interesting to see how the application of mannitol- and glucose-containing algal hydrolysates from enzymatic pre-processing influenced L-lysine production in the SEA-7 strain (Figure 5-29 B). Again, the strain immediately started to grow without lag-phase and consumed mannitol (56 mM) and glucose (14 mM) simultaneously. Compared to cultivation on mannitol-rich extract (Figure 5-29 A) and pure mannitol (Figure 5-21 G), the strain utilized the substrates within only 13 h and showed a higher maximum specific growth (0.36 h^{-1}), comparable to that obtained for the *C. glutamicum* wild-type ATCC 13032 (Becker et al. 2011). This behaviour underlined the high vitality of the constructed strain and the high suitability of the used seaweed extract. The significantly increased specific growth rate revealed a synergistic use of the two carbon sources. During co-consumption of glucose and mannitol, fructose, which was derived from mannitol oxidation, accumulated and peaked at 18.3 mM after 9 h, and was later co-consumed together with mannitol (Figure 5-29 B). It was interesting to note that precisely at this time point, when glucose was no longer present, the re-uptake of fructose started. Unlike in other bacteria, the phosphotransferase systems in *C. glutamicum* are not influenced by catabolite repression and are therefore constitutively expressed, which generally allows the co-consumption of sugar mixtures, including glucose and fructose (Wang et al. 2016b; Yokota and Lindley 2005). In this respect, it could be assumed that the strain was not able to handle the overall increased carbon influx, when grown on mannitol plus glucose. Considering the production performance, SEA-7 accumulated L-lysine to a final titer of 18.1 mM, corresponding to an overall L-lysine yield of 252 mol per mol mannitol plus glucose (Figure 5-30). Taken together, this strategy was an important proof of concept, impressively demonstrating the use of seaweed for the production of L-lysine. The constructed strain SEA-7 emerged as high-yield producer.

Table 5-12: Growth and production characteristics of the tailor-made producer *C. glutamicum* SEA-7 during batch cultivation using hydrolysate from the brown algae *L. digitata* and *D. antarctica*. The mannitol-rich *L. digitata* hydrolysate was obtained by hydrothermal extraction, while the mannitol/glucose-rich hydrolysate was obtained by an additional enzymatic hydrolysis step. The hydrolysate from *D. antarctica* was obtained by hydrothermal extraction with ethanol and sulfuric acid. The data represent the initial growth phase, linked to fructose accumulation (shown in white, Figure 5-29 A-B) for strain SEA-7 on mannitol and mannitol/glucose containing hydrolysate from *L. digitata* and the entire cultivation period of non-fructose accumulating SEA-7 on pure mannitol (Figure 5-21 G) and hydrolysate from *D. antarctica* (Figure 5-32). The given data comprise the specific rates for growth (μ), substrate uptake (q_S),L-lysine production (q_{Lys}) and the yields for L-lysine ($Y_{Lys/S}$), biomass ($Y_{X/S}$) and by-products (fructose (Frc), trehalose (Tre), lactate (Lac), acetate (Ace)). The data represent mean values and deviations from three biological replicates.

Strain	SEA-7	SEA-7	SEA-7	SEA-7
Algae species	-	*L. digitata*	*L. digitata*	*D. antarctica*
Substrate	pure mannitol	mannitol-containing hydrolysate	mannitol/glucose -containing hydrolysate	mannitol/glucose/ fructose-containing hydrolysate
μ [h^{-1}]	0.25 ± 0.02	0.33 ± 0.01	0.36 ± 0.00	0.20 ± 0.01
q_{Lys} [mmol g^{-1} h^{-1}]	1.58 ± 0.05	1.13 ± 0.02	1.08 ± 0.02	1.48 ± 0.01
q_S [mmol g^{-1} h^{-1}]	5.3 ± 0.1	5.0 ± 0.3	7.3 ± 0.2	3.6 ± 0.1
$Y_{Lys/S}$ [mmol mol^{-1}]	299.5 ± 4.8	226.1 ± 10.4	147.0 ± 5.7	409.3 ± 7.5
$Y_{X/S}$ [g mol^{-1}]	47.8 ± 5.4	65.5 ± 3.2	49.0 ± 1.6	53.9 ± 2.8
$Y_{Frc/Mtl}$ [mmol mol^{-1}]	< 0.01	79.7 ± 9.7	464.9 ± 12.4	-
$Y_{Lac/S}$ [mmol mol^{-1}]	< 0.01	< 0.01	< 0.01	< 0.01
$Y_{Tre/S}$ [mmol mol^{-1}]	1.8 ± 0.2	3.9 ± 0.9	7.4 ± 0.9	2.5 ± 0.1
$Y_{Ace/S}$ [mmol mol^{-1}]	<0.01	< 0.01	< 0.01	< 0.01

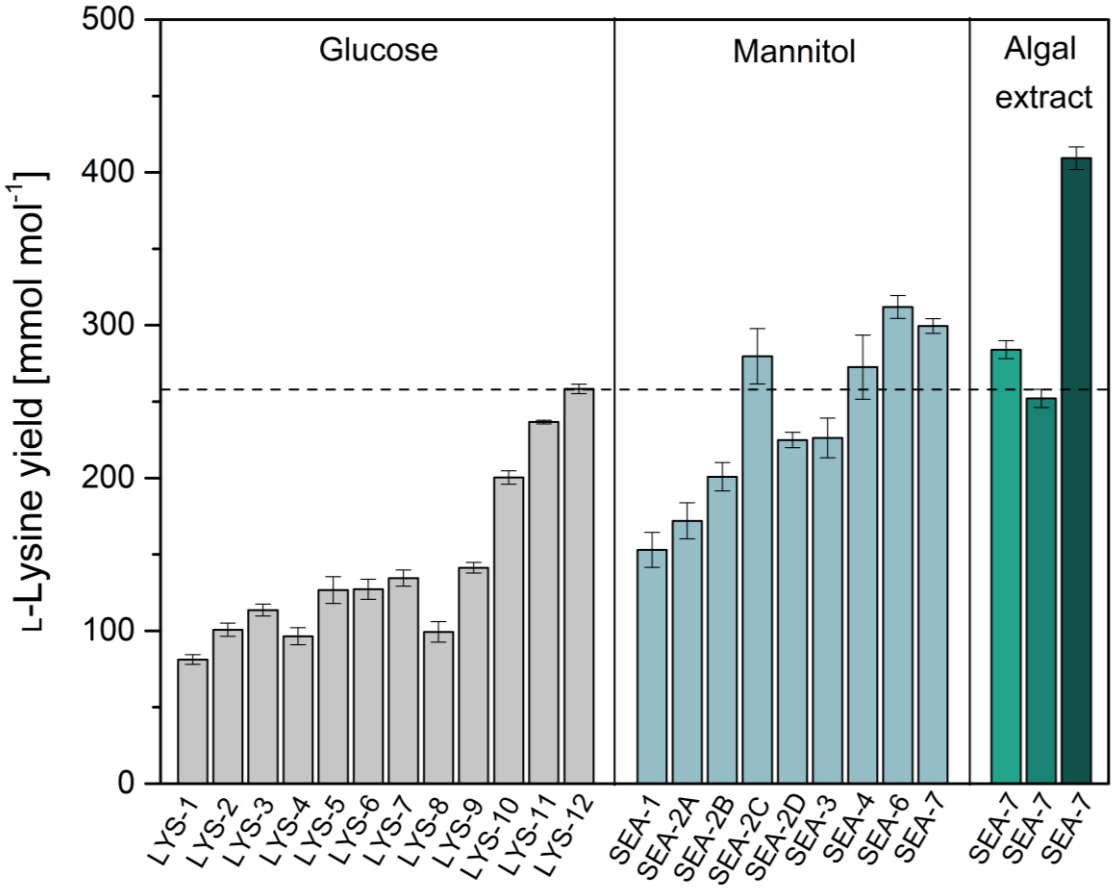

Figure 5-30: Systems metabolic engineering of *C. glutamicum* for L-lysine production from mannitol and mannitol containing seaweed extract. The figure shows the L-lysine yield for the different strains SEA-1, SEA-2A, SEA-2B, SEA-2C, SEA-2D, SEA-3, SEA-4, SEA-6, and SEA-7 constructed in this work, using mannitol (light turquoise bars), mannitol-containing extracts (light green bars) and mannitol/glucose-containing extracts from the brown algae *L. digitata* (green bars) and mannitol/glucose/fructose-containing extracts from the brown algae *D. antarctica* (dark green bars). The data represent mean values and deviations from three biological replicates. For comparison, data from previous metabolically engineered glucose-optimized *C. glutamicum* strains, i.e. producers LYS-1 to LYS-12 are shown (grey bars) (Becker et al. 2011).

5.6.3 Production of L-lysine from hydrolyzed *Durvillaea antarctica* waste

The large brown seaweed *D. antarctica* (Chamisso) Hariot is an endemic species of the Southern Hemisphere presenting a subantarctic distribution (Lizée-Prynne et al. 2016; Mansilla et al. 2012; Mansilla et al. 2017). In Chile, it is known as "*cochayuyo*" and mainly found in rocky habitats of the Chilean shoreline and the ocean as bull kelp forests. While the local population to some extent eats the dry stipes of the algae (Mansilla et al. 2012; Uribe et al. 2018), the soft fronds (blades) are the main valuable part processed for human consumption, typically leaving the rest as a waste (Figure 5-31 B). The commercialization of the macroalgae has increased by more than 400 % over the last decade and reached a production volume of 8,000 tons in 2014 (Ferdouse et al. 2018), enabling international trade to other countries (Uribe et al. 2018).

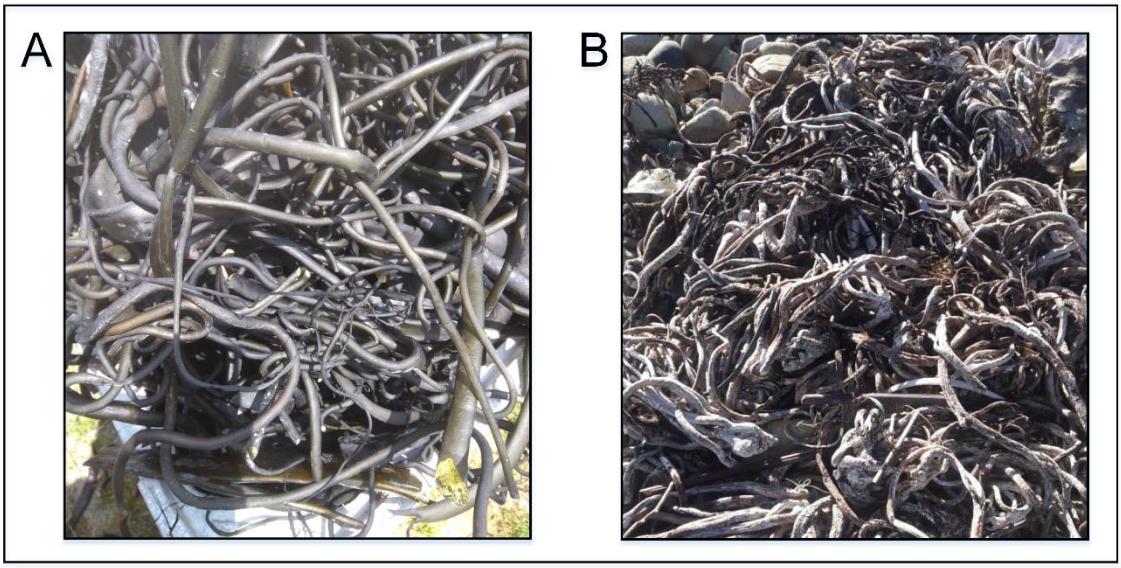

Figure 5-31: The figure represents the sun-dried blades and stipes of *D. antarctica* used for commercial purposes (A) and the waste products, especially the holder and parts of the blades, which are produced during harvesting and drying (B).

As shown in Figure 5-31, harvesting and drying of *D. antarctica* produces enormous amounts of waste, involving especially the holdfasts and parts of the blades. In a further proof of concept, the use of this waste for L-lysine production was investigated. Therefore, the best L-lysine-producing strain *C. glutamicum* SEA-7 was cultivated on extracts from the seaweed (Figure 5-32).

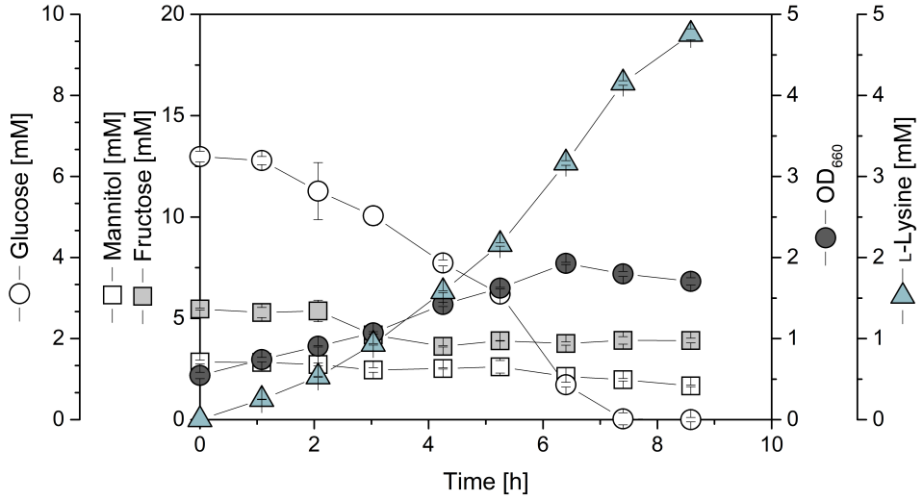

Figure 5-32: Growth and production performance of the tailor-made L-lysine producer *C. glutamicum* SEA-7 on mannitol/glucose-rich algal hydrolysate from *D. antarctica.* Cultivation was performed on mineral salt medium, supplemented with algal extract. The data represent mean values and corresponding standard deviations from three biological replicates.

As shown in Figure 5-32, the strain quickly consumed glucose and showed efficient L-lysine production. SEA-7 accumulated L-lysine to a titer of 4.8 mM, corresponding to an overall L-lysine yield of 409 mmol per mol mannitol plus glucose plus fructose (Figure 5-30). During the time period of glucose depletion, mannitol and fructose remained rather untouched, but were taken up afterwards. This behavior was different to that observed for the *L. digitata* hydrolysates. Eventually, it was related to the reduced growth of SEA-7 on the *D. antarctica* hydrolysate (Table 5-12). The medium likely contained an increased level of salt, which originated from the pre-treatment of the seaweed with sulphuric acid. In addition, the sugar level was not as high as for *L. digitata*. The experiment, however, showed, that *C. glutamicum* could also handle the more detrimental raw material. Future optimization of the upfront processing could help to make the extract more bioavailable.

6 Conclusion and Outlook

The use of more sustainable raw materials is one of the most relevant tasks to achieve a greener production. Admittedly, biotechnology still largely relies on first and second-generation renewables. As an example L-lysine, a premium feed additive, is primarily manufactured from starch, raw sugar and molasses (Becker et al. 2005; Becker et al. 2011; Gopinath et al. 2011; Hirao et al. 1989; Ikeda 2017; Seibold et al. 2006; Tateno et al. 2007a, 2007b; Xu et al. 2018). At this point, seaweed biomass is emerging a highly promising alternative third-generation renewable to produce L-lysine in the future. Seaweed build-up occurs quickly, is independent from arable land, fertilizers, and fresh water (Kraan 2013; McHugh 2003; Poblete-Castro et al. 2020; Torres et al. 2019; van Hal et al. 2014) and fixes CO_2 from the atmosphere, thereby reducing ocean acidification. In this regard, this work focused on utilization of the sugar alcohol mannitol, a major carbohydrate in many seaweeds (Groisillier et al. 2015; Iwamoto and Shiraiwa 2005; Wei et al. 2013) using metabolically engineered *C. glutamicum* cell factories. Based on the construction of the basic producer SEA-1, which provided L-lysine from mannitol, at least to a weak extent, fluxomics and metabolomics were used to gain a better understanding of the underlying metabolism and identify targets for strain optimization. The data indicated bottlenecks in mannitol catabolism and NADPH supply, which could then be addressed by iterative optimization cycles. The finally created strain SEA-7 harbored 16 genetic modifications and accumulated L-lysine with a yield of 300 mmol mol^{-1} and a specific production rate of 1.6 mmol g^{-1} h^{-1}. When tested in a fed-batch process, SEA-7 reached a L-lysine titer of 76 g L^{-1} within only 35 h and a maximal productivity of 2.13 g L^{-1} h^{-1}. In this regard, SEA-7 displays the first cell factory capable of utilizing mannitol for high-level L-lysine production. The strain also performed well when hydrolysates from the brown algae *Laminaria digitata* and *Durvillaea antarctica* were used. Hereby, the fermentation was implemented into a cascaded value chain towards maximal sustainability. For *L. digitata*, the extract was pre-processed to recover pure alginate and the residual sugars were used and found highly suitable for L-lysine production. For *D. antarctica*, the hydrolysate was obtained from the waste parts of the algae, discharged during the processing of the leaves for human consumption.

The excellent performance of SEA-7 and the demonstrated value chain from seaweed to L-lysine can serve as a model for the production of other biotechnologically relevant products from marine biomass. In this context, biopolymer building blocks such as 5-aminovalerate, glutarate and 1,5-diaminopentane are highly attractive, since they directly accessible from L-lysine (Kind et al. 2010a; Kind et al. 2010b; Rohles et al. 2016).

Another interesting product, derived from L-lysine catabolism is the non-proteinogenic amino acid L-pipecolic acid (Fujii et al. 2002; Pérez-García et al. 2017a), which serves as a precursor to form pharmaceutical drugs (Pérez-García et al. 2017a; Pérez-García et al. 2016).

From the point of substrate utilization, further metabolic engineering could aim at extending the substrate spectrum of *C. glutamicum* towards alginate, since the structural polysaccharide is abundant in many brown algae species (Kawai and Murata 2016; Wei et al. 2013). Simultaneous utilization of alginate and mannitol could be also interesting from the fact that the catabolism of alginate requires NADH, which is provided by the oxidation of mannitol (Wargacki et al. 2012). This substrate coupling could replenish the NAD^+ pool, while additionally utilizing the entire carbon repertoire of the macroalgae. Furthermore, the substrate spectrum of *C. glutamicum* SEA-7 could be expanded by considering other algae species as raw material, such as red algae, since these contain a higher carbohydrate content than brown algae, that can range up to 84 % of their dry weight (Wei et al. 2013). Red algae, especially the species *Gelidium amansii*, mainly consist of agar, carrageenan, and cellulose (Wei et al. 2013), which can be easily broken down into the sugar monomers glucose, mannose, and galactose by combined acid treatment and subsequent enzymatic saccharification (Kim et al. 2011). Inherently, *C. glutamicum* is able to utilize both substrates (glucose and mannose) via glucose/mannose-specific phosphotransferase system (Moon et al. 2007; Parche et al. 2001), but not galactose (Barrett et al. 2004). On this basis, further metabolic engineering of *C. glutamicum* SEA-7 would solely require activated utilization of galactose as substrate. Besides carbohydrates, macroalgae have a large repertoire of hydrocolloids, vitamins, fatty acids, proteins and amino acids, minerals and pigments (Torres et al. 2019), suggesting cascaded biorefinery to fully harness all valuable compounds while reducing the amount of waste produced (Torres et al. 2019; van Hal et al. 2014). By using a biorefinery approach, a more sustainable and thus economically more efficient production of industrially important products can be achieved (Poblete-Castro et al. 2020; Torres et al. 2019; van Hal et al. 2014). The production of L-lysine from residual sugars could display one vital element of such an ocean based sustainable bio-production.

7 Appendix

7.1 Primers

Site-specific primers used for the construction of the transformation vectors are listed in Table 7-1.

Table 7-1: Specific primer sequences used for the construction of the transformation vectors.

No.	Sequence (5´- 3´)	Plasmid
PR$_{\Delta mtlR}$_1	AATTGGGATCCTCTAGACCCGGTTCATGATCACGCATCCA	pClik int *sacB* Δ*mtlR*
PR$_{\Delta mtlR}$_2	GCAAAAGATCCCGCTGCTCAGTGAAAAAGTTACCACGGAA	
PR$_{\Delta mtlR}$_3	TTCCGTGGTAACTTTTTCACTGAGCAGCGGGATCTTTTGC	
PR$_{\Delta mtlR}$_4	CGCTAGCGATTTAAATCCCACCGTCACGTTAAATCCGTGT	
PR$_{Psod_mak}$_1	GGTTATGGCCACAAGAGTAACTCTGCTTTTATCCGATCAG	pClik int *sacB* P_{sod} *mak*
PR$_{Psod_mak}$_2	CTGATCGGATAAAAGCAGAGTTACTCTTGTGGCCATAACC	
PR$_{Psod_mak}$_3	AATTGGGATCCTCTAGACCCAGCATTATGGCTTAAAGCAC	
PR$_{Psod_mak}$_4	CCGCTAGCGATTTAAATCCCATCCGATGCTGCTGATTTGT	
PR$_{Psod_mak}$_5	GAGCCAGAAAAGCCGTAGTCTAGCTGCCAATTATTCCGGG	
PR$_{Psod_mak}$_6	AAATCGATACCTATACGCATGGGTAAAAAATCCTTTCGTA	
PR$_{Psod_mak}$_7	TACGAAAGGATTTTTTACCCATGCGTATAGGTATCGATTT	
PR$_{Psod_mak}$_8	CCCGGAATAATTGGCAGCTAGACTACGGCTTTTCTGGCTC	
PR$_{Psod_scrK}$_1	AATTGGGATCCTCTAGACCCAGCATTATGGCTTAAAGCAC	pClik int *sacB* P_{sod} *scrK*
PR$_{Psod_scrK}$_2	CCGCTAGCGATTTAAATCCCATCCGATGCTGCTGATTTGT	
PR$_{Psod_scrK}$_3	GAGCCAGAAAAGCCGTAGTCTAGCTGCCAATTATTCCGGG	
PR$_{Psod_scrK}$_4	CCCGGAATAATTGGCAGCTAGACTACGGCTTTTCTGGCTC	
PR$_{Psod_scrK}$_5	TACGAAAGGATTTTTTACCCATGAATAATGTTTTATGTAT	
PR$_{Psod_scrK}$_6	ATACATAAAACATTATTCATGGGTAAAAAATCCTTTCGTA	
PR$_{Psod_scrK}$_7	GTGAAGTTGAAGGTGATTAGCTCTGCTTTTATCCGATCAG	
PR$_{MtlD}$_fw_1	TCATCGGCATGGGTGTCATGCCTTCCGCAGTGCGCAAGCG	pClik int *sacB mtlD*^{GCA}
PR$_{MtlD}$_rev_2	GTAGCCGATTTCCTTGATGTCATCGCGGTCGCCGTCGGTG	
PR$_{TS1_MtlD}$_rev_3	CGCTTGCGCACTGCGGAAGGCATGACACCCATGCCGATGA	
PR$_{TS1_MtlD}$_fw_4	AATTGGGATCCTCTAGACCCGGCGCAGCGATGGCCACATA	
PR$_{TS2_MtlD}$_fw_5	CACCGACGGCGACCGCGATGACATCAAGGAAATCGGCTAC	
PR$_{TS2_MtlD}$_rev_6	CCGCTAGCGATTTAAATCCCGAATGACAAAATATCGGTGC	
PR$_{tuf_pntAB}$_1	AATTGGGATCCTCTAGACCCGGTAGTAGGCGGTGTCACTG	pClik int *sacB* P_{tuf} *pntAB*
PR$_{tuf_pntAB}$_2	CATTCGCAGGGTAACGGCCAAGCTGAGGCTGCTTCTGGTA	
PR$_{tuf_pntAB}$_3	TACCAGAAGCAGCCTCAGCTTGGCCGTTACCCTGCGAATG	
PR$_{tuf_pntAB}$_4	CTTGGTATGCCAATTCGCATTGTATGTCCTCCTGGACTTC	
PR$_{tuf_pntAB}$_5	GAAGTCCAGGAGGACATACAATGCGAATTGGCATACCAAG	
PR$_{tuf_pntAB}$_6	AGTTTTAGTCGAGACCTTCATTACAGAGCTTTCAGGATTG	
PR$_{tuf_pntAB}$_7	CAATCCTGAAAGCTCTGTAATGAAGGTCTCGACTAAAACT	
PR$_{tuf_pntAB}$_8	CCGCTAGCGATTTAAATCCCTTAGGATCTGGCGCAACACC	

Table 7-1: *(Continued from previous page)* Specific primer sequences used for the construction of the transformation vectors.

No.	Sequence (5´- 3´)	Plasmid
PR239$_{gapN_epi_fw}$	GATCCTCGAGCTATTATTTGCTGTTTGACA	pClik 5a MCS
PR240$_{gapN_epi_rev}$	GATCGGATCCCAATCAACCACTGTGTTAAA	*gapN*
PR$_{TS1_GapN_fw_}$1	CTGCGTTAATTAACAATTGGTCTAGATGCGGATCTTGTGG	
PR$_{TS1_GapN_rev_}$2	CATTCGCAGGGTAACGGCCAACCACAATTCGGTCAGTGAG	pClik int *sacB* P_{tuf}
PR$_{TS2_GapN_rev_}$3	AATCCCGGGTCTAGAGGATCGCATATGGGGTGCAAGGTTAATAC	*gapN*
PR$_{Eftu_GapN_fw_}$4	CTCACTGACCGAATTGTGGTTGGCCGTTACCCTGCGAATG	

7.2 Codon optimization

To enhance the expression level of NADP-dependent glyceraldehyde 3-phosphate dehydrogenase (GapN) from *Streptococcus mutans* the codon usage was adjusted to the codon usage preferred by *C. glutamicum*. The gene cluster alignment of the native *gapN* gene along with the codon-optimized version is given in Figure 7-1.

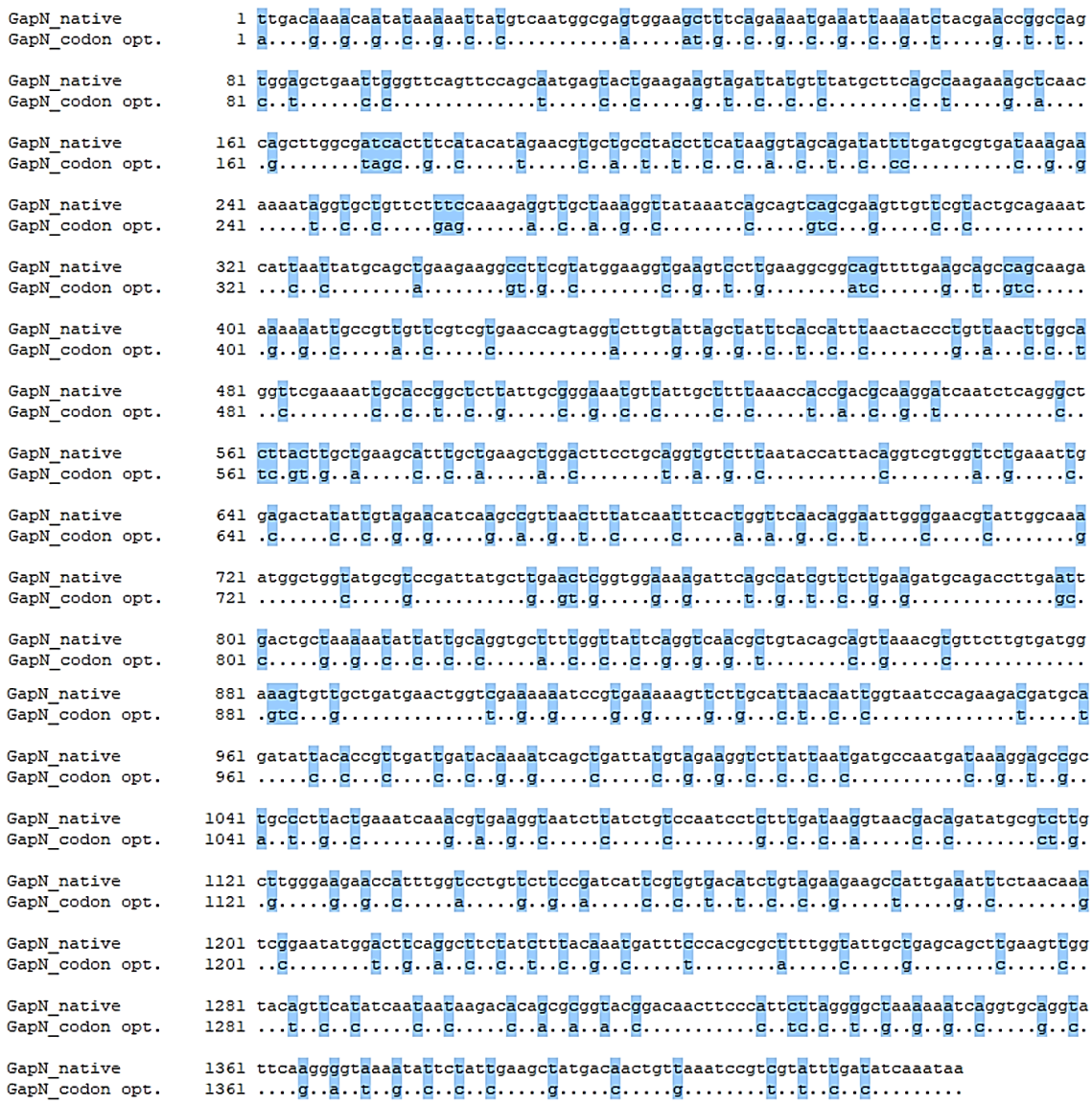

Figure 7-1: Gene cluster alignment of the native *gapN* sequence and the codon-optimized *gapN* sequence from *S. mutans*. The upper row represent the native *gapN* sequence from *S. mutans* while the lower stand represent the sequence for the codon-optimized *gapN* gene. Letters that are highlighted in blue have been changed. The alignment of the two sequences was performed in Clone Manager Professional 9 (Sci-Ed Software, Denver, USA). (Tuesday, February 11, 2020 10:09:38).

7.3 ^{13}C Metabolic flux analysis

For metabolic flux analysis in mannitol-grown *C. glutamicum* cells the major net fluxes through the carbon core metabolism were determined using a correlation factor of $f = 1.49$. This factor was inferred from glucose-grown *C. glutamicum* (Table 7-2). Shown are experimental labeling data of mannitol-grown L-lysine producing *C. glutamicum* strains of the mass isotopomers of proteinogenic L-alanine from GC-MS measurement (exp), subsequently corrected for natural isotope abundance (corr) according to (van Winden et al. 2002) (Table 7-3), used to derive the PP pathway flux (Table 7-4).

Table 7-2: Determination of the correlation factor. The determination of the correlation factor is based on the constant ^{13}C labeling information obtained from the recently generated glucose-grown L-lysine producer strains (LYS-1 to LYS-12). In order to determine the SFL data of the strains LYS-1 to LYS-12, the data of these strains were taken from previous work (Becker et al. 2011).

Strain	SFL [%]	$v_{Zwf,lb}$ [%]	v_{Zwf} [%]	Factor
LYS-1	12.6	36.1	56.2	1.56
LYS-2	11.5	41.2	62.2	1.51
LYS-3	11.4	41.0	60.2	1.47
LYS-4	11.2	43.1	62.1	1.44
LYS-5	11.5	39.8	57.2	1.44
LYS-6	11.0	43.4	64.8	1.49
LYS-7	11.0	42.5	61.4	1.44
LYS-8	11.3	40.4	59.0	1.46
LYS-9	11.1	41.7	64.0	1.54
LYS-10	10.5	45.7	70.2	1.54
LYS-11	10.1	48.8	75.6	1.55
LYS-12	8.9	57.4	83.6	1.46
				∅ 1.49

Table 7-3: Mass isotopomer distribution of proteinogenic L-alanine from GC-MS measurement (exp). The data were corrected for natural isotope abundance (corr) (van Winden et al. 2002). The strains were grown either on 99 % [1-^{13}C] glucose (G), 99 % [1-^{13}C] fructose (F) or 99 % [1-^{13}C] mannitol (M).

Strain **Substrate**	M exp	M+1 exp	M+2 exp	M+3 exp	M corr	M+1 corr	M+2 corr	M+3 corr
SEA-1, M	0.385 ± 0.000	0.450 ± 0.000	0.124 ± 0.001	0.002 ± 0.000	0.506 ± 0.000	0.490 ± 0.000	0.004 ± 0.001	0.000 ± 0.000
SEA-1, G	0.607 ± 0.000	0.282 ± 0.000	0.089 ± 0.001	0.022 ± 0.000	0.784 ± 0.000	0.210 ± 0.000	0.006 ± 0.001	0.000 ± 0.000
SEA-1, F	0.419 ± 0.000	0.424 ± 0.000	0.119 ± 0.001	0.038 ± 0.000	0.540 ± 0.000	0.441 ± 0.000	0.019 ± 0.001	0.000 ± 0.000
SEA-2B, M	0.397 ± 0.000	0.442 ± 0.000	0.122 ± 0.001	0.001 ± 0.000	0.523 ± 0.000	0.476 ± 0.000	0.003 ± 0.001	0.000 ± 0.000
SEA-3, M	0.387 ± 0.000	0.447 ± 0.000	0.125 ± 0.001	0.001 ± 0.000	0.508 ± 0.000	0.486 ± 0.000	0.006 ± 0.001	0.000 ± 0.000
SEA-2D, M	0.557 ± 0.000	0.327 ± 0.000	0.095 ± 0.001	0.002 ± 0.000	0.494 ± 0.000	0.481 ± 0.000	0.002 ± 0.001	0.000 ± 0.000
SEA-7, M	0.387 ± 0.000	0.449 ± 0.000	0.121 ± 0.001	0.001 ± 0.000	0.498 ± 0.000	0.481 ± 0.000	0.019 ± 0.001	0.002 ± 0.000

Table 7-4: Relative PP pathway flux in L-lysine producing *C. glutamicum* strains. The strains were grown on 99 % [1-^{13}C] mannitol. The previously obtained correlation factor (f = 1.49) was used to correct the relative PP pathway flux of mannitol-grown strains.

Strain	$v_{Zwf,lb}$ [%]	Factor [-]	v_{Zwf} [%]
SEA-1	3.8 ± 0.1	1.49	5.7 ± 0.2
SEA-2B	11.2 ± 0.1	1.49	16.7 ± 0.2
SEA-3	5.3 ± 0.1	1.49	7.9 ± 0.2
SEA-2D	3.1 ± 0.1	1.49	4.6 ± 0.2
SEA-7	4.3 ± 0.1	1.49	6.4 ± 0.2

Table 7-5: Relative mannitol catabolic fluxes in mannitol-grown *C. glutamicum* stains. Mean values and deviations were calculated on basis of corresponding measurements (Table 5-9 and Table 5-11).

Strain	$v_{Mtl,in}$ [%]	$v_{Frc,out}$ [%]	$v_{Frc,in}$ [%]	v_{Zwf} [%]	v_{Mak} [%]	$v_{PTS,Frc}$ [%]
SEA-1	100	26.2 ± 1.4	73.8 ± 1.4	5.7 ± 0.2	n.i.*	73.8 ± 1.4
SEA-2B	100	18.4 ± 1.3	81.7 ± 1.3	16.7 ± 0.2	11.0 ± 0.2	70.7 ± 1.5
SEA-3	100	8.2 ± 1.8	91.8 ± 1.8	7.9 ± 0.2	2.2 ± 0.2	89.6 ± 2.0
SEA-2D	100	0.0 ± 0.0	100.0 ± 0.0	4.6 ± 0.2	n.i.*	100.0 ± 0.0
SEA-7	100	0.0 ± 0.0	100 ± 0.0	6.4 ± 0.2	0.7 ± 0.2	99.3 ± 0.0

*n.i. not included, since enzyme not contained

Table 7-6: Relative flux through the lower glycolysis at the level of NAD-dependent glyceraldehyde 3-phosphate dehydrogenase (v_{GapA}) and NADP-dependent glyceraldehyde 3-phosphate dehydrogenase (v_{GapN}) in mannitol-grown *C. glutamicum* strains. Mean values and deviations were calculated on basis of corresponding measurements (Table 5-9 and Table 5-11).

Strain	$v_{Frc,in}$ [%]	$v_{G6P,Tre}$ [%]	$v_{G6P,Ana}$ [%]	$v_{F6P,Ana}$ [%]	$v_{R5P,Ana}$ [%]	$v_{E4P,Ana}$ [%]	$v_{GapA,Ana}$ [%]	$v_{Zwf\,/\,6}$ [%]	v_{GapA} [%]	v_{GapN} [%]
SEA-1	73.8 ± 1.4	0.3 ± 0.0	0.8 ± 0.0	1.2 ± 0.1	3.5 ± 0.2	1.1 ± 0.1	0.5 ± 0.0	0.9 ± 0.0	130.9 ± 3.9	n.i.*
SEA-2B	81.7 ± 1.3	0.3 ± 0.0	0.8 ± 0.0	1.2 ± 0.1	3.4 ± 0.2	1.1 ± 0.1	0.5 ± 0.0	2.8 ± 0.0	143.2 ± 3.8	n.i.*
SEA-3	91.8 ± 1.8	0.3 ± 0.1	0.8 ± 0.1	1.2 ± 0.1	3.5 ± 0.4	1.1 ± 0.1	0.5 ± 0.1	1.3 ± 0.0	143.2 ± 6.0	23.0 ± 1.8
SEA-2D	100.0 ± 0.0	0.3 ± 0.0	1.1 ± 0.1	1.6 ± 0.1	4.6 ± 0.3	1.4 ± 0.1	0.7 ± 0.1	0.8 ± 0.0	179.2 ± 1.5	n.i.*
SEA-7	100 ± 0.0	0.2 ± 0.0	1.0 ± 0.1	1.5 ± 0.2	4.7 ± 0.2	1.3 ± 0.1	0.6 ± 0.1	1.0 ± 0.0	143.2 ± 2.1	36.2 ± 1.5

*n.i. not included, since enzyme not contained

Table 7-7: Relative flux through the lower glycolysis at the level of enolase (v_{Eno}) in mannitol-grown *C. glutamicum* strains. Mean values and deviations were calculated on basis of corresponding measurements (Table 5-9 and Table 5-11).

Strain	v_{GapA} [%]	v_{GapN} [%]	$v_{3P,Ana}$ [%]	$v_{3P,Gly}$ [%]	v_{Eno} [%]
SEA-1	130.9 ± 3.9	n.i.*	5.2 ± 0.3	0.2 ± 0.0	125.6 ± 3.9
SEA-2B	143.2 ± 3.8	n.i.*	5.1 ± 0.3	0.5 ± 0.0	137.8 ± 3.9
SEA-3	143.2 ± 6.0	23.0 ± 1.8	5.2 ± 0.6	0.7 ± 0.1	160.4 ± 6.0
SEA-2D	179.2 ± 1.5	n.i.*	6.7 ± 0.5	0.2 ± 0.0	172.3 ± 2.0
SEA-7	143.2 ± 2.1	36.2 ± 1.5	6.2 ± 0.7	0.5 ± 0.0	172.7 ± 2.8

*n.i. not included, since enzyme not contained

Table 7-8: Relative net flux through anaplerotic carboxylation ($v_{Pyc,net}$) in mannitol-grown *C. glutamicum* strains. Mean values and deviations were calculated on basis of corresponding measurements (Table 5-9 and Table 5-11).

Strain	$v_{OAA,Ana}$ [%]	$v_{Akg,Ana}$ [%]	$v_{Akg,Glu}$ [%]	$v_{OAA,Lys}$ [%]	$v_{Pyc,net}$ [%]
SEA-1	3.5 ± 0.2	6.7 ± 0.3	0.6 ± 0.0	10.5 ± 0.1	21.3 ± 1.5
SEA-2B	3.5 ± 0.2	6.6 ± 0.4	0.9 ± 0.1	12.8 ± 0.6	23.8 ± 0.7
SEA-3	3.5 ± 0.4	6.7 ± 0.7	1.0 ± 0.1	15.9 ± 1.0	27.1 ± 2.2
SEA-2D	4.5 ± 0.3	8.7 ± 0.7	0.4 ± 0.0	24.3 ± 0.5	38.0 ± 1.5
SEA-7	4.2 ± 0.5	8.0 ± 0.9	1.0 ± 0.0	31.6 ± 0.5	44.8 ± 1.9

Table 7-9: Relative flux through pyruvate dehydrogenase (v_{Pdh}) in mannitol-grown *C. glutamicum* strains. Mean values and deviations were calculated on basis of corresponding measurements (Table 5-9 and Table 5-11).

Strain	v_{Eno} [%]	$v_{Pyr,Lys}$ [%]	$v_{Pyr,Ana}$ [%]	$v_{Pyc,net}$ [%]	$v_{Pyr,Lac}$ [%]	$v_{Pyr,Ala}$ [%]	v_{Pdh} [%]
SEA-1	125.6 ± 3.9	10.5 ± 0.1	11.6 ± 0.5	21.3 ± 1.5	1.0 ± 0.1	0.1 ± 0.1	81.0 ± 5.3
SEA-2B	137.8 ± 3.9	12.8 ± 0.6	11.4 ± 0.5	23.8 ± 0.7	0.0 ± 0.0	0.0 ± 0.0	89.8 ± 5.1
SEA-3	160.4 ± 6.0	15.9 ± 1.0	11.6 ± 1.0	27.1 ± 2.2	0.0 ± 0.0	0.0 ± 0.0	105.8 ± 10.1
SEA-2D	172.3 ± 2.0	24.3 ± 0.5	15.1 ± 0.9	38.0 ± 1.5	0.0 ± 0.0	0.0 ± 0.0	94.9 ± 4.9
SEA-7	172.7 ± 2.8	31.6 ± 0.5	15.6 ± 1.2	44.8 ± 1.9	0.0 ± 0.0	0.0 ± 0.0	80.7 ± 6.3

Table 7-10: Relative flux through the TCA cycle in mannitol-grown *C. glutamicum* strains. Mean values and deviations were calculated on basis of corresponding measurements (Table 5-9 and Table 5-11).

Strain	v_{Pdh} [%]	$v_{AcCoA,Ana}$ [%]	v_{Cis} [%]	$v_{Akg,Ana}$ [%]	$v_{Akg,Glu}$ [%]	v_{Akd} [%]
SEA-1	81.0 ± 5.3	12.7 ± 0.6	68.3 ± 6.0	6.7 ± 0.3	0.6 ± 0.0	61.0 ± 6.0
SEA-2B	89.8 ± 5.1	12.4 ± 0.7	77.4 ± 5.8	6.6 ± 0.4	0.9 ± 0.1	69.9 ± 5.8
SEA-3	105.8 ± 10.1	12.7 ± 1.4	93.0 ± 11.5	6.7 ± 0.7	1.0 ± 0.1	85.3 ± 11.5
SEA-2D	94.9 ± 4.9	16.5 ± 1.2	78.4 ± 6.1	8.7 ± 0.7	0.4 ± 0.0	69.3 ± 6.1
SEA-7	80.7 ± 6.3	15.2 ± 1.7	65.5 ± 8.1	8.0 ± 0.9	1.0 ± 0.0	56.5 ± 8.1

Table 7-11: *In vitro* activity of malic enzyme in *C. glutamicum* SEA-1, SEA-2D, and SEA-7. The cultivation of the different strains was conducted in mannitol mineral salt medium at 30 °C. The data represent mean values and deviations from three biological replicates.

Strain	Specific activity (mU mg^{-1})
SEA-1	163 ± 9
SEA-2D	158 ± 4
SEA-7	111 ± 7

Table 7-12: Relative flux through the TCA cycle in mannitol-grown *C. glutamicum* strains. The relative flux of malic enzyme (v_{Mae}) in strains SEA-2D and SEA-7 was assumed to be equal to that of SEA-1, based on the unchanged malic enzyme activity (Table 7-11).

Strain	$v_{OAA,Ana}$ [%]	$v_{Akg,Ana}$ [%]	$v_{Akg,Glu}$ [%]	$v_{OAA,Lys}$ [%]	$v_{Pyc,net}$ [%]	v_{Mae} [%]	v_{Pyc} [%]
SEA-1	3.5 ± 0.2	6.7 ± 0.3	0.6 ± 0.0	10.5 ± 0.1	21.3 ± 1.5	22.6 ± 1.5	43.9 ± 1.5
SEA-2D	4.5 ± 0.3	8.7 ± 0.7	0.4 ± 0.0	24.3 ± 0.5	38.0 ± 1.5	22.6 ± 1.5	60.6 ± 1.5
SEA-7	4.2 ± 0.5	8.0 ± 0.9	1.0 ± 0.0	31.6 ± 0.5	44.8 ± 1.9	22.6 ± 1.5	67.4 ± 1.9

Table 7-13: *In vitro* activity of membrane-bound transhydrogenase PntAB in *C. glutamicum* SEA-1, SEA-2D, and SEA-7. The cultivation of the different strains was conducted in mannitol mineral salt medium at 30 °C. The data represent mean values and deviations from three biological replicates.

	Transhydrogenase PntAB	
Strain	(mU mg^{-1} total protein)	(mU mg^{-1} membrane protein)
SEA-1	< 0.1	< 0.1
SEA-2D	28.8 ± 1.8	497.9 ± 30.8
SEA-7	31.8 ± 3.2	578.0 ± 57.8

Table 7-14: Relative flux through PntAB in mannitol-grown *C. glutamicum* strains. For determination of the NADPH requirement for anabolism, the previously estimated demand of 16.4 mmol NADPH (g biomass)$^{-1}$ (Wittmann and de Graaf 2005) and the obtained biomass yields of the strains SEA-1, SEA-2D and SEA-7 (Table 5-9 and Table 5-11) were used.

Strain	$v_{NADPH,Anabolism}$ [%]	v_{Lys} [%]	v_{Zwf} [%]	v_{GapN} [%]	v_{Cis} [%]	v_{Mae} [%]	v_{PntAB} [%]
SEA-1	66.3 ± 3.3	9.0 ± 0.1	5.7 ± 0.2	n.i.*	68.3 ± 6.0	22.6 ± 1.5	n.i.*
SEA-2D	85.8 ± 6.4	22.4 ± 0.5	4.6 ± 0.2	n.i.*	78.4 ± 6.1	22.6 ± 1.5	65.2 ± 0.4
SEA-7	78.9 ± 8.9	30.0 ± 0.5	6.4 ± 0.2	36.2 ± 1.5	65.5 ± 8.1	22.6 ± 1.5	61.7 ± 1.0

*n.i. not included, since enzyme not contained

7.4 Elementary flux mode analysis

Table 7-15 depicts the reactions of the carbon core metabolism of mannitol-grown cells, which were used for elementary flux mode analysis.

Table 7-15: Metabolic network of mannitol-grown *C. glutamicum* SEA-1 and SEA-7 used for elementary flux mode analysis. The additional substrate-specific reactions, which are present in the SEA-7 strain but not in the L-lysine basic producer strain SEA-1 are highlighted in blue.

Reaction no.	Description/genes	Reaction
1	mannitol import	'--> MTL[e]'
2	L-lysine export	'LYS[c] -->'
3	biomass export	'biomass[c] -->'
4	ATP maintenance export	'ATPmaintenance[c] -->'
5	carbon dioxide export	'CO2[c] -->'
6	carbon dioxide import	'--> CO2ex[c]'
7	oxygen import	'--> O2[c]'
8	ammonium import	'--> NH3[c]'
9	hydrogen sulphide import	'--> H2S[c]'
10	*mtlD*	'MTL[e] + NAD[c] --> FRU[c] + NADH[c]'
11	pts_{Man}	'FRU[c] + PEP[c] --> F6P[c] + PYR[c]'
12	*mak*	'FRU[c] + ATP[c] --> F6P[c] + ADP[c]'
13	pts_{Frc}	'FRU[c] + PEP[c] --> F1P[c] + PYR[c]'
14	*pfkB*	'ATP[c] + F1P[c] --> ADP[c] + FBP[c]'
15	*pfkA*	'ATP[c] + F6P[c] --> ADP[c] + FBP[c]'
16	*fbp*	'FBP[c] --> F6P[c]'
17	*pgi*	'F6P[c] <==> G6P[c]'
18	*zwf*	'G6P[c] + NADP[c] --> GLC-LAC[c] + NADPH[c]'
19	*opcA*	'GLC-LAC[c] --> 6-PG[c]'
20	*gnd*	'6-PG[c] + NADP[c] --> RIB-5P[c] + CO2[c] + NADPH[c]'
21	*rpe*	'RIB-5P[c] <==> XYL-5P[c]'
22	*rpi*	'RIB-5P[c] <==> RIBO-5P[c]'
23	*tkt1*	'RIBO-5P[c] + XYL-5P[c] <==> S7P[c] + GAP[c]'
24	*tal*	'S7P[c] + GAP[c] <==> E-4P[c] + F6P[c]'
25	*tkt2*	'E-4P[c] + XYL-5P[c] <==> F6P[c] + GAP[c]'
26	*fda*	'FBP[c] <==> GAP[c] + DAHP[c]'
27	*tpi*	'DAHP[c] <==> GAP[c]'
28	*gapA*	'GAP[c] + NAD[c] <==> 13-PG[c] + NADH[c]'
29	*gapN*	GAP[c] + NADP[c] --> 3-PG[c] + NADPH[c]'
30	*pgk*	'ADP[c] + 13-PG[c] --> ATP[c] + 3-PG[c]'
31	*gpmAB*	'3-PG[c] <==> 2-PG[c]'
32	*eno*	'2-PG[c] <==> PEP[c]'
33	*pyk*	'PEP[c] + ADP[c] --> PYR[c] + ATP[c]'
34	*aceEF*	'PYR[c] + NAD[c] --> AC-CoA[c] + NADH[c] + CO2[c]'
35	*gltA*	'AC-CoA[c] + OAA[c] --> CIT[c]'
36	*acn*	'CIT[c] <==> ICI[c]'
37	*icd*	'ICI[c] + NADP[c] --> AKG[c] + CO2[c] + NADPH[c]'
38	*kgd*	'AKG[c] + NAD[c]--> SUCC-CoA[c] + NADH[c] + CO2[c]'
39	*sucCD*	'SUCC-CoA[c] + ADP[c] --> SUCC[c] + ATP[c]'
40	*sdhAB*	'SUCC[c] + MK[c] <==> FUM[c] + MKH2[c]'

Table 7-15: *(Continued from previous page)* Metabolic network of mannitol-grown *C. glutamicum* SEA-1 and SEA-7 used for elementary flux mode analysis.

Reaction no.	Description/genes	Reaction
41	*fumC*	'FUM[c] <==> MAL[c]'
42	*mdh*	'MAL[c] + NAD[c] --> OAA[c] + NADH[c]'
43	*aceA*	'ICI[c] --> GLYOXY[c] + SUCC[c]'
44	*aceB*	'GLYOXY[c] + AC-CoA[c] --> MAL[c]'
45	*pyc*	'PYR[c] + ATP[c] + CO2[c] --> OAA[c] + ADP[c]'
46	*pyc*	'PYR[c] + ATP[c] + CO2ex[c] --> OAA[c] + ADP[c]'
47	*ppc*	'PEP[c] + CO2[c] --> OAA[c]'
48	*ppc*	'PEP[c] + CO2ex[c] --> OAA[c]'
49	*pck*	'OAA[c] + ATP[c] --> PEP[c] + ADP[c] + CO2[c]'
50	*malE*	'MAL[c] + NADP[c] --> PYR[c] + CO2[c] + NADPH[c]'
51	*gdh*	'AKG[c] + NH3[c] + NADPH[c] --> GLU[c] + NADP[c]'
52	*aspC*	'OAA[c] + GLU[c] <==> ASP[c] + AKG[c]'
53	*lysC*	'ASP[c] + ATP[c] --> ASP-P[c] + ADP[c]'
54	*asd*	'ASP-P[c] + NADPH[c] --> ASP-SA[c] + NADP[c]'
55	*dapA*	'ASP-SA[c] + PYR[c] --> DHP[c]'
56	*dapB*	'DHP[c] + NADPH[c] --> THDP[c] + NADP[c]'
57	*dapD*	'THDP[c] + SUCC-CoA[c] --> SAP[c]'
58	*dapC*	'SAP[c] + GLU[c] --> SADP[c] + AKG[c]'
59	*dapE*	'SADP[c] --> SUCC[c] + DAP[c]'
60	*ddh*	'THDP[c] + NADPH[c] + NH3[c] --> DAP[c] + NADP[c]'
61	*lysA*	'DAP[c] --> LYS[c] + CO2[c]'
62	ATP maintenance	'ATP[c] --> ADP[c] + ATPmaintenance[c]'
63	energy metabolism	'NADH[c] + (0.5) O2[c] + (2) ADP[c] --> NAD[c] + (2) ATP[c]'
64	energy metabolism	'MKH2[c] + (0.5) O2[c] + (2) ADP[c] --> MK[c] + (2) ATP[c]'
65	*pntAB*	'NADP[c] + NADH[c] --> NADPH[c] + NAD[c]'
66	biomass synthesis	'(6.231) NH3[c] + (0.233) H2S[c] + (0.205) G6P[c] + (0.308) F6P[c] + (0.879) RIBO-5P[c] + (0.268) E-4P[c] + (0.129) GAP[c] + (1.295) 3-PG[c] + (0.652) PEP[c] + (2.604) PYR[c] + (3.177) AC-CoA[c] + (1.680) OAA[c] + (1.224) AKG[c] + (16.429) NADPH[c] + (67.79) ATP[c] + (3.111) NAD[c] --> biomass[c] + (16.429) NADP[c] + (2.537) CO2[c] + (67.79) ADP[c] + (3.111) NADH[c]'

7.5 Data from ^{13}C metabolic flux analysis in *C. glutamicum* strains

For metabolic flux analysis the *C. glutamicum* strains SEA-2B, SEA-3, and SEA-2D were analyzed with regard to their metabolic as well as their isotopic steady state (Figure 7-2, Figure 7-3, and Figure 7-4).

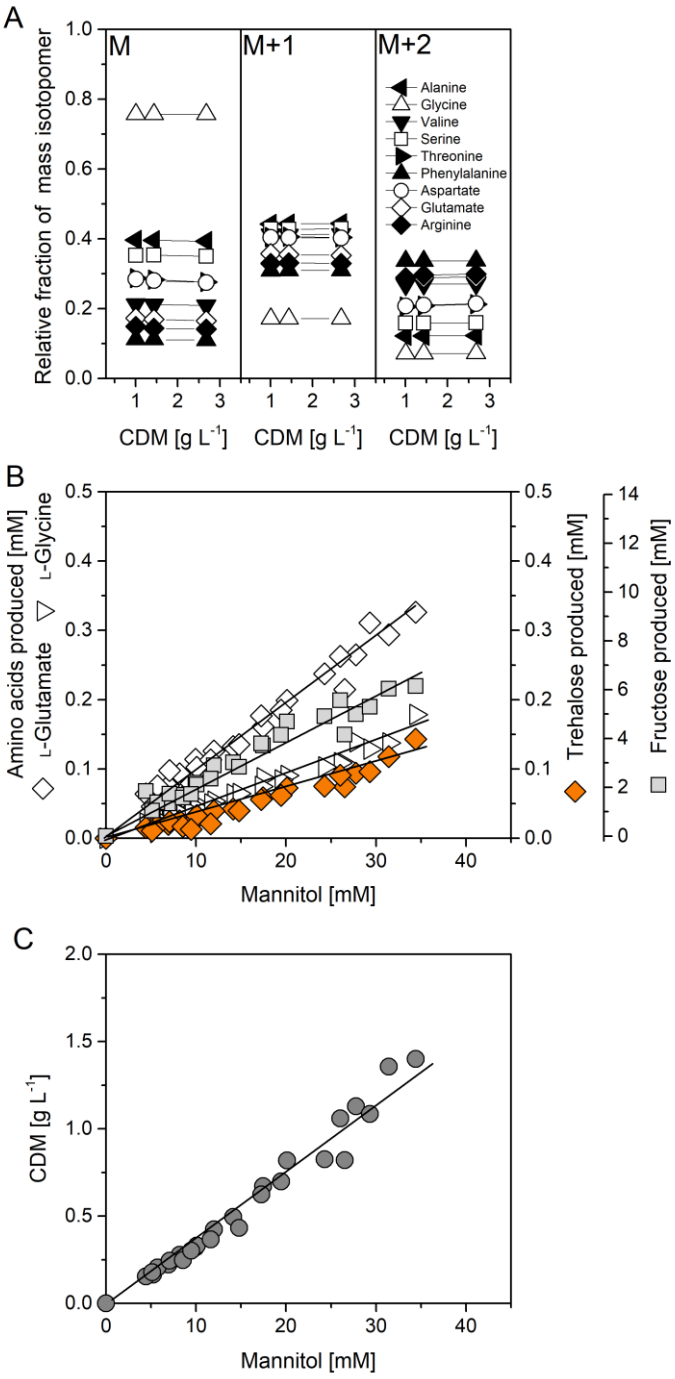

Figure 7-2: Verification of isotopic (A) and metabolic (B, C) steady-state of L-lysine-producing *C. glutamicum* SEA-2B on mineral salt medium containing mannitol as the sole carbon source. The data represent the initial growth phase of the cultivated *C. glutamicum* SEA-2B mutant, which was determined by fructose accumulation and is highlighted in white in the cultivation profile (Figure 5-10) and are derived from three biological replicates.

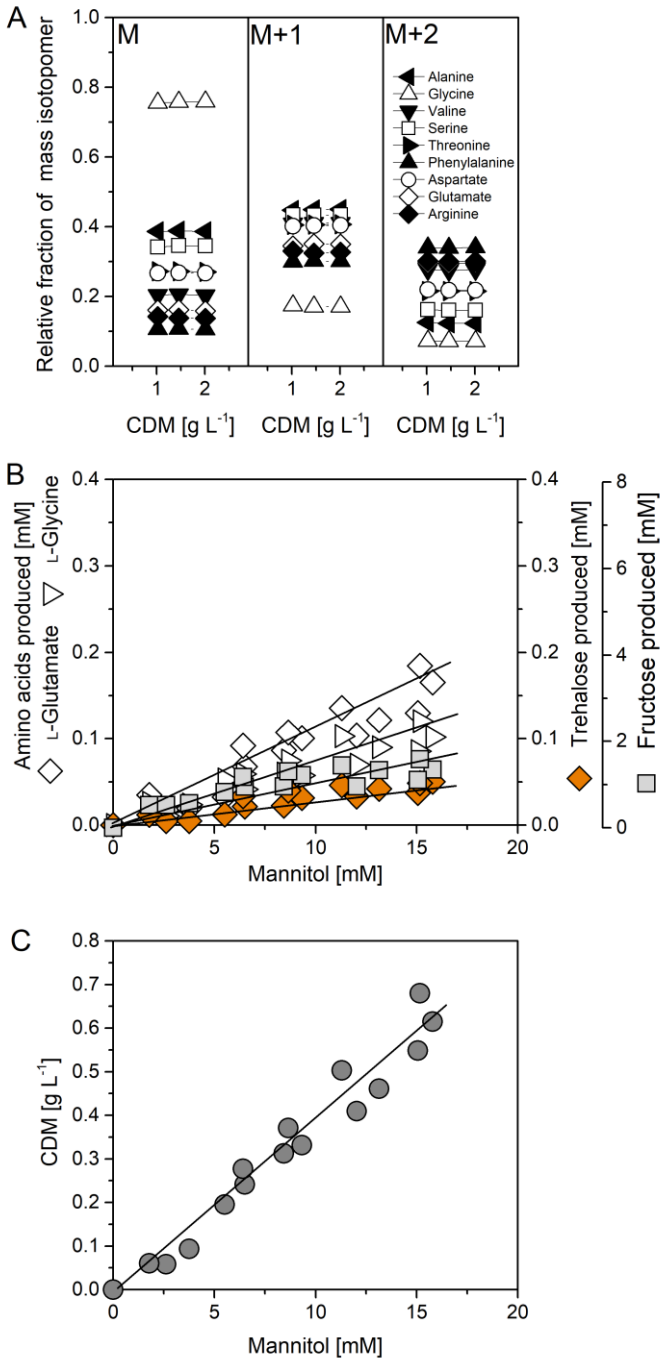

Figure 7-3: Verification of isotopic (A) and metabolic (B, C) steady-state of L-lysine-producing *C. glutamicum* SEA-3 on mineral salt medium containing mannitol as the sole carbon source. The data represent the initial growth phase of the cultivated *C. glutamicum* SEA-3 mutant, which was determined by fructose accumulation and is highlighted in white in the cultivation profile (Figure 5-14) and are derived from three biological replicates

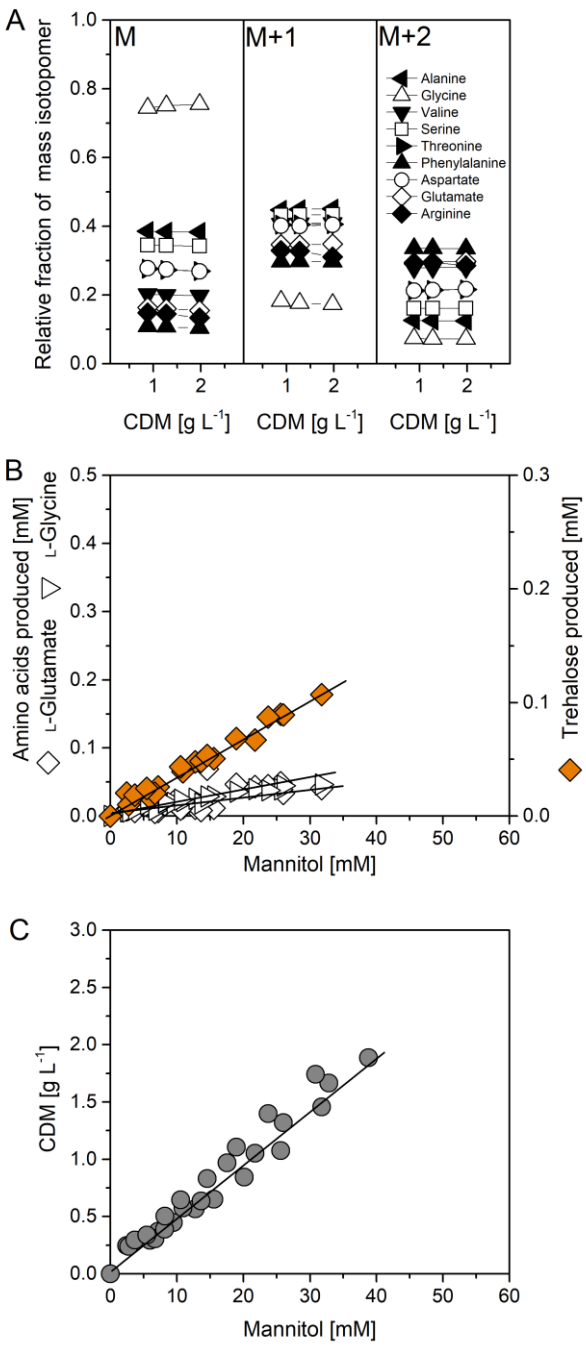

Figure 7-4: Verification of isotopic (A) and metabolic (B, C) steady-state of L-lysine-producing *C. glutamicum* SEA-2D on mineral salt medium containing mannitol as the sole carbon source. The data represent the early exponential growth phase of the cultivated *C. glutamicum* strain and are derived from three biological replicates.

To investigate the intracellular flux distribution of *C. glutamicum* SEA-7, the strain was first analyzed with regard to its metabolic as well as its isotopic steady state (Figure 7-5).

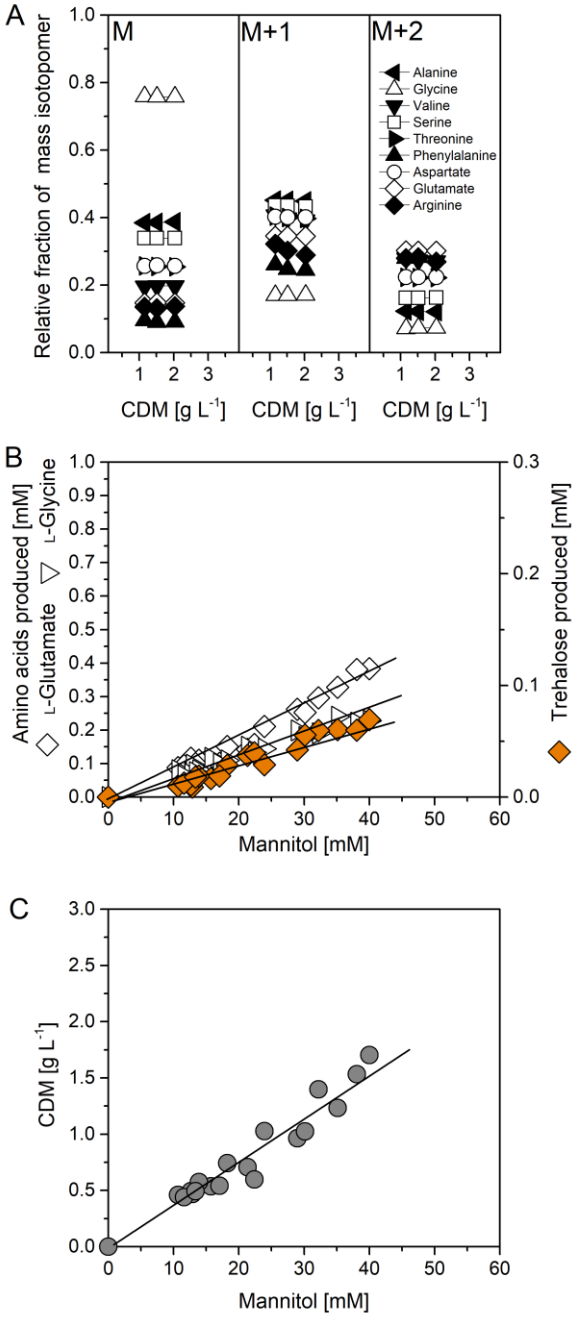

Figure 7-5: Verification of isotopic (A) and metabolic (B, C) steady-state of the tailor-made L-lysine-producing strain *C. glutamicum* SEA-7 on mineral salt medium containing mannitol as the sole carbon source. The data represent the early exponential growth phase of the cultivated *C. glutamicum* strain and are derived from three biological replicates.

8 Abbreviations and Symbols

Abbreviations

2-OG	2-oxoglutarate
3PG	3-phosphoglycerate
ABC	ATP-binding cassette transporter
ABU	α-aminobutyric acid
AcCoA	acetyl CoA
Ace	acetate
aceA	gene, encoding isocitrate lyase
aceB	gene, encoding malate synthase
aceEF	gene, encoding pyruvate dehydrogenase
acn	gene, encoding aconitase
Ala	alanine
Ana	anabolism
AraA	arabinose isomerase
AraB	ribulokinase
AraD	ribulose 5-phosphate 4-epimerase
AraE	H^+-transporter for arabinose
asd	gene, encoding aspartate semialdehyde dehydrogenase
aspC	gene, encoding aspartate aminotransferase
ATCC	American Type Culture Collection
ATG	adenine-thymidine-guanine, start codon
atlR	gene, encoding a mannitol/arabitol dependent transcriptional repressor
AtlR	mannitol/arabitol dependent transcriptional repressor
ATP	adenosine triphosphate
BHI	brain heart infusion
BHI^{kan}	brain heart infusion with kanamycin
$BHI^{kan+tet}$	brain heart infusion with kanamycin and tetracycline
BHIS	brain heart infusion with sorbitol
bp	base pair
BSA	bovine serum albumin
C_3	metabolite containing three carbon atoms
C_4	metabolite containing four carbon atoms
CDW	cell dry weight
CDM	cell dry mass
cis	gene, encoding citrate synthase
CM	complex medium
CO_2	carbon dioxide
crtB	gene, encoding phytoene synthase
crtEb	gene, encoding lycopene elongase
crtI	gene, encoding phytoene desaturase
dapA	gene, encoding dihydrodipicolinate synthase
dapB	gene, encoding dihydrodipicolinate reductase
dapC	gene, encoding succinyl-aminoketopimelate transaminase
dapD	gene, encoding tetrahydrodipicolinate succinylase
dapE	gene, encoding succinyl-L-diaminopimelate desuccinylase
dapF	gene, encoding diaminopimelate epimerase
dATP	deoxyadenosine triphosphate
dCTP	deoxycytidine triphosphate

dGTP	deoxyguanosine triphosphate
ddh	gene, encoding diaminopimelate dehydrogenase
DHB	dihydroxybenzoic acid
DMSO	dimethyl sulfoxide
DNA	deoxyribonucleic acid
DTT	dithiothreitol
dTTP	deoxythymidine triphosphate
E4P	erythrose 4-phosphate
EI	general PTS-component enzyme I
EII	general PTS-component enzyme II
EII_{Glc}	glucose-specific PTS component
EII_{Fru}	fructose-specific PTS component
EII_{Suc}	sucrose-specific PTS component
eftu	gene, encoding elongation factor tu
EMP	Emden-Meyerhof-Parnas
eno	gene, encoding enolase
Eno	enolase
Eq	equation
f	correlation factor
F6P	fructose 6-phosphate
FADH	flavin adenine dinucleotide, reduced
fda	gene, encoding fructose bisphosphate aldolase
Fda	fructose bisphosphate aldolase
fbp	gene, encoding fructose 1,6 bisphosphatase
Fbp	fructose 1,6-bisphosphatase
Frc	fructose
fumC	gene, encoding fumarase
G6P	glucose 6-phosphate
G6PDH	glucose 6-phosphate dehydrogenase
Gap	glyceraldehyde 3-phosphate
gapA	gene, encoding NAD-dependent glyceraldehyde 3-phosphate dehydrogenase
GapA	NAD-dependent glyceraldehyde 3-phosphate dehydrogenase
gapB	gene, encoding NAD(P)-dependent glyceraldehyde 3-phosphate dehydrogenase
GapB	NAD(P)-dependent glyceraldehyde 3-phosphate dehydrogenase
GapDH	glyceraldehyde 3-phosphate deydrogenase
gapN	gene, encoding NADP-dependent glyceraldehyde 3-phosphate dehydrogenase in *S. mutans*
GapN	NADP-dependent glyceraldehyde 3-phosphate dehydrogenase in *S. mutans*
GC	gas chromatography
GC-MS	gas chromatography-mass spectrometry
gdh	gene, encoding glutamate dehydrogenase
GHG	greenhouse gases
gltA	gene, encoding citrate synthase
GlK	glucokinase
Glu	glutamate
Gly	glycine
gnd	gene, encoding 6-phosphogluconate dehydrogenase
gpmAB	gene, encoding phosphoglycerate mutase
GRAS	generally recognized as safe
GTG	guanine-thymine-guanine, start codon
GTP	guanosine triphosphate
hom	gene, encoding homoserine dehydrogenase

HPr	histidine protein
HPLC	high-performance liquid chromatography
icd	gene, encoding isocitrate dehydrogenase
int	integrative
iolT1	gene, encoding *myo*-inositol transporter 1
IolT1	*myo*-inositol transporter 1
iolT2	gene, encoding *myo*-inositol transporter 2
IolT2	*myo*-inositol transporter 2
kan	kanamycin
kan^R	kanamycin resistance
kb	kilo base pairs
kgd	gene, encoding α-ketoglutarate dehydrogenase
Lac	lactate
lb	lower boundary
lysA	gene, encoding diaminopimelate decarboxylase
lysC	gene, encoding aspartate kinase
lysE	gene, encoding lysine permease
lysE	lysine permease
M	mass
mak	gene, encoding fructokinase in *E. coli*
Mak	fructokinase in *E. coli*
malE	gene, encoding malic enzyme
MBDSTFA	*N*-methyl-*N*-tert-butyldimethylsilyl-trifluoro-acetamide
MSTFA	*N*-methyl-*N*-trimethylsilyl-trifluoroacetamide
MCS	multiple cloning site
mdh	gene, encoding malate dehydrogenase
mqo	gene, encoding malate:quinone oxidoreductase
MID	mass isotopomer distribution
MID_{corr}	mass isotopomer distribution corrected for natural isotopes
Mtl	mannitol
mtlD	gene, encoding mannitol 2-dehydrogenase
mtlD	mannitol 2-dehydrogenase
mtlR	gene, encoding a mannitol/arabitol dependent transcriptional repressor
mtlR	mannitol/arabitol dependent transcriptional repressor
mtlT	gene, encoding mannitol/ribitol MFS-type transporter
mtlT	mannitol/ribitol transporter
n.d.	not determined
NAD(P)	nicotinamide adenine dinucleotide (phosphate), oxidized
NAD(P)H	nicotinamide adenine dinucleotide (phosphate), reduced
NMR	nuclear magnetic resonance
odc	gene, encoding oxaloacetate decarboxylase
OD	optical density
OPA	ortho-phthaldialdehyde
opcA	gene, encoding a putative subunit of glucose 6-phosphate dehydrogenase
ORI	origin of replication
PCR	polymerase chain reaction
PEP	Phosphoenolpyruvate
pck	gene, encoding phosphoenolpyruvate carboxykinase
pdh	gene, encoding pyruvate dehydrogenase
PBS	phosphate-buffered saline
pfkA	gene, encoding 6-phosphofructokinase

PfkA	6-phosphofructokinase
pfkB	gene, encoding fructose 1-phosphate kinase
PfkB	fructose 1-phosphate kinase
pgi	gene, encoding phosphoglucoisomerase
Pgi	phosphoglucoisomerase
pgk	gene, encoding phosphoglycerate kinase
pgl	gene, encoding 6-phosphogluconolactonase
pntAB	gene, encoding membrane-bound nicotinamide nucleotide transhydrogenase in *E. coli*
PntAB	membrane-bound nicotinamide nucleotide transhydrogenase in *E. coli*
ppc	gene, encoding phosphoenolpyruvate carboxylase
PP	pentose phosphate
PTS	phosphotransferase system
PTS_{Glc}	glucose-specific phosphotransferase system
PTS_{Frc}	fructose-specific phosphotransferase system
pts_{Frc}	gene, encoding fructose-specific phosphotransferase system
pts_{Man}	gene, encoding mannose-specific phosphotransferase system
PTS_{Suc}	sucrose-specific phosphotransferase system
pyc	gene, encoding pyruvate carboxylase
Pyc	pyruvate carboxylase
pyk	gene, encoding pyruvate kinase
Pyr	pyruvate
R5P	ribose 5-phosphate
RbsK1	ribokinase 1
Rbsk2	ribokinase 2
rbtT	gene, encoding mannitol/ribitol MFS-type transporter
RbtT	mannitol/ribitol MFS-type transporter
rpe	gene, encoding ribulose 5-phosphate epimerase
Rpe	ribulose 5-phosphate epimerase
rpi	gene, encoding ribose 5-phosphate epimerase
Rpi	ribose 5-phosphate epimerase
sacB	gene, encoding levansucrase in *B. subtilis*
ScrB	sucrose 6-phosphate hydrolase in *B. subtilis*
scrK	gene, encoding fructokinase in *C. acetobutylicum*
ScrK	fructokinase in *C. acetobutylicum*
sdhAB	gene, encoding succinate dehydrogenase
SFL	summed fractional labeling
SIM	selective ion monitoring
sod	gene, encoding superoxide dismutase
sucCD	succinyl-CoA-synthetase
TAE	buffer consisting of Tris, EDTA and acetic acid
tal	gene, encoding transaldolase
TCA	tricarboxylic acid
tet	tetracycline
tkt	gene, encoding transketolase
tkt operon	genes, encoding transketolase operon
TMS	trimethylsilyl
tpi	gene, encoding triosephosphate isomerase
Tre	trehalose
$TSPd_4$	3-(trimethylsilyl)propionic-2,2,3,3-d_4 acid
v	flux
XylA	xylose isomerase

xylB	gene, encoding xylulokinase
XylB	xylulokinase in *E. coli*
XylK	xylulokinase in *E. coli*
zwf	gene, encoding glucose 6-phosphate dehydrogenase

Proteinogenic amino acids

A	Ala	alanine
D	Asp	aspartic acid
E	Glu	glutamic acid
G	Gly	glycine
K	Lys	lysine
M	Met	methionine
V	Val	valine

Symbols

μ	specific growth rate	$[h^{-1}]$
g	gravitation constant	$[m\ s^{-2}]$
q_{Mtl}	specific mannitol uptake rate	$[mmol\ g^{-1}\ h^{-1}]$
q_{Lys}	specific lysine production rate	$[mmol\ g^{-1}\ h^{-1}]$
T	temperature	[°C]
t	time	[min] or [h]
U	unit	$[\mu mol\ min^{-1}]$
$Y_{Ala/Mtl}$	alanine yield	$[mmol^{-1}\ mol^{-1}]$
$Y_{Ace/Mtl}$	acetate yield	$[mmol^{-1}\ mol^{-1}]$
$Y_{Frc/Mtl}$	fructose yield	$[mmol^{-1}\ mol^{-1}]$
$Y_{Glu/Mtl}$	glutamate yield	$[mmol^{-1}\ mol^{-1}]$
$Y_{Gly/Mtl}$	glycine yield	$[mmol^{-1}\ mol^{-1}]$
$Y_{Lac/Mtl}$	lactate yield	$[mmol^{-1}\ mol^{-1}]$
$Y_{Lys/Mtl}$	lysine yield	$[mmol^{-1}\ mmol^{-1}]$ or $[mmol^{-1}\ mol^{-1}]$
$Y_{Tre/Mtl}$	trehalose yield	$[mmol^{-1}\ mol^{-1}]$
$Y_{X/Mtl}$	biomass yield	$[g\ mol^{-1}]$

9 References

Abe, S, Takayama, K-I, and Kinoshita, S. (1967). Taxonomical studies on glutamic acid-producing bacteria. *The Journal of General and Applied Microbiology, 13*(3), 279-301.

Adams, JMM, Toop, TA, Donnison, IS, and Gallagher, JA. (2011). Seasonal variation in *Laminaria digitata* and its impact on biochemical conversion routes to biofuels. *Bioresource Technology, 102*(21), 9976-9984.

Akagawa, E, Kurita, K, Sugawara, T, Nakamura, K, Kasahara, Y, Ogasawara, N, and Yamane, K. (1995). Determination of a 17484 bp nucleotide sequence around the 39° region of the *Bacillus subtilis* chromosome and similarity analysis of the products of putative ORFs. *Microbiology, 141*(12), 3241-3245.

Alaswad, A, Dassisti, M, Prescott, T, and Olabi, AG. (2015). Technologies and developments of third generation biofuel production. *Renewable and Sustainable Energy Reviews, 51*, 1446-1460.

Aldor, IS, Krawitz, DC, Forrest, W, Chen, C, Nishihara, JC, Joly, JC, and Champion, KM. (2005). Proteomic Profiling of Recombinant *Escherichia coli* in High-Cell-Density Fermentations for Improved Production of an Antibody Fragment Biopharmaceutical. *Applied and Environmental Microbiology, 71*(4), 1717-1728.

Alexandratos, N, and Bruinsma, J. (2012). World agriculture towards 2030/2050: The 2012 revision. Rome: ESA Working Paper No. 12-03, Rome FAO.

Alfonsín, V, Maceiras, R, and Gutiérrez, C. (2019). Bioethanol production from industrial algae waste. *Waste Management, 87*, 791-797.

Anusree, M, Wendisch, VF, and Nampoothiri, KM. (2016). Co-expression of endoglucanase and β-glucosidase in *Corynebacterium glutamicum* DM1729 towards direct lysine fermentation from cellulose. *Bioresource Technology, 213*, 239-244.

Bae, HW, Kim, HJ, Moon, JO, Jang, Jw, Kim, JC, Kim, TH, Sung, JS, Lee, KH, Kim, DC, Kim, HJ, Bae, HA, and Lim, SJ. (2016). *Corynebacterium* sp. transformed with a fructokinase gene derived from *Escherichia* sp. and process for preparing L-amino acid using the same *EP2694638B1*.

Balat, M. (2011). Production of bioethanol from lignocellulosic materials via the biochemical pathway: A review. *Energy Conversion and Management, 52*(2), 858-875.

Baritugo, K-A, Kim, HT, David, Y, Choi, J-i, Hong, SH, Jeong, KJ, Choi, JH, Joo, JC, and Park, SJ. (2018). Metabolic engineering of *Corynebacterium glutamicum* for fermentative production of chemicals in biorefinery. *Applied Microbiology and Biotechnology, 102*(9), 3915-3937.

Barrett, E, Stanton, C, Zelder, O, Fitzgerald, G, and Ross, RP. (2004). Heterologous Expression of Lactose- and Galactose-Utilizing Pathways from Lactic Acid Bacteria in *Corynebacterium glutamicum* for Production of Lysine in Whey. *Applied and Environmental Microbiology, 70*(5), 2861-2866.

Bartek, T, Makus, P, Klein, B, Lang, S, and Oldiges, M. (2008). Influence of L-isoleucine and pantothenate auxotrophy for L-valine formation in *Corynebacterium glutamicum* revisited by metabolome analyses. *Bioprocess and Biosystems Engineering, 31*(3), 217-225.

Barton, N, Horbal, L, Starck, S, Kohlstedt, M, Luzhetskyy, A, and Wittmann, C. (2018). Enabling the valorization of guaiacol-based lignin: Integrated chemical and biochemical production of *cis*,*cis*-muconic acid using metabolically engineered *Amycolatopsis* sp ATCC 39116. *Metabolic Engineering, 45*, 200-210.

Becker, J, Buschke, N, Bücker, R, and Wittmann, C. (2010). Systems level engineering of *Corynebacterium glutamicum*–Reprogramming translational efficiency for superior production. *Engineering in Life Sciences, 10*(5), 430-438.

Becker, J, Gießelmann, G, Hoffmann, SL, and Wittmann, C. (2016). *Corynebacterium glutamicum* for Sustainable Bioproduction: From Metabolic Physiology to Systems Metabolic Engineering. In H. Zhao & A.-P. Zeng (Eds.), *Synthetic Biology – Metabolic Engineering* (pp. 217-263). Cham: Springer International Publishing.

Becker, J, Klopprogge, C, Herold, A, Zelder, O, Bolten, CJ, and Wittmann, C. (2007). Metabolic flux engineering of L-lysine production in *Corynebacterium glutamicum*—over expression and modification of G6P dehydrogenase. *Journal of Biotechnology, 132*(2), 99-109.

Becker, J, Klopprogge, C, Zelder, O, Heinzle, E, and Wittmann, C. (2005). Amplified Expression of Fructose 1,6-Bisphosphatase in *Corynebacterium glutamicum* Increases In Vivo Flux through the Pentose Phosphate Pathway and Lysine Production on Different Carbon Sources. *Applied and Environmental Microbiology, 71*(12), 8587-8596.

Becker, J, Kuhl, M, Kohlstedt, M, Starck, S, and Wittmann, C. (2018a). Metabolic engineering of *Corynebacterium glutamicum* for the production of *cis*, *cis*-muconic acid from lignin. *Microbial Cell Factories, 17*(1), 115.

Becker, J, Rohles, CM, and Wittmann, C. (2018b). Metabolically engineered *Corynebacterium glutamicum* for bio-based production of chemicals, fuels, materials, and healthcare products. *Metabolic Engineering, 50*, 122-141.

Becker, J, Schäfer, R, Kohlstedt, M, Harder, BJ, Borchert, NS, Stöveken, N, Bremer, E, and Wittmann, C. (2013). Systems metabolic engineering of *Corynebacterium glutamicum* for production of the chemical chaperone ectoine. *Microbial Cell Factories, 12*(1), 110.

Becker, J, and Wittmann, C. (2012a). Bio-based production of chemicals, materials and fuels – *Corynebacterium glutamicum* as versatile cell factory. *Current Opinion in Biotechnology, 23*(4), 631-640.

Becker, J, and Wittmann, C. (2012b). Systems and synthetic metabolic engineering for amino acid production – the heartbeat of industrial strain development. *Current Opinion in Biotechnology, 23*(5), 718-726.

Becker, J, and Wittmann, C. (2015). Advanced Biotechnology: Metabolically Engineered Cells for the Bio-Based Production of Chemicals and Fuels, Materials, and Health-Care Products. *Angewandte Chemie International Edition, 54*(11), 3328-3350.

Becker, J, and Wittmann, C. (2019). A field of dreams: Lignin valorization into chemicals, materials, fuels, and health-care products. *Biotechnology Advances, 37*(6), 107360.

Becker, J, Zelder, O, Häfner, S, Schröder, H, and Wittmann, C. (2011). From zero to hero—Design-based systems metabolic engineering of *Corynebacterium glutamicum* for L-lysine production. *Metabolic Engineering, 13*(2), 159-168.

Behera, S, Singh, R, Arora, R, Sharma, NK, Shukla, M, and Kumar, S. (2015). Scope of Algae as Third Generation Biofuels. *Frontiers in Bioengineering and Biotechnology, 2*(90).

Behrens, S, Mitchell, WJ, and Bahl, H. (2001). Molecular analysis of the mannitol operon of *Clostridium acetobutylicum* encoding a phosphotransferase system and a putative PTS-modulated regulator. *Microbiology, 147*(1), 75-86.

Bellmann, A, Vrljić, M, Pátek, M, Sahm, H, Krämer, R, and Eggeling, L. (2001). Expression control and specificity of the basic amino acid exporter LysE of *Corynebacterium glutamicum*. *Microbiology, 147*(7), 1765-1774.

Bendt, AK, Burkovski, A, Schaffer, S, Bott, M, Farwick, M, and Hermann, T. (2003). Towards a phosphoproteome map of *Corynebacterium glutamicum*. *PROTEOMICS, 3*(8), 1637-1646.

Benkert, P, Biasini, M, and Schwede, T. (2011). Toward the estimation of the absolute quality of individual protein structure models. *Bioinformatics (Oxford, England), 27*(3), 343-350.

Berg, JM, Tymoczko, JL, Gatto, GJ, and Stryer, L. (2018). Stryer Biochemie (8 ed.). Berlin: Springer Spektrum

Bernofsky, C, and Swan, M. (1973). An improved cycling assay for nicotinamide adenine dinucleotide. *Analytical Biochemistry, 53*(2), 452-458.

Bjerregaard, R, Valderrama, D, Sims, N, Radulovich, R, James, D, Capron, M, Forster, J, Goudey, C, Yarish, C, Hopkins, K, Rust, M, and McKinnie, C. (2016). Seaweed Aquaculture for Food Security, Income Generation and Environmental Health in Tropical Developing Countries. Washington, D.C.: World Bank Group.

Blombach, B, Riester, T, Wieschalka, S, Ziert, C, Youn, J-W, Wendisch, VF, and Eikmanns, BJ. (2011). *Corynebacterium glutamicum* Tailored for Efficient Isobutanol Production. *Applied and Environmental Microbiology, 77*(10), 3300-3310.

Bolten, CJ. (2010). Bio-based Production of L-methionine in *Corynebacterium Glutamicum*. In C. Wittmann (Ed.), *Ibvt-Schriftenreihe* (Vol. 48). Göttingen: Cuvillier Verlag.

Bolten, CJ, Kiefer, P, Letisse, F, Portais, J-C, and Wittmann, C. (2007). Sampling for Metabolome Analysis of Microorganisms. *Analytical Chemistry, 79*(10), 3843-3849.

Bommareddy, RR, Chen, Z, Rappert, S, and Zeng, A-P. (2014). A *de novo* NADPH generation pathway for improving lysine production of *Corynebacterium glutamicum* by rational design of the coenzyme specificity of glyceraldehyde 3-phosphate dehydrogenase. *Metabolic Engineering, 25*, 30-37.

Born, TL, and Blanchard, JS. (1999). Structure/function Studies on Enzymes in the Diaminopimelate Pathway of Bacterial Cell Wall Biosynthesis. *Current Opinion in Chemical Biology, 3*(5), 607-613.

Bott, M, and Niebisch, A. (2003). The respiratory chain of *Corynebacterium glutamicum*. *Journal of Biotechnology, 104*(1), 129-153.

Bottoms, CA, Smith, PE, and Tanner, JJ. (2002). A structurally conserved water molecule in Rossmann dinucleotide-binding domains. *Protein Science, 11*(9), 2125-2137.

Brune, I, Brinkrolf, K, Kalinowski, J, Pühler, A, and Tauch, A. (2005). The individual and common repertoire of DNA-binding transcriptional regulators of *Corynebacterium glutamicum*, *Corynebacterium efficiens*, *Corynebacterium diphtheriae* and *Corynebacterium jeikeium* deduced from the complete genome sequences. *BMC Genomics, 6*(86), 1471-2164.

Buijs, NA, Siewers, V, and Nielsen, J. (2013). Advanced biofuel production by the yeast *Saccharomyces cerevisiae*. *Current Opinion in Chemical Biology, 17*(3), 480-488.

Buschke, N, Becker, J, Schäfer, R, Kiefer, P, Biedendieck, R, and Wittmann, C. (2013a). Systems metabolic engineering of xylose-utilizing *Corynebacterium glutamicum* for production of 1,5-diaminopentane. *Biotechnology Journal, 8*(5), 557-570.

Buschke, N, Schäfer, R, Becker, J, and Wittmann, C. (2013b). Metabolic engineering of industrial platform microorganisms for biorefinery applications–optimization of substrate spectrum and process robustness by rational and evolutive strategies. *Bioresource Technology, 135*, 544-554.

Buschke, N, Schröder, H, and Wittmann, C. (2011). Metabolic engineering of *Corynebacterium glutamicum* for production of 1,5-diaminopentane from hemicellulose. *Biotechnology Journal, 6*(3), 306-317.

Cahn, JKB, Werlang, CA, Baumschlager, A, Brinkmann-Chen, S, Mayo, SL, and Arnold, FH. (2017). A General Tool for Engineering the NAD/NADP Cofactor Preference of Oxidoreductases. *ACS Synthetic Biology, 6*(2), 326-333.

Chades, T, Scully, SM, Ingvadottir, EM, and Orlygsson, J. (2018). Fermentation of Mannitol Extracts From Brown Macro Algae by Thermophilic *Clostridia*. *Frontiers in Microbiology, 9*, 1931-1931.

Chassagnole, C, Noisommit-Rizzi, N, Schmid, JW, Mauch, K, and Reuss, M. (2002). Dynamic modeling of the central carbon metabolism of *Escherichia coli*. *Biotechnology and Bioengineering, 79*(1), 53-73.

Chemler, JA, Fowler, ZL, McHugh, KP, and Koffas, MAG. (2010). Improving NADPH availability for natural product biosynthesis in *Escherichia coli* by metabolic engineering. *Metabolic Engineering, 12*(2), 96-104.

Chen, N, Du, J, Liu, H, and Xu, Q. (2009). Elementary mode analysis and metabolic flux analysis of L-glutamate biosynthesis by *Corynebacterium glutamicum*. *Annals of Microbiology, 59*(2), 317.

Chen, Z, Huang, J, Wu, Y, Wu, W, Zhang, Y, and Liu, D. (2017). Metabolic engineering of *Corynebacterium glutamicum* for the production of 3-hydroxypropionic acid from glucose and xylose. *Metabolic Engineering, 39*, 151-158.

Chen, Z, Liu, G, Zhang, J, and Bao, J. (2019). A preliminary study on L-lysine fermentation from lignocellulose feedstock and techno-economic evaluation. *Bioresource Technology, 271*, 196-201.

Cheng, J, Chen, P, Song, A, Wang, D, and Wang, Q. (2018). Expanding lysine industry: industrial biomanufacturing of lysine and its derivatives. *Journal of Industrial Microbiology & Biotechnology, 45*(8), 719-734.

Cherniak, R, O'Neill, EB, and Sheng, S. (1998). Assimilation of Xylose, Mannose, and Mannitol for Synthesis of Glucuronoxylomannan of *Cryptococcus neoformans* Determined by ^{13}C Nuclear Magnetic Resonance Spectroscopy. *Infection and Immunity, 66*(6), 2996-2998.

Choi, JH, Lee, SJ, Lee, SJ, and Lee, SY. (2003). Enhanced production of insulin-like growth factor I fusion protein in *Escherichia coli* by coexpression of the down-regulated genes identified by transcriptome profiling. *Applied and Environmental Microbiology, 69*(8), 4737-4742.

Christensen, B, Thykær, J, and Nielsen, J. (2000). Metabolic characterization of high- and low-yielding strains of *Penicillium chrysogenum*. *Applied Microbiology and Biotechnology, 54*(2), 212-217.

Cirilli, M, Zheng, R, Scapin, G, and Blanchard, JS. (2003). The Three-Dimensional Structures of the *Mycobacterium tuberculosis* Dihydrodipicolinate Reductase−NADH−2,6-PDC and −NADPH−2,6-PDC Complexes. Structural and Mutagenic Analysis of Relaxed Nucleotide Specificity. *Biochemistry, 42*(36), 10644-10650.

Cleto, S, Jensen, JVK, Wendisch, VF, and Lu, TK. (2016). *Corynebacterium glutamicum* Metabolic Engineering with CRISPR Interference (CRISPRi). *ACS Synthetic Biology, 5*(5), 375-385.

Cremer, J, Eggeling, L, and Sahm, H. (1991). Control of the Lysine Biosynthesis Sequence in *Corynebacterium glutamicum* as Analyzed by Overexpression of the Individual Corresponding Genes. *Applied and Environmental Microbiology, 57*(6), 1746-1752.

Crow, VL, and Wittenberger, CL. (1979). Separation and properties of NAD^+- and $NADP^+$-dependent glyceraldehyde-3-phosphate dehydrogenases from *Streptococcus mutans*. *Journal of Biological Chemistry, 254*(4), 1134-1142.

Davis, T, Yamada, M, Elgort, M, and Saier Jr, MH. (1988). Nucleotide sequence of the mannitol (mtl) operon in *Escherichia coli*. *Molecular microbiology, 2*(3), 405-412.

de Hollander, JJ, Eswilder, R, and Noordover, JAC. (1998). Amino Acid Fermentation Process. *U.S. Patent No. 5,763,230.*

Dhar, KS, Wendisch, VF, and Nampoothiri, KM. (2016). Engineering of *Corynebacterium glutamicum* for xylitol production from lignocellulosic pentose sugars. *Journal of Biotechnology, 230*, 63-71.

Dominguez, H, and Lindley, ND. (1996). Complete Sucrose Metabolism Requires Fructose Phosphotransferase Activity in *Corynebacterium glutamicum* To Ensure Phosphorylation of Liberated Fructose. *Applied and Environmental Microbiology, 62*(10), 3878-3880.

Dominguez, H, Rollin, C, Guyonvarch, A, Guerquin-Kern, J-L, Cocaign-Bousquet, M, and Lindley, ND. (1998). Carbon-flux distribution in the central metabolic pathways of *Corynebacterium glutamicum* during growth on fructose. *European Journal of Biochemistry, 254*(1), 96-102.

Eggeling, L. (2013). Aminosäuren. In H. Sahm, G. Antranikian, K.-P. Stahmann, & R. Takors (Eds.), *Industrielle Mikrobiologie* (pp. 109-126). Berlin, Heidelberg: Springer Berlin Heidelberg.

Eggeling, L, and Bott, M. (2015). A giant market and a powerful metabolism: L-lysine provided by *Corynebacterium glutamicum*. *Applied Microbiology and Biotechnology, 99*(8), 3387-3394.

Eggeling, L, Oberle, S, and Sahm, H. (1998). Improved L-lysine yield with *Corynebacterium glutamicum*: use of *dapA* resulting in increased flux combined with growth limitation. *Applied Microbiology and Biotechnology, 49*(1), 24-30.

Eggeling, L, and Sahm, H. (1999). L-Glutamate and L-lysine: traditional products with impetuous developments. *Applied Microbiology and Biotechnology, 52*(2), 146-153.

Eikmanns, BJ. (2005). Central Metabolism: Tricarboxylic Acid Cycle and Anaplerotic Reactions. In L. Eggeling & M. Bott (Eds.), *Handbook of Corynebacterium glutamicum* (pp. 241-276): CRC Press: Boca Ration.

Eikmanns, BJ, Eggeling, L, and Sahm, H. (1993). Molecular aspects of lysine, threonine, and isoleucine biosynthesis in *Corynebacterium glutamicum*. *Antonie van Leeuwenhoek, 64*(2), 145-163.

Eikmanns, BJ, Follettie, MT, Griot, MU, and Sinskey, AJ. (1989). The phosphoenolpyruvate carboxylase gene of *Corynebacterium glutamicum*: molecular cloning, nucleotide sequence, and expression. *Molecular and General Genetics MGG, 218*(2), 330-339.

Eikmanns, BJ, Kleinertz, E, Liebl, W, and Sahm, H. (1991a). A family of *Corynebacterium glutamicum*/*Escherichia coli* shuttle vectors for cloning, controlled gene expression, and promoter probing. *Gene, 102*(1), 93-98.

Eikmanns, BJ, Metzger, M, Reinscheid, D, Kircher, M, and Sahm, H. (1991b). Amplification of three threonine biosynthesis genes in *Corynebacterium glutamicum* and its influence on carbon flux in different strains. *Applied Microbiology and Biotechnology, 34*(5), 617-622.

Eikmanns, BJ, Rittmann, D, and Sahm, H. (1995). Cloning, sequence analysis, expression, and inactivation of the *Corynebacterium glutamicum icd* gene encoding isocitrate dehydrogenase and biochemical characterization of the enzyme. *Journal of Bacteriology, 177*(3), 774-782.

Evonik. (2019). Product Information Biolys®. April 2019. from https://animal-nutrition.evonik.com/product/feed-additives/en/products/bio-amino-acids/l-lysine/

FAO. (2019). FAO yearbook. Fishery and Aquaculture Statistics 2017. Rome. Available from www.fao.org/fishery/static/Yearbook/YB2017_USBcard/index.htm

Ferdouse, F, Lovestad Holdt, S, Smith, R, Murua, P, and Yang, Z. (2018). The global status of seaweed production, trade and utilization.: FAO Globefish Research Programme, 124. Rome. 120 pp.

Fertah, M, Belfkira, A, Dahmane, Em, Taourirte, M, and Brouillette, F. (2017). Extraction and characterization of sodium alginate from Moroccan *Laminaria digitata* brown seaweed. *Arabian Journal of Chemistry, 10*, S3707-S3714.

Figge, RM, Ramseier, TM, and Saier, M. (1994). The mannitol repressor (MtlR) of *Escherichia coli*. *Journal of Bacteriology, 176*(3), 840-847.

Förster, J, Famili, I, Fu, P, Palsson, BØ, and Nielsen, J. (2003). Genome-scale reconstruction of the *Saccharomyces cerevisiae* metabolic network. *Genome Research, 13*(2), 244-253.

Fujii, T, Mukaihara, M, Agematu, H, and Tsunekawa, H. (2002). Biotransformation of L-Lysine to L-Pipecolic Acid Catalyzed by L-Lysine 6-Aminotransferase and Pyrroline-5-carboxylate Reductase. *Bioscience, Biotechnology, and Biochemistry, 66*(3), 622-627.

Gaida, SM, Liedtke, A, Jentges, AHW, Engels, B, and Jennewein, S. (2016). Metabolic engineering of *Clostridium cellulolyticum* for the production of *n*-butanol from crystalline cellulose. *Microbial Cell Factories, 15*(1), 6.

Georgi, T, Rittmann, D, and Wendisch, VF. (2005). Lysine and glutamate production by *Corynebacterium glutamicum* on glucose, fructose and sucrose: Roles of malic enzyme and fructose-1,6-bisphosphatase. *Metabolic Engineering, 7*(4), 291-301.

Gerstmeir, R, Cramer, A, Dangel, P, Schaffer, S, and Eikmanns, BJ. (2004). RamB, a novel transcriptional regulator of genes involved in acetate metabolism of *Corynebacterium glutamicum*. *Journal of Bacteriology, 186*(9), 2798-2809.

Gerstmeir, R, Wendisch, VF, Schnicke, S, Ruan, H, Farwick, M, Reinscheid, D, and Eikmanns, BJ. (2003). Acetate metabolism and its regulation in *Corynebacterium glutamicum*. *Journal of Biotechnology, 104*(1–3), 99-122.

Gibson, DG, Young, L, Chuang, R-Y, Venter, JC, Hutchison, CA, and Smith, HO. (2009). Enzymatic assembly of DNA molecules up to several hundred kilobases. *Nature Methods, 6*(5), 343-345.

Gießelmann, G, Dietrich, D, Jungmann, L, Kohlstedt, M, Jeon, EJ, Yim, SS, Sommer, F, Zimmer, D, Mühlhaus, T, Schroda, M, Jeong, KJ, Becker, J, and Wittmann, C. (2019). Metabolic Engineering of *Corynebacterium glutamicum* for High-Level Ectoine Production: Design, Combinatorial Assembly, and Implementation of a Transcriptionally Balanced Heterologous Ectoine Pathway. *Biotechnology Journal, 14*(9), 1800417.

Goh, CS, and Lee, KT. (2010). A visionary and conceptual macroalgae-based third-generation bioethanol (TGB) biorefinery in Sabah, Malaysia as an underlay for renewable and sustainable development. *Renewable and Sustainable Energy Reviews, 14*(2), 842-848.

Goodfellow, M, Collins, MD, and Minnikin, DE. (1976). Thin-layer Chromatographic Analysis of Mycolic Acid and Other Long-chain Components in Whole-organism Methanolysates of Coryneform and Related Taxa. *Microbiology, 96*(2), 351-358.

Gopinath, V, Meiswinkel, TM, Wendisch, VF, and Nampoothiri, KM. (2011). Amino acid production from rice straw and wheat bran hydrolysates by recombinant pentose-utilizing *Corynebacterium glutamicum*. *Applied Microbiology and Biotechnology, 92*(5), 985-996.

Gorke, B, and Stulke, J. (2008). Carbon catabolite repression in bacteria: many ways to make the most out of nutrients. *Nature Reviews Microbiology, 6*(8), 613-624.

Gourdon, P, Baucher, MF, Lindley, ND, and Guyonvarch, A. (2000). Cloning of the malic enzyme gene from *Corynebacterium glutamicum* and role of the enzyme in lactate metabolism. *Applied and Environmental Microbiology, 66*(7), 2981-2987.

Groisillier, A, Labourel, A, Michel, G, and Tonon, T. (2015). The Mannitol Utilization System of the Marine Bacterium *Zobellia galactanivorans*. *Applied and Environmental Microbiology, 81*(5), 1799.

Guex, N, Diemand, A. and Peitsch, M.C. (1999). SWISS-MODEL and the Swiss-Pdb Viewer: an environment for comparative protein modeling. *Biochemical Society Transactions, 18*, 2714-2723.

Hagino, H, and Nakayama, K. (1974). L-Phenylalanine Production by Analog-resistant Mutants of *Corynebacterium glutamicum*. *Agricultural and Biological Chemistry, 38*(1), 157-161.

Han, JES. (1929). Monosodium Glutamate as a Chemical Condiment. *Industrial & Engineering Chemistry, 21*(10), 984-987.

Hartmann, M, Tauch, A, Eggeling, L, Bathe, B, Möckel, B, Pühler, A, and Kalinowski, J. (2003). Identification and characterization of the last two unknown genes, *dapC* and *dapF*, in the succinylase branch of the L-lysine biosynthesis of *Corynebacterium glutamicum*. *Journal of Biotechnology, 104*(1-3), 199-211.

Hasunuma, T, Sanda, T, Yamada, R, Yoshimura, K, Ishii, J, and Kondo, A. (2011). Metabolic pathway engineering based on metabolomics confers acetic and formic acid tolerance to a recombinant xylose-fermenting strain of *Saccharomyces cerevisiae*. *Microbial Cell Factories, 10*(1), 2.

Haug, A, Larsen, B, and Smidsrød, O. (1974). Uronic acid sequence in alginate from different sources. *Carbohydrate Research, 32*(2), 217-225.

Hayashi, M, Mizoguchi, H, Shiraishi, N, Obayashi, M, Nakagawa, S, Imai, J-i, Watanabe, S, Ota, T, and Ikeda, M. (2002). Transcriptome Analysis of Acetate Metabolism in *Corynebacterium glutamicum* Using a Newly Developed Metabolic Array. *Bioscience, Biotechnology, and Biochemistry, 66*(6), 1337-1344.

Hayashi, M, Ohnishi, J, Mitsuhashi, S, Yonetani, Y, Hashimoto, S, and Ikeda, M. (2006). Transcriptome analysis reveals global expression changes in an industrial L-lysine producer of *Corynebacterium glutamicum*. *Bioscience, Biotechnology, and Biochemistry, 70*(2), 546-550.

Heider, SA, Peters-Wendisch, P, and Wendisch, VF. (2012). Carotenoid biosynthesis and overproduction in *Corynebacterium glutamicum*. *BMC Microbiology, 12*(198), 1471-2180.

Helanto, M, Aarnikunnas, J, Palva, A, Leisola, M, and Nyyssölä, A. (2006). Characterization of genes involved in fructose utilization by *Lactobacillus fermentum*. *Archives of Microbiology, 186*(1), 51-59.

Henstra, SA, Duurkens, RH, and Robillard, GT. (2000). Multiple phosphorylation events regulate the activity of the mannitol transcriptional regulator MtlR of the *Bacillus stearothermophilus* phosphoenolpyruvate-dependent mannitol phosphotransferase system. *Journal of Biological Chemistry, 275*(10), 7037-7044.

Henstra, SA, Tuinhof, M, Duurkens, RH, and Robillard, GT. (1999). The *Bacillus stearothermophilus* Mannitol Regulator, MtlR, of the Phosphotransferase System: A DNA-binding protein, regulated by HPr and $IICB^{mtl}$-dependent phosphorylation. *Journal of Biological Chemistry, 274*(8), 4754-4763.

Hermann, T. (2003). Industrial production of amino acids by coryneform bacteria. *Journal of Biotechnology, 104*(1), 155-172.

Hermann, T, Finkemeier, M, Pfefferle, W, Wersch, G, Krämer, R, and Burkovski, A. (2000). Two-dimensional electrophoretic analysis of *Corynebacterium glutamicum* membrane fraction and surface proteins. *Electrophoresis, 21*(3), 654-659.

Hermann, T, Pfefferle, W, Baumann, C, Busker, E, Schaffer, S, Bott, M, Sahm, H, Dusch, N, Kalinowski, J, Pühler, A, Bendt, AK, Krämer, R, and Burkovski, A. (2001). Proteome analysis of *Corynebacterium glutamicum*. *Electrophoresis, 22*(9), 1712-1723.

Hirao, T, Nakano, T, Azuma, T, Sugimoto, M, and Nakanishi, T. (1989). L-Lysine production in continuous culture of an L-lysine hyperproducing mutant of *Corynebacterium glutamicum*. *Applied Microbiology and Biotechnology, 32*(3), 269-273.

Hirasawa, T, and Shimizu, H. (2017). Glutamic Acid Fermentation: Discovery of Glutamic Acid-Producing Microorganisms, Analysis of the Production Mechanism, Metabolic Engineering, and Industrial Production Process. In C. Wittmann, Liao, J.C. (Ed.), *Industrial Biotechnology* (pp. 339-360): Wiley-VCH Verlag GmbH & Co.

Hoffmann, SL, Jungmann, L, Schiefelbein, S, Peyriga, L, Cahoreau, E, Portais, J-C, Becker, J, and Wittmann, C. (2018). Lysine production from the sugar alcohol mannitol: Design of the cell factory *Corynebacterium glutamicum* SEA-3 through integrated analysis and engineering of metabolic pathway fluxes. *Metabolic Engineering, 47*, 475-487.

Honeyman, AL, and Curtiss III, R. (2000). The mannitol-specific enzyme II (*mtlA*) gene and the *mtlR* gene of the PTS of *Streptococcus mutans*. *Microbiology, 146*(7), 1565-1572.

Honeyman, AL, and Curtiss, R. (1992). Isolation, characterization, and nucleotide sequence of the *Streptococcus mutans* mannitol-phosphate dehydrogenase gene and the mannitol-specific factor III gene of the phosphoenolpyruvate phosphotransferase system. *Infection and Immunity, 60*(8), 3369-3375.

Horn, SJ, Aasen, IM, and Østgaard, K. (2000a). Ethanol production from seaweed extract. *Journal of Industrial Microbiology and Biotechnology, 25*(5), 249-254.

Horn, SJ, Aasen, IM, and Østgaard, K. (2000b). Production of ethanol from mannitol by *Zymobacter palmae*. [journal article]. *Journal of Industrial Microbiology and Biotechnology, 24*(1), 51-57.

Hossain, ABMS, Saleh, AA, Aishah, S, Boyce, AN, Chowdhury, PP, and Naqiuddin, M. (2008). Bioethanol Production from Agricultural Waste Biomass as a Renewable Bioenergy Resource in Biomaterials, Berlin, Heidelberg.

Hou, X, From, N, Angelidaki, I, Huijgen, WJJ, and Bjerre, A-B. (2017). Butanol fermentation of the brown seaweed *Laminaria digitata* by *Clostridium beijerinckii* DSM-6422. *Bioresource Technology, 238*, 16-21.

Hou, X, Hansen, JH, and Bjerre, A-B. (2015). Integrated bioethanol and protein production from brown seaweed *Laminaria digitata*. *Bioresource Technology, 197*, 310-317.

Hughes, AD, Kelly, MS, Black, KD, and Stanley, MS. (2012). Biogas from Macroalgae: is it time to revisit the idea? *Biotechnology for Biofuels, 5*(1), 86.

Hüser, AT, Chassagnole, C, Lindley, ND, Merkamm, M, Guyonvarch, A, Elišáková, V, Pátek, M, Kalinowski, J, Brune, I, Pühler, A, and Tauch, A. (2005). Rational Design of a *Corynebacterium glutamicum* Pantothenate Production Strain and Its Characterization by Metabolic Flux Analysis and Genome-Wide Transcriptional Profiling. *Applied and Environmental Microbiology, 71*(6), 3255-3268.

HYPERCHEM, v. (1999) (Version Hypercube Inc.). Gainsville, Florida, USA.

Iddar, A, Valverde, F, Serrano, A, and Soukri, A. (2002). Expression, purification, and characterization of recombinant nonphosphorylating NADP-dependent glyceraldehyde-3-phosphate dehydrogenase from *Clostridium acetobutylicum*. *Biochemical Journal, 25*(3), 519-526.

Ikeda, K. (2002). New Seasonings. *Chemical Senses, 27*(9), 847-849.

Ikeda, M. (2003). Amino acid production processes. *Advances in Biochemical Engineering / Biotechnology, 79*, 1-35.

Ikeda, M. (2006). Towards bacterial strains overproducing L-tryptophan and other aromatics by metabolic engineering. *Applied Microbiology and Biotechnology, 69*(6), 615-626.

Ikeda, M. (2017). Lysine Fermentation: History and Genome Breeding. In A. Yokota & M. Ikeda (Eds.), *Amino Acid Fermentation* (pp. 73-102). Tokyo: Springer Japan.

Ikeda, M, and Katsumata, R. (1992). Metabolic Engineering To Produce Tyrosine or Phenylalanine in a Tryptophan-Producing *Corynebacterium glutamicum* Strain. *Applied and Environmental Microbiology, 58*(3), 781-785.

Ikeda, M, Mitsuhashi, S, Tanaka, K, and Hayashi, M. (2009). Reengineering of a *Corynebacterium glutamicum* L-arginine and L-citrulline producer. *Applied and Environmental Microbiology, 75*(6), 1635-1641.

Ikeda, M, and Nakagawa, S. (2003). The *Corynebacterium glutamicum* genome: features and impacts on biotechnological processes. *Applied Microbiology and Biotechnology, 62*(2-3), 99-109.

Ikeda, M, Nakanishi, K, Kino, K, and Katsumata, R. (1994). Fermentative production of tryptophan by a stable recombinant strain of *Corynebacterium glutamicum* with a modified serine-biosynthetic pathway. *Bioscience, Biotechnology, and Biochemistry, 58*(4), 674-678.

Ikeda, M, Noguchi, N, Ohshita, M, Senoo, A, Mitsuhashi, S, and Takeno, S. (2015). A third glucose uptake bypass in *Corynebacterium glutamicum* ATCC 31833. *Applied Microbiology and Biotechnology, 99*(6), 2741-2750.

Ikeda, M, Ohnishi, J, Hayashi, M, and Mitsuhashi, S. (2006). A genome-based approach to create a minimally mutated *Corynebacterium glutamicum* strain for efficient L-lysine production. *Journal of Industrial Microbiology and Biotechnology, 33*(7), 610-615.

Ikeda, M, Ozaki, A, and Katsumata, R. (1993). Phenylalanine production by metabolically engineered *Corynebacterium glutamicum* with the *pheA* gene of *Escherichia coli*. *Applied Microbiology and Biotechnology, 39*(3), 318-323.

Insights, GM. (2016). Lysine, Methionine Market Size For Animal Nutrition, Potential, Industry Outlook, Regional Analysis, Application Development, Competitive Landscape & Forecast, 2019 - 2025. Retrieved 11 March 2020. from https://www.gminsights.com/industry-analysis/lysine-methionine-market

Inui, M, Kawaguchi, H, Murakami, S, Vertès, AA, and Yukawa, H. (2004a). Metabolic Engineering of *Corynebacterium glutamicum* for Fuel Ethanol Production under Oxygen-Deprivation Conditions. *Journal of Molecular Microbiology and Biotechnology, 8*(4), 243-254.

Inui, M, Murakami, S, Okino, S, Kawaguchi, H, Vertès, AA, and Yukawa, H. (2004b). Metabolic analysis of *Corynebacterium glutamicum* during lactate and succinate productions under oxygen deprivation conditions. *Journal of Molecular Microbiology and Biotechnology, 7*(4), 182-196.

Ishino, S, Mizukami, T, Yamaguchi, K, Katsumata, R, and Araki, K. (1988). Cloning and Sequencing of the *meso*-Diaminopimelate-D-dehydrogenase (*ddh*) Gene of *Corynebacterium glutamicum*. *Agricultural and Biological Chemistry, 52*(11), 2903-2909.

Iwamoto, K, and Shiraiwa, Y. (2005). Salt-regulated mannitol metabolism in algae. *Marine Biotechnology, 7*(5), 407-415.

Jackson, JB. (2003). Proton translocation by transhydrogenase. *FEBS Letters, 545*(1), 18-24.

Jäger, W, Schäfer, A, Kalinowski, J, and Pühler, A. (1995). Isolation of insertion elements from gram-positive *Brevibacterium*, *Corynebacterium* and *Rhodococcus* strains using the *Bacillus subtilis sacB* gene as a positive selection marker. *FEMS Microbiology Letters, 126*(1), 1-6.

Jäger, W, Schäfer, A, Pühler, A, Labes, G, and Wohlleben, W. (1992). Expression of the *Bacillus subtilis sacB* gene leads to sucrose sensitivity in the gram-positive bacterium *Corynebacterium glutamicum* but not in *Streptomyces lividans*. *Journal of Bacteriology, 174*(16), 5462-5465.

Jang, SS, Shirai, Y, Uchida, M, and Wakisaka, M. (2012). Production of Mono Sugar from Acid Hydrolysis of Seaweed. *African Journal of Biotechnology, 11*.

Jetten, MS, Follettie, MT, and Sinskey, AJ. (1995). Effect of different levels of aspartokinase on the lysine production by *Corynebacterium lactofermentum*. *Applied Microbiology and Biotechnology, 43*(1), 76-82.

Jetten, MSM, and Sinskey, AJ. (1995). Recent Advances in the Physiology and Genetics of Amino Acid-Producing Bacteria. *Critical Reviews in Biotechnology, 15*(1), 73-103.

Jiang, L-Y, Zhang, Y-Y, Li, Z, and Liu, J-Z. (2013). Metabolic engineering of *Corynebacterium glutamicum* for increasing the production of L-ornithine by increasing NADPH availability. *Journal of Industrial Microbiology & Biotechnology, 40*(10), 1143-1151.

Jojima, T, Fujii, M, Mori, E, Inui, M, and Yukawa, H. (2010). Engineering of sugar metabolism of *Corynebacterium glutamicum* for production of amino acid L-alanine under oxygen deprivation. *Applied Microbiology and Biotechnology, 87*(1), 159-165.

Kabus, A, Georgi, T, Wendisch, VF, and Bott, M. (2007). Expression of the *Escherichia coli pntAB* genes encoding a membrane-bound transhydrogenase in *Corynebacterium glutamicum* improves L-lysine formation. *Applied Microbiology and Biotechnology, 75*(1), 47-53.

Kadam, SU, Tiwari, BK, and O'Donnell, CP. (2015). Extraction, structure and biofunctional activities of laminarin from brown algae. *International Journal of Food Science & Technology, 50*(1), 24-31.

Kalinowski, J, Bathe, B, Bartels, D, Bischoff, N, Bott, M, Burkovski, A, Dusch, N, Eggeling, L, Eikmanns, BJ, Gaigalat, L, Goesmann, A, Hartmann, M, Huthmacher, K, Krämer, R, Linke, B, McHardy, AC, Meyer, F, Möckel, B, Pfefferle, W, Pühler, A, Rey, DA, Rückert, C, Rupp, O, Sahm, H, Wendisch, VF, Wiegräbe, I, and Tauch, A. (2003). The complete *Corynebacterium glutamicum* ATCC 13032 genome sequence and its impact on the production of L-aspartate-derived amino acids and vitamins. *Journal of Biotechnology, 104*(1–3), 5-25.

Kalinowski, J, Cremer., J, Bachmann, B, Eggeling, L, Sahm, H, and Pühler, A. (1991). Genetic and biochemical analysis of the aspartokinase from *Corynebacterium glutamicum*. *Molecular Microbiology, 5*(5), 1197-1204.

Kase, H, and Nakayama, K. (1972). Production of L-Threonine by Analog-resistant Mutants. *Agricultural and Biological Chemistry, 36*(9), 1611-1621.

Katsumata, R, and Ikeda, M. (1993). Hyperproduction of Tryptophan in *Corynebacterium glutamicum* by Pathway Engineering. *Bio/Technology, 11*(8), 921-925.

Kawaguchi, H, Sasaki, M, Vertès, AA, Inui, M, and Yukawa, H. (2009). Identification and Functional Analysis of the Gene Cluster for L-Arabinose Utilization in *Corynebacterium glutamicum*. *Applied and Environmental Microbiology, 75*(11), 3419-3429.

Kawaguchi, H, Vertès, AA, Okino, S, Inui, M, and Yukawa, H. (2006). Engineering of a Xylose Metabolic Pathway in *Corynebacterium glutamicum*. *Applied and Environmental Microbiology, 72*(5), 3418-3428.

Kawai, S, and Murata, K. (2016). Biofuel Production Based on Carbohydrates from Both Brown and Red Macroalgae: Recent Developments in Key Biotechnologies. *International Journal of Molecular Science, 17*(2).

Kelle, R, Hermann, T, and Bathe, B. (2005). L-Lysine Production. In L. Eggeling & M. Bott (Eds.), *Handbook of Corynebacterium glutamicum* (pp. 465-488): CRC Press: Boca Raton.

Kiefer, P, Heinzle, E, and Wittmann, C. (2002). Influence of glucose, fructose and sucrose as carbon sources on kinetics and stoichiometry of lysine production by *Corynebacterium glutamicum*. *Journal of Industrial Microbiology and Biotechnology, 28*(6), 338-343.

Kiefer, P, Heinzle, E, Zelder, O, and Wittmann, C. (2004). Comparative metabolic flux analysis of lysine-producing *Corynebacterium glutamicum* cultured on glucose or fructose. *Applied and Environmental Microbiology, 70*(1), 229-239.

Kim, H, Heinzle, E, and Wittmann, C. (2006). Deregulation of aspartokinase by single nucleotide exchange leads to global flux rearrangement in the central metabolism of *Corynebacterium glutamicum*. *Journal of Microbiology and Biotechnology, 16*, 1174-1179.

Kim, HT, Baritugo, K-A, Oh, YH, Hyun, SM, Khang, TU, Kang, KH, Jung, SH, Song, BK, Park, K, Kim, I-K, Lee, MO, Kam, Y, Hwang, YT, Park, SJ, and Joo, JC. (2018). Metabolic Engineering of *Corynebacterium glutamicum* for the High-Level Production of Cadaverine That Can Be Used for the Synthesis of Biopolyamide 510. *ACS Sustainable Chemistry & Engineering, 6*(4), 5296-5305.

Kim, N-J, Li, H, Jung, K, Chang, HN, and Lee, PC. (2011). Ethanol production from marine algal hydrolysates using *Escherichia coli* KO11. *Bioresource Technology, 102*(16), 7466-7469.

Kimura, K. (1963). The effect of biotin on the amino acid biosynthesis by *Micrococcus glutamicus*. *The Journal of General and Applied Microbiology, 9*(2), 205-212.

Kind, S, Becker, J, and Wittmann, C. (2013). Increased lysine production by flux coupling of the tricarboxylic acid cycle and the lysine biosynthetic pathway-Metabolic engineering of the availability of succinyl-CoA in *Corynebacterium glutamicum*. *Metabolic Engineering, 15*, 184-195.

Kind, S, Jeong, WK, Schröder, H, and Wittmann, C. (2010a). Systems-wide metabolic pathway engineering in *Corynebacterium glutamicum* for bio-based production of diaminopentane. *Metabolic Engineering, 12*(4), 341-351.

Kind, S, Jeong, WK, Schröder, H, Zelder, O, and Wittmann, C. (2010b). Identification and elimination of the competing *N*-acetyldiaminopentane pathway for improved production of diaminopentane by *Corynebacterium glutamicum*. *Applied and Environmental Microbiology, 76*(15), 5175-5180.

Kind, S, Neubauer, S, Becker, J, Yamamoto, M, Völkert, M, von Abendroth, G, Zelder, O, and Wittmann, C. (2014). From zero to hero–Production of bio-based nylon from renewable resources using engineered *Corynebacterium glutamicum*. *Metabolic Engineering, 25*, 113-123.

Kinoshita, S. (2005). A short history of the birth of the amino acid industry in Japan. In L. Eggeling & M. Bott (Eds.), *Handbook of Corynebacterium glutamicum* (pp. 3-6): CRC Press: Boca Raton.

Kinoshita, S, Udaka, S, and Shimono, M. (1957). Studies on the amino acid fermentation. Part I: Production of L-glutamic acid by various microorganisms *The Journal of General and Applied Microbiology, 3*(3), 193-205.

Kircher, M, and Pfefferle, W. (2001). The fermentative production of L-lysine as an animal feed additive. *Chemosphere, 43*(1), 27-31.

Kirchner, O, and Tauch, A. (2003). Tools for genetic engineering in the amino acid-producing bacterium *Corynebacterium glutamicum*. *Journal of Biotechnology, 104*(1), 287-299.

Kjeldsen, KR, and Nielsen, J. (2009). In silico genome-scale reconstruction and validation of the *Corynebacterium glutamicum* metabolic network. *Biotechnology and Bioengineering, 102*(2), 583-597.

Kobayashi, M, Itoyama, T, Mitani, Y, and Usui, N. (2011). Method for producing basic amino acid. *EP Patent 1182261 B1*.

Koffas, M, and Stephanopoulos, G. (2005). Strain improvement by metabolic engineering: lysine production as a case study for systems biology. *Current Opinion in Biotechnology, 16*(3), 361-366.

Kohlstedt, M, Starck, S, Barton, N, Stolzenberger, J, Selzer, M, Mehlmann, K, Schneider, R, Pleissner, D, Rinkel, J, Dickschat, JS, Venus, J, J, BJHvD, and Wittmann, C. (2018). From lignin to nylon: Cascaded chemical and biochemical conversion using metabolically engineered *Pseudomonas putida*. *Metabolic Engineering, 47*, 279-293.

Kotrba, P, Inui, M, and Yukawa, H. (2003). A single V317A or V317M substitution in Enzyme II of a newly identified β-glucoside phosphotransferase and utilization system of *Corynebacterium glutamicum* R extends its specificity towards cellobiose. *Microbiology, 149*(6), 1569-1580.

Kraan, S. (2013). Mass-cultivation of carbohydrate rich macroalgae, a possible solution for sustainable biofuel production. *Mitigation and Adaptation Strategies for Global Change, 18*(1), 27-46.

Krömer, JO, Bolten, CJ, Heinzle, E, Schröder, H, and Wittmann, C. (2008). Physiological response of *Corynebacterium glutamicum* to oxidative stress induced by deletion of the transcriptional repressor McbR. *Microbiology, 154*(12), 3917-3930.

Krömer, JO, Fritz, M, Heinzle, E, and Wittmann, C. (2005). In vivo quantification of intracellular amino acids and intermediates of the methionine pathway in *Corynebacterium glutamicum*. *Analytical biochemistry, 340*(1), 171-173.

Krömer, JO, Heinzle, E, Schröder, H, and Wittmann, C. (2006a). Accumulation of Homolanthionine and Activation of a Novel Pathway for Isoleucine Biosynthesis in *Corynebacterium glutamicum* McbR Deletion Strains. *Journal of Bacteriology, 188*(2), 609-618.

Krömer, JO, Heinzle, E, and Wittmann, C. (2006b). Quantification of *S*-adenosyl methionine in microbial cell extracts. *Biotechnology Letters, 28*(2), 69-71.

Krömer, JO, Sorgenfrei, O, Klopprogge, K, Heinzle, E, and Wittmann, C. (2004). In-Depth Profiling of Lysine-Producing *Corynebacterium glutamicum* by Combined Analysis of the Transcriptome, Metabolome, and Fluxome. *Journal of Bacteriology, 186*(6), 1769-1784.

Kumar, S, Smith, KP, Floyd, JL, and Varela, MF. (2011). Cloning and molecular analysis of a mannitol operon of phosphoenolpyruvate-dependent phosphotransferase (PTS) type from *Vibrio cholerae* O395. *Archives of Microbiology, 193*(3), 201-208.

Lange, A, Becker, J, Schulze, D, Cahoreau, E, Portais, J-C, Haefner, S, Schröder, H, Krawczyk, J, Zelder, O, and Wittmann, C. (2017). Bio-based succinate from sucrose: High-resolution ^{13}C metabolic flux analysis and metabolic engineering of the rumen bacterium *Basfia succiniciproducens*. *Metabolic Engineering, 44*, 198-212.

Laslo, T, von Zaluskowski, P, Gabris, C, Lodd, E, Rückert, C, Dangel, P, Kalinowski, J, Auchter, M, Seibold, G, and Eikmanns, BJ. (2012). Arabitol Metabolism of *Corynebacterium glutamicum* and Its Regulation by AtlR. *Journal of Bacteriology, 194*(5), 941-955.

Latifi, AM, Sadegh Nejad, E, and Babavalian, H. (2015). Comparison of Extraction Different Methods of Sodium Alginate from Brown Alga *Sargassum* sp. Localized in the Southern of Iran. *Journal of Applied Biotechnology Reports, 2*(2), 251-255.

Lee, JH, Sung, BH, Kim, MS, Blattner, FR, Yoon, BH, Kim, JH, and Kim, SC. (2009). Metabolic engineering of a reduced-genome strain of *Escherichia coli* for L-threonine production. *Microbial Cell Factories, 8*(1), 2.

Lee, SY, and Park, J. (2010). Integration of Systems Biology with Bioprocess Engineering: L-Threonine Production by Systems Metabolic Engineering of *Escherichia Coli*. *Advances in Biochemical Engineering/Biotechnology, 120*, 1-19.

Li, L, Wada, M, and Yokota, A. (2007). Cytoplasmic proteome reference map for a glutamic acid-producing *Corynebacterium glutamicum* ATCC 14067. *PROTEOMICS, 7*(23), 4317-4322.

Liebl, W. (2005). *Corynebacterium* Taxonomy. In L. Eggeling & M. Bott (Eds.), *Handbook of Corynebacterium glutamicum* (pp. 9-34): CRC Press: Boca Raton.

Lindner, SN, Seibold, GM, Krämer, R, and Wendisch, VF. (2011). Impact of a new glucose utilization pathway in amino acid-producing *Corynebacterium glutamicum*. *Bioengineered Bugs, 2*(5), 291-295.

Liu, DY, Liu, CH, Lai, MT, Lin, HK, and Hseu, TH. (2007a). Global gene expression profiling of wild type and *lysC* knockout *Escherichia coli* W3110. *FEMS Microbiology Letters, 276*(2), 202-206.

Liu, Q, Ouyang, S-p, Kim, J, and Chen, G-Q. (2007b). The impact of PHB accumulation on L-glutamate production by recombinant *Corynebacterium glutamicum*. *Journal of Biotechnology, 132*(3), 273-279.

Lizée-Prynne, D, López, B, Tala, F, and Thiel, M. (2016). No sex-related dispersal limitation in a dioecious, oceanic long-distance traveller: the bull kelp *Durvillaea antarctica*. *Botanica Marina, 59*(1), 39-50.

Ma, C, Zhang, L, Dai, J, and Xiu, Z. (2010). Relaxing the coenzyme specificity of 1,3-propanediol oxidoreductase from *Klebsiella pneumoniae* by rational design. *Journal of Biotechnology, 146*(4), 173-178.

MacArtain, P, Gill, CIR, Brooks, M, Campbell, R, and Rowland, IR. (2007). Nutritional Value of Edible Seaweeds. *Nutrition Reviews, 65*(12), 535-543.

Magnus, J, Hollwedel, D, Oldiges, M, and Takors, R. (2006). Monitoring and Modeling of the Reaction Dynamics in the Valine/Leucine Synthesis Pathway in *Corynebacterium glutamicum*. *Biotechnology Progress, 22*, 1071-1083.

Manns, D, Nielsen, MM, Bruhn, A, Saake, B, and Meyer, AS. (2017). Compositional variations of brown seaweeds *Laminaria digitata* and *Saccharina latissima* in Danish waters. *Journal of Applied Phycology, 29*(3), 1493-1506.

Mansilla, A, Ávila, M, and Yokoya, NS. (2012). Current knowledge on biotechnological interesting seaweeds from the Magellan Region, Chile. *Revista Brasileira de Farmacognosia, 22*, 760-767.

Mansilla, AO, Avila, M, and Cáceres, J. (2017). Reproductive biology of *Durvillaea antarctica* (Chamisso) Hariot in the sub-Antartic ecoregion of Magallanes (51–56° S). *Journal of Applied Phycology, 29*(5), 2567-2574.

Marx, A, de Graaf, AA, Wiechert, W, Eggeling, L, and Sahm, H. (1996). Determination of the fluxes in the central metabolism of *Corynebacterium glutamicum* by nuclear magnetic resonance spectroscopy combined with metabolite balancing. *Biotechnology and Bioengineering, 49*(2), 111-129.

Marx, A, Eikmanns, BJ, Sahm, H, de Graaf, AA, and Eggeling, L. (1999). Response of the Central Metabolism in *Corynebacterium glutamicum* to the use of an NADH-Dependent Glutamate Dehydrogenase. *Metabolic engineering, 1*(1), 35-48.

Marx, A, Hans, S, Möckel, B, Bathe, B, and de Graaf, AA. (2003). Metabolic phenotype of phosphoglucose isomerase mutants of *Corynebacterium glutamicum*. *Journal of Biotechnology, 104*(1), 185-197.

Matsumoto, Ki, Tobitani, K, Aoki, S, Song, Y, Ooi, T, and Taguchi, S. (2014). Improved production of poly(lactic acid)-like polyester based on metabolite analysis to address the rate-limiting step. *AMB Express, 4*(1), 83.

Matsumura, H, and Miyachi, S. (1980). [43] Cycling assay for nicotinamide adenine dinucleotides. In A. San Pietro (Ed.), *Methods in Enzymology* (Vol. 69, pp. 465-470): Academic Press.

Mazat, JP, and Patte, JC. (1976). Lysine-sensitive aspartokinase of *Escherichia coli* K12. Synergy and autosynergy in an allosteric V system. *Biochemistry, 15*(18), 4053-4058.

Mazumdar, S, Bang, J, and Oh, MK. (2014). L-lactate production from seaweed hydrolysate of *Laminaria japonica* using metabolically engineered *Escherichia coli*. *Applied Biochemistry and Biotechnology, 172*(4), 1938-1952.

Mchardy, AC, Goesmann, A, Pühler, A, and Meyer, F. (2004). Development of joint application strategies for two microbial gene finders. *Bioinformatics (Oxford, England), 20*(10), 1622–1631.

McHardy, AC, Tauch, A, Rückert, C, Pühler, A, and Kalinowski, J. (2003). Genome-based analysis of biosynthetic aminotransferase genes of *Corynebacterium glutamicum*. *Journal of Biotechnology, 104*(1-3), 229-240.

McHugh, DJ. (2003). A guide to the seaweed industry. Rome: FAO Fisheries Technical Paper No. 441, Rome.

Melzer, G, Esfandabadi, ME, Franco-Lara, E, and Wittmann, C. (2009). Flux Design: In silico design of cell factories based on correlation of pathway fluxes to desired properties. *BMC Systems Biology, 3*(1), 120.

Mimitsuka, T, Sawai, H, Hatsu, M, and Yamada, K. (2007). Metabolic Engineering of *Corynebacterium glutamicum* for Cadaverine Fermentation. *Bioscience, Biotechnology, and Biochemistry, 71*, 2130-2135.

Mizukami, T, Hamu, A, Ikeda, M, Oka, T, and Katsumata, R. (1994). Cloning of the ATP Phosphoribosyl Transferase Gene of *Corynebacterium glutamicum* and Application of the Gene to L-Histidine Production. *Bioscience, Biotechnology, and Biochemistry, 58*(4), 635-638.

Molenaar, D, van der Rest, ME, Drysch, A, and Yücel, R. (2000). Functions of the Membrane-Associated and Cytoplasmic Malate Dehydrogenases in the Citric Acid Cycle of *Corynebacterium glutamicum*. *Journal of Bacteriology, 182*(24), 6884-6891.

Moon, M-W, Kim, H-J, Oh, T-K, Shin, C-S, Lee, J-S, Kim, S-J, and Lee, J-K. (2005). Analyses of enzyme II gene mutants for sugar transport and heterologous expression of fructokinase gene in *Corynebacterium glutamicum* ATCC 13032. *FEMS Microbiology Letters, 244*(2), 259-266.

Moon, M-W, Park, S-Y, Choi, S-K, and Lee, J-K. (2007). The phosphotransferase system of *Corynebacterium glutamicum*: features of sugar transport and carbon regulation. *Journal of Molecular Microbiology and Biotechnology, 12*(1-2), 43-50.

Mori, M, and Shiio, I. (1987). Pyruvate Formation and Sugar Metabolism in an Amino Acid-Producing Bacterium, *Brevibacterium flavum*. *Agricultural and Biological Chemistry, 51*(1), 129-138.

Moritz, B, Striegel, K, de Graaf, AA, and Sahm, H. (2000). Kinetic properties of the glucose-6-phosphate and 6 phosphogluconate dehydrogenases from *Corynebacterium glutamicum* and their application for predicting pentose phosphate pathway flux in vivo. *European Journal of Biochemistry, 267*(12), 3442-3452.

Naik, SN, Goud, VV, Rout, PK, and Dalai, AK. (2010). Production of first and second generation biofuels: A comprehensive review. *Renewable and Sustainable Energy Reviews, 14*(2), 578-597.

Nakayama, K, and Araki, K. (1973). Process for producing L-lysine. *US Patent 3708395*.

Nakayama, K, Araki, K, and Kase, H. (1978). Microbial Production of Essential Amino Acids with *Corynebacterium Glutamicum* Mutants. In M. Friedman (Ed.), *Nutritional Improvement of Food and Feed Proteins* (pp. 649-661). Boston, MA: Springer US.

Nentwich, SS, Brinkrolf, K, Gaigalat, L, Hüser, AT, Rey, DA, Mohrbach, T, Marin, K, Pühler, A, Tauch, A, and Kalinowski, J. (2009). Characterization of the LacI-type transcriptional repressor RbsR controlling ribose transport in *Corynebacterium glutamicum* ATCC 13032. *Microbiology, 155*(1), 150-164.

Netzer, R, Krause, M, Rittmann, D, Peters-Wendisch, PG, Eggeling, L, Wendisch, VF, and Sahm, H. (2004). Roles of pyruvate kinase and malic enzyme in *Corynebacterium glutamicum* for growth on carbon sources requiring gluconeogenesis. *Archives of Microbiology, 182*(5), 354-363.

Neushul, P. (1989). Seaweed for War: California's World War I Kelp Industry. *Technology and Culture, 30*(3), 561-583.

Nielsen, J, Larsson, C, van Maris, A, and Pronk, J. (2013). Metabolic engineering of yeast for production of fuels and chemicals. *Current Opinion in Biotechnology, 24*(3), 398-404.

Nolden, L, Ngouoto-Nkili, CE, Bendt, AK, Krämer, R, and Burkovski, A. (2001). Sensing nitrogen limitation in *Corynebacterium glutamicum*: the role of *glnK* and *glnD*. *Molecular Microbiology, 42*(5), 1281-1295.

Ohnishi, J, Katahira, R, Mitsuhashi, S, Kakita, S, and Ikeda, M. (2005). A novel *gnd* mutation leading to increased L-lysine production in *Corynebacterium glutamicum*. *FEMS Microbiology Letters, 242*(2), 265-274.

Ohnishi, J, Mitsuhashi, S, Hayashi, M, Ando, S, Yokoi, H, Ochiai, K, and Ikeda, M. (2002). A novel methodology employing *Corynebacterium glutamicum* genome information to generate a new L-lysine-producing mutant. *Applied Microbiology and Biotechnology, 58*(2), 217-223.

Okino, S, Suda, M, Fujikura, K, Inui, M, and Yukawa, H. (2008). Production of D-lactic acid by *Corynebacterium glutamicum* under oxygen deprivation. *Applied Microbiology and Biotechnology, 78*(3), 449-454.

Omumasaba, CA, Okai, N, Inui, M, and Yukawa, H. (2004). *Corynebacterium glutamicum* Glyceraldehyde-3-Phosphate Dehydrogenase Isoforms with Opposite, ATP-Dependent Regulation. *Journal of Molecular Microbiology and Biotechnology, 8*(2), 91-103.

Ozaki, A, Katsumata, R, Oka, T, and Furuya, A. (1984). Functional expression of the genes of *Escherichia coli* in gram-positive *Corynebacterium glutamicum*. *Molecular and General Genetics MGG, 196*(1), 175-178.

Parche, S, Burkovski, A, Sprenger, GA, Weil, B, Krämer, R, and Titgemeyer, F. (2001). *Corynebacterium glutamicum*: a dissection of the PTS. *Journal of Molecular Microbiology and Biotechnology, 3*(3), 423-428.

Parekh, S, Vinci, VA, and Strobel, RJ. (2000). Improvement of microbial strains and fermentation processes. *Applied Microbiology and Biotechnology, 54*(3), 287-301.

Park, S-D, Lee, J-Y, Sim, S-Y, Kim, Y, and Lee, H-S. (2007). Characteristics of methionine production by an engineered *Corynebacterium glutamicum* strain. *Metabolic engineering, 9*(4), 327-336.

Peng, X, Okai, N, Vertès, AA, Inatomi, K-i, Inui, M, and Yukawa, H. (2011). Characterization of the mannitol catabolic operon of *Corynebacterium glutamicum*. *Applied Microbiology and Biotechnology, 91*(5), 1375-1387.

Pérez-García, F, Max Risse, J, Friehs, K, and Wendisch, VF. (2017a). Fermentative production of L-pipecolic acid from glucose and alternative carbon sources. *Biotechnology Journal, 12*(7), 1600646.

Pérez-García, F, Peters-Wendisch, P, and Wendisch, VF. (2016). Engineering *Corynebacterium glutamicum* for fast production of L-lysine and L-pipecolic acid. *Applied Microbiology and Biotechnology, 100*(18), 8075-8090.

Pérez-García, F, Ziert, C, Risse, JM, and Wendisch, VF. (2017b). Improved fermentative production of the compatible solute ectoine by *Corynebacterium glutamicum* from glucose and alternative carbon sources. *Journal of Biotechnology, 258*, 59-68.

Peters-Wendisch, P, Stolz, M, Etterich, H, Kennerknecht, N, Sahm, H, and Eggeling, L. (2005). Metabolic engineering of *Corynebacterium glutamicum* for L-serine production. *Applied and Environmental Microbiology, 71*(11), 7139-7144.

Peters-Wendisch, PG, Schiel, B, Wendisch, VF, Katsoulidis, E, Mockel, B, Sahm, H, and Eikmanns, BJ. (2001). Pyruvate carboxylase is a major bottleneck for glutamate and lysine production by *Corynebacterium glutamicum*. *Journal of Molecular Microbiology and Biotechnology, 3*(2), 295-300.

Petersen, S, de Graaf, AA, Eggeling, L, Möllney, M, Wiechert, W, and Sahm, H. (2000). *In Vivo* Quantification of Parallel and Bidirectional Fluxes in the Anaplerosis of *Corynebacterium glutamicum*. *Journal of Biological Chemistry, 275*(46), 35932-35941.

Pisabarro, A, Malumbres, M, Mateos, LM, Oguiza, JA, and Martín, JF. (1993). A cluster of three genes (*dapA*, *orf2*, and *dapB*) of *Brevibacterium lactofermentum* encodes dihydrodipicolinate synthase, dihydrodipicolinate reductase, and a third polypeptide of unknown function. *Journal of Bacteriology, 175*(9), 2743-2749.

Poblete-Castro, I, Hoffmann, S, Becker, J, and Wittmann, C. (2020). Cascaded valorization of seaweed using microbial cell factories. *Current Opinion in Biotechnology, 65*, 102-113.

Pompejus, M, Kröger, B, Schröder, H, Zelder, O, and Haberhauer, G. (2004). *Corynebacterium glutamicum* genes encoding proteins involved in membrane synthesis and membrane transport*., US Patent 6696561*.

Postma, PW, Lengeler, JW, and Jacobson, GR. (1993). Phosphoenolpyruvate:carbohydrate phosphotransferase systems of bacteria. *Microbiological Reviews, 57*(3), 543-594.

Prasad Maharjan, R, and Ferenci, T. (2003). Global metabolite analysis: the influence of extraction methodology on metabolome profiles of *Escherichia coli*. *Analytical Biochemistry, 313*(1), 145-154.

Qian, Z-G, Xia, X-X, and Lee, SY. (2011). Metabolic engineering of *Escherichia coli* for the production of cadaverine: A five carbon diamine. *Biotechnology and Bioengineering, 108*(1), 93-103.

Raamsdonk, LM, Teusink, B, Broadhurst, D, Zhang, N, Hayes, A, Walsh, MC, Berden, JA, Brindle, KM, Kell, DB, Rowland, JJ, Westerhoff, HV, van Dam, K, and Oliver, SG. (2001). A functional genomics strategy that uses metabolome data to reveal the phenotype of silent mutations. *Nature Biotechnology, 19*(1), 45-50.

Radmacher, E, Vaitsikova, A, Burger, U, Krumbach, K, Sahm, H, and Eggeling, L. (2002). Linking central metabolism with increased pathway flux: L-valine accumulation by *Corynebacterium glutamicum*. *Applied and Environmental Microbiology, 68*(5), 2246-2250.

Reddy, SG, Scapin, G, and Blanchard, JS. (1996). Interaction of pyridine nucleotide substrates with *Escherichia coli* dihydrodipicolinate reductase: thermodynamic and structural analysis of binary complexes. *Biochemistry, 35*(41), 13294-13302.

Reed, JL, Vo, TD, Schilling, CH, and Palsson, BO. (2003). An expanded genome-scale model of *Escherichia coli* K-12 (*i*JR904 GSM/GPR). *Genome Biology, 4*(9), R54.

Riedel, C, Rittmann, D, Dangel, P, Möckel, B, Petersen, S, Sahm, H, and Eikmanns, BJ. (2001). Characterization of the phosphoenolpyruvate carboxykinase gene from *Corynebacterium glutamicum* and significance of the enzyme for growth and amino acid production. *Journal of Molecular Microbiology and Biotechnology, 3*(4), 573-583.

Ritthausen, H. (1866). Ueber die Glutaminsäure. *Journal für Praktische Chemie, 99*(1), 454-462.

Rohles, CM, Gießelmann, G, Kohlstedt, M, Wittmann, C, and Becker, J. (2016). Systems metabolic engineering of *Corynebacterium glutamicum* for the production of the carbon-5 platform chemicals 5-aminovalerate and glutarate. *Microbial Cell Factories, 15*(1), 154.

Ryu, S, and Karim, MN. (2011). A whole cell biocatalyst for cellulosic ethanol production from dilute acid-pretreated corn stover hydrolyzates. *Applied Microbiology and Biotechnology, 91*(3), 529-542.

Sahm, H, Eggeling, L, and de Graaf, AA. (2000). Pathway analysis and metabolic engineering in *Corynebacterium glutamicum*. *Biological Chemistry, 381*(9-10), 899-910.

Sahm, H, Eggeling, L, Eikmanns, B, and Krämer, R. (1995). Metabolic design in amino acid producing bacterium *Corynebacterium glutamicum*. *FEMS Microbiology Reviews, 16*(2-3), 243-252.

Sand, j. (2005). A Short History of MSG: Good Science, Bad Science, and Taste Cultures. *Gastronomica, 5*(4), 38-49.

Sasaki, M, Jojima, T, Inui, M, and Yukawa, H. (2008). Simultaneous utilization of D-cellobiose, D-glucose, and D-xylose by recombinant *Corynebacterium glutamicum* under oxygen-deprived conditions. *Applied Microbiology and Biotechnology, 81*(4), 691-699.

Sasaki, M, Jojima, T, Kawaguchi, H, Inui, M, and Yukawa, H. (2009). Engineering of pentose transport in *Corynebacterium glutamicum* to improve simultaneous utilization of mixed sugars. *Applied Microbiology and Biotechnology, 85*(1), 105-115.

Sauer, U, Canonaco, F, Heri, S, Perrenoud, A, and Fischer, E. (2004). The Soluble and Membrane-bound Transhydrogenases UdhA and PntAB Have Divergent Functions in NADPH Metabolism of *Escherichia coli*. *Journal of Biological Chemistry, 279*(8), 6613-6619.

Sauer, U, and Eikmanns, BJ. (2005). The PEP–pyruvate–oxaloacetate node as the switch point for carbon flux distribution in bacteria. *FEMS Microbiology Reviews, 29*(4), 765-794.

Sawada, K, Zen-in, S, Wada, M, and Yokota, A. (2010). Metabolic changes in a pyruvate kinase gene deletion mutant of *Corynebacterium glutamicum* ATCC 13032. *Metabolic Engineering, 12*(4), 401-407.

Scapin, G, Reddy, SG, and Blanchard, JS. (1996). Three-Dimensional Structure of *meso*-Diaminopimelic Acid Dehydrogenase from *Corynebacterium glutamicum*. *Biochemistry, 35*(42), 13540-13551.

Schaffer, S, and Burkovski, A. (2005). Proteomics. In L. Eggeling & M. Bott (Eds.), *Handbook of Corynebacterium glutamicum* (pp. 99-118): CRC Press: Boca Raton.

Schaffer, S, Weil, B, Nguyen, V, Dongmann, G, Günther, K, Nickolaus, M, Hermann, T, and Bott, M. (2001). A high-resolution reference map for cytoplasmic and membrane-associated proteins of *Corynebacterium glutamicum*. *Electrophoresis, 22*, 4404-4422.

Schiefelbein, S. (2014). Improved L-Lysine Production in *Corynebacterium glutamicum* by Rational Strain Engineering. Saarland University.

Schiener, P, Black, KD, Stanley, MS, and Green, DH. (2015). The seasonal variation in the chemical composition of the kelp species *Laminaria digitata*, *Laminaria hyperborea*, *Saccharina latissima* and *Alaria esculenta*. *Journal of Applied Phycology, 27*(1), 363-373.

Schmid, R, Uhlemann, E-M, Nolden, L, Wersch, G, Hecker, R, Hermann, T, Marx, A, and Burkovski, A. (2000). Response to nitrogen starvation in *Corynebacterium glutamicum*. *FEMS Microbiology Letters, 187*(1), 83-88.

Schneider, J, Niermann, K, and Wendisch, VF. (2011). Production of the amino acids L-glutamate, L-lysine, L-ornithine and L-arginine from arabinose by recombinant *Corynebacterium glutamicum*. *Journal of Biotechnology, 154*(2–3), 191-198.

Schneider, K, Schütz, V, John, GT, and Heinzle, E. (2010). Optical device for parallel online measurement of dissolved oxygen and pH in shake flask cultures. *Bioprocess and Biosystems Engineering, 33*(5), 541-547.

Schrumpf, B, Schwarzer, A, Kalinowski, J, Pühler, A, Eggeling, L, and Sahm, H. (1991). A functionally split pathway for lysine synthesis in *Corynebacterium glutamicium*. *Journal of Bacteriology, 173*(14), 4510-4516.

Schwechheimer, SK, Becker, J, Peyriga, L, Portais, J-C, and Wittmann, C. (2018). Metabolic flux analysis in *Ashbya gossypii* using ^{13}C-labeled yeast extract: industrial riboflavin production under complex nutrient conditions. *Microbial Cell Factories, 17*(1), 162.

Scrutton, NS, Berry, A, and Perham, RN. (1990). Redesign of the coenzyme specificity of a dehydrogenase by protein engineering. *Nature, 343*(6253), 38-43.

Seibold, G, Auchter, M, Berens, S, Kalinowski, J, and Eikmanns, BJ. (2006). Utilization of soluble starch by a recombinant *Corynebacterium glutamicum* strain: Growth and lysine production. *Journal of Biotechnology, 124*(2), 381-391.

Shen, Y, Chen, X, Peng, B, Chen, L, Hou, J, and Bao, X. (2012). An efficient xylose-fermenting recombinant *Saccharomyces cerevisiae* strain obtained through adaptive evolution and its global transcription profile. *Applied Microbiology and Biotechnology, 96*(4), 1079-1091.

Shiio, I, Ôtsuka, S-I, and Takahashi, M. (1962). Effect of Biotin on the Bacterial Formation of Glutamic Acid: I. Glutamate Formation and Cellular Permeability of Amino Acids*. *The Journal of Biochemistry, 51*(1), 56-62.

Shiio, I, Ôtsuka, S-I, and Tsunoda, T. (1959). Glutamic acid formation from glucose by bacteria. I. Enzymes of the Embden-Meyerhof-Parnas pathway, the Krebs cycle, and the glyoxylate bypass in cell extracts of *Brevibacterium flavum* No. 2247. *The Journal of Biochemistry, 46*(10), 1303-1311.

Shiio, I, Sasaki, A, Nakamori, S, and Sano, K. (1973). Production of L-Isoleucine by AHV Resistant Mutants of *Brevibacterium flavum*. *Agricultural and Biological Chemistry, 37*(9), 2053-2061.

Shiio, I, Toride, Y, and Sugimoto, S-I. (1984). Production of Lysine by Pyruvate Dehydrogenase Mutants of *Brevibacterium flavum*. *Agricultural and Biological Chemistry, 48*(12), 3091-3098.

Shiratsuchi, M, Kuronuma, H, Kawahara, Y, Yoshihara, Y, Miwa, H, and Nakamori, S. (1995). Simultaneous and High Fermentative Production of L-Lysine and L-Glutamic Acid Using a Strain of *Brevibacterium lactofermentum*. *Bioscience, Biotechnology, and Biochemistry, 59*(1), 83-86.

Silberbach, M, Schäfer, M, Hüser, AT, Kalinowski, J, Pühler, A, Krämer, R, and Burkovski, A. (2005). Adaptation of *Corynebacterium glutamicum* to Ammonium Limitation: a Global Analysis Using Transcriptome and Proteome Techniques. *Applied and Environmental Microbiology, 71*(5), 2391-2402.

Sindelar, G, and Wendisch, VF. (2007). Improving lysine production by *Corynebacterium glutamicum* through DNA microarray-based identification of novel target genes. *Applied Microbiology and Biotechnology, 76*(3), 677-689.

Smith, KM, Cho, K-M, and Liao, JC. (2010). Engineering *Corynebacterium glutamicum* for isobutanol production. *Applied Microbiology and Biotechnology, 87*(3), 1045-1055.

Soma, Y, Inokuma, K, Tanaka, T, Ogino, C, Kondo, A, Okamoto, M, and Hanai, T. (2012). Direct isopropanol production from cellobiose by engineered *Escherichia coli* using a synthetic pathway and a cell surface display system. *Journal of Bioscience and Bioengineering, 114*(1), 80-85.

Sonntag, K, Eggeling, L, De Graaf, AA, and Sahm, H. (1993). Flux partitioning in the split pathway of lysine synthesis in *Corynebacterium glutamicum*. *European Journal of Biochemistry, 213*(3), 1325-1331.

Sonoki, T, Takahashi, K, Sugita, H, Hatamura, M, Azuma, Y, Sato, T, Suzuki, S, Kamimura, N, and Masai, E. (2018). Glucose-Free *cis*,*cis*-Muconic Acid Production via New Metabolic Designs Corresponding to the Heterogeneity of Lignin. *ACS Sustainable Chemistry & Engineering, 6*(1), 1256-1264.

Spaans, SK, Weusthuis, RA, van der Oost, J, and Kengen, SWM. (2015). NADPH-generating systems in bacteria and archaea. *Frontiers in Microbiology, 6*, 742-742.

Stackebrandt, E, Rainey, FA, and Ward-Riney, NL. (1997). Proposal for a New Hierarchic Classification System, *Actinobacteria* classis nov. *International Journal of Systematic and Evolutionary Microbiology, 47*(2), 479-491.

Stansen, C, Uy, D, Delaunay, S, Eggeling, L, Goergen, J-L, and Wendisch, VF. (2005). Characterization of a *Corynebacterium glutamicum* Lactate Utilization Operon Induced during Temperature-Triggered Glutamate Production. *Applied and Environmental Microbiology, 71*(10), 5920-5928.

Takeno, S, Hori, K, Ohtani, S, Mimura, A, Mitsuhashi, S, and Ikeda, M. (2016). L-Lysine production independent of the oxidative pentose phosphate pathway by *Corynebacterium glutamicum* with the *Streptococcus mutans gapN* gene. *Metabolic Engineering, 37*, 1-10.

Takeno, S, Murata, R, Kobayashi, R, Mitsuhashi, S, and Ikeda, M. (2010). Engineering of *Corynebacterium glutamicum* with an NADPH-Generating Glycolytic Pathway for L-Lysine Production. *Applied and Environmental Microbiology, 76*(21), 7154-7160.

Tan, KT, Lee, KT, and Mohamed, AR. (2008). Role of energy policy in renewable energy accomplishment: The case of second-generation bioethanol. *Energy Policy, 36*(9), 3360-3365.

Tateno, T, Fukuda, H, and Kondo, A. (2007a). Direct production of L-lysine from raw corn starch by *Corynebacterium glutamicum* secreting *Streptococcus bovis* α-amylase using *cspB* promoter and signal sequence. *Applied Microbiology and Biotechnology, 77*(3), 533-541.

Tateno, T, Fukuda, H, and Kondo, A. (2007b). Production of L-Lysine from starch by *Corynebacterium glutamicum* displaying α-amylase on its cell surface. *Applied Microbiology and Biotechnology, 74*(6), 1213-1220.

Tauch, A. (2005). Native Plasmids of Amino Acid–Producing Corynebacteria. In L. Eggeling & M. Bott (Eds.), *Handbook of Corynebacterium glutamicum* (pp. 57-80): CRC Press: Boca Raton.

Tedesco, S, and Stokes, J. (2017). Valorisation to biogas of macroalgal waste streams: a circular approach to bioproducts and bioenergy in Ireland. *Chemical Papers, 71*(4), 721-728.

Theobald, U, Mailinger, W, Baltes, M, Rizzi, M, and Reuss, M. (1997). In vivo analysis of metabolic dynamics in *Saccharomyces cerevisiae*: I. Experimental observations. *Biotechnology and Bioengineering, 55*.

Thierbach, G, Kalinowski, J, Bachmann, B, and Pühler, A. (1990). Cloning of a DNA fragment from *Corynebacterium glutamicum* conferring aminoethyl cysteine resistance and feedback resistance to aspartokinase. *Applied Microbiology and Biotechnology, 32*(4), 443-448.

Tonouchi, N, and Ito, H. (2017). Present Global Situation of Amino Acids in Industry. In A. Yokota & M. Ikeda (Eds.), *Amino Acid Fermentation* (pp. 3-14). Tokyo: Springer Japan.

Torres, MD, Kraan, S, and Domínguez, H. (2019). Seaweed biorefinery. *Reviews in Environmental Science and Bio/Technology, 18*(2), 335-388.

Toyoda, K, and Inui, M. (2016). Regulons of global transcription factors in Corynebacterium glutamicum. *Applied Microbiology and Biotechnology, 100*(1), 45-60.

Tsuge, Y, Kato, N, Yamamoto, S, Suda, M, and Inui, M. (2019). Enhanced production of D-lactate from mixed sugars in *Corynebacterium glutamicum* by overexpression of glycolytic genes encoding phosphofructokinase and triosephosphate isomerase. *Journal of Bioscience and Bioengineering, 127*(3), 288-293.

Tweeddale, H, Notley-McRobb, L, and Ferenci, T. (1998). Effect of Slow Growth on Metabolism of *Escherichia coli*, as Revealed by Global Metabolite Pool ("Metabolome") Analysis. *Journal of bacteriology, 180*(19), 5109-5116.

Udaka, S. (1960). Screening method for microorganisms accumulating metabolites and its use in the isolation of *Micrococcus glutamicus*. *Journal of Bacteriology, 79*(5), 754-755.

Uribe, E, Vega-Gálvez, A, Vargas, N, Pasten, A, Rodríguez, K, and Ah-Hen, KS. (2018). Phytochemical components and amino acid profile of brown seaweed *Durvillaea antarctica* as affected by air drying temperature. *Journal of Food Science and Technology, 55*(12), 4792-4801.

van der Wal, H, Sperber, BLHM, Houweling-Tan, B, Bakker, RRC, Brandenburg, W, and López-Contreras, AM. (2013). Production of acetone, butanol, and ethanol from biomass of the green seaweed *Ulva lactuca*. *Bioresource Technology, 128*, 431-437.

van Hal, JW, Huijgen, WJJ, and López-Contreras, AM. (2014). Opportunities and challenges for seaweed in the biobased economy. *Trends in Biotechnology, 32*(5), 231-233.

van Winden, WA, Wittmann, C, Heinzle, E, and Heijnen, JJ. (2002). Correcting mass isotopomer distributions for naturally occurring isotopes. *Biotechnology and Bioengineering, 80*(4), 477-479.

Vardon, DR, Franden, MA, Johnson, CW, Karp, EM, Guarnieri, MT, Linger, JG, Salm, MJ, Strathmann, TJ, and Beckham, GT. (2015). Adipic acid production from lignin. *Energy & Environmental Science, 8*(2), 617-628.

Velasco, AM, Leguina, JI, and Lazcano, A. (2002). Molecular Evolution of the Lysine Biosynthetic Pathways. *Journal of Molecular Evolution, 55*(4), 445-449.

Vergara-Fernández, A, Vargas, G, Alarcón, N, and Velasco, A. (2008). Evaluation of marine algae as a source of biogas in a two-stage anaerobic reactor system. *Biomass and Bioenergy, 32*(4), 338-344.

Vickery, HB, and Schmidt, CLA. (1931). The History of the Discovery of the Amino Acids. *Chemical Reviews, 9*(2), 169-318.

Voet, D, Voet, JG, and Pratt, CW. (1999). Fundamentals of Biochemistry. New York: Wiley & Sons.

von der Osten, CH, Barbas III, CF, Wong, C-H, and Sinskey, AJ. (1989). Molecular cloning, nucleotide sequence and fine-structural analysis of the *Corynebacterium glutamicum fda* gene: structural comparison of *C. glutamicum* fructose-1,6-biphosphate aldolase to class I and class II aldolases. *Molecular microbiology, 3*(11), 1625-1637.

Vrljic, M, Sahm, H, and Eggeling, L. (1996). A new type of transporter with a new type of cellular function: L-lysine export from *Corynebacterium glutamicum*. *Molecular Microbiology, 22*(5), 815-826.

Wang, D, Kim, DH, and Kim, KH. (2016a). Effective production of fermentable sugars from brown macroalgae biomass. *Applied Microbiology and Biotechnology, 100*(22), 9439-9450.

Wang, J, Zhu, J, Bennett, GN, and San, KY. (2011). Succinate production from sucrose by metabolic engineered *Escherichia coli* strains under aerobic conditions. *Biotechnology Progress, 27*(5), 1242-1247.

Wang, Z, Chan, SHJ, Sudarsan, S, Blank, LM, Jensen, PR, and Solem, C. (2016b). Elucidation of the regulatory role of the fructose operon reveals a novel target for enhancing the NADPH supply in *Corynebacterium glutamicum*. *Metabolic Engineering, 38*, 344-357.

Wargacki, AJ, Leonard, E, Win, MN, Regitsky, DD, Santos, CNS, Kim, PB, Cooper, SR, Raisner, RM, Herman, A, Sivitz, AB, Lakshmanaswamy, A, Kashiyama, Y, Baker, D, and Yoshikuni, Y. (2012). An Engineered Microbial Platform for Direct Biofuel Production from Brown Macroalgae. *Science, 335*(6066), 308-313.

Watanabe, S, Hamano, M, Kakeshita, H, Bunai, K, Tojo, S, Yamaguchi, H, Fujita, Y, Wong, S-L, and Yamane, K. (2003). Mannitol-1-Phosphate Dehydrogenase (MtlD) Is Required for Mannitol and Glucitol Assimilation in *Bacillus subtilis*: Possible Cooperation of *mtl* and *gut* Operons. *Journal of Bacteriology, 185*(16), 4816-4824.

Waterhouse, A, Bertoni, M, Bienert, S, Studer, G, Tauriello, G, Gumienny, R, Heer, FT, de Beer, TAP, Rempfer, C, Bordoli, L, Lepore, R, and Schwede, T. (2018). SWISS-MODEL: homology modelling of protein structures and complexes. *Nucleic acids research, 46*(W1), W296-W303.

Wehrmann, A, Phillipp, B, Sahm, H, and Eggeling, L. (1998). Different modes of diaminopimelate synthesis and their role in cell wall integrity: a study with *Corynebacterium glutamicum*. *Journal of Bacteriology, 180*(12), 3159-3165.

Wei, N, Quarterman, J, and Jin, Y-S. (2013). Marine macroalgae: an untapped resource for producing fuels and chemicals. *Trends in Biotechnology, 31*(2), 70-77.

Weinberger, S, and Gilvarg, C. (1970). Bacterial distribution of the use of succinyl and acetyl blocking groups in diaminopimelic acid biosynthesis. *Journal of Bacteriology, 101*(1), 323-324.

Wendisch, VF. (2003). Genome-wide expression analysis in *Corynebacterium glutamicum* using DNA microarrays. *Journal of biotechnology, 104*(1), 273-285.

Wendisch, VF. (2017). L-Lysine. In C. Wittmann, Liao, J.C. (Ed.), *Industrial Biotechnology* (pp. 361-390). Weinheim, Germany: Wiley-VCH Verlag GmbH & Co.

Wendisch, VF, Bott, M, Kalinowski, J, Oldiges, M, and Wiechert, W. (2006). Emerging *Corynebacterium glutamicum* systems biology. *Journal of Biotechnology, 124*(1), 74-92.

White, PJ. (1983). The Essential Role of Diaminopimelate Dehydrogenase in the Biosynthesis of Lysine by *Bacillus sphaericus*. *Microbiology, 129*(3), 739-749.

Wisselink, HW, Weusthuis, RA, Eggink, G, Hugenholtz, J, and Grobben, GJ. (2002). Mannitol production by lactic acid bacteria: a review. *International Dairy Journal, 12*(2–3), 151-161.

Wittmann, C. (2002). Metabolic Flux Analysis Using Mass Spectrometry. *Advances in Biochemical Engineering/Biotechnology, 74*, 39-64.

Wittmann, C. (2007). Fluxome analysis using GC-MS. *Microbial cell factories, 6*, 6-6.

Wittmann, C. (2010). Analysis and engineering of metabolic pathway fluxes in *Corynebacterium glutamicum*. *Advances in Biochemical Engineering/Biotechnology, 120*, 21-49.

Wittmann, C, and Becker, J. (2007). The L-Lysine Story: From Metabolic Pathways to Industrial Production. In V. Wendisch, (ed.) (Ed.), *Amino Acid Biosynthesis - Pathways, Regulation and Metabolic Engineering* (Vol. 5, pp. 39-70): Springer Berlin Heidelberg.

Wittmann, C, and de Graaf, AA. (2005). Metabolic Flux Analysis in *Corynebacterium glutamicum*. In L. Eggeling & M. Bott (Eds.), *Handbook of Corynebacterium glutamicum*: CRC Press: Boca Raton.

Wittmann, C, Hans, M, and Heinzle, E. (2002). In vivo analysis of intracellular amino acid labelings by GC/MS. *Analytical Biochemistry, 307*, 379-382.

Wittmann, C, and Heinzle, E. (2001a). Application of MALDI-TOF MS to lysine-producing *Corynebacterium glutamicum*. *European Journal of Biochemistry, 268*(8), 2441-2455.

Wittmann, C, and Heinzle, E. (2001b). Modeling and Experimental Design for Metabolic Flux Analysis of Lysine-Producing *Corynebacteria* by Mass Spectrometry. *Metabolic Engineering, 3*(2), 173-191.

Wittmann, C, and Heinzle, E. (2002). Genealogy Profiling through Strain Improvement by Using Metabolic Network Analysis: Metabolic Flux Genealogy of Several Generations of Lysine-Producing Corynebacteria. *Applied and Environmental Microbiology, 68*(12), 5843-5859.

Wittmann, C, Kiefer, P, and Zelder, O. (2004a). Metabolic fluxes in *Corynebacterium glutamicum* during lysine production with sucrose as carbon source. *Applied and Environmental Microbiology, 70*(12), 7277-7287.

Wittmann, C, Kim, HM, and Heinzle, E. (2004b). Metabolic network analysis of lysine producing *Corynebacterium glutamicum* at a miniaturized scale. *Biotechnology and Bioengineering, 87*(1), 1-6.

Wittmann, C, Krömer, JO, Kiefer, P, Binz, T, and Heinzle, E. (2004c). Impact of the cold shock phenomenon on quantification of intracellular metabolites in bacteria. *Analytical Biochemistry, 327*.

Woo, HM, Noack, S, Seibold, GM, Willbold, S, Eikmanns, BJ, and Bott, M. (2010). Link between Phosphate Starvation and Glycogen Metabolism in *Corynebacterium glutamicum*, Revealed by Metabolomics. *Applied and Environmental Microbiology, 76*(20), 6910-6919.

Wyman, CE, Dale, BE, Elander, RT, Holtzapple, M, Ladisch, MR, and Lee, YY. (2005). Coordinated development of leading biomass pretreatment technologies. *Bioresource Technology, 96*(18), 1959-1966.

Xu, J-Z, Ruan, H-Z, Chen, X-L, Zhang, F, and Zhang, W. (2019). Equilibrium of the intracellular redox state for improving cell growth and L-lysine yield of *Corynebacterium glutamicum* by optimal cofactor swapping. *Microbial Cell Factories, 18*(1), 65.

Xu, J-Z, Wu, Z-H, Gao, S-J, and Zhang, W. (2018). Rational modification of tricarboxylic acid cycle for improving L-lysine production in *Corynebacterium glutamicum*. *Microbial Cell Factories, 17*(1), 105.

Yamamoto, S, Suda, M, Niimi, S, Inui, M, and Yukawa, H. (2013). Strain optimization for efficient isobutanol production using *Corynebacterium glutamicum* under oxygen deprivation. *Biotechnology and Bioengineering, 110*(11), 2938-2948.

Yeh, P, Sicard, AM, and Sinskey, AJ. (1988). General organization of the genes specifically involved in the diaminopimelate-lysine biosynthetic pathway of *Corynebacterium glutamicum*. *Molecular and General Genetics MGG, 212*(1), 105-111.

Yim, SS, Choi, JW, Lee, SH, Jeon, EJ, Chung, W-J, and Jeong, KJ. (2017). Engineering of *Corynebacterium glutamicum* for Consolidated Conversion of Hemicellulosic Biomass into Xylonic Acid. *Biotechnology Journal, 12*(11).

Yokota, A, and Lindley, ND. (2005). Central metabolism: Sugar Uptake and Conversion. In L. Eggeling & M. Bott (Eds.), *Handbook of Corynebacterium glutamicum* (pp. 215-240): CRC Press: Boca Raton.

Yukawa, H, Omumasaba, CA, Nonaka, H, Kós, P, Okai, N, Suzuki, N, Suda, M, Tsuge, Y, Watanabe, J, and Ikeda, Y. (2007). Comparative analysis of the *Corynebacterium glutamicum* group and complete genome sequence of strain R. *Microbiology, 153*(4), 1042-1058.

Zhan, M, Kan, B, Dong, J, Xu, G, Han, R, and Ni, Y. (2019). Metabolic engineering of Corynebacterium glutamicum for improved l-arginine synthesis by enhancing NADPH supply. *Journal of Industrial Microbiology & Biotechnology, 46*(1), 45-54.

Zhang, B, Carlson, R, and Srienc, F. (2006). Engineering the Monomer Composition of Polyhydroxyalkanoates Synthesized in *Saccharomyces cerevisiae*. *Applied and Environmental Microbiology, 72*(1), 536-543.